Assessing the relationship between nanoparticle physicochemical characteristics and biological interactions; optimisation of *in vitro* techniques and protocols.

Thesis submitted in accordance with the requirements of
the University of Liverpool for the degree of Doctor in Philosophy
by

Christopher A. W. David

December 2016

This thesis is the result of my own work. The material contained within the thesis has not been presented, either wholly or in part, for any other degree or qualification.

Christopher A. W. David

This research was carried out in the
Department of Molecular and Clinical Pharmacology
University of Liverpool, UK

Acknowledgements

A PhD, as I have come to find, is much more than an academic qualification; it is an opportunity for personal growth. I have had the privilege throughout this time to experience many things which have shaped me as an individual. For all that has been done since Andrew, Neill, and Marco huddled around a webcam and saw the potential in me to afford this undertaking, I am truly grateful.

For the opportunity, ongoing guidance, and example of what can be achieved through diligent work, Andrew, from one Welshman to another; diolch yn fawr iawn.

Neill, as a supervisor, mentor, and good friend, I think it best to thank you in terms befitting local custom; ta la.

I would like to thank Steve, Marco, Jay, and the rest of the Rannard Group for your hospitality and sharing of expertise during my time spent in your department. The collaboration, which has been vital to my project, has been much appreciated.

If I were to try to summarise everything that the members of the Department of Molecular and Clinical Pharmacology have done for me throughout my PhD, it would not do them justice. The early mornings, late nights, and all manner of activities, be they scaling mountains or consuming copious amounts of beef from swords, have left me with many fond memories. I consider myself very lucky to have been accepted into this group, who I now regard as family.

Finally, I would like to thank my parents for their love and support. You have encouraged me throughout all of my endeavours, and instilled in me the importance of committing myself fully to any task and performing to the best of my abilities. I cannot begin to describe how much I appreciate all that you have done.

Abbreviations

µCi	Microcurie
µg	Microgram
µl	Microlitre
µm	Micrometre
µM	Micromolar
°C	Degree celsius
ACU	Atmospheric control unit
AUC	Area under the curve
AIHA	Autoimmune haemolytic anaemia
AIM2	Absent in melanoma 2
ANOVA	Analysis of variance
AO	Acridine orange
APC	Antigen presenting cells
API	Active pharmaceutical ingredient
APTT	Activated partial thromboplastin time
ASC	Apoptosis-associated speck-like protein containing caspase recruitment domain
Atg4	Cysteine protease Atg4
ATP	Adenosine triphosphate
BLQ	Below limit of quantification
C3	Complement component 3
C3a	Complement component 3 cleavage fragment a
C3b	Complement component 3 cleavage fragment b
C5	Complement component 5
C60	Fullerene of 60 carbon atoms
C70	Fullerene of 70 carbon atoms
CC_{50}	Concentration producing 50% cytotoxicity
CD	Cluster of differentiation
CFSE	Carboxyfluorescein succinimidyl ester
C_{max}	Maximum fluorescence
CM-H_2DCFDA	Chloromethyl 2',7'-dichlorofluorescin diacetate
CO_2	Carbon dioxide
COX	Cyclooxygenase
CpG-ODN	CpG oligodeoxynucleotides
CPM	Counts per minute
DAMP	Danger-associated molecular pattern
DC	Dendritic cell
DCF	2',7'-dichlorofluorescin
DDH_2O	Double-distilled water
DITMA	Drug-induced thrombotic microangiopathy

dl	Decilitre
DLS	Dynamic light scattering
DMEM	Dulbecco's Modified Eagle's Medium
DMF	Dimethylformamide
DMSO	Dimethyl sulfoxide
DNA	Deoxyribonucleic acid
DPBS	Dulbecco's phosphate buffered saline
E. coli MC1061	*Escherichia coli* strain MC1061
EGDMA	Ethylene glycol dimethacrylate
EIA	Enzyme immunoassay
ELISA	Enzyme-linked immunosorbent assay
EPR	Enhanced permeability and retention
EU	Endotoxin units
EU-NCL	European Nanomedicine Characterization Laboratory
Ex/Em	Excitation/emission
FBS	Fetal bovine serum
FDA	Food and Drug Administration
FoxP3	Forkhead box P3
G2	Generation 2
GFP-LC3	Microtubule-associated protein 1A/1B-light chain 3 vector fused to green fluorescent protein
GPIIb/IIIa	Glycoprotein integrin receptor IIb/IIIa
GMP	Good manufacturing practice
GSH	Reduced glutathione
GSSG	Oxidised glutathione
h	Hour
HBSS	Hanks' balanced salt solution
HCV	Hepatitis C virus
HEPES	4-(2-hydroxyethyl)-1-piperazineethanesulfonic acid
HIV	Human immunodeficiency virus
HMGB	High mobility group box
HPMA	N-(2-Hydroxypropyl) methacrylamide
iC3b	Inactivated complement component 3 cleavage fragment b
ICE	IL-1β converting enzyme
IFN	Interferon
IFNα	Interferon alpha
IFNγ	Interferon gamma
IL	Interleukin
JSLE	Juvenile systemic lupus erythematosus
K2EDTA	Dipotassium ethylenediaminetetraacetic acid
l	Litre
LAL	Limulus amoebocyte lysate
LB	Luria-Bertani
LPB	Lipopolysaccharide binding protein

LC3B	Microtubule-associated protein 1A/1B-light chain 3B
LDH	Lactate dehydrogenase
LP	Leukocyte proliferation
LPS	Lipopolysaccharide
M	Molar
MAC	Membrane attack complex
MAPK	Mitogen activated protein kinase
MD2	Lymphocyte antigen 96
mg	Milligram
MHC	Major histocompatibility complex
MIAME	Minimum information about a microarray experiment
ml	Millilitre
mM	Millimolar
MR	Magnetic resonance
MSU	Monosodium urate
mTOR	Mechanistic target of rapamycin
MTS	3-(4,5-dimethylthiazol-2-yl)-5-(3-carboxymethoxyphenyl)-2-(4-sulfophenyl)-2H-tetrazolium)
MTT	3-(4,5-dimethylthiazol-2-yl)-2,5-diphenyltetrazolium bromide
mV	Millivolt
MWCNT	Multi-walled carbon nanotube
NaCl	Sodium chloride
NAD	Nicotinamide adenine dinucleotide
NAD^+	Oxidised nicotinamide adenine dinucleotide
$NADH^+/H^+$	Reduced nicotinamide adenine dinucleotide
NBCD	Non-biological complex drugs
NCI-NCL	National Cancer Institute's Nanotechnology Characterisation Laboratory
NDCI	Nanomaterial Data Curation Initiative
NF-κB	Nuclear factor kappa-light-chain-enhancer of activated B cells
NK	Natural killer
NLR	NOD-like receptor
NLRC4	NLR family CARD domain containing 4
NLRP3	NLR family pyrin domain containing 3
nm	Nanometre
nM	Nanomolar
p53	Cellular tumor antigen p53
p62	Ubiquitin-binding protein p62
PAMAM	Poly(amidoamine)
PAMP	Pathogen-associated molecular pattern
PBMC	Peripheral blood mononuclear cell
PCC	Physicochemical characteristics
PD-1	Programmed cell death 1

pDC	Plasmacytoid dendritic cell
PdI	Polydispersity index
PDT	Photodynamic therapy
PEG	Poly(ethylene glycol)
PEG-PL	Poly(ethylene glycol)-phospholipid
pg	Picogram
pH	Potential of hydrogen
PHA	Phytohemagglutinin
PIC	Protease inhibitor cocktail
PK	Pharmacokinetic
PLMA	Poly(lauryl methacrylate)
pM	Picomolar
PMMA	Poly(methyl methacrylate)
PRR	Pattern recognition receptor
PSGL	P-selectin glycoprotein ligand
PT	Prothrombin time
PVP	Polyvinyl pyrolidone
QSAR	Quantitative structure-activity relationship
RAU	Relative absorbance units
R. shaeroides	*Rhodobacter sphaeroides*
REDOX	Reduction-oxidation
RES	Reticuloendothelial system
RFU	Relative fluorescence units
RNA	Ribonucleic acid
ROS	Reactive oxygen species
rpm	Revolutions per minute
RPMI-1640	Roswell Park Memorial Institute 1640 Medium
s	Seconds
SAR	Structure-activity relationship
SDS	Sodium dodecyl sulfate
SEM	Scanning electron microscopy
SPION	Superparamagnetic iron oxide nanoparticle
SWCNT	Single walled carbon nanotube
TEM	Transmission electron microscopy
Th	T helper cell
THF	Tetrahydrofuran
TLR	Toll-like receptor
T_{max}	Time to maximum fluorescence
TMC-TPP	Trimesoyl chloride tripolyphosphate
TNFα	Tumour necrosis factor alpha
Treg	FoxP3+ T cells
TRPS	Tunable resistive pulse sensing
TT	Thrombin time
U	Units
UV	Ultraviolet
XRD	X-ray diffraction

List of communications

Peer reviewed publications

David, C. (2016). Preclinical assessment of G2':2000PEG-pHPMA100EGDMA0.8 polymeric nanoparticles. *JOIN*, 1(2):49.

David, C.A., Owen, A., and Liptrott N.J. (2016). Determining the relationship between nanoparticle characteristics and immunotoxicity: Key challenges and approaches. *Nanomedicine (Lond)*, 11(11):1447-64.

Conference presentations

David, C.A.W., Rannard, S., Owen, A., and Liptrott, N.J. (2016, August). *Preclinical assessment of G2':2000PEG-pHPMA100EGDMA0.8 polymeric nanoparticles.* Poster session presented at the Nanomedicine's Early Career Researchers Meeting 2016, Swansea, UK.

David, C., Owen, A. and Liptrott, N.J. (2016, July). *Determining the physicochemical characteristics of nanoparticles that relate to negative effects on cellular health using in vitro systems.* Poster session presented at the University of Liverpool ITM Research Day, Liverpool, UK.

David, C.A.W., Owen, A., and Liptrott, N.J. (2015, December). *Determining the physicochemical characteristics of nanoparticles that relate to negative effects on cellular health using in vitro systems.* Poster session presented at the European Nanomedicine Meeting, Grenoble, France.

David, C.A.W., Raymant, M., Owen, A., and Liptrott, N.J. (2015, November). *Utility of kinetic measurement of oxidative stress in nanotoxicological assay development.* Poster session presented at the Nanotechnology in Medicine, Manchester, UK.

David, C., Owen, A., and Liptrott, N.J. (2015, August). *Optimisation of methodology to assess the impact of nanomaterials on autophagy.* Poster session presented at the BSNM Young Researcher Meeting, Liverpool, UK.

David, C., Liptrott, N.J., and Owen, A. (2015, March). *Optimisation of higher throughput assays for assessing the impact of nanomaterials on autophagy.* Poster session presented at the University of Liverpool Poster Day, Liverpool, UK.

Abstract

The development and implementation of nanomaterials for a variety of clinical applications is increasing as their utility in improving healthcare is demonstrated. However, consideration must be given to appropriate pre-clinical testing to fully translate these materials into clinical use.

A library of 22 nanomaterials, both commercially available and those developed in-house, were subject to an assay cascade forming the basis of a preclinical *in vitro* assessment which utilised a broad and widely accessible range of techniques. The library comprised numerous material classes; metallic (gold, silver, iron oxide, titanium dioxide, zinc oxide), non-metal (silica), and polymeric (polystyrene, liposome, emulsion, polydendron), varying in manufacturer stated particle size, charge, and functionalization.

Chapter 2 details characterisation of the size and zeta potential of the nanomaterial library in biologically relevant matrices. When combined with information provided by the manufacturers regarding stabilisation and surface functionalization, where available, these measures allowed associations to be made between nanoparticle physicochemical characteristics and the biological effects observed in subsequent chapters. Inherent optical properties of the nanomaterials in biologically relevant matrices and sample sterility were assessed in order to gain indication of any potential incompatibility with subsequent assays.

The haemocompatibility of nanomaterials is of primary concern in their application as nanomedicines, especially those administered intravenously. The work presented in Chapter 3 assessed the haemolytic potential of a subset of nanomaterials. All nanomaterial treatments were found to result in a lower level of complement activation compared to untreated cells, and cases of prolongation or reduction in plasma coagulation times via the extrinsic, intrinsic, and common pathways were observed.

In Chapter 4 the impact of nanomaterials on pro-inflammatory and anti-inflammatory cytokine secretion by primary immune cells demonstrated. Endotoxin was shown to exacerbate the inflammatory responses toward tested nanoparticles. Further to this; the inhibitory effects of polystyrene nanoparticles to caspase-1 activity described in the literature was confirmed. Proliferation in primary human leukocytes was shown to be significantly affected by certain nanomaterials where particular variants of silver and silica nanoparticles had antiproliferative and proliferation effects, respectively.

The work presented in Chapter 5 describes the development and utilisation of screening methodologies to investigate the influence of nanomaterials on reactive oxygen species generation, reduced glutathione and autophagy. Trends have been observed within assays e.g. the reduction in levels of autophagy appears to be linked with surface charge of the nanomaterials with the most negative having the greatest effect.

Chapter 6 details the application of methods optimised throughout the thesis

to perform a preclinical assessment on a novel class of polymeric nanomaterial termed polydendrons. It was found that variants composed of a higher ratio of novel G2' initiator demonstrated less immunogenic potential than those with an equal ratio to PEG.

Given the heterogeneity of engineered nanomaterials in terms of composition, coatings, particle characteristics and functionalization, the identification of particle characteristics that influence biological interactions will enable the rational design of future nanomaterials. The work presented in this thesis has found associations between nanoparticle characteristics and biological effects. These included concentration-dependent correlations between zeta potential and reactive oxygen species generation, and nanoparticle size and autophagic impact. Additionally, the need for thorough physicochemical characterisation, to generate as many parameters as possible for determining structure-activity relationships, has been presented. The methodologies used, and developed, throughout this thesis will aid future preclinical characterisation of novel nanomaterials.

Contents

Acknowledgements **i**

Abbreviations **ii**

List of communications **vi**

Abstract **vii**

1 General introduction **1**

2 Pre-screen to determine sterility, physicochemical characteristics and optical properties of nanomaterial library. **46**

3 Investigating the association between nanoparticle characteristics and blood compatibility **89**

4 Nanoparticle physicochemical characteristics and their potential immunogenicity **118**

5 Development and optimisation of *in vitro* cellular health and cytotoxicity protocols **152**

6 Preclinical biocompatibility assessment of hyperbranched polydendrons with the potential for drug delivery vehicles **208**

7 General discussion **247**

References **255**

Chapter 1

General introduction

Contents

1.1 Introduction 3

1.2 Physicochemical characterisation of nanoparticles 3

1.3 Interaction of nanoparticles with components of the immune system 6

1.3.1 Nanoparticle involvement in cytokine generation 8

1.3.2 Nanoparticle antigenicity 14

1.4 Interaction of nanoparticles with components of the blood 16

1.4.1 Nanoparticle-protein corona 18

1.5 Links between immunological and haematological systems 22

1.5.1 Leukocyte pro-coagulant activity 22

1.5.2 Complement activation 23

1.5.3 Platelet activation and immune stimulation 25

1.5.4 Haemolytic potential 26

1.6 Challenges in assessing the biocompatibility of novel, engineered, nanoparticles 27

1.6.1 Contamination 27

1.6.2 Nanoparticle interference with assays 29

1.6.3 Nanoparticle physicochemical characteristics in biological matrices 31

1.7 Considerations for specific patient populations 33

1.8 Efforts for standardisation in nanoparticle testing 39

1.9 Nanomaterials assessed in thesis 40

1.10 Aims of thesis 44

1.1 Introduction

The application of nanotechnology in a healthcare setting offers many novel therapeutic strategies that may improve existing therapies and diagnostics. Advantages of nanoformulation that can translate to medical benefits include improvements in bioavailability, biodistribution, and reduced clearance compared to conventional formulations (Alexis et al., 2008; Szabo and Zelko, 2015). Additionally, there are opportunities for targeted therapies which may reduce undesirable effects in cell types other than those targeted, and co-formulation that may alleviate pill burden in diseases such as HIV (Giardiello et al., 2016) as well as simplifying dosing strategies by enabling parenteral long-acting depot formulations (Tatham et al., 2015). While there are obvious advantages to the application of nanotechnology, it is entirely possible that it will not be a case of "one size fits all" and that certain drugs may only be compatible with particular nanoparticles or nanoformulation strategies (Rannard and Owen, 2009), or routes of administration (Vauthier, 2012).

1.2 Physicochemical characterisation of nanoparticles

Size, charge, hydrophobicity, and shape are some of the numerous characteristics that can be tuned by the manufacturing process. Modification of these properties can alter the biological interactions of these nanoparticles. For example, uptake of gold nanoparticles by epithelial cells has been shown to be size-dependent where the rate increases with decreasing nanoparticle size (Yao et al., 2015), and hydrophobic modification of glycol chitosan nanoparticles increased uptake in cancer cells (Nam et al., 2009).

Options for characterisation of physicochemical characteristics are dictated by

the preparation state of the material, and the desired characteristic to be evaluated (Thompson, 2010). Size, surface area, and morphology (shape and aspect ratio), can be measured directly by microscopy (scanning electron microscopy SEM, transmission electron microscopy TEM), however these methodologies require deposition to substrate for those materials in the liquid phase (Stratton et al., 2013). Size measurements may also be performed in suspension by dynamic light scattering (DLS) (Kato et al., 2009) or tunable resistive pulse sensing (TRPS) (Izon Science, 2015). Turbidity spectroscopy is used to assess sample turbidity (Elsayed and Cevc, 2011). Nanoparticle surface charge in suspension is determined by zeta potential (Clogston and Patri, 2011). Surface hydrophobicity is most commonly assessed by contact angle measurements and hydrophobic interaction chromatography (Murthy and Harivardhan Reddy, 2006). Crystallinity can be assessed via X-ray diffraction (XRD) (Ingham, 2015), and porosity by small angle X-ray scattering (Li et al., 2016), or gas adsorption (Zielinski and Kettle, 2013).

Efforts by the National Cancer Institute's Nanotechnology Characterisation Laboratory (NCI-NCL) (http://ncl.cancer.gov/) to associate nanomaterial physicochemical characteristics and biocompatibility have been summarised in Figure 1.1. Since the inception of the NCI-NCL in 2004 more than 300 different particles have been characterised (National Cancer Institute, 2013). From this extensive dataset it has been observed that smaller, more positively charged nanoparticles are associated with a higher potential for cytotoxicity due to surface reactivity, while those of negative charge are cleared by the renal and, potentially, biliary systems. Larger hydrophobic nanoparticles, with low solubility, are subject to recognition and clearance by the reticuloendothelial system while those more hydrophilic (soluble) are associated with enhanced permeability and retention in tissues (McNeil, 2009).

The heterogeneity of nanoparticles being produced by various inventors is a

major advantage as it provides many options for the treatment of a broad range of diseases by enabling numerous strategies for the formulation of therapeutic compounds as well as allowing interactions with other therapeutics. However, the broad spectrum of nanoparticle classes, in addition to their physicochemical characteristics, presents a challenge in determining their biocompatibility. A

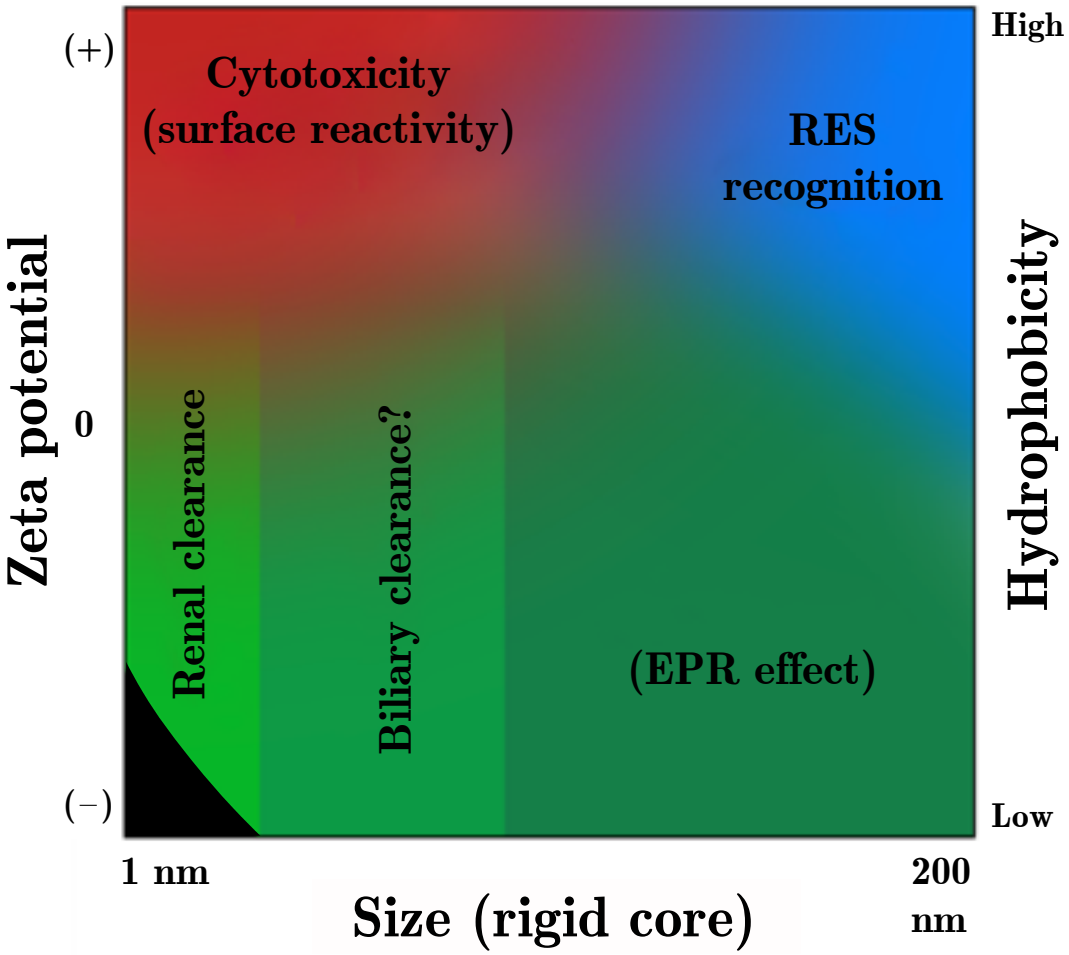

Figure 1.1: Qualitative representation of trends in relationships between independent variables of particle size (neglecting contributions from attached coatings and biologics), particle zeta potential (surface charge), and solubility with the dependent variable of biocompatibility - which includes the route of uptake and clearance (shown in green), cytotoxicity (red), and RES recognition (blue). Acronyms used; RES - reticuloendothelial system, EPR - enhanced permeability and retention. Adapted from "Nanoparticle therapeutics: A personal perspective," by S. E. McNeil, 2009, *Wiley Interdisciplinary Reviews - Nanomedicine and Nanobiotechnology*, *1(3)*, p. 268. Copyright 2009 by John Wiley and Sons. Adapted with permission.

balance should be found between nanoparticle characteristics that favour the delivery of therapeutic agents while simultaneously not resulting in issues around either toxicity or undesirable interactions with the immune system. Clearly therefore, a rational understanding of how nanoparticle physical properties relate to their biological interactions is required for the efficient development of beneficial materials.

1.3 Interaction of nanoparticles with components of the immune system

There are many well-described interactions of nanoparticles with cells of the immune system (Zolnik et al., 2010). The reasons for these interactions may be linked to specific nanoparticle properties, in particular size and charge (Frohlich, 2012; Kettler et al., 2014; Shang et al., 2014). Many nanoparticles are within the size range of microorganisms that the immune system has evolved to recognise, with many signatures in common with invading pathogens (Petersen et al., 2011).

The mechanism by which nanoparticles are internalised varies between immune cell types. As demonstrated in Figure 1.2 this includes, but is not limited to, phagocytosis, endocytosis, passive uptake, and receptor-interaction based uptake. Phagocytosis (a process performed by macrophages, monocytes, neutrophils, dendritic cells, and mast cells) leads to the capture and internalisation of nanoparticles in phagosomes which in turn undergo lysosomal degradation (Luzio et al., 2007). While this is an effective tool for removing biological pathogens, not all nanoparticles are so simply degraded. The pH environment of the phagolysosome may affect the stability of the nanoparticle leading to the release of metallic ions in the case of metallic nanoparticles (Knaapen et al., 2004). These in turn can disrupt mitochondrial processes and generate reactive oxygen species (ROS) through Fenton type reactions (Knaapen et al., 2004). A similar effect can be observed in

clathrin-mediated (McMahon and Boucrot, 2011) and clathrin-independent endocytosis (Kirkham and Parton, 2005) where degradation occurs following lysosomal fusion with the endosome. Caveolin-mediated endosomes bypass lysosomal degradation (Benmerah and Lamaze, 2007) the mechanism of which is being explored for its potential for intracellular delivery of nanomaterials (Medina-Kauwe, 2007).

Nanoparticles which translocate passively through cellular membranes (Treuel et al., 2013), or those which escape phagocytic/endocytic vesicles are then able to come in direct contact with intracellular proteins and organelles (Krpetic et al., 2014), with the potential to interact in a detrimental manner. Internalised nanoparticles have been shown to interfere with the normal autophagic process (Huang et al., 2015) and also as a result modulate the NLRP3 inflammasome (Zhong et al., 2016).

Interaction with cell surface receptors leads to the internalisation of nanoparticles, usually displaying surface motifs such as proteins and polysaccharides (Salatin and Yari Khosroushahi, 2017), although this is not a necessity as scavenger receptors have been shown to bind polystyrene via the action of macrophage receptor with collagenous structure (MARCO) (Kanno et al., 2007). Activation of receptor associated pathways as a result of the binding of nanoparticles has been demonstrated where Toll-like receptor 4 (TLR4) signal transduction followed binding of polyethylenimine-coated SPIONs (Mulens-Arias et al., 2015).

In addition to size and charge, hydrophobicity has also been demonstrated to be an important factor in the recognition of nanoparticles by the immune system (Moyano et al., 2012). As many intracellular danger-associated molecular patterns (DAMPs) are hydrophobic in nature their release upon cellular damage signals to the immune system to respond to this damage (Seong and Matzinger, 2004). Hydrophobic nanoparticles have been shown to more likely induce an immune response than those which are less hydrophobic (Shima et al., 2015). As more classes/types of nanomaterials are created it is entirely possible that

further nanoparticle characteristics will be recognised for their association with biocompatibility, and nanoparticles may be stratified for their interactions with the immune system by class-specific properties.

1.3.1 Nanoparticle involvement in cytokine generation

The *in vitro* cytokine production by human peripheral blood mononuclear cells in response to nanomaterials has been shown to have good correlation to that observed *in vivo* (Dobrovolskaia and McNeil, 2013). As such, the use of cytokines as biomarkers of immunomodulatory properties of nanomaterials has been proposed and utilised by numerous sources (Dobrovolskaia, 2015; Dobrovolskaia and McNeil, 2013; Elsabahy and Wooley, 2013). A series of cytokines have been established as being particularly pertinent in monitoring immune responses towards nanoparticles, namely TNFα, IL1β, IL-6, IL-8, IL-10, IL-12, IFNα, IFNβ, and IFNγ (Potter et al., 2015).

Cytokines are a class of growth factor proteins used in extracellular signalling, which trigger differentiation or proliferation following binding to cell-surface receptors. The actions of numerous cytokines overlap one another, and can act synergistically, or antagonistically. Their roles in modulating immune responses, homeostasis, and inducing the expression of growth factors, imparts a high degree of biological importance. Four cytokines, namely IFNγ, TNFα, IL-1β, and IL-10, were chosen for assessment in Chapter 4, informed by their presence in the literature for their implications with nanomaterials (Dobrovolskaia, 2015; Dobrovolskaia and McNeil, 2013; Elsabahy and Wooley, 2013), and being a subset of those assessed in the standard protocol developed by the NCI-NCL for their assessments of nanomaterials (Potter et al., 2015).

IFNγ, a type II interferon, is a cytokine with pleotropic immune activity inducing both proinflammatory and antiinflammatory responses (Teixeira et al., 2005). It is known to be involved in both innate and adaptive immune responses

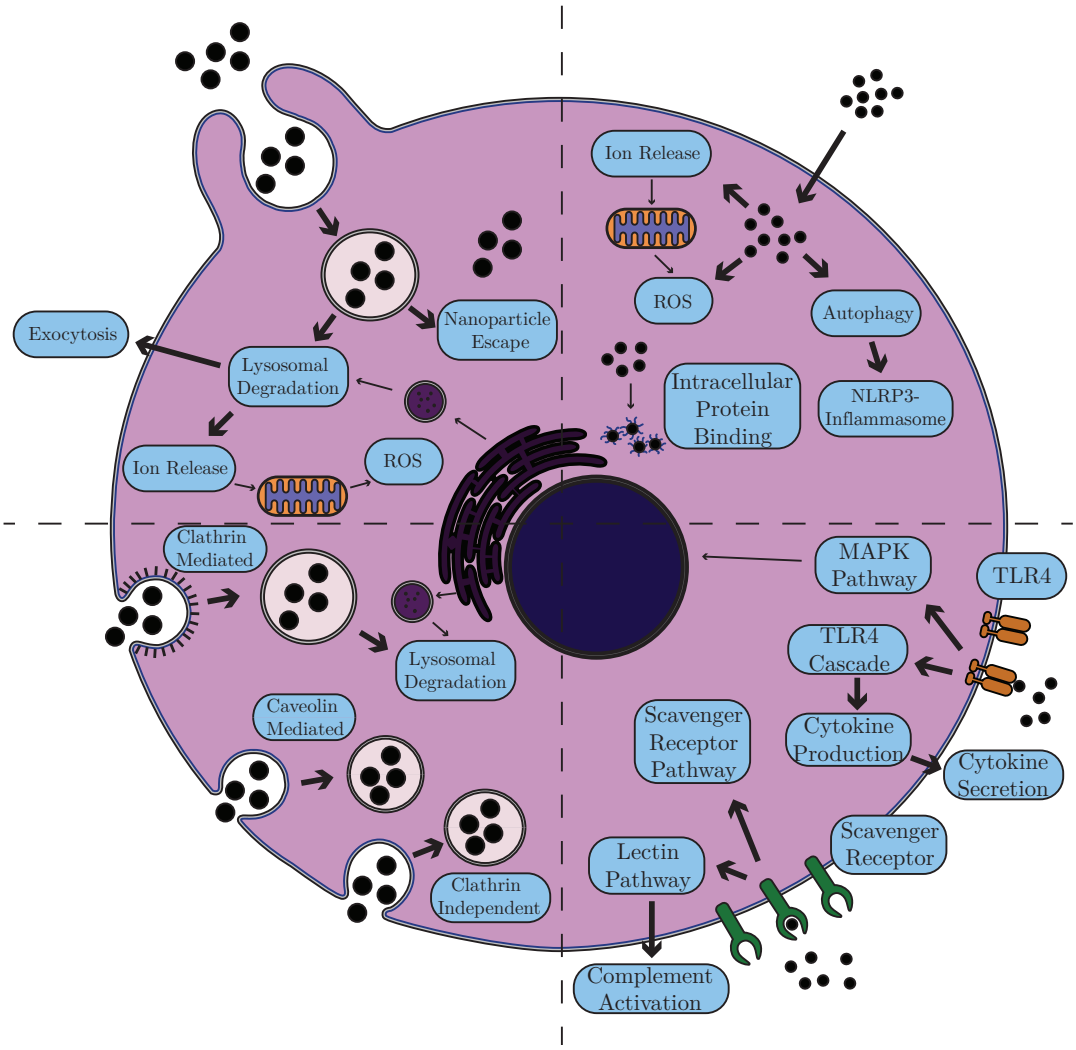

Figure 1.2: Routes of entry determine nanoparticle intracellular effects, and extracellular consequences. Internalisation of nanomaterials includes, but is not limited to, endocytosis (including phagocytosis), receptor-binding, and passive uptake. The fate, and associated intracellular effects of these mechanisms include lysosomal degradation, generation of by-products such as metal ions which can induce reactive oxygen species generation in mitochondria, direct interference with intracellular processes involved in autophagy and the NLRP3-inflammasome, and activation of intracellular cascades such as the scavenger receptor pathway, TLR4 cascade, MAPK pathway, and the lectin pathway. Extracellular consequences include exocytosis, cytokine secretion, and complement activation. Effects displayed here are non-exhaustive, some being ubiquitous and not limited to individual modes of entry to the cell. Acronyms used; ROS - reactive oxygen species, NLRP3 - NLR family pyrin domain containing 3, TLR4 - Toll-like receptor 4, MAPK - mitogen activated protein kinase.

against pathogens, tumors, in addition to maintaining immune homeostasis (Lin and Young, 2013). Primary activities include priming macrophages for enhanced microbial killing and inflammatory activation by TLRs (Su et al., 2015), and upregulating MHC class I (Zhou, 2009) and class II (Giroux et al., 2003) antigen processing and presentation. IFNγ is produced primarily by natural killer (NK) cells, T cells and NKT cells (Lin and Young, 2013), as well as macrophages (Darwich et al., 2009), B cells (Ballesteros-Tato et al., 2014), innate lymphoid cells (ILCs) (Cella et al., 2014). Its receptor is expressed ubiquitously by almost all cell types (Lin and Young, 2013). Induction of IFNγ has been demonstrated by human peripheral blood mononuclear cells in response to 8 nm zinc oxide nanoparticles (Hanley et al., 2009).

TNFα is a proinflammatory cytokine primarily secreted by activated macrophages and induces expression of other autocrine growth factors, and induces signalling pathways that lead to proliferation or death (Papadakis and Targan, 2000). It also increases the permeability of local vascular epithelia to enhance the movement of cells and soluble molecules into tissues (Hofmann et al., 2002). TNFα activates NF-κB (Schutze et al., 1995; Wajant et al., 2003), which is in turn involved in the transcriptional activation of inflammatory-related genes in response to TNF and IL-1 (Baud and Karin, 2001), LPS (Andreakos et al., 2004), and reactive oxygen species (Morgan and Liu, 2011). Silica nanoparticles have been shown to induce generation of TNFα in Huh7 cells (Christen and Fent, 2016).

IL-1β is produced by activated macrophages and other antigen presenting cells. *In vivo* it generates co-stimulation of antigen presenting cells (APCs) and Th17 cells, resulting in inflammation (Garlanda et al., 2013). In addition to its role as a mediator of the inflammatory response, IL-1β is involved in a variety of cellular activities including cell proliferation, differentiation, and apoptosis. It is produced as a proprotein which is proteolytically processed to its active form by

caspase 1 (CASP1/ICE) (Denes et al., 2012). In the THP1 cell line, 15 nm silver nanoparticles have been found to generate secretion of IL-1β by causing increased activity of caspase-1, and the NLRP3 inflammasome (Simard et al., 2015).

Generation of proinflammatory cytokines IL-1β and IL-18 (Latz et al., 2013) through immune stimulation can lead to the generation of oxidative stress. This is the primary mode of toxicity for some nanomaterials following accumulation in cells as demonstrated in Figure 1.2. Release of these cytokines requires activation of the NLRP3 inflammasome (Sorbara and Girardin, 2011).

Inflammasomes are a group of cytosolic protein complexes within the innate immune system which play a role in regulating inflammation in response to various stimuli (Guo et al., 2015). The innate immune system utilises a series of pattern recognition receptors (PRRs) in order to differentiate pathogenic or host-derived signals of cellular stress. PRRs are expressed by epithelial cells, monocytes, macrophages, dendritic cells, neutrophils, as well as adaptive immune cells (Mogensen, 2009). PRRs include Toll-like receptors (TLRs), involved in early innate immune response to pathogens, and cytoplasmic NOD-like receptors (NLRs) which detect conserved microbial factors termed pathogen-associated molecular patterns (PAMPs) as well as host-derived DAMPs (Mogensen, 2009). NLRs are involved in the assembly of inflammasomes in response to PAMP/DAMP recognition Davis et al. (2011). Subtypes include NLRP3, NLRC4, absent in melanoma 2 (AIM2), and non-canonical inflammasomes (Guo et al., 2015). The nomenclature of inflammasome subtypes relate to the protein scaffold upon which the inflammasome forms, while the functional basis revolves around a sensory molecule, the adapter protein apoptosis-associated speck-like protein containing caspase recruitment domain (ASC), and caspase 1 (Guo et al., 2015). Of all inflammasome subtypes NLRP3 has been subject to the most detailed characterisation (Wree et al., 2014). Its activation by endogenous and exogenous danger signals leads to the release of mature IL-1β via the action of caspase-1 (Franchi et al., 2009).

Formerly known as IL-1β converting enzyme (ICE), the activation of caspase-1 is known to be the rate-limiting step in inflammation due to IL-1β or IL-18 (Jo et al., 2016). In its active form, caspase-1 is a cysteine protease involved in the processing and maturation of these cytokines. Endogenous signals which activate NLRP3 include extracellular uric acid and adenosine triphosphate (ATP), and cytosolic DNA (Jo et al., 2016). Alongside these, the NLRP3 inflammasome is activated by crystalline particles. Such particles play roles in the pathogenesis of diseases including gout (Kingsbury et al., 2011), Altzheimer's (Heneka et al., 2013), and respiratory conditions such as asbestosis and silicosis (Dostert et al., 2008). This mechanism has been exploited as a target of vaccine adjuvants such as alum (Eisenbarth et al., 2008). Nanoparticles, including silica and titanium dioxide, have been shown to activate the NLRP3 inflammasome in macrophages through release of ATP (Baron et al., 2015).

Secretion of IL-10 is a hallmark of dendritic cells (DC) (Saraiva and O'Garra, 2010), macrophages (Ouyang et al., 2011), and regulatory (TR1-like) T cells (Wraith, 2016). IL-10 promotes differentiation of B cells to IL-10-secreting regulatory B cells (Wraith, 2016). Among functions including maintaining homeostasis of tissue epithelial layers facilitating tissue-healing process in injuries resulting from infection or inflammation, IL-10 plays a role in repressing proinflammatory responses (Ouyang et al., 2011). This anti-inflammatory function results from inhibition of APCs to present MHC class II, and costimulatory molecule B7-1/B7-2 expression (Couper et al., 2008). Additionally, IL-10 production by TR1-like cells can inhibit activation of helper (CD4+) and cytotoxic (CD8+) T cells that are specific for other peptides presented by the same APC, thereby mediating bystander suppression (Couper et al., 2008; Wraith, 2016). Treatment of macrophages with iron oxide nanoparticles for 24 hours has been shown to result in IL-10 production (Rojas et al., 2016).

It should be noted that the mechanisms of nanoparticle recognition and pre-

sentation to the immune system differs from that of graft rejection. Allograft rejection is primarily mediated by T lymphocytes (Ingulli, 2010). T cells, through a process termed allorecognition, recognize non-host major histocompatibility complex (MHC) molecules via direct or indirect pathways (LaRosa et al., 2007). In the direct pathway, alloreactive T cells recognize intact donor MHC molecules on APCs in the transplanted tissue (Larsen et al., 1990). In the indirect pathway, alloreactive T cells are presented with antigen derived from donor MHC molecules by antigen presenting cells in a self-restricted manner (Game and Lechler, 2002). Graft damage incurs following naïve T cells activation and transition to effector T cells by mechanisms that include direct T cell cytotoxicity and classic delayed-type hypersensitivity (Le Moine et al., 2002).

Biomedical implants, through the process of implantation, result in physical damage which leads to blood-material interactions, provisional matrix formation, acute inflammation, chronic inflammation, granulation tissue development, foreign body reaction, and fibrosis/fibrous capsule development (Anderson et al., 2008). The provisional matrix describes the initial thrombus at the tissue-material interface (Anderson et al., 2008). Chemoattractants, cytokines, growth factors, mitogens, and other bioactive agents present in the provisional matrix is conducive with inflammatory and wound healing responses (Anderson et al., 2008).

The mechanisms of degradation of metallic implants, specifically metal-on-metal prostheses and metal-on-polyethylene, has been found to involve the generation of nanoparticles (Vasconcelos et al., 2016). Commonly used hip prostheses are primarily composed of metallic alloys, most commonly cobalt-chromium-molybdenum and titanium-aluminum-vanadium, and their bearing surface can be composed of different materials (Vasconcelos et al., 2016). It has been shown that, depending on the particular materials composing the implant, at the site of wear can generate metallic nanoparticles in the <100 nm range (Billi et al.,

2012; Brown et al., 2007; Catelas et al., 2003; Doorn et al., 1998; Germain et al., 2003; Pourzal et al., 2011), and polymeric particles of 100-10000 nm Tipper et al. (2006). The origination of nanoparticles from implants is not limited to the common site of wear, as evidenced by titanium-based particles produced by different regions of hip implants such as the femoral stem and/or acetabular cup Milosev and Remskar (2009).

1.3.2 Nanoparticle antigenicity

Currently, nanoparticle antigenicity is not well understood. Antigenicity involving plasma B cells generating antibodies against the nanoparticles, or functional groups, such as peptides, attached to the particle surface has been described (Dobrovolskaia and McNeil, 2007). Since nanoparticle specific antibodies should only influence the effectiveness of particle-based products, for example by modulating cellular interactions or biodistribution, it is more probable that antibodies which recognise the functional ligands present on the nanoparticle surface may cause similar clinical results as those seen for biotechnology-derived therapeutic proteins (Kivisakk et al., 2000; Swanson et al., 2004). Nanoparticle-specific antibody formation has been reported. In particular these relate to monoclonal antibody responses to C60 fullerenes, as well as an instance of polyclonal C60-specific antibodies with a subpopulation shown to cross-react with C70 fullerene (Braden et al., 2000; Chen et al., 1998). PEGylation (the functionalization of nanoparticles with polyethylene glycol chains) has been used to reduce their immunogenic potential, but the production of anti-PEG antibodies has also been reported (Ishida et al., 2007; Wang et al., 2007).

Unwanted immune stimulation is a hurdle for the development of some nanomaterials, but it does also present an opportunity for the formulation of certain therapeutics, in particular, antigens to be utilised in vaccines. The use of nanoparticles as adjuvants has been reported by numerous studies (Zhao et al., 2014).

Poly(methyl methacrylate) (PMMA) nanoparticles have been shown to induce long-lasting antibody titres in response to HIV-2 whole virus vaccine in mice, and the antibody response was 100-fold higher than that of standard adjuvant (Stieneker et al., 1991). Similarly, the levels of specific antibodies produced in the immunisation of animals with colloidal gold conjugated antigens were higher than that generated by other adjuvants while the amount of antigen required to achieve this response was an order of magnitude lower than for immunisation with Freund's complete adjuvant (Dykman et al., 2004). The reason for this may be due to greater accumulation of the antigen in cells such as dendritic cells allowing greater presentation of the therapeutic antigen to the adaptive immune system.

Concerning the formulation of vaccines, the generation of inflammation is desirable when nanoparticles are targeted to dendritic cells (DCs). DCs have the ability to induce and modulate the immune response. DCs play a key role in the activation of T cells and as such are a principal target for most vaccines. Utilization of "danger signals" in vaccine design (DC activating non-host signals) combined with specific antigen to induce the desired immune response type is a common approach (Reddy et al., 2006). As mentioned earlier, nanoparticle size can govern their immunostimulatory profile with plasmacytoid DCs (pDCs) showing preferential uptake of nanoparticles <200 nm, resulting in the production of IFNα while phagocytosis by monocytic DCs (mDCs) of 500-1000 nm particles induced TNFα (Rettig et al., 2010). Similarly, gadolinium containing nanoparticles have been reported to possess antitumor activity resulting from their ability to induce the maturation of immature DCs (Yang et al., 2010). Stimulation of DCs by TMC-TPP nanoparticles has been shown to induce differentiation of T cells to inflammatory Th17 (Keijzer et al., 2013). The opposite effect was observed following DC stimulation by PLGA nanoparticles where not only was TH17 differentiation inhibited but also differentiation of naïve CD4+ T cells to FoxP3+ T cells (Treg cells) was observed. The anti-inflammatory role which Treg cells

play in self-antigen tolerance, inhibition of T cell response, cytokine release, as well as NK and CD4+ cell activity would not be favourable for a vaccine-based application. Determination of the favourable characteristics of nanoparticles that are correlated with the desired effect is vital to the development of future nanomaterials for use as a vaccines.

The application of knowledge regarding the biodistribution and accumulation of nanomaterials *in vivo* (Almeida et al., 2011) is highly important when interpreting immunogenicity not only regarding use as adjuvants but for general safety. Passive and active accumulation of nanoparticles in multiple sites increase the concern of off-target toxicity. The relationship between administration route and biodistribution of nanoparticles is intrinsically linked. However, there exists no thorough evaluation of route of administration, and how it relates to cytotoxicity following tissue accumulation.

1.4 Interaction of nanoparticles with components of the blood

Many nanoparticles have been shown to influence a number of haematological components and processes (Ilinskaya and Dobrovolskaia, 2013). In their normal homeostatic role platelets facilitate coagulation and are involved in the thrombogenic process to stop bleeding (Packham, 1994). Platelet activation and thrombus formation have been found to occur in response to nanomaterials in the systemic circulation (Radomski et al., 2005). Platelet aggregation following the activation of glycoprotein integrin receptor GPIIb/IIIa has been observed for both single walled carbon nanotubes (SWCNT) and multi-walled carbon nanotubes (MWCNT) in a particle size-dependant manner (Radomski et al., 2005). Platelet activation has also been strongly associated with GPIIb/IIIa activation by silver ions released from silver nanoparticles (Jun et al., 2011; Laloy et al., 2014) and in-

creased intracellular calcium ion concentration resulting from silica nanoparticles (Nemmar et al., 2015). The interaction of charged polystyrene latex nanoparticles has been found to cause physical bridging of platelets in a GPIIb/IIIa independent manner (Smyth et al., 2015).

The properties of size, charge, functionalization with charged surface groups such as amines, and hydrophobicity can determine thrombogenicity of nanoparticles resulting from altering prothrombin times and activated partial thromboplastin times, as well as the mechanism by which coagulation is induced (Ilinskaya and Dobrovolskaia, 2013). Anionic polystyrene latex nanoparticles caused platelet aggregation via upregulation of adhesion receptors, while their cationic counterparts initiated platelet aggregation following destabilization of cell membrane integrity (McGuinnes et al., 2011). Amine-functionalized nanoparticles reduced thrombin production via depletion of factors VII and IX in a size dependent manner (Oslakovic et al., 2012). It has been shown that these characteristics hold greater influence over thrombogenicity than does the basic composition of a given material (Ilinskaya and Dobrovolskaia, 2013). Cationic, but not neutral or anionic, PAMAM dendrimers cause platelet aggregation (Dobrovolskaia et al., 2012b; Jones et al., 2012). The size-dependence of polystyrene nanoparticles to cause coagulation has been suggested because 220 nm but not 24 nm particles exhibited this effect (Oslakovic et al., 2012).

A number of techniques can be utilised for the assessment of coagulation. These include clot-based tests, chromogenic assays, direct chemical measurements, and ELISAs (Bates and Weitz, 2005; Walenga and Hoppensteadt, 2004). Of these, clot-based and chromogenic assays are used commonly applied clinically and in the assessment of material impact on coagulation (Bates and Weitz, 2005). The methodology chosen for nanomaterial assessment in Section 3.2.2.2 is consistent with the protocol forming part of the assay cascade used by the National Cancer Institute's Nanotechnology Characterisation Laboratory in their assess-

ments of nanomaterials (Neun et al., 2015b). This format of testing separately assessed coagulation times via the extrinsic (prothrombin time - PT), intrinsic (activated partial thromboplastin time - APTT), and common (thrombin time - TT) pathways in order to elucidate where, if present, in these pathways any changes occurred as a result of treating plasma with nanomaterials. For the purposes of this evaluation the common coagulation pathway is able to be assessed in isolation using thrombin to induce coagulation, however biologically the common pathway is not exclusive from either extrinsic nor intrinsic pathways. Under normal physiological conditions it is not directly activated in the manner that the intrinsic is initiated by binding of Factor XII to anionic or hydrophilic surfaces (Vogler and Siedlecki, 2009), or the extrinsic through vascular injury (Owens and Mackman, 2010). Activation of this pathway provides a means in which to further probe any pro- or anticoagulant effects of nanomaterials. Prolongation or reduction of coagulation times via the extrinsic or intrinsic pathways in the absence of effect on the common pathway means that materials are acting upon coagulation factors necessary earlier in the cascade. In the case of nanomaterials altering coagulation times via extrinsic/intrinsic pathways and the common pathway it can be elucidated that the effect is based on nanomaterial action upon multiple targets. Directly assessing coagulation time via the common pathway enables confirmation of these observations.

1.4.1 Nanoparticle-protein corona

The inherent physicochemical characteristics of nanoparticles, when introduced to a biological or any protein containing matrix, result in nanoparticle-protein associations termed the corona. The corona is composed of layers of adsorbed proteins and molecules to the nanoparticle surface providing the interface which directly interacts with the biological system (Walczyk et al., 2010). As exemplified in Figure 1.3a, the composition of the corona changes over time (Tenzer

et al., 2013). Known as the Vroman effect; proteins present in high concentration but of low affinity, such as albumin and fibrinogen, will exchange with those of higher affinity over time (Vroman et al., 1980). A great deal of effort has been put into the characterisation of coronal composition (Tenzer et al., 2013), as well as elucidation of the kinetics, affinities, and stoichiometries of nanoparticle-protein association and dissociation (Cedervall et al., 2007). These are areas of importance as it is the corona that governs the biological distribution and fate of the nanoparticle (Aggarwal et al., 2009; Gunawan et al., 2014), and understanding of this effect may assist in the rational design of nanomaterials.

Coronal formation has the potential for detrimental effects on the nanoparticle's structure and function. Highlighted in Figure 1.3a; protein binding has been shown to accelerate the dissolution of zinc oxide, cadmium selenium quantum dots, iron oxides, aluminium oxides and oxyhydroxides (Xia et al., 2008), resulting in the release of metallic ions which in turn may result in the generation of reactive oxygen species. Reconstruction of the surface crystalline structure through energy release following protein binding has been shown as a potential mechanism, extrapolating work by Gilbert et al. on zinc sulphide nanoparticles (Gilbert et al., 2004). Opsonization of the nanoparticle surface is known to reduce the circulation time of nanoparticles by enhancing uptake by the RES (Chonn et al., 1992), or forming a "molecular signature" (Aggarwal et al., 2009) marking the nanoparticles for uptake and clearance by immune cells (Goppert and Muller, 2005).

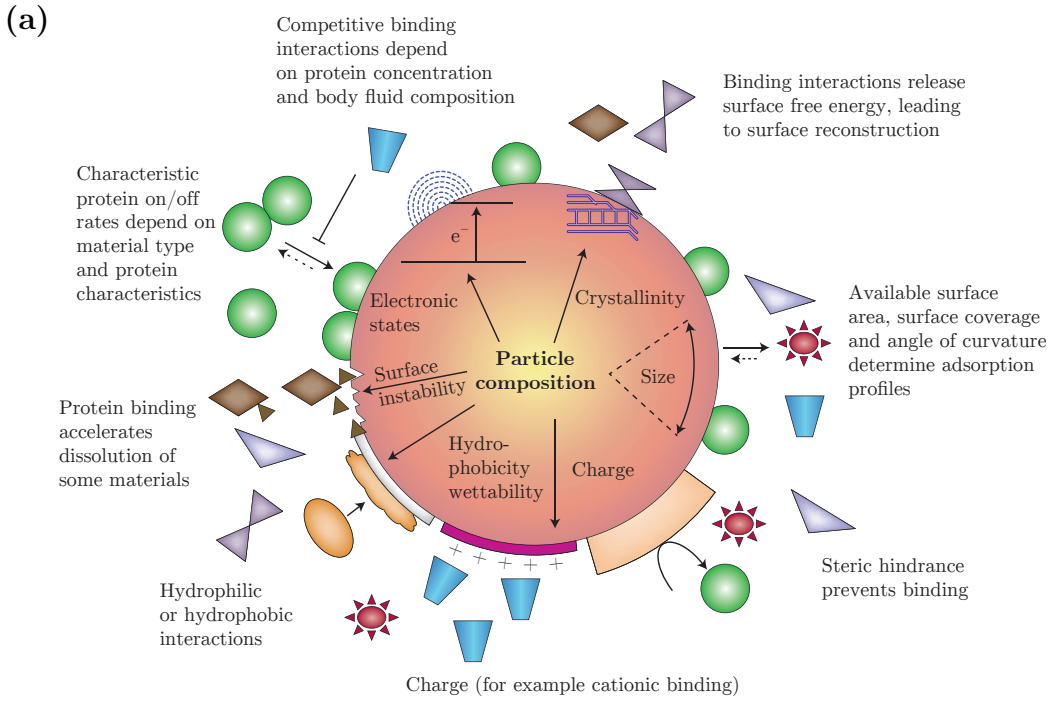
(a)
Competitive binding interactions depend on protein concentration and body fluid composition
Binding interactions release surface free energy, leading to surface reconstruction
Characteristic protein on/off rates depend on material type and protein characteristics
e⁻
Electronic states
Crystallinity
Particle composition
Surface instability
Size
Available surface area, surface coverage and angle of curvature determine adsorption profiles
Protein binding accelerates dissolution of some materials
Hydro-phobicity wettability
Charge
Steric hindrance prevents binding
Hydrophilic or hydrophobic interactions
Charge (for example cationic binding)

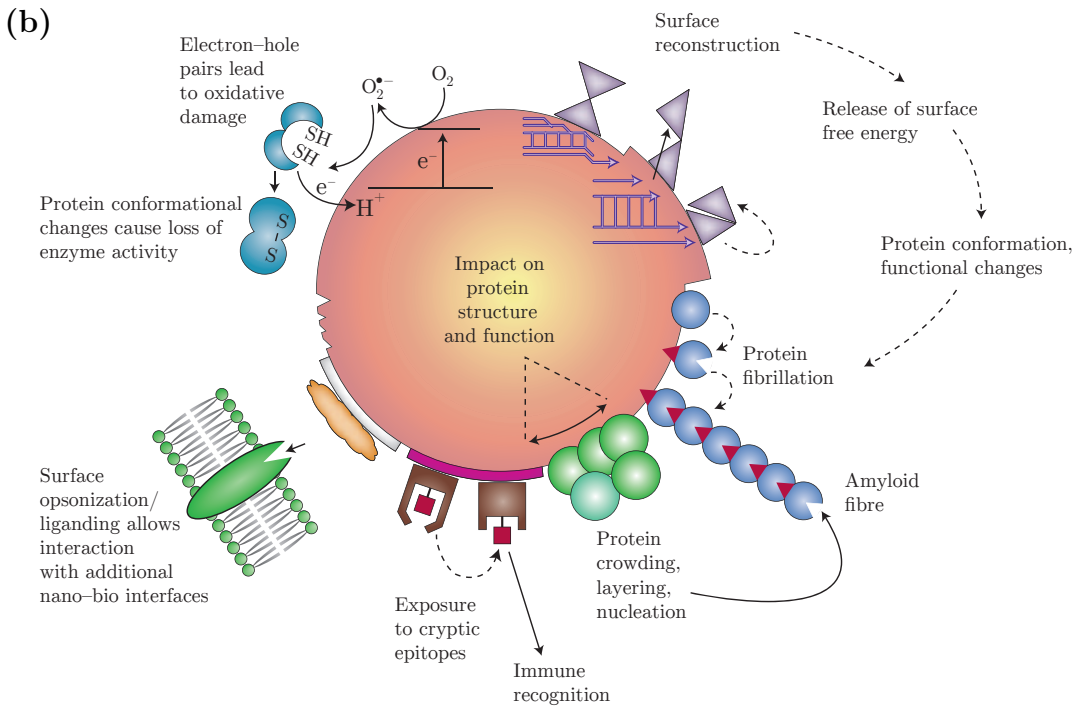

Figure 1.3: The nanoparticle-protein corona constitutes a primary nano-bio interface determining nanoparticle function and fate in biological systems. (a) Nanomaterial physicochemical characteristics associated with corona formation in a biological environment including size, charge, hydrophobicity, and surface functionalization Protein association/disassociation rates, competitive binding interactions, and the protein composition of the nanoparticle environment cause dynamic changes in coronal composition. (b) Potential modulations in protein structure and function resulting from nanoparticle surface interaction which may generate adverse biological effects contributing to disease pathogenesis. Coloured symbols represent charged, lipophilic, conformationally flexible proteins, catalytic enzymes with sensitive thiol groups, and fibril forming proteins. Adapted from "Understanding biophysicochemical interactions at the nano-bio interface," by A. E. Nel, L. Mädler, D. Velegol, T. Xia, E. M. Hoek, P. Somasundaran, F. Klaessig, V. Castranova, M. Thompson, 2009, *Nature Materials, 8(7)*, p. 547. Copyright 2009 by Nature Publishing Group. Adapted with permission.

Adhesion of proteins to the nanoparticle surface has been shown to impart conformational changes of the proteins leading to exposure of cryptic epitopes (Figure 1.3b) which may result in possible detection as non-self (Nel et al., 2009). Such conformational changes may result in a loss of enzyme activity, as exemplified by the interaction of silica nanoparticles with lysozyme (Vertegel et al., 2004).

The effect of protein on the colloidal stability of a nanoparticle suspension is known to vary, either sterically stabilising or destabilising leading to aggregation, depending on parameters including nanoparticle physicochemical characteristics and the composition of the medium (Moore et al., 2015). Establishment of the protein corona has been shown to reduce the haemolytic potential of nanomaterials by negating the effects of strong surface charge (Martinez et al., 2015; Paula et al., 2012; Tenzer et al., 2013).

1.5 Links between immunological and haematological systems

Immunological and haematological systems do not function in isolation and have evolved to work cooperatively to both detect infection and ensure resolution of the response. There are a number of examples of how nanoparticles interact with one system, which in turn activates the other.

1.5.1 Leukocyte pro-coagulant activity

Leukocytes play key roles in the regulation of thrombin formation (Bouchard and Tracy, 2003) having an influence over inflammation, wound healing, and atherosclerosis. Monocytes and neutrophils are recruited by activated platelets at sites of thrombogenesis (von Bruhl et al., 2012). This is achieved via recogni-

tion of P-selectin on the activated platelet by leukocyte P-selectin glycoprotein ligand (PSGL)-1 resulting in conformation changes in β2 integrins (Totani and Evangelista, 2010) leading to potent procoagulant activity. Induction of tissue factor synthesis, the presence of which is necessary for the production of thrombin, leads to thrombus formation (Niemetz, 1972).

Contamination of materials can have a great effect on the pro-coagulant activity of leukocytes. It has been shown that the presence of endotoxin confers leukocytes with considerable procoagulant activity (Niemetz and Fani, 1971). Contamination of nanomaterials by endotoxin may cause false positives in many immunological assays and it has been demonstrated that cationic PAMAM dendrimers enhance the procoagulant activity induced by endotoxin (Dobrovolskaia et al., 2012b; Ilinskaya and Dobrovolskaia, 2014).

1.5.2 Complement activation

The complement system is a vital component of the innate immune system with functions involved in homeostasis, pathogen recognition, and determining the appropriate immune response be it innate or adaptive (Dunkelberger and Song, 2010). It is a multicomponent system made up of over 30 membrane-associated and soluble proteins (Sarma and Ward, 2011).

Complement component C3 plays a central role in the activation of complement system. Its activation is required for the classical, lectin, and alternative pathways of complement activation (Freedman, 1987). Complement activation results in C3 cleavage to C3a, an anaphylatoxin mediating chemotaxis and inflammation (Peng et al., 2009), and C3b fragments by C3 convertases (Arumugam et al., 2006). C3b covalently binds to the activating surface participating in the self-activation loop of complement activation via the alternate pathway (Nesargikar et al., 2012). C3b may also bind to the C4b2a complex to form C5 convertase which cleaves C5 into C5a, an anaphylatoxin exerting multiple inflam-

matory responses which include the recruitment of phagocytes (Sarma and Ward, 2011), and C5b (Song et al., 2000) in turn initiating formation of the membrane attack complex (MAC) (Nesargikar et al., 2012). MAC, formed by the interaction of C5b with C6, C7, C8 and C9, inserts into cell membranes creating functional pores resulting in lysis of microbial cells or apoptosis (Morgan, 1999).

C3b activity is regulated by two-site cleavage by Factor I, in the presence of co-factors Factor H or CR1, yielding inactivated C3b (iC3b) blocking the formation of C3 and C5 convertase enzymes (Fraczek and Martin, 2010). The immunoassay used in Section 3.2.4 quantifies the iC3b present in plasma. By assessing complement activation in this manner any form of modulation can be observed. This methodology, when utilised as a preliminary screen, allows higher throughput and reduction of time compared more laborious methodologies such as single component activities or haemolytic assays (Kirschfink and Mollnes, 2003). The utility of these assays still stand as they can be later used to further elucidate any observed interactions in greater detail, as well as being used in tandem to highlight and/or negate any potential nanoparticle-based interference. Nanoparticles have been shown to activate the complement system following intravenous injection (Peter and Moghimi, 2012). Opsonization of nanomaterials by iC3b can lead to their recognition and internalization by phagocytic cells (Boraschi et al., 2012), while this is not as efficient as opsonization by other active fragments of C3 (Freedman, 1987).

Numerous studies have pointed towards complement activation being a contributing factor in the development of hypersensitivity and anaphylaxis as a response to the systemic presence of nanoparticles (Chanan-Khan et al., 2003; Dobrovolskaia et al., 2008a; Zolnik et al., 2010). Hypersensitivity reactions have been reported for the liposomal formulation Doxil (Szebeni et al., 2011), and there is evidence that this is mediated by complement activation (Chanan-Khan et al., 2003). It has been described that polymeric nanoparticles consisting of

PEG-PL (block copolymers of poloxamer and poloxamine) can activate complement exclusively via the lectin pathway (Moghimi et al., 2015). This mechanism is normally reserved for the recognition of repeating and charged motifs of certain polysaccharides (Hollmig et al., 2009).

1.5.3 Platelet activation and immune stimulation

The link between platelet activation and immune stimulation is multifactorial and double-edged. While thrombogenesis can influence immune stimulation, along with various thrombogenic factors being able to inhibit or augment immune responses, the opposite is also true where immune stimulation increases thrombogenic potential. Proinflammatory cytokines and endotoxin induce tissue factor production on leukocytes, which in turn initiates extrinsic coagulation via thrombin (FIIa) generation (Chu, 2011). Complement activation leads to enrichment of platelet plasma membrane surfaces with negatively charged phospholipids which have been shown to amplify coagulation (Sims et al., 1989).

Thrombogenic function is just one of the numerous activities which platelets have within homeostasis. The involvement of platelets within immune stimulation has gained recognition in recent years (Franco et al., 2015; Speth et al., 2013). Platelets carry numerous receptors including TLRs, and express immunomodulatory molecules and cytokines (Li et al., 2012). An example of how nanoparticles may cause immune stimulation via platelets has been demonstrated previously where multi-walled nanotubes were shown to induce the release of platelet membrane microparticles capable of stimulating other immune cells (De Paoli Lacerda et al., 2011). Further studies are warranted on the interaction of platelets and immune cells with respect to nanoparticle effects on both cell types.

1.5.4 Haemolytic potential

The mechanisms of nanoparticle-mediated haemolysis are not yet fully understood. Haemolysis is the result of damage to red blood cells and may be used as a measure of cell viability in response to contact with materials in addition to possibly leading to anaemia (Love et al., 2012b). Many studies currently exist which describe the haemolytic potential of various nanomaterials, while only some suggestions concerning their mode of action (Dobrovolskaia et al., 2008a) primarily membrane disruption via interactions with red blood cell membrane phosphatidylcholine (Nash et al., 1966; Razzaboni and Bolsaitis, 1990). Charge has been shown to strongly influence whether nanoparticles cause haemolysis. This process has been related to the disruption of cell membranes via pore formation following the integration of charged nanoparticles into existing membrane defects (Leroueil et al., 2008). The potential for nanoparticles to become ionised (Choi et al., 2011), surface groups (Nash et al., 1966; Razzaboni and Bolsaitis, 1990), and cationic charge seem to be parameters likely to have an effect. Materials which exhibit this trend include silica nanoparticles (Rabolli et al., 2010; Zhao et al., 2011) as well as numerous others via the presence of unprotected amines on the nanoparticle surface such as PAMAM (Domanski et al., 2004), carbosilane (Bermejo et al., 2007), polypropylene imine (Agashe et al., 2007), and polylysine (Shah et al., 2000) dendrimers, which have been associated with erythrocyte damage in a dose dependent manner. The haemolytic potential of silver nanoparticles has been well described in numerous sources (Chen et al., 2015; Choi et al., 2011; Laloy et al., 2014). It has been demonstrated that with increasing hydrophilicity the haemolytic potential increases (Saha et al., 2014).

The presence of a protein corona has been shown to have a protective effect, and the haemolytic potential of gold nanoparticles featuring both hydrophobic and hydrophilic surface functionalization was reduced (Saha et al., 2014). This

effect has also been described by Tenzer et al. wherein the presence of protein corona on silica nanoparticles negated their haemolytic activity as well as a reduced level of thrombocyte activation compared to pristine nanoparticles (Tenzer et al., 2013).

1.6 Challenges in assessing the biocompatibility of novel, engineered, nanoparticles

1.6.1 Contamination

The potential for nanomaterial contamination is intrinsically linked to the associated manufacturing process. Bacterial endotoxin, or lipopolysaccharide (LPS), is a contaminant that can be introduced to nanomaterials during the manufacturing process or in handling which elicits a strong immune response upon exposure (Smulders et al., 2012). LPS, a component of the outer membrane of Gram-negative bacteria, activates B cells, monocytes, macrophages, and other APCs via Toll-like receptor 4 (TLR4) and lymphocyte antigen 96 (MD2) (Bryant et al., 2010). Recognition is enhanced by the accessory proteins lipopolysaccharide binding protein (LBP) and CD14 (Park and Lee, 2013). Activation of monocytes and macrophages by LPS results in the release of cytokines and costimulatory molecules including TNFα, IL-1β, IL-6, IL-12, and IL-23 (Arango Duque and Descoteaux, 2014; Dobrovolskaia and Vogel, 2002). It has been shown that endotoxin can exacerbate inflammatory responses to nanoparticles (Bianchi et al., 2015; Cesta et al., 2010; Shi et al., 2010; Vallhov et al., 2006). LPS has been demonstrated to have a proliferative effect on B cells Xu et al. (2008), and CD4 and $CD8^+$ T cells *in vivo* (Tough et al., 1997). Variation in the structure of

LPS exists between bacterial source Lukacova et al. (2008), and these can result is varying modes of action. LPS from *R. sphaeroides* is a potent antagonist of TLR4 signalling, and can be exploited as an assay control to negate any possible endotoxin effect (InvivoGen, 2007).

As a result of the potent proinflammatory activity the presence of endotoxin in nanomedicines whose administration to individuals in an already diseased state leads to the question of how this, in combination with potential nanoparticle associated immunomodulation, may affect an already compromised immune system.

Various methods of depyrogenation or purification may be employed for the inactivation or extraction of endotoxin from biotechnology products, however, not all may be suitable for nanomaterials (Dobrovolskaia and McNeil, 2012). Depyrogenation via prolonged exposure to extreme temperature ($\leq$30 minutes at $\leq$200°C), while highly effective in inactivating endotoxin on glassware and tools used in nanomaterial synthesis, may not be tolerated by the nanomaterials themselves especially if containing biological components, targeting ligands, or drugs (Dobrovolskaia and McNeil, 2012). Other sterilization methods are known to be incompatible with classes of nanomaterials, such as gamma irradiation applied to silver colloids (Subbarao, 2012) or gold nanoparticles (Franca et al., 2010).

The formulation of nanomedicines can represent complicated, multistep processes often involving the use of volatile chemicals and reagents. These volatile agents must be removed to prevent toxicity being generated by carry-over from contaminants within the formulation process (Crist et al., 2013). The cytotoxic analysis of a preparation of gold nanorods both pre- and post-purification has demonstrated the effects which can result from residual manufacturing components (Leonov et al., 2008). Removal of cetyltrimethylammonium bromide, a cationic surfactant used in the production of nanorods, using polystyrenesulfonate resulted in the preparation having a "comparable toxicity to a standard

phosphate buffer solution" when evaluated via MTT in a human nasopharyngeal carcinoma cell line (Leonov et al., 2008). This observation has also been described by some sources where the toxicological potential of carbon nanotubes has been assessed (Kagan et al., 2006; Shvedova et al., 2003). The production of carbon nanotubes requires catalysis by transition metals (Hofmann et al., 2009). Most frequently these are iron, nickel, and copper. As free ions, these metals have been shown to induce oxidative stress via the production of reactive oxygen species (Figure 1.2) (Diabate et al., 2002; Voelkel et al., 2003). Chemical contamination of this type has been detected in commercially available preparations of carbon nanotubes where, following purification, the material was no longer deemed toxic (Pulskamp et al., 2007).

1.6.2 Nanoparticle interference with assays

A number of *in vitro* assays have been adopted for use with nanomaterials (Love et al., 2012a). Their translation to use in nanotoxicology is mainly due to their track record of versatility, simplicity, and reproducibility. As has become apparent in recent years; the appropriateness to apply these methodologies with little consideration to how novel materials may lead to spurious assay outcomes (Kroll et al., 2012). Determining the appropriateness of assays for this end is complicated by the intrinsic complexity of nanoparticles. As such, suitable inhibition/enhancement controls should be included in this analysis when possible.

Adsorption of protein to the surface of nanoparticles reduces the concentration of free protein available for quantification. The polarity of nanoparticles can enhance or reduce their potential for binding proteins from a biological matrix. This is particularly evident by the reduction in measurable IL-8 due to adsorption to a titanium dioxide preparation (Kroll et al., 2012). In this study depletion of recombinant IL-8 concentration in a cell-free system was observed via ELISA following 24 hours incubation with titanium dioxide nanoparticles. Similarly, TLR9

and IL-1β binding to citrate-stabilized gold nanoparticles has been documented (Sumbayev et al., 2013; Tsai et al., 2012). The ability of nanoparticles to interact with, and inactivate enzymes is a consideration which reaches beyond the potential *in vitro* and *in vivo* effects. Numerous methods for testing the toxicity of nanomaterials rely on enzymatic function. The potential for interaction dictates that further considerations be made so as not to generate data which may not be representative of the material but merely an artefact of experimental interference (Maccormack et al., 2012). Few assays have been implicated with this form of interference to date. One that has been brought to light is the LDH assay. Inactivation of lactate dehydrogenase as a result of adsorption to nanoparticle surfaces has been presented as a mechanism by which the LDH assay can produce results which are not an accurate representation of nanoparticle action (Kroll et al., 2012; Maccormack et al., 2012).

Studying the haemotoxic effects of nanomaterials lends the opportunity for a number of methodological issues relating to the basic properties of nanoparticles under investigation. Techniques applied to these studies have a high potential for material-based interference. The turbidity of nanoparticle preparations is known to interfere with platelet aggregometry, the principal of which relies on the optical assessment of the decrease in turbidity due to platelet aggregation. A potential solution for this is to utilize alternative measurement methods such as flow cytometry. Systems utilising magnets, such as those used for measuring platelet activation, have the potential to be incompatible with magnetic nanoparticles. When subjected to the magnetic field a region of higher concentration may establish, the effect of which may skew any observations and not be representative of a uniform distribution.

Proliferation is commonly evaluated using the MTT assay, but there are numerous mechanisms by which this can be incompatible with nanomaterials. A potential issue with the use of this assay is that it relies on the metabolic conver-

sion of the MTT compound. Materials which promote/alter mitochondrial biogenesis cause artificially high signal which could be mistaken as pro-proliferative (Wang et al., 2010). Differences in rates of tetrazolium production is reflective of the metabolic state of the cells (Berridge et al., 2005; Berridge and Tan, 1993). It is known that activated lymphocytes are more metabolically active than non-activated, which may reflect altered metabolism rather than proliferation (Mosmann, 1983). The effect of nanoparticles on metabolism and proliferation would be difficult to discern so the use of further methods such as [^{3}H]-thymidine incorporation and CFSE could be utilised.

The issues described here hold equal validity not only for toxicity assays but also immunotoxicity as the reagents employ similar strategies for generation of a measurable result i.e. absorbance, fluorescence. As such, the potential for nanoparticle-based assay interference must be considered throughout assay development and data interpretation.

1.6.3 Nanoparticle physicochemical characteristics in biological matrices

To determine structure-activity relationships and define meaningful trends, it is necessary to accurately measure physicochemical characteristics. The application of nanomaterials under biological conditions, both *in vitro* and *in vivo*, require in-depth knowledge of their physicochemical properties in relevant matrices. Due to the complexity of biological matrices, it is not sufficient to assume that characteristics determined under minimal conditions (i.e. under vacuum, or in water) are still valid in the rational design and development for given purposes. The size, charge, surface chemistry, stability, and a host of other properties can be directly and dramatically altered by the medium in which the nanoparticles are suspended, all of which may affect how the materials interact with biological

processes (Hall et al., 2007; Treuel et al., 2014).

Not only is it important to produce accurate and appropriate measurements of the physicochemical characteristics of nanomaterials, but it must be appreciated that the production of such materials is often a complex multistep process. Changes in particle size and/or charge can affect particle biodistribution, immunological impact and broader aspects of safety for nanoparticles made of the same material (Dobrovolskaia et al., 2012a,b). While polydispersity within and between preparations must be expected, this batch-to-batch variability must be strictly monitored and accounted for to minimize downstream issues.

The issue of determining biologically meaningful *in vitro* assays which can inform downstream *in vivo* studies is further complicated by the choice of appropriate cellular models and endpoints. *In vitro* cytotoxicity assays performed in immune cell lines are known to not be good indicators of nanoparticle immunotoxicity *in vivo* (Dobrovolskaia, 2015). This results from the inability of a single cell line to accurately represent the various populations of immune cells, nor allowing for evaluation of the immune cell systemic function (Dobrovolskaia, 2015). Assays known to demonstrate good *in vitro-in vivo* correlation with human and animal models include haemolysis, complement activation, cytokine secretion, opsonisation and phagocytosis (Dobrovolskaia, 2015; Dobrovolskaia and McNeil, 2013). While cellular responses to nanomaterials in these *in vitro* assays does not guarantee the same to occur *in vivo*, these assays demonstrate great utility in identifying cases of cause for concern where nanomaterials may generate potentially detrimental effects when applied to *in vivo* models.

Linked with this is the need to choose relevant and efficacious controls as well as determine any interaction between the nanomaterial and assay itself. To exemplify this issue, it was earlier mentioned that numerous cytotoxicity assays are prone to nanoparticle-related interference. Without detailing the choice of cell line or endpoint, the choice of controls and assay interaction potential shall be

discussed. The cytotoxic compound of choice must be sufficiently potent within the given cell line to generate toxicity and, ideally, have a mode of action similar to that which would be expected from a nanomaterial. While this is desirable, tetrazolium salts such as MTS/MTT which detect the REDOX potential of cells would not be necessarily compatible with ROS generators such as dicumarol which can lead to overestimation of cellular viability and proliferation (Collier and Pritsos, 2003). Similarly, compounds which affect cell membrane integrity should be used with care in the LDH assay, especially when comparing results of different cytotoxicity assays. Cell-free preparations of assays can be considered vital as a means to not only generate a baseline but also to observe any concentration dependent interactions that may occur. This can be invaluable in fluorogenic assays such as DCF where a threshold for interference may exist (Kroll et al., 2009). As mentioned earlier, the inclusion of inhibition/enhancement controls can assist in determining whether observations are a result of cellular interactions with nanomaterials or solely due to the presence of the nanomaterial. This is becoming routine in Limulus amoebocyte lysate (LAL)-based assays for measuring endotoxin in which a nanomaterial sample is spiked with a known amount of endotoxin and assessed for enhanced or diminished recovery (Neun and Dobrovolskaia, 2011). The underlying principal is translatable to a host of assays in which inducers or inhibitors of the desired effect can be introduced in addition to nanomaterials. Although logical, these considerations are widely overlooked, potentially resulting in misleading conclusions being drawn.

1.7 Considerations for specific patient populations

Research efforts examining the biocompatibility of nanomaterials primarily use blood, as well as immune cells, from healthy volunteers to assess potential inter-

actions. However, the intended populations often have differential immunological profiles compared to healthy volunteers. It is, therefore, vital that these aspects be considered when testing novel engineered nanomaterials.

The broad concepts of "immunological frailty", a term encompassing all situations in which the immune response is not adequate, and how they relate to potential interactions with nanomaterials has been described (Boraschi, 2014) and highlights the relative lack of experimental evidence in such populations compared to investigations in healthy volunteer cells and tissues. There is evidence to suggest that the genetic background of the test organism can influence the outcome of biocompatibility testing. Gustafsson et al. showed that the response to titanium dioxide nanoparticles in rats was strain-specific, indicating that genetics plays a role in the response to nanomaterials (Gustafsson et al., 2014). Existing data on the effects of nanoparticles in animal models reflecting immunological frailty, dysregulated immunity, and immune-compromised states, show that nanoparticles can have greater, or an additive, toxicological effect to that resulting from the diseased state (Li et al., 2014). The can be the result of Reduced protection mechanism, compromised immunity, and impaired self-repair ability (Li et al., 2014). However, how closely animal models can reflect the situation in humans with respect to disease states is an ongoing issue surrounding many fields of research, and it seems likely that obtaining *ex vivo* samples from patients with specific conditions may complement other pre-clinical evaluations, prior to Phase I trials.

As one would expect, potential side effects and immune interactions by nanomaterials may be further influenced by dysregulation of the immune system in disease. HIV is a pertinent example of this, wherein the disease is underpinned by complex multifactorial immunomodulation, and treatment paradigms are currently being investigated for improvement via the application of nanoformulation (Mamo et al., 2010).

There exist several parallels between the immunological effects of nanomaterials and those of the diseased state. These effects include some generated by chronic inflammation such as rheumatoid arthritis, cancer, and even hepatitis and HIV.

As mentioned previously, the activation of TH17 type response by TMC-TPP nanoparticles leads to the generation of IL-17 (Keijzer et al., 2013). The generation of this particular proinflammatory factor is of interest in the pathogenesis of rheumatoid arthritis, as its production in the synovial tissue has been shown to promote destructive collagen arthritis in an IL-1 independent manner in murine models (Lubberts et al., 2001), and act synergistically with IL-1 and TNFα (Leonaviciene et al., 2004).

The pathogenesis of cancer is intrinsically linked to a multitude of cytokines generated by the innate and adaptive immune systems including IL-1, IL-6, IL-12, IFNγ, TNFα (Sheen et al., 2014). All of these have also been shown to be generated in response to, and associated with cellular interactions with various nanoparticles including silver (IL-1) (Simard et al., 2015), MWCNT (IL-6) (He et al., 2011), and zinc oxide (IL-12, IFNγ, TNFα) (Hanley et al., 2009). As a platform for immunotherapy nanoparticles are being studied due to their known induction of various immunostimulatory cytokines which are proposed to exacerbate, and illicit, a greater immune response against cancerous cells.

Mechanisms proposed to result in apoptosis in HCV and HIV-infected cells include loss of cell membrane integrity, mitochondrial dysfunction, and generation of ROS (Alimonti et al., 2003). Silica (Wei et al., 2015) and titanium dioxide (Novak et al., 2012) nanoparticles have been shown to alter cell membrane integrity in a charge- and concentration-dependent manner. Oxidative stress and the generation of reactive oxygen species is directly relatable to mitochondrial dysfunction (Figure 1.2) (Rego and Oliveira, 2003). A large number of nanomaterials have a similar effect (Manke et al., 2013). HIV has been shown to interfere

with the autophagic process via inhibition in dendritic cells, and induction in macrophages (Dinkins et al., 2014), while HCV has been shown to increase levels of autophagy in infected cells (Vescovo et al., 2014). Inhibition (Stern et al., 2012) or induction (Panzarini et al., 2013) of autophagy by nanomaterials (Figure 1.2) is also common to the actions of HIV and HCV. Therefore, it seems likely that certain material compositions should not be progressed for certain applications.

Immunocompromised individuals can be defined as having a substantially weakened immune system, and this was originally thought to be the case in HIV infection. However, it is now known that the situation is not clear cut since a patients' immunological profile varies with the type of viral populations infecting them, and their response to antiretroviral therapy (Annison et al., 2013). Infection with HIV leads to a decline in CD4+ T cells, but treatment with antiretrovirals may produce a resurgence in the number of these cells. However, it has been shown that although the number of CD4+ T cells increases, their functional capacity is diminished in chronic infection. This has been demonstrated by the increased expression of the receptor programmed death 1 (PD-1), a negative regulator of activated T-cells (Day et al., 2006). Cells expressing high levels of PD-1 were shown to be functionally exhausted, hyporesponsive due to continuous antigenic stimulus (Ozkazanc et al., 2016; Yi et al., 2010), compared to uninfected cells suggesting HIV+ patients are immunocompromised (Breton et al., 2013). However, the reasons for this exhaustion of the immune system are unclear, and several hypotheses have been proposed (Khaitan and Unutmaz, 2011). An interesting hypothesis for the ongoing inflammation seen in HIV, which may be linked to T cell exhaustion, is the discovery that HIV itself can induce an inflammatory form of programmed cell death termed pyroptosis. Dotish et al. showed that HIV can directly induce pyroptosis in CD4+ T cells via inflammasome activation, and that this process could be blocked by inhibiting caspase-1 (Doitsh et al., 2014). Interestingly, nanoparticles have been shown to interact with inflammasomes,

NLRP3 in particular (Figure 1.2) (Baron et al., 2015), and carbon nanoparticles have been shown to induce pyroptosis (Reisetter et al., 2011). This is an important consideration for the application of nanoparticles either in the treatment of HIV infection or when nanoparticles may be applied in HIV+ patients for concomitant health issues e.g. raised cholesterol or infections. As a condition where chronic dosing is a reality which cannot be overlooked, the long term effects of any nanoformulation must be considered, and is something being investigating with interest.

Effects such as these may be tolerable in a healthy model but be potentially incompatible with the diseased state. It is also possible for the opposite to be true, where the observable effect is unacceptable under healthy conditions, whereas its effect on the diseased state may not be as pronounced and within a range where the potential benefits outweigh the negative outcomes. As is demonstrated in Figure 1.4 the primary considerations of the nanomaterial itself, the immune system to which it will be introduced, and the disease on which it will act, are not mutually exclusive. The intersections of biocompatibility and treatment response weigh heavily in the development of nanomedicines. Often overlooked is the immune response relating the disease to the immune state, and also how the nanomaterial has influence over these. To be able to create a truly appropriate model for the design of nanomedicines, a holistic approach such as this must be adopted.

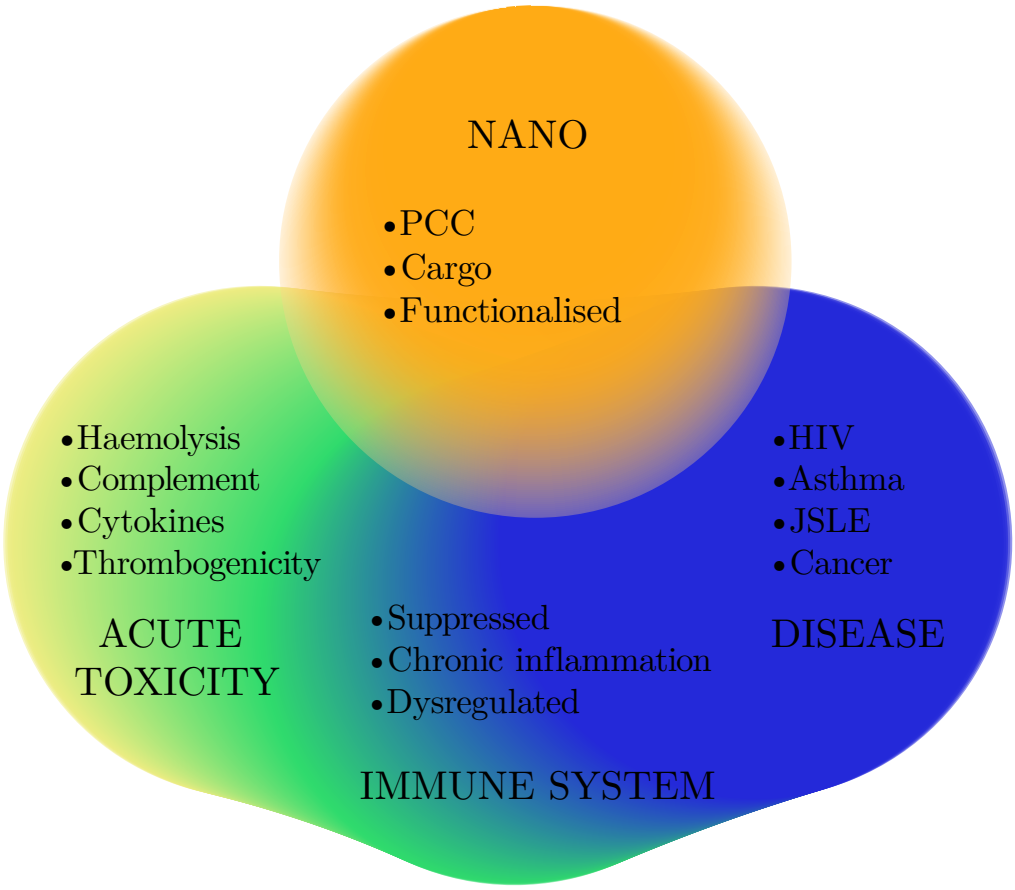

Figure 1.4: Key challenges in compatibility of nanoparticles as nanomedicines. Considerations involved in the design, analysis, and application of nanomaterial for the treatment of disease linking the material specific, immune state, and particular disease. A more holistic approach incorporating investigation of immunological status and genetic variability in genes encoding immune signalling proteins will allow a more holistic approach to the biocompatibility testing of novel engineered nanomaterials. Acronyms used; PCC - physicochemical characteristics, HIV - human immunodeficiency virus, JSLE - juvenile systemic lupus erythematosus.

1.8 Efforts for standardisation in nanoparticle testing

To truly determine relationships between nanoparticle characteristics, the necessity to apply a more standardised approach to assays has become apparent in order to correctly assess how nanoparticles interact with biological systems. Many researchers involved in the development of nanomaterials use well-defined assays to assess biocompatibility e.g. investigation of cytotoxicity by using MTT assays. However, there are reports of contradictory test results from cell-based assays (Krug and Wick, 2011; Schrurs and Lison, 2012). Unexpected variability can arise in such assays by differences in media composition, passage time of cell lines, and the source of the serum used in routine cell culture media. The NCI-NCL has been at the forefront of promoting harmonisation of assays to determine nanoparticle interactions with biological systems and offers standardised methodologies for its assessment. Given the increasing development of nanomaterials across Europe, a need has been identified to begin to regulate the preclinical evaluation of novel engineered nanomaterials as well as provide a platform for the translation of these materials into clinical studies. The recently established European Nanomedicine Characterization Laboratory (EU-NCL) (http://www.euncl.eu/) shares the same ethos as the NCI-NCL in the provision of a standardised characterisation of nanomedicines to aid in their translation to the clinic and facilitate nanomedicine development. Currently, researchers and developers in Europe have to gather preclinical data from a multitude of non-integrated providers which may result in interlaboratory variability and, therefore, conflicting results. A major ambition of the EU-NCL is to tackle that obstacle by providing an open-access EU-wide characterisation infrastructure and maintain Europe as internationally competitive in nanomedicine development. EU-NCL offers a unique integrated

solution ensuring access to high-quality data, experience, and facilities throughout Europe for a large range of medical applications. EU-NCL is a multi-centre infrastructure which is intended to overcome current fragmentation and to improve quality and efficiency of translation by drawing on expertise across Europe. The involvement of multiple analytical centres guarantees direct access to different domains in the nanomedicine communities and other stakeholders while maintaining the bandwidth to engage with Europe's most promising candidates. It is envisaged that using this integrated approach, EU-NCL will also be able to determine critical nanoparticle characteristics that relate to biological effects, without compromising confidentiality with developers. As such, this will enable researchers to access anonymised information to inform future rational design of nanomaterials.

1.9 Nanomaterials assessed in thesis

The nanoparticles used throughout this work were chosen to represent broader classes of nanomaterials with predominance in the literature; metallic (gold, silver, iron oxide, titanium dioxide, zinc oxide), non-metal (silica), and polymeric (polystyrene, liposome, emulsion, polydendron), varying in manufacturer stated particle size, charge, and functionalization. Additionally, choices were subject to nanomaterial availability at the time of the project.

Two types of gold nanoparticle were included in this work. The first being sodium citrate-stabilised gold nanoparticles, 10 nm in size. The second type being 11 nm gold nanoparticles to which a mix matrix coating composed of peptides CVVVT-ol and HS-PEG had been applied as described by Duchesne et al. (2008). Both of these gold nanoparticle variants have previously been shown to augment peripheral blood mononuclear cell (PBMC) proliferation in response to phytohemagglutinin, and increase production of cytokines IL-10 and IFN-γ (Liptrott

et al., 2014). Gold nanoparticles are a promising candidate material for drug delivery systems and cancer therapeutics (Arvizo et al., 2010).

Two types of silver nanoparticles were obtained for this work which differed in their surface stabilisation; sodium polyacrylate (1-10 nm), and sodium citrate (20 nm). Silver nanoparticles show potential for range of biomedical applications which include diagnosis, treatment, drug delivery, medical device coating, and for personal health care (Ge et al., 2014; Zhang et al., 2016).

Three variants of iron oxide nanoaprticles, all featuring differing surface stabilisation, were applied to the assessments in this thesis. Two of these, namely Endorem and Ferumoxytol, are currently applied clinically. Endorem is a superparamagnetic iron oxide nanoparticle (SPION) magnetic resonance (MR) contrast agent, composed of nano-sized iron oxide crystals coated with dextran or carboxydextran (160 nm) (Wang, 2011). Ferumoxytol is 30 nm carboxymethyldextran-coated iron oxide nanoparticles (Neubert et al., 2015) used in the treatment of iron deficiency anemia in patients with chronic kidney disease (Coyne, 2009; Schwenk, 2010). JGC is a 6.9 nm diethylaminoethyl dextran coated SPION developed for use in labelling macrophages (Sharkey et al., 2017). In addition to these applications, superparamagnetic iron oxide nanoparticles have been developed as delivery systems, for magnetic hyperthermia (local heat source in the case of tumor therapy) (Gupta and Gupta, 2005; Neuberger et al., 2005), and extensively used as contrast agents for morphological imaging (Lee et al., 2006; Li et al., 2013).

Titanium (IV) oxide nanoparticles were procured for this work. These were 21 nm in size as described by the manufacturer, supplied as a nanopowder. Titanium dioxide nanoparticles are being developed for use in advanced imaging and nanotherapeutics (Yuan et al., 2010). Such applications include photosensitizers for use in photodynamic therapy (PDT) (Szacilowski et al., 2005), use in various skin care products as a novel treatment for acne vulgaris, recurrent condyloma accumi-

nata, atopic dermatitis, hyperpigmented skin lesions, and other non-dermatologic diseases (Wiesenthal et al., 2011). Titanium dioxide nanoparticles also show antibacterial properties under UV light irradiation (Montazer et al., 2011; Yuan et al., 2010) and utility as drug carriers (Shi et al., 2013).

Three zinc oxide nanoparticles were chosen for use in this work. These comprised a 35 nm zinc oxide nanoparticle surface-stabilised with 3-aminopropyl triethoxysilane, and 50 and 100 nm zinc oxides supplied as nanopowder. Zinc oxide, as a potential nanotherapeutic, offers a platform of low toxicity and biodegradability (Zhang et al., 2013). Through exploiting the range of zinc oxide nanostructures, all possessing properties advantageous for particular applications (Zhong Lin, 2004), this material is being developed for biomedical imaging (fluorescence, magnetic resonance, positron emission tomography, dual-modality imaging), drug delivery, gene delivery, and biosensing (Xiong, 2013; Zhang et al., 2013).

Three types of silica nanoparticles were chosen for inclusion in the library of nanomaterials; 50 and 310 nm, both of which stabilised with L-arginine, and a 100 nm silica nanoparticle supplied as a nanopowder. The latter has been shown to trigger caspase-1 cleavage and IL-1β secretion in human macrophages and keratinocytes (Yazdi et al., 2010). Silica has been described as one of the most promising inorganic materials for nanovaccinology and delivery system design (Zhao et al., 2014). They have shown utility in applications including selective tumour targeting (Ow et al., 2005), real-time multimodal imaging (Benezra et al., 2011), and vaccine delivery (Zhao et al., 2014).

Polystyrene nanoparticles featuring surface stabilisation by either quaternary ammonium or sulphonate were purchased. These two distinct forms were then subdivided into three nanoparticle sizes; 180, 275, 440 and 180, 300, 440 nm respectively. Quaternary ammonium surface functionalization has previously demonstrated antimicrobial activity (Xue et al., 2015), as well as low gastrointestinal uptake when applied for use in oral vaccination (Kim et al., 2012).

Sulphonated polystyrene nanoparticles have been found to have a high affinity for binding protein due to high surface energy (Pitek et al., 2012). Additionally, a 245 nm sulphonate-stabilised polystyrene was shown trigger human dendritic cell maturation resulting in enhanced CD4+ T cell activation (Frick et al., 2012). Polystyrene nanoparticles are able to conjugate to a variety of antigens through surface-modification with various functional groups (Kalkanidis et al., 2006). However, use of polystyrene nanoparticles is limited to model systems as they are not biodegradable and cannot be cleared from circulation following therapeutic action (Solaro et al., 2010).

Non-targeted/loaded liposomes composed constituent lipids DSPC, DSPE-PEG(200), DSPE-PEG(2000)-maleimide, and cholesterol prepared using the thin lipid film process as described by King et al. (2016) were included in this library of nanomaterials. Liposomes show great potential for the delivery of chemotherapeutics via entrapment in their internal structure (Crommelin and Storm, 2003; Metselaar and Storm, 2005; Minko et al., 2006). As a platform for vaccine delivery they offer a number of ways in which an antigen or adjuvant may be delivered. These include encapsulation in the core of the liposome, incorporation with the lipid bilayer, or adsortion on the surface for presentation to APCs (Alving, 1991; Alving et al., 1980; Saupe et al., 2006). Liposomes can be modified to generate an immunogenic response by modifying the surface of the particle by adding a ligand (Saupe et al., 2006), antigen (Alving et al., 1980) or lipid. Cationic liposomes have been demonstrated as more potent than anionic or neutral liposomes for generating a cell-mediated immune response (Nakanishi et al., 1999).

Additionally an unloaded nanoemulsion composed of castor oil, ethyl acetate, and a novel in-house developed non-gelled branched polymer stabiliser (Hobson et al., 2013) was included. Nanoemulsions have shown great promise in improving the oral bioavailability and intestinal permeation of poorly water-soluble drugs through encapsulation within the emulsion droplet structure (Hobson et al.,

2017). Furthermore, they have shown potential for use as vaccines (Zhao et al., 2014) through their ability to carry antigens inside their core structure (Shah et al., 2010).

Finally nanoparticles of a novel polymeric material class termed polydendrons were subject to assessment in this thesis. These polydendrons were composed of N-(2-Hydroxypropyl) methacrylamide (HPMA) monmers polymerised with novel G2' and 2000PEG initiator (Figure 6.1b), at 50:50 and 75:25 ratios as described by Hatton (2015). Of each ratio there were two sizes; 161, 378 nm and 157, 264 nm respectively. These dendrimer-like materials were developed to mimic the surface functionality of dendrimers but at much higher molecular weights and size than conventional dendrimers (Hatton, 2015). The small size of dendrimers limits extensive drug incorporation internally, though their dendritic nature and branching allows for drug conjugation to the surface of the polymeric structure (Svenson and Tomalia, 2005). Currently, dendrimers pose promising candidates as drug nanocarriers for their well-defined structures, loading capacities, and potential for surface functionalization (Madaan et al., 2014), but are hindered by lengthy and costly syntheses (Hatton, 2015).

1.10 Aims of thesis

The overall aim of this thesis was to associate specific nanoparticle characteristics with targets linked to cellular health, including cellular health, immuno- and haemocompatibility. Additionally, to identify issues that might hinder the biological characterisation of these materials and develop methodologies to overcome them.

Chapter 2 details a "pre-screen" applied to a library of 22 nanomaterials, both commercially available and those developed in-house. Contamination with endotoxin or intact microbes was assessed, followed by characterisation of physic-

ochemical properties; specifically size, charge, and optical properties, conducted in a range of experimentally relevant matrices. Chapter 3 explores the effects of nanomaterials on plasma coagulation, as well as potential haemolytic activity, and influence on complement activation. Chapter 4 evaluates the generation of cytokine secretion, influence over caspase-1, and inflammasome activation, in response to nanoparticles by primary human peripheral blood mononuclear cells. Chapter 5 investigates the cytotoxic potential of nanomaterials in human cell lines, and the impact on cellular health; in particular reactive oxygen species generation, reduced glutathione content, and autophagy. The suitability of commercially available fluorogenic probes for kinetic measurement of oxidative stress was explored to demonstrate the utility of such methodologies in nanotoxicological assay development. Chapter 6 applies the methodologies described, and developed, in previous chapters of this thesis to provide a preclinical assessment of a class of novel nanomaterials termed hyperbranched polydendrons.

Chapter 2

Pre-screen to determine sterility, physicochemical characteristics and optical properties of nanomaterial library.

Contents

2.1 Introduction 48

2.2 Methods 54

2.2.1 Materials 54

2.2.2 Determination of endotoxin concentration in commercial and in-house nanoparticle samples 56

2.2.3 Assessment of possible viable microbial contamination . . 58

2.2.4 Physical and optical characterization 58

2.2.4.1 Rheometry of media used for dispersion and subsequent DLS analysis 58

2.2.4.2 Dynamic light scattering and zeta potential . . . 58

2.2.4.3 Evaluation of absorption and emission spectra in experimentally-relevant matrices 59

2.3 Results 61

2.3.1 Endotoxin content and recovery 61

2.3.2 Microbial presence 65

2.3.3 Dynamic light scattering and zeta potential 66

2.3.4 Evaluation of nanomaterial absorption and emission spectra in various matrices 72

2.4 Discussion 83

2.1 Introduction

Nanomaterials are being increasingly utilised in a wide range of applications spanning industrial uses (Stark et al., 2015), cosmetics (Raj et al., 2012), pharmaceuticals (Sheth et al., 2012), and more. As a focus for the work presented here, a number of the nanomaterials being studied are examples of, or are similar to, those produced with the intention to come in close contact with, or have a route of entry into the body e.g. gold, iron oxide, silica. Furthermore, as mentioned in Section 1.9, others have been chosen with respect to their extensive presence in the literature in *in vitro* studies e.g. polystyrene. The size of nanoparticles allows them to interact at cellular and sub-cellular levels (Shang et al., 2014). When introduced in such proximity to biological organisms their behaviour is something that needs to be more clearly defined, particularly with respect to detrimental effects on health. This creates the requirement for comprehensive assessment of the nanomaterial's physicochemical characteristics and biological effects prior to their approval in the same way as with new medical devices, pharmaceuticals, biosimilars, and non-biological complex drugs (NBCD) (U.S. Food and Drug Administration, 2015).

There are numerous reports in the literature of a variety of toxic effects attributed to nanoparticles which have been extensively reviewed elsewhere (Srivastava et al., 2015; Yah et al., 2012). However, to clearly define potential nanoparticle toxicity, contamination of nanomaterials cannot be overlooked whether this is biological or chemical in nature (Pulskamp et al., 2007).

Residual chemical contamination from nanoparticle synthesis may also result in potentially false positive results in cytotoxicity, and further downstream immunological, assays. This has been observed in commercially available preparations of carbon nanotubes where, following purification, the material was no longer deemed toxic (Pulskamp et al., 2007). However this is beyond the scope

of the project.

The matrix in which the nanoparticles are suspended tends to be minimal, which reduces the risk of microbial growth (Venkitanarayanan et al., 1999), but this is not guaranteed. Novel bacteria-derived surface coatings (Moon et al., 2014), or isolated bacterial targeting ligands (Brenza et al., 2011) increase the potential for contamination with bacterial structural components such as lipopolysaccharide (LPS or endotoxin).

Bacterial endotoxin is a contaminant which elicits a strong immune response upon exposure (Smulders et al., 2012). Endotoxin is a component of Gram-negative bacterial cell walls and can contaminate nanomaterials during the manufacturing process or in handling. It has been shown that endotoxin can exacerbate inflammatory responses to nanoparticles (Li and Boraschi, 2016). The removal of endotoxin from nanomaterial preparations is problematic and, as discussed in Section 1.6.1, methodologies such as UV irradiation, heat treatment, and gamma irradiation have been shown to change the physicochemical characteristics of nanoparticles (Franca et al., 2010). Given the difficulty in removing endotoxin from nanoparticle preparations, it is clear that its presence during production should be kept to a minimum. Products which have reached the stage of GMP manufacture are of a lower concern due to stringent controls, but prior to the scaling and transfer of materials to GMP manufacture it is necessary to gain a preclinical understanding of any compatibility issues without false positives generated by LPS. Production of novel nanomaterials by academic institutions or small companies, whose resources do not allow for stringent monitoring of endotoxin contamination at all stages of manufacture, are most at risk of rejection due to incompatibility resulting from contamination (Crist et al., 2013). This is a possible issue as many such producers of nanomaterials may not have access to biological safety cabinets or other methods of aseptic procedures. Such considerations should be addressed as best as possible prior to submission for biological

assessment to reduce incurred costs and time wasted by having to meet these issues retrospectively by modifying the formulation/production process.

Guidelines are in place for endotoxin presence in production. The FDA states "For medical devices... the limit is 0.5 EU/ml or 20 EU/device for products that directly or indirectly contact the cardiovascular system and lymphatic system. For devices in contact with cerebrospinal fluid, the limit is 0.06 EU/ml or 2.15 EU/device. For devices that are in direct or indirect contact with the intraocular environment, a lower endotoxins limit may apply." (U.S. Food and Drug Administration, 2012a). The "gold standard" method of assessing endotoxin contamination is the gel clot assay which relies on lysate from the blood of *Limulus amoebocyte* horseshoe crabs. The Limulus amoebocyte lysate (LAL) assay has been adapted in many ways to serve the analysis of endotoxin due to its sensitivity and consistency (Duff, 1983). However, nanomaterials have been shown to interfere with this method of quantification (Dobrovolskaia et al., 2010; Smulders et al., 2012) requiring careful interpretation of data generated. Dobrovolskaia et al. have shown that citrate stabilised gold nanoparticles can reduce the detected endotoxin content, while assessment of PLMA nanoparticles led to an overestimation (Dobrovolskaia et al., 2010). Such interference relates to the over and underestimation of endotoxin content. Inhibition/enhancement controls where test materials are spiked with a known amount of endotoxin provide a means to observe this effect. To obtain a valid result it is possible that additional techniques should be utilised as appropriate for certain materials (Neun and Dobrovolskaia, 2011).

With respect to interference nanomaterials possess novel properties e.g. gold nanoparticles with enhanced optical characteristics for photothermal therapy (Huang et al., 2007) or improved catalytic properties (Mikami et al., 2013), and quantum dots with specific emission spectra for advanced imaging (Chang et al., 2008). It is for this reason why they are developed and chosen for use over their

macro-scale counterparts. Although these properties are desirable for the end product, they can make characterisation a challenging task (Baer, 2011). Such optical properties include absorption at particular wavelengths (surface plasmon resonance) (Noguez, 2007), increased scattering of light, as well as excitation and emission at particular wavelengths (Kelly et al., 2003). These can all be affected by the particular conditions and immediate environment of the nanoparticle (Link and El-Sayed, 1999), and are inherent properties which can not only interfere with tests of their biological interactions, but also with their basic structural analysis. Their spectral characteristics should, as good practice, be assessed before any assays in which their presence may interfere with any optical measurements (Gonzales et al., 2010). The potential for nanomaterials to interfere with assays is a factor that is often overlooked (Ong et al., 2014) and given the broad range of nanomaterials which exhibit this quality; appropriate assay choices should be made alongside thorough characterization.

The size and uniformity of dispersion of nanomaterials is determined and controlled by factors in their manufacturing process (Rajput, 2015). To guarantee that the intended size has indeed been produced, a direct determination is necessary. There are a great number of methods employed to perform this task, the majority of which require the material to be removed from its intended medium (Stratton et al., 2013). Techniques such as scanning electron microscopy (SEM) and transmission electron microscopy (TEM) are pertinent examples of this, where imaging and size determination is performed under vacuum and requires samples to be fixed and dried (Stadtländer, 2007). An accurate measurement of dry particle size can be gained, but this is not as useful a piece of information as would be the hydrodynamic size (Baalousha and Lead, 2012) which accounts for the solvation layers around the nanoparticle in liquid. Dynamic light scattering (DLS) is a sizing method which allows the materials to be observed in their native buffer creating an applicable representation of the material's size (Kato

et al., 2009). A secondary, yet valuable metric generated using dynamic light scattering is the polydispersity index (PdI) of a given material. This provides a measure of the broadness of the size distribution of the material preparation. A larger PdI value relates to a more distributed representation of particle sizes within the formulation, meaning that attributing cytotoxic/unwanted effects to a particular size of the nanoparticle can be difficult or inaccurate (Murdock et al., 2008).

Often paired with DLS is an assessment of the nanoparticle's zeta potential (Clogston and Patri, 2011), which is the surface charge of a particle in colloidal suspension. Routinely this measurement is performed in water, and while this may be the medium in which the material is supplied by the manufacturer, it may not be the buffer in which the material is finally suspended when it comes in contact with biological systems. As zeta potential measurements are strongly influenced by the pH and ionic strength of the dispersing medium, Clogston et al. recommend measurements be performed in 10 mM NaCl due to its extensive characterisation, and the ability to generate highly reproducible data (Clogston and Patri, 2011). Colloidal stability of nanomaterials is maintained either by electrostatic interaction with the buffer or steric stabilisation by polymeric coating of the particle surface, the latter being unaffected by changes in ionic balance of the buffer (Wandee et al., 2009). As the zeta potential is a key indicator of particle stability for materials in solution which are not sterically stabilised, where a zeta potential of greater than ±30 mV is a hallmark of colloidal stability (Larsson et al., 2012), it is important to have information generated in conditions appropriate to the experimental setup.

The aim of this chapter was to perform a "pre-screen" of the nanoparticles that would be investigated in subsequent chapters of this thesis. This approach was employed to ensure the robustness of subsequent experimentation; particularly to rule out potential false positives or negatives.

Contamination with endotoxin or intact microbes was assessed initially, prior to the investigation of the physicochemical properties, specifically size and charge, and optical properties of test materials in order to determine possible interference with downstream assays, the analysis of which was conducted in a range of experimentally relevant matrices.

This work has been conducted on the materials listed in Table 2.1, which covers a broad range of material classes, particle size and charge. The data in this table was provided by the manufacturers/suppliers.

2.2 Methods

2.2.1 Materials

Emulsion (Hobson et al., 2013) and JGC were prepared as part of ongoing, separate, research projects at the University of Liverpool (Liverpool, UK). Endorem was purchased from Guerbet GmbH (Sulzbach, Germany), Ferumoxytol was purchased from AMAG Pharmaceuticals (Massachusetts, USA). Colloidal gold was purchased from British Biocell (Cardiff, UK), and mix-matrix coating was applied as described previously (Duchesne et al., 2008). Liposome (non-targeted, as described by King et al. (2016)) was provided by Lynda Harris from the University of Manchester (Manchester, UK). Quaternary ammonium functionalized polystyrene (180nm, 275nm, 440nm), sulphonate functionalized polystyrene (180nm, 300nm, 440nm), L-arginine stabilized silica (50nm, 310nm) and sodium polyacrylate stabilized silver were purchased from Sciventions (Toronto, Canada). Nano-SiO2 was purchased from Invivogen (San Diego, USA). Sodium citrate stabilized silver, titanium (IV) oxide, zinc oxide dispersion, zinc oxide nanopowder (<50nm, <100nm), RPMI-1640, Dulbecco's Modified Eagle's Medium (DMEM), and Fetal Bovine Serum (FBS) were purchased from Sigma-Aldrich (Dorset, UK). EndoLISA kit was purchased from Hyglos (Bernried, Germany). LB Broth (Hi-Salt), and Agar No 1 Bacteriological were purchased from Lab M (Lancashire, UK).

Designation	Size (nm)	Hydrodynamic size (nm)	PdI	Zeta potential (mV)	Stabiliser	Surface groups
Polystyrene 1	180	N/A	N/A	52.2	N/A	quaternary ammonium
Polystyrene 2	180	N/A	N/A	-40.9	N/A	sulphonate
Polystyrene 3	275	N/A	N/A	42.2	N/A	quaternary ammonium
Polystyrene 4	300	N/A	N/A	-37.2	N/A	sulphonate
Polystyrene 5	440	N/A	N/A	39.2	N/A	quaternary ammonium
Polystyrene 6	440	N/A	N/A	-34.9	N/A	sulphonate
Gold 1	10	N/A	N/A	N/A	sodium citrate	N/A
Gold 2	11	N/A	N/A	N/A	N/A	N/A
Silver 1	1-10	N/A	N/A	-39	sodium polyacrylate	N/A
Silver 2	20	N/A	N/A	N/A	sodium citrate	N/A
Endorem	N/A	160	N/A	-6.8	sodium citrate	mannitol
Ferumoxytol	N/A	30	N/A	-30.55	N/A	carboxyl
JGC	6.9	52.3	0.275	20.2	N/A	diethylaminoethyl dextran
Titanium (IV) oxide	21	N/A	N/A	N/A	N/A	N/A
Zinc oxide 1	35	100	N/A	N/A	3-aminopropyl triethoxysilane	N/A
Zinc oxide 2	50	N/A	N/A	N/A	N/A	N/A
Zinc oxide 3	100	N/A	N/A	N/A	N/A	N/A
Silica 1	50	N/A	N/A	-34.7	L-arginine	N/A
Silica 2	310	N/A	N/A	-37.1	L-arginine	N/A
Silica 3	100	N/A	N/A	N/A	N/A	N/A
Liposome	N/A	174	N/A	N/A	N/A	N/A
Emulsion	N/A	345.73	0.141	N/A	N/A	N/A

Table 2.1: Nanomaterials being assessed in this chapter including information provided by the manufacturers on their size, hydrodynamic size measured by DLS, polydispersity index, zeta potential, stabiliser, and surface groups. N/A - information not available from manufacturers.

2.2.2 Determination of endotoxin concentration in commercial and in-house nanoparticle samples

Endotoxin contamination was assessed using the EndoLISA kit as outlined in the protocol provided by the manufacturer. Briefly, the LPS standard was reconstituted in endotoxin-free water. From this stock a 5-point dilution series was prepared with a maximum of 50 EU/ml, three 1:10 dilution steps from this, and a 0 EU/ml standard of endotoxin-free water. Nanomaterials were prepared to the concentrations displayed in Table 2.2 at final a volume of 250 µl in duplicate. Dilutions from stock concentrations were made with endotoxin-free water. One of each material replicate was spiked with endotoxin at a final concentration of 5 EU/ml to assess potential inhibition or enhancement in recovery. Preparations were performed in endotoxin-free glassware.

100 µl of each standard, material dilution, and endotoxin spiked material dilution were added to the ELISA plate in duplicate. Binding was carried out for 90 minutes at 37°C with shaking at 450 rpm.

The plate was washed twice with 150 µl of wash buffer. The plate was tapped on paper towel to ensure complete removal of contents following each wash. 100 µl of assay reagent was added to each well. Detection was performed immediately, and again following a 90 minute incubation at 37°C. Fluorometric analysis was performed on a Varioskan Flash Multimode Plate Reader (Thermo Scientific, Massachusetts, USA).

Endotoxin content was calculated by a linear regression model applied to the standard curve, following blank correction of the data, using Microsoft Excel (2013).

Endotoxin percentage recovery was calculated in endotoxin spiked samples and accepted when recovery fell within the range of 50-200% (U.S. Food and Drug Administration, 2012a; European Medicines Agency, 2010). If recovery was

outside of the acceptable range, further dilutions above the maximum valid dilution of the relevant material were prepared to determine if this was a result of concentration or material dependent effects.

Material	Tested concentration	
Polystyrene 1	100 µg/ml	1 µg/ml
Polystyrene 2	100 µg/ml	1 µg/ml
Polystyrene 3	100 µg/ml	1 µg/ml
Polystyrene 4	100 µg/ml	1 µg/ml
Polystyrene 5	100 µg/ml	1 µg/ml
Polystyrene 6	100 µg/ml	1 µg/ml
Gold 1	100 pg/ml	1 pg/ml
Gold 2	100 pg/ml	1 pg/ml
Silver 1	100 µg/ml	1 µg/ml
	500 pg/ml	250 pg/ml
Silver 2	100 µg/ml	1 µg/ml
Endorem	100 µg/ml	1 µg/ml
	500 pg/ml	250 pg/ml
Ferumoxytol	100 µg/ml	1 µg/ml
	500 pg/ml	250 pg/ml
JGC	100 µg/ml	1 µg/ml
Titanium (IV) oxide	100 µg/ml	1 µg/ml
Zinc oxide 1	100 µg/ml	1 µg/ml
Zinc oxide 2	100 µg/ml	1 µg/ml
Zinc oxide 3	100 µg/ml	1 µg/ml
Silica 1	100 µg/ml	1 µg/ml
Silica 2	100 µg/ml	1 µg/ml
Silica 3	100 µg/ml	1 µg/ml
Liposome	1/10	1/100
Emulsion	1/10	1/100

Table 2.2: Concentrations of nanomaterials used for endotoxin content measurement.

2.2.3 Assessment of possible viable microbial contamination

Nanomaterials were streaked on plates of Luria-Bertani (LB) Agar at neat concentrations or at 10 mg/ml in deionised water for those in powder form. *E. coli* MC1061 was used as a positive control and deionized water as a negative control. All preparations were performed in triplicate.

The plates were incubated for 24 hours at 37°C, following which visual inspection for signs of microbial growth was performed and photographic records made.

2.2.4 Physical and optical characterization

2.2.4.1 Rheometry of media used for dispersion and subsequent DLS analysis

The viscosity of chosen media; deionized water, RPMI-1640, RPMI-1640 supplemented with FBS to 10% final volume, DMEM, and DMEM supplemented with FBS to 10% final volume, were measured using a microVISC (RheoSense, California, USA). Measurements were performed at room temperature in triplicate.

2.2.4.2 Dynamic light scattering and zeta potential

Nanoparticle size and surface charge were measured using a Zetasizer Nano ZS (Malvern, Malvern, UK). Measurements were performed in a DTS1060 folded capillary cell at room temperature, using the automatic attenuation selection and optimum measurement position seeking settings of the Zetasizer Software. Number of runs and run duration were automatically determined by the software, and 3 measurements were performed per sample. Experimentally determined viscosities of media from Section 2.2.4.1 were substituted to the software

for size calculation. Measurements were performed in deionized water, RPMI-1640, RPMI-1640 supplemented with FBS to 10% final volume, DMEM, and DMEM supplemented with FBS to 10% final volume. Materials were prepared at concentrations producing an attenuator index of 6-8 as recommended by the manufacturer.

Z-average intensity weighted mean hydrodynamic size, peak mean intensity size, polydispersity index, and zeta potential were recorded. The average and standard deviation for each parameter of the triplicate measurements was calculated.

2.2.4.3 Evaluation of absorption and emission spectra in experimentally-relevant matrices

Absorption and emission spectra of materials suspended at three concentrations denoted High, Mid, and Low (actual concentrations displayed in Table 2.3) in 100 µl of deionised water, RPMI-1640, RPMI-1640 supplemented with FBS to 10% final volume, DMEM, and DMEM supplemented with FBS to 10% final volume were assessed using CLARIOstar (BMG Labtech, Ortenberg, Germany) in 96-well microplates.

Wavelengths of absorption and emission maxima were calculated using MARS Data Analysis Software (BMG Labtech).

Material	Low	Mid	High
Polystyrene 1	50 µg/ml	100 µg/ml	200 µg/ml
Polystyrene 2	50 µg/ml	100 µg/ml	200 µg/ml
Polystyrene 3	50 µg/ml	100 µg/ml	200 µg/ml
Polystyrene 4	50 µg/ml	100 µg/ml	200 µg/ml
Polystyrene 5	50 µg/ml	100 µg/ml	200 µg/ml
Polystyrene 6	50 µg/ml	100 µg/ml	200 µg/ml
Gold 1	250 pM	500 pM	1 nM
Gold 2	250 pM	500 pM	1 nM
Silver 1	50 µg/ml	100 µg/ml	200 µg/ml
Silver 2	2.5 µg/ml	5 µg/ml	10 µg/ml
Endorem	50 µg/ml	100 µg/ml	200 µg/ml
Ferumoxytol	50 µg/ml	100 µg/ml	200 µg/ml
JGC	50 µg/ml	100 µg/ml	200 µg/ml
Titanium (IV) oxide	50 µg/ml	100 µg/ml	200 µg/ml
Zinc oxide 1	50 µg/ml	100 µg/ml	200 µg/ml
Zinc oxide 2	50 µg/ml	100 µg/ml	200 µg/ml
Zinc oxide 3	50 µg/ml	100 µg/ml	200 µg/ml
Silica 1	50 µg/ml	100 µg/ml	200 µg/ml
Silica 2	50 µg/ml	100 µg/ml	200 µg/ml

Table 2.3: Concentrations and dilution factors used to assess absorption and emission spectra of nanomaterials.

2.3 Results

2.3.1 Endotoxin content and recovery

Some interference with the quantification of endotoxin content was observed as highlighted in Table 2.4. Materials such as polystyrene 2 and 3 demonstrated a possible additive effect which was resolved at lower concentration. Silver 1 conversely had an inhibitory effect which again was rectified by further sample dilution. With regard to percentage recovery of spiked samples silver 1, Endorem, and Ferumoxytol all fell outside the accepted 50-200% recovery range at higher concentrations (Figure 2.1b, 2.1c). Interestingly JGC fell below the 50% threshold to 24.88% at 1 µg/ml (Figure 2.1c) which could be a result of an underlying concentration-dependent effect.

Material	Tested concentration	Endotoxin content (EU/ml)	Tested concentration	Endotoxin content (EU/ml)
Polystyrene 1	100 µg/ml	1.97	1 µg/ml	BLQ
Polystyrene 2	100 µg/ml	2.02	1 µg/ml	3.55
Polystyrene 3	100 µg/ml	2.74	1 µg/ml	1.27
Polystyrene 4	100 µg/ml	1.37	1 µg/ml	0.73
Polystyrene 5	100 µg/ml	2.27	1 µg/ml	1.13
Polystyrene 6	100 µg/ml	1.04	1 µg/ml	1.93
Gold 1	100 pg/ml	BLQ	1 pg/ml	BLQ
Gold 2	100 pg/ml	BLQ	1 pg/ml	BLQ
Silver 1	100 µg/ml	1.63	1 µg/ml	2.98
	500 pg/ml	0.50	250 pg/ml	1.91
Silver 2	100 µg/ml	1.41	1 µg/ml	2.06
Endorem	100 µg/ml	BLQ	1 µg/ml	0.61
	500 pg/ml	0.02	250 pg/ml	0.07
Ferumoxytol	100 µg/ml	BLQ	1 µg/ml	BLQ
	500 pg/ml	1.47	250 pg/ml	4.40
JGC	100 µg/ml	107.80	1 µg/ml	2.99
Titanium (IV) oxide	100 µg/ml	BLQ	1 µg/ml	BLQ
Zinc oxide 1	100 µg/ml	BLQ	1 µg/ml	BLQ
Zinc oxide 2	100 µg/ml	BLQ	1 µg/ml	BLQ
Zinc oxide 3	100 µg/ml	BLQ	1 µg/ml	BLQ
Silica 1	100 µg/ml	1.36	1 µg/ml	1.37
Silica 2	100 µg/ml	2.26	1 µg/ml	2.4
Silica 3	100 µg/ml	BLQ	1 µg/ml	BLQ
Liposome	1/10	18.44	1/100	3.19
Emulsion	1/10	3.11	1/100	1.29

Table 2.4: Endotoxin content measured from the concentrations stated. Text coloured red demonstrated a possible additive effect. Text coloured blue demonstrated a possible interference effect. BLQ - below limit of quantification (0.05 EU/ml).

(a)

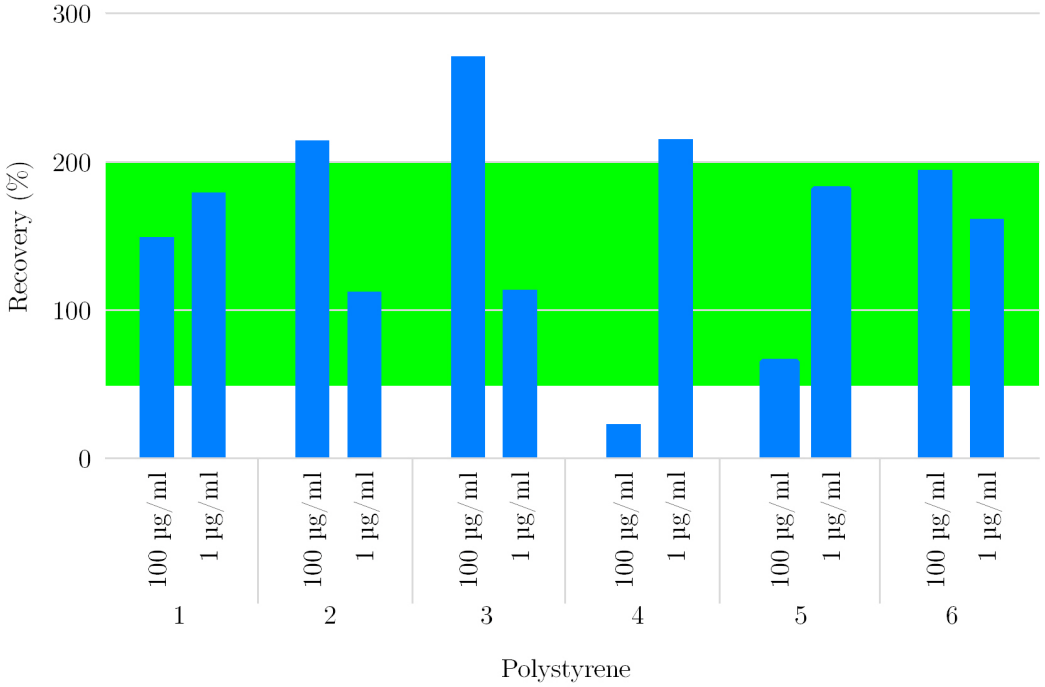
300
200
100
0
Recovery (%)
100 µg/ml
1 µg/ml
1
2
3
4
5
6
Polystyrene

(b)

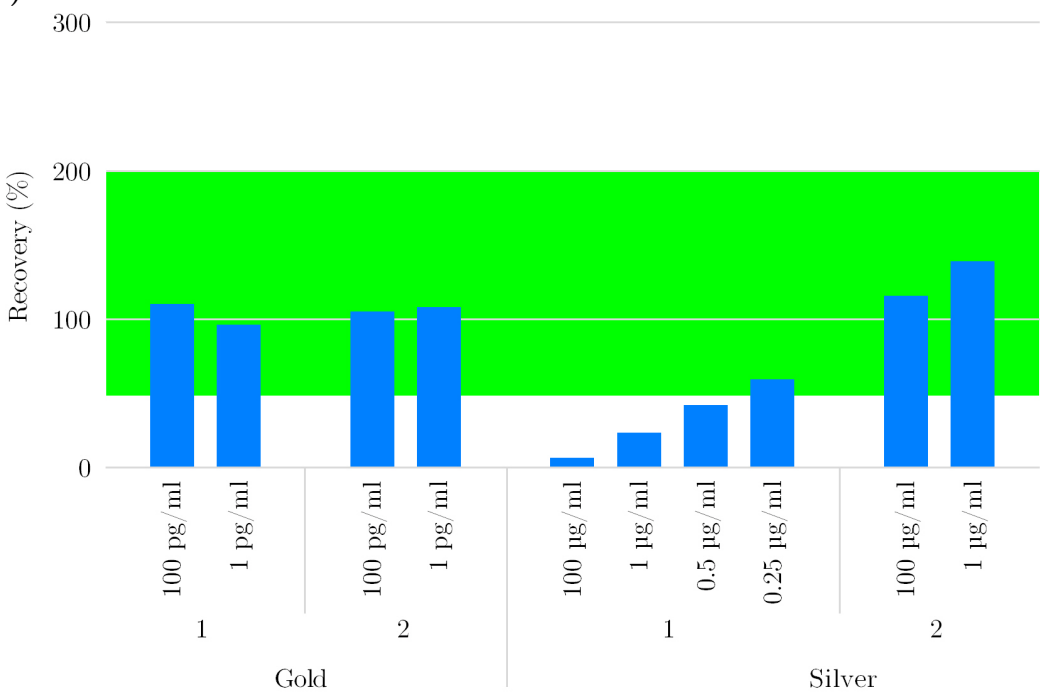
300
200
100
0
Recovery (%)
100 pg/ml
1 pg/ml
100 µg/ml
1 µg/ml
0.5 µg/ml
0.25 µg/ml
1
2
Gold
Silver

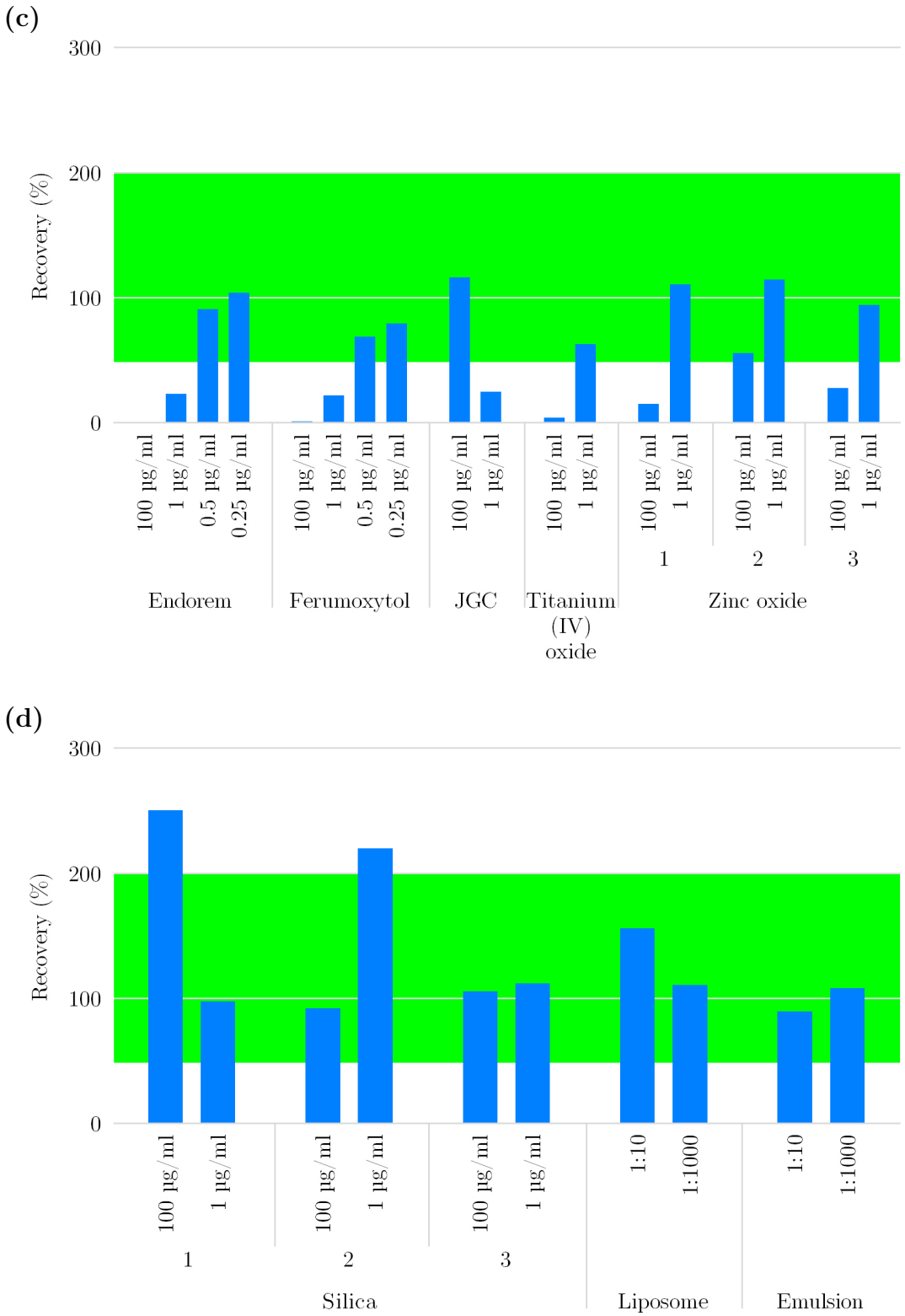

Figure 2.1: Percentage endotoxin recovery from endotoxin spiked nanomaterials at stated concentrations. Green shaded region highlights the acceptable 50-200% range of recovery.

2.3.2 Microbial presence

The positive control plates all demonstrated bacterial growth of *E. coli* (Figure 2.2a), while no bacterial growth was observed in the negative control (Figure 2.2b) or any of the nanomaterials assessed (Figure 2.2c) following 24 hour incubation.

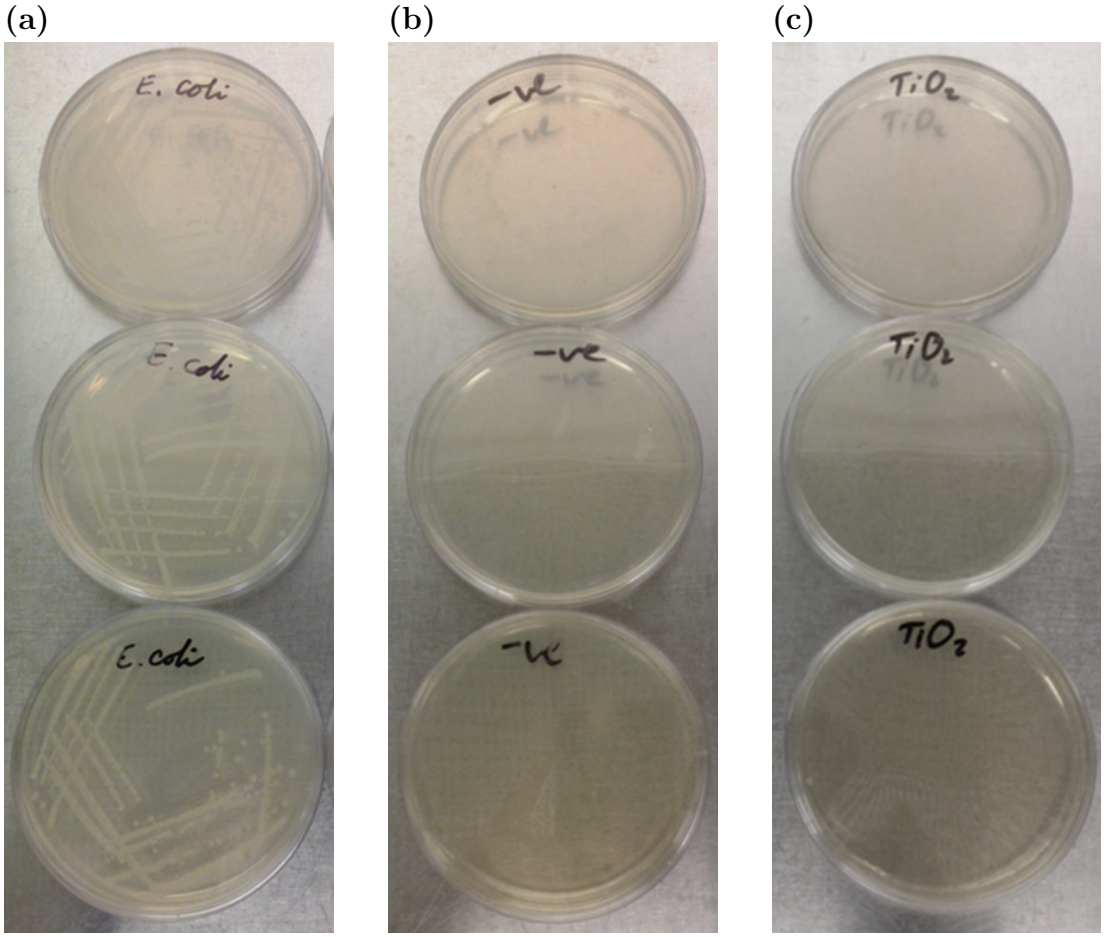

Figure 2.2: LB agar plates following 24 hours incubation after streaking of (a) Positive control *E. coli*. (b) Negative control deionised water. (c) Example of nanomaterial; titanium (IV) oxide.

2.3.3 Dynamic light scattering and zeta potential

Size measurements were performed on liposome and emulsion by their respective manufacturers utilising an identical protocol to the one in this work. The high degree of similarity of Z-average size in deionised water to stated sizes shows no degradation, or reduction in the stability of the materials during storage (Table 2.1). Similarity by this measurement was found in the polystyrene samples, with 5 and 6 matching the manufacturer stated sizes, as well as Endorem. Conversely, stark disparity was observed in all other materials ranging from upwards of twice the stated size, to titanium (IV) oxide, zinc oxides 2 and 3, and silicas 2 and 3 being micron-sized.

The Z-average size of polystyrene 5 displayed an increase to micron size in RPMI-1640 and DMEM, an eleven- and sevenfold increase over its size in water respectively. Unlike the metal oxides there was no visible precipitation, only turbidity due to the concentration of material. Supplementation of RPMI-1640 and DMEM with FBS resulted in fold increases of 1.5 and 1.2 respectively with regard to polystyrene 5. Both zinc oxide and titanium dioxide suspended at a concentration of 1 mg/ml formed a visible precipitate once introduced to RPMI-1640 and DMEM, both with and without supplementation with FBS, prior to measurement. This loss of colloidal stability has resulted in their respective hydrodynamic diameters no longer being nanoscale.

Nanoparticle peak mean intensity sizes were found not to be influenced by the presence of large aggregates, as evidenced by the sizes of silicas 2 and 3 being a half and a third of their equivalent Z-average sizes in deionised water (Table 2.6). Nanoparticle sizes by this measure were observed not to succumb to the skew imparted by an additional distribution resultant from protein supplementation. Henceforth, nanoparticle sizes will be displayed by this measurement unless stated otherwise.

Overall, nanoparticle suspensions in FBS-supplemented media demonstrated smaller size than those in unsupplemented media. The presence of protein could have provided some stabilising effect on the colloidal suspensions, protecting them from aggregation due to the salt content of culture media.

A zeta potential of greater than ±30 mV is a hallmark of colloidal stability (Larsson et al., 2012). All of the materials when suspended in culture media supplemented with FBS displayed zeta potentials which are indicative of instability and high likelihood of flocculation (Table 2.8). The presence of protein resulted in all materials, with the exception of JGC, irrespective of their polarity in deionised water, demonstrating negative zeta potentials.

Material	Expected value	Deionised water	RPMI-1640	RPMI-1640 10% FBS	DMEM	DMEM 10% FBS
Polystyrene 1	180	198.47	6157.00	526.90	5574.67	330.80
Polystyrene 2	180	230.83	184.77	234.60	324.33	187.77
Polystyrene 3	275	281.73	9021.67	678.27	6329.67	450.27
Polystyrene 4	300	402.53	319.10	392.03	274.63	315.43
Polystyrene 5	440	439.77	4931.00	667.77	3137.67	538.47
Polystyrene 6	440	440.80	387.30	449.80	319.10	322.97
Gold 1	10	143.36	810.60	87.66	553.33	37.85
Gold 2	11	45.77	64.55	29.98	83.99	99.01
Silver 1	1-10	64.64	199.87	104.57	313.53	67.78
Silver 2	20	126.13	80.98	192.17	413.50	88.46
Endorem	160	138.50	116.60	102.70	82.57	75.13
Ferumoxytol	30	70.55	54.54	29.43	72.44	72.89
JGC	6.9/52.3	131.97	47.91	26.46	27.86	27.19
Titanium (IV) oxide	21	1457.00	3718.67	2193.67	2117.00	263.03
Zinc oxide 1	35/100	117.69	19853.33	1906.33	9640.33	251.30
Zinc oxide 2	50	4964.00	3943.00	7768.67	1891.33	844.97
Zinc oxide 3	100	1483.00	1913.33	2035.67	1510.67	1659.00
Silica 1	50	101.56	657.87	67.35	108.61	84.75
Silica 2	310	1105.07	2530.33	279.67	682.03	89.29
Silica 3	100	3494.33	3564.67	870.17	2080.33	483.77
Liposome	174	175.70	154.63	159.93	127.67	115.60
Emulsion	345.73	370.70	301.13	282.27	251.80	213.33

Table 2.5: Nanoparticle Z-average intensity weighted mean hydrodynamic size (nm) determined via dynamic light scattering in deionized water, RPMI-1640, RPMI-1640 supplemented with FBS to 10% final volume, DMEM, and DMEM supplemented with FBS to 10% final volume. Expected values include size/hydrodynamic size where available.

Material	Expected value	Deionised water	RPMI-1640	RPMI-1640 10% FBS	DMEM	DMEM 10% FBS
Polystyrene 1	180	208.10	892.67	1169.93	5258.00	358.47
Polystyrene 2	180	244.23	199.37	261.13	406.33	211.07
Polystyrene 3	275	298.40	153.82	926.93	5489.67	568.43
Polystyrene 4	300	475.17	353.33	453.47	302.93	354.47
Polystyrene 5	440	464.30	4683.00	802.50	3405.67	643.23
Polystyrene 6	440	490.47	418.57	497.97	352.63	354.23
Gold 1	10	20.26	821.23	31.99	662.37	25.69
Gold 2	11	19.87	18.15	16.71	14.48	13.90
Silver 1	1-10	120.90	308.70	142.73	440.77	93.41
Silver 2	20	166.33	120.57	368.33	486.83	178.17
Endorem	160	175.17	176.13	163.70	112.33	110.73
Ferumoxytol	30	173.43	32.51	33.27	20.34	20.09
JGC	6.9/52.3	191.23	55.85	38.42	36.01	36.70
Titanium (IV) oxide	21	1656.33	3318.33	2132.67	2197.67	329.27
Zinc oxide 1	35/100	79.09	0.59	489.33	693.16	406.00
Zinc oxide 2	50	2754.00	302.93	611.67	1918.67	1369.00
Zinc oxide 3	100	1529.00	1599.33	2176.33	1673.33	1796.67
Silica 1	50	67.55	756.60	130.80	66.51	58.68
Silica 2	310	521.10	274.80	400.63	342.87	322.33
Silica 3	100	1160.07	646.20	1062.60	1012.87	691.70
Liposome	174	189.77	169.80	179.27	139.50	134.50
Emulsion	345.73	421.07	335.67	344.20	287.50	244.30

Table 2.6: Nanoparticle peak mean intensity size (nm) determined via dynamic light scattering in deionized water , RPMI-1640, RPMI-1640 supplemented with FBS to 10% final volume, DMEM, and DMEM supplemented with FBS to 10% final volume. Expected values include size/hydrodynamic size where available.

Material	Expected value	Deionised water	RPMI-1640	RPMI-1640 10% FBS	DMEM	DMEM 10% FBS
Polystyrene 1	N/A	0.03	0.46	0.46	0.28	0.34
Polystyrene 2	N/A	0.14	0.07	0.10	0.39	0.16
Polystyrene 3	N/A	0.04	0.47	0.27	0.25	0.22
Polystyrene 4	N/A	0.15	0.09	0.15	0.12	0.21
Polystyrene 5	N/A	0.04	0.23	0.19	0.15	0.23
Polystyrene 6	N/A	0.10	0.13	0.16	0.09	0.08
Gold 1	N/A	0.25	0.39	0.43	0.40	0.72
Gold 2	N/A	0.30	0.18	0.28	0.33	0.60
Silver 1	N/A	0.49	0.41	0.26	0.39	0.30
Silver 2	N/A	0.52	0.42	0.74	0.36	0.61
Endorem	N/A	0.44	0.42	0.41	0.32	0.42
Ferumoxytol	N/A	0.43	0.36	0.58	0.39	0.24
JGC	0.28	0.29	0.27	0.36	0.25	0.50
Titanium (IV) oxide	N/A	0.09	0.72	0.42	0.35	0.24
Zinc oxide 1	N/A	0.38	1.00	0.93	0.55	0.56
Zinc oxide 2	N/A	0.32	0.58	1.00	0.40	0.63
Zinc oxide 3	N/A	0.30	0.54	0.19	0.28	0.34
Silica 1	N/A	0.55	0.50	0.59	0.30	0.57
Silica 2	N/A	0.65	1.00	0.46	0.69	0.45
Silica 3	N/A	0.68	0.78	0.87	0.82	0.78
Liposome	N/A	0.07	0.09	0.11	0.08	0.14
Emulsion	0.14	0.26	0.25	0.23	0.20	0.26

Table 2.7: Nanoparticle polydispersity index (PdI) determined via dynamic light scattering in deionized water, RPMI-1640, RPMI-1640 supplemented with FBS to 10% final volume, DMEM, and DMEM supplemented with FBS to 10% final volume.

Material	Expected value	Deionised water	RPMI-1640	RPMI-1640 10% FBS	DMEM	DMEM 10% FBS
Polystyrene 1	52.2	52.07	23.60	-9.99	6.55	-10.82
Polystyrene 2	-40.9	-21.63	-49.53	-7.02	-45.70	-12.90
Polystyrene 3	42.2	45.57	22.30	-8.47	7.85	-11.71
Polystyrene 4	-37.2	-42.27	-46.83	-7.93	-52.23	-12.15
Polystyrene 5	39.2	40.33	20.50	-7.97	13.00	-11.02
Polystyrene 6	-34.9	-35.73	-50.67	-6.51	-33.10	-9.00
Gold 1	N/A	-19.70	-26.03	-10.97	-20.30	-10.57
Gold 2	N/A	-4.00	-4.72	-12.40	-4.49	-6.31
Silver 1	-39	-45.73	-48.43	-16.27	-47.17	-14.93
Silver 2	N/A	-42.53	-19.33	-11.39	-30.33	-9.65
Endorem	-6.8	-22.87	-4.30	-4.40	-4.96	-3.54
Ferumoxytol	-30.55	-10.98	-5.24	-10.80	-9.83	-16.50
JGC	20.2	40.13	8.05	3.78	7.01	1.77
Titanium (IV) oxide	N/A	15.33	-9.76	-8.15	-6.32	-14.43
Zinc oxide 1	N/A	26.27	-9.97	-9.64	0.21	-13.97
Zinc oxide 2	N/A	16.97	-28.77	-7.04	-12.30	-10.83
Zinc oxide 3	N/A	21.93	-23.53	-5.83	-13.63	-10.00
Silica 1	-34.7	-15.90	-26.40	-8.78	-18.97	-11.77
Silica 2	-37.1	-28.60	-20.00	-8.53	-26.83	-12.57
Silica 3	N/A	-26.10	-21.73	-8.60	-28.20	-8.45
Liposome	N/A	-20.13	-3.78	-2.30	-4.00	-3.55
Emulsion	N/A	-4.55	-6.44	-7.76	-5.94	-10.85

Table 2.8: Nanoparticle zeta potential (mV) determined in deionized water, RPMI-1640, RPMI-1640 supplemented with FBS to 10% final volume, DMEM, and DMEM supplemented with FBS to 10% final volume.

2.3.4 Evaluation of nanomaterial absorption and emission spectra in various matrices

To better visualise any observable trends, the wavelengths of maximal absorption and emission at given concentrations were plotted in relation to the other test materials within individual matrices. It can be seen that generally in both types of culture media, with and without supplementation with FBS, the polystyrene have a highly similar absorption maximum across the three concentrations (Figures 2.3b to e). Similar trends were observed in the maximum emission wavelengths generated in RPMI-1640 (Figure 2.4b), and in both cell culture media containing of FBS (Figures 2.4c, 2.4e).

While the assessment of both maximal absorption and emission generated discrete wavelengths, which have been displayed here, they were however not of sufficiently high intensity with regard to their relative absorbance/fluorescence units to generate cause for concern when considering applying further assays to these nanomaterials.

(a)

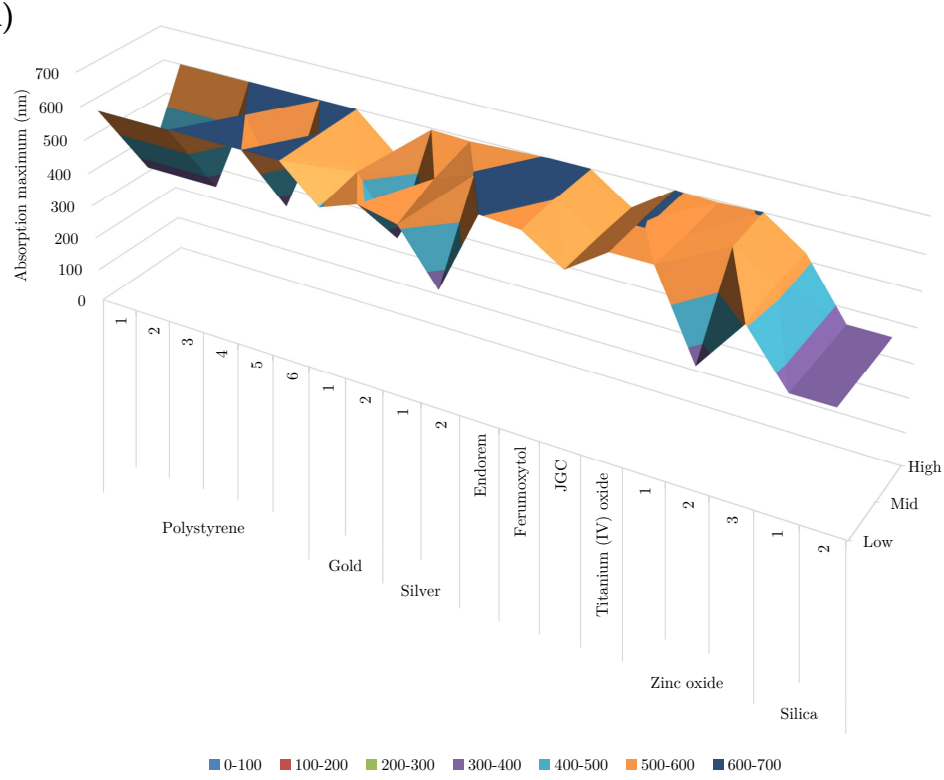

Material	Absorbance maximum (nm) in deionized water		
	Low	Mid	High
Polystyrene 1	601	356	601
Polystyrene 2	601	356	601
Polystyrene 3	601	356	601
Polystyrene 4	601	601	601
Polystyrene 5	601	356	601
Polystyrene 6	601	601	601
Gold 1	496	521	501
Gold 2	536	356	596
Silver 1	511	561	591
Silver 2	356	601	596
Endorem	601	601	601
Ferumoxytol	591	601	601
JGC	516	521	521
Titanium (IV) oxide	596	601	601
Zinc oxide 1	596	591	596
Zinc oxide 2	356	591	601
Zinc oxide 3	506	526	521
Silica 1	356	356	356
Silica 2	356	356	356

(b)

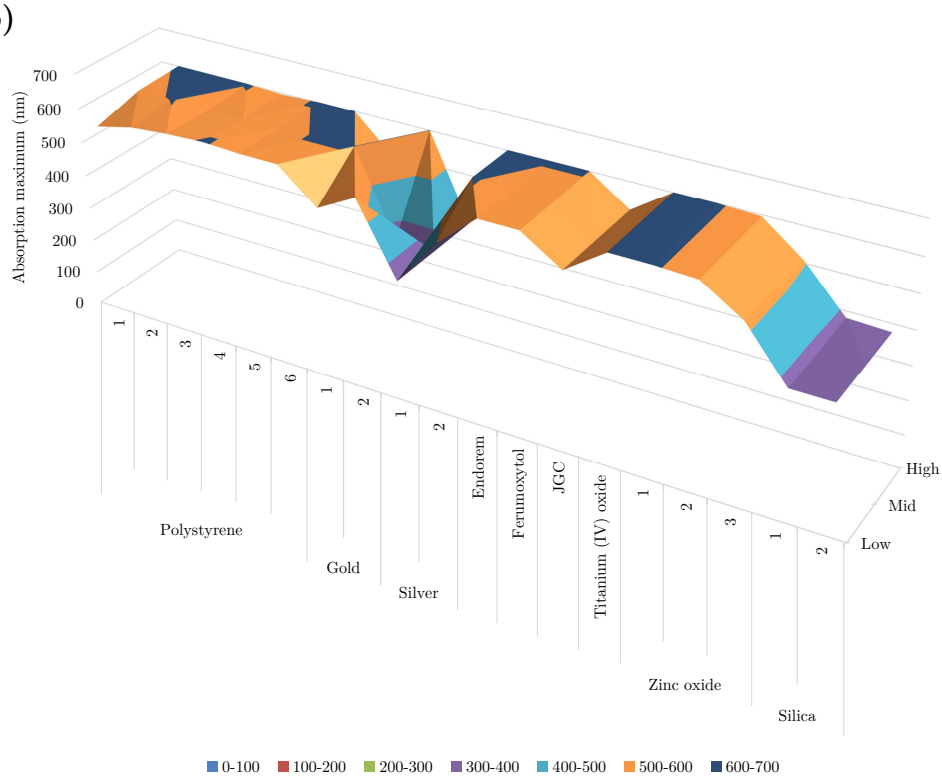

Material	Absorbance maximum (nm) in RPMI-1640		
	Low	Mid	High
Polystyrene 1	561	596	601
Polystyrene 2	586	601	601
Polystyrene 3	596	591	601
Polystyrene 4	601	596	596
Polystyrene 5	596	596	601
Polystyrene 6	596	601	601
Gold 1	501	601	496
Gold 2	561	356	601
Silver 1	356	356	356
Silver 2	496	601	601
Endorem	596	596	601
Ferumoxytol	596	596	601
JGC	521	521	521
Titanium (IV) oxide	601	601	601
Zinc oxide 1	601	601	601
Zinc oxide 2	596	596	596
Zinc oxide 3	521	521	506
Silica 1	376	376	381
Silica 2	376	376	376

(c)

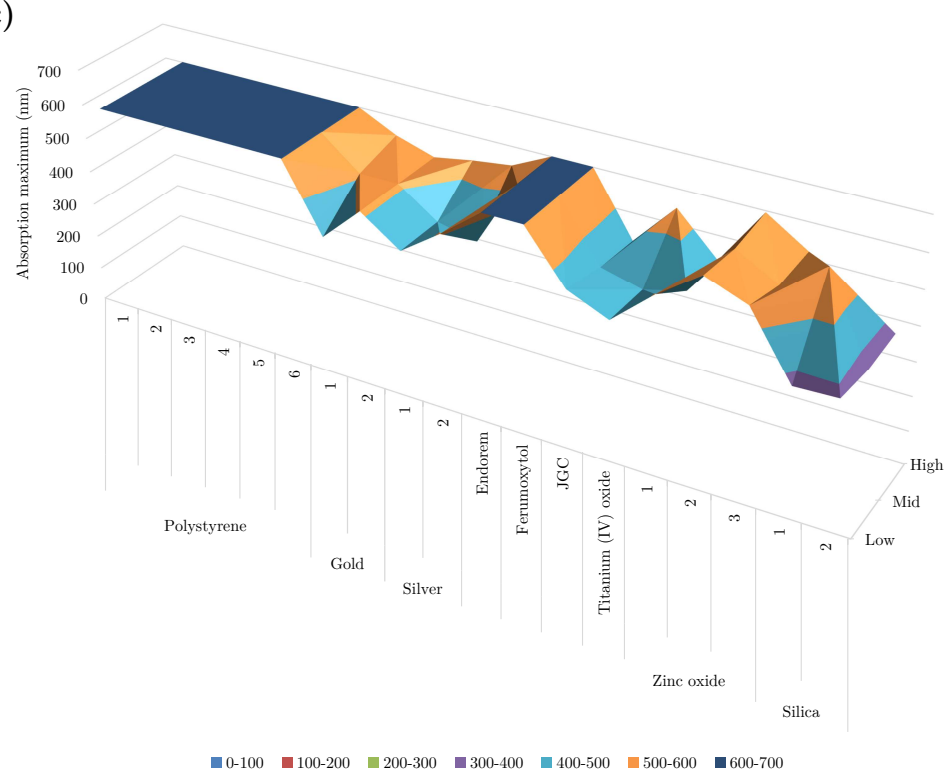

Material	Absorbance maximum (nm) in RPMI-1640 10% FBS		
	Low	Mid	High
Polystyrene 1	601	601	601
Polystyrene 2	601	601	601
Polystyrene 3	601	601	601
Polystyrene 4	601	601	601
Polystyrene 5	601	601	601
Polystyrene 6	601	601	601
Gold 1	406	511	546
Gold 2	511	511	511
Silver 1	431	431	531
Silver 2	511	406	546
Endorem	601	601	601
Ferumoxytol	601	601	601
JGC	456	431	421
Titanium (IV) oxide	406	401	546
Zinc oxide 1	511	431	431
Zinc oxide 2	596	581	596
Zinc oxide 3	551	516	521
Silica 1	371	601	376
Silica 2	376	356	361

(d)

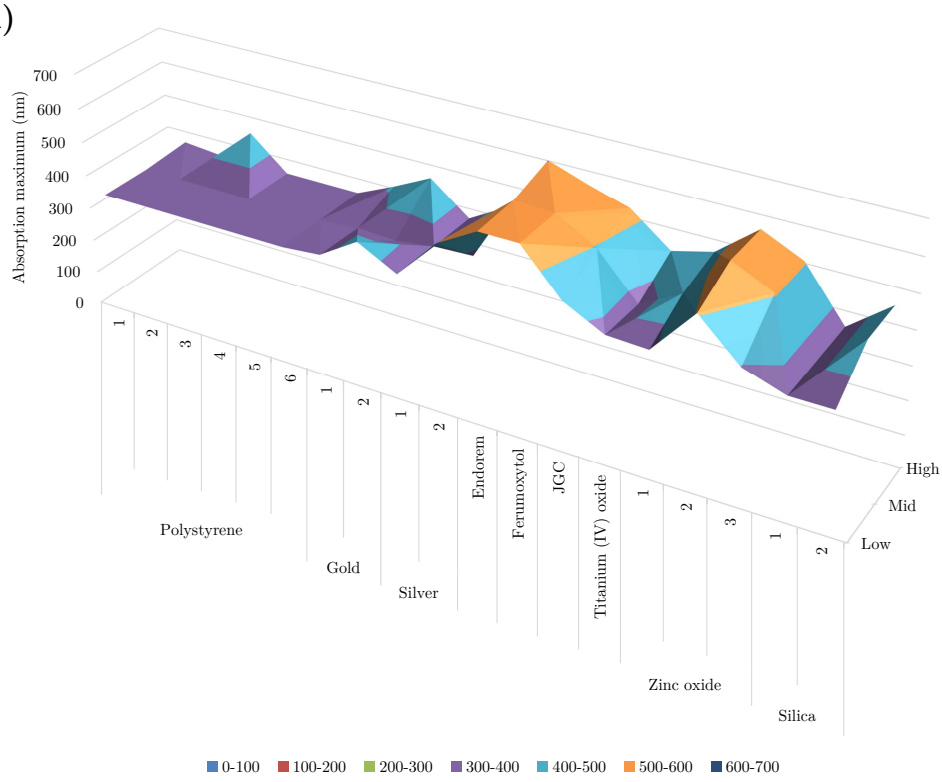

Material	Absorbance maximum (nm) in DMEM		
	Low	Mid	High
Polystyrene 1	356	356	366
Polystyrene 2	356	356	356
Polystyrene 3	356	356	451
Polystyrene 4	356	356	356
Polystyrene 5	356	356	356
Polystyrene 6	356	356	356
Gold 1	366	361	406
Gold 2	436	356	461
Silver 1	376	371	371
Silver 2	496	376	436
Endorem	561	566	601
Ferumoxytol	561	561	561
JGC	436	496	526
Titanium (IV) oxide	376	371	436
Zinc oxide 1	371	436	466
Zinc oxide 2	506	561	561
Zinc oxide 3	396	506	506
Silica 1	356	356	356
Silica 2	356	451	451

(e)

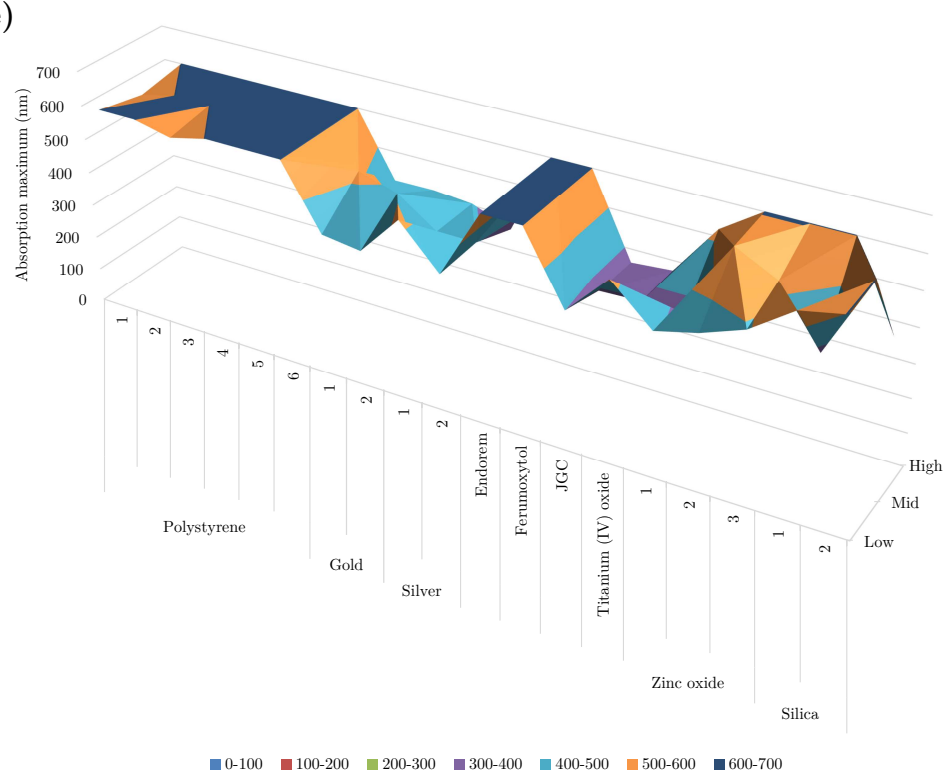

Material	Absorbance maximum (nm) in DMEM 10% FBS		
	Low	Mid	High
Polystyrene 1	601	576	601
Polystyrene 2	601	601	601
Polystyrene 3	576	601	601
Polystyrene 4	601	601	601
Polystyrene 5	601	601	601
Polystyrene 6	601	601	601
Gold 1	416	521	406
Gold 2	401	486	416
Silver 1	521	406	406
Silver 2	401	406	361
Endorem	601	601	601
Ferumoxytol	601	601	601
JGC	401	366	361
Titanium (IV) oxide	521	371	371
Zinc oxide 1	416	371	521
Zinc oxide 2	446	591	601
Zinc oxide 3	491	531	601
Silica 1	576	371	601
Silica 2	601	601	356

Figure 2.3: Graphical representations of maximum absorption wavelengths, and associated wavelengths (nm), of nanomaterials suspended in (a) Deionized water. (b) RPMI-1640. (c) RPMI-1640 supplemented with FBS to 10% final volume. (d) DMEM. (e) DMEM supplemented with FBS to 10% final volume.

(a)

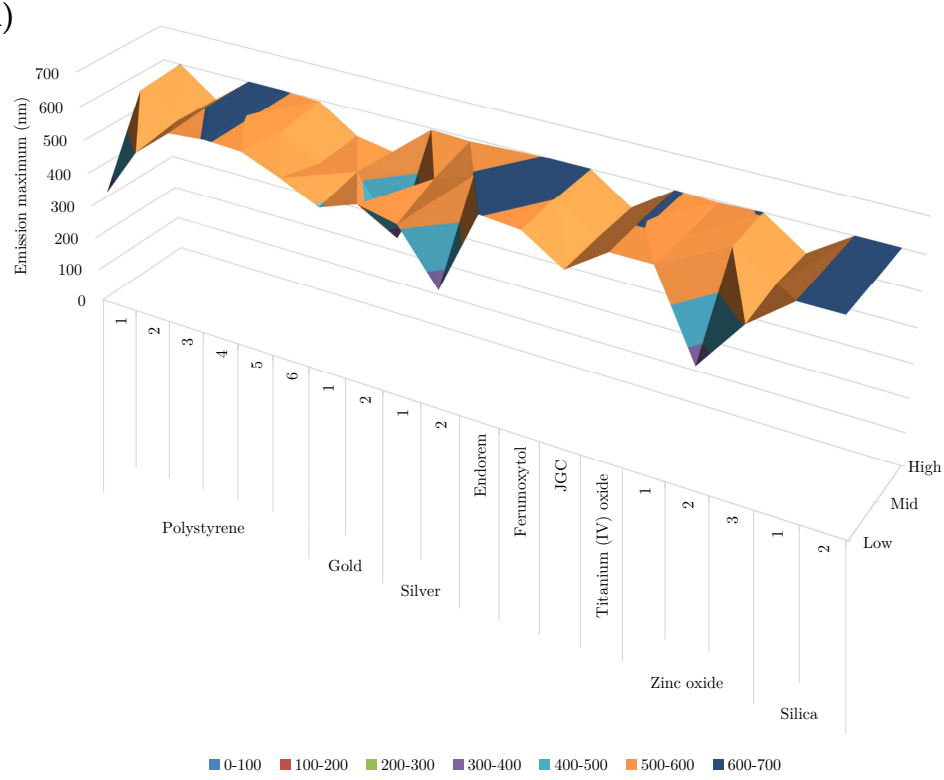

Material	Emission maximum (nm) in deionized water		
	Low	Mid	High
Polystyrene 1	356	591	601
Polystyrene 2	506	526	521
Polystyrene 3	591	601	601
Polystyrene 4	601	601	601
Polystyrene 5	596	581	596
Polystyrene 6	551	516	521
Gold 1	496	521	501
Gold 2	536	356	596
Silver 1	511	561	591
Silver 2	356	601	596
Endorem	601	601	601
Ferumoxytol	591	601	601
JGC	516	521	521
Titanium (IV) oxide	596	601	601
Zinc oxide 1	596	591	596
Zinc oxide 2	356	591	601
Zinc oxide 3	506	526	521
Silica 1	601	601	601
Silica 2	601	601	601

(b)

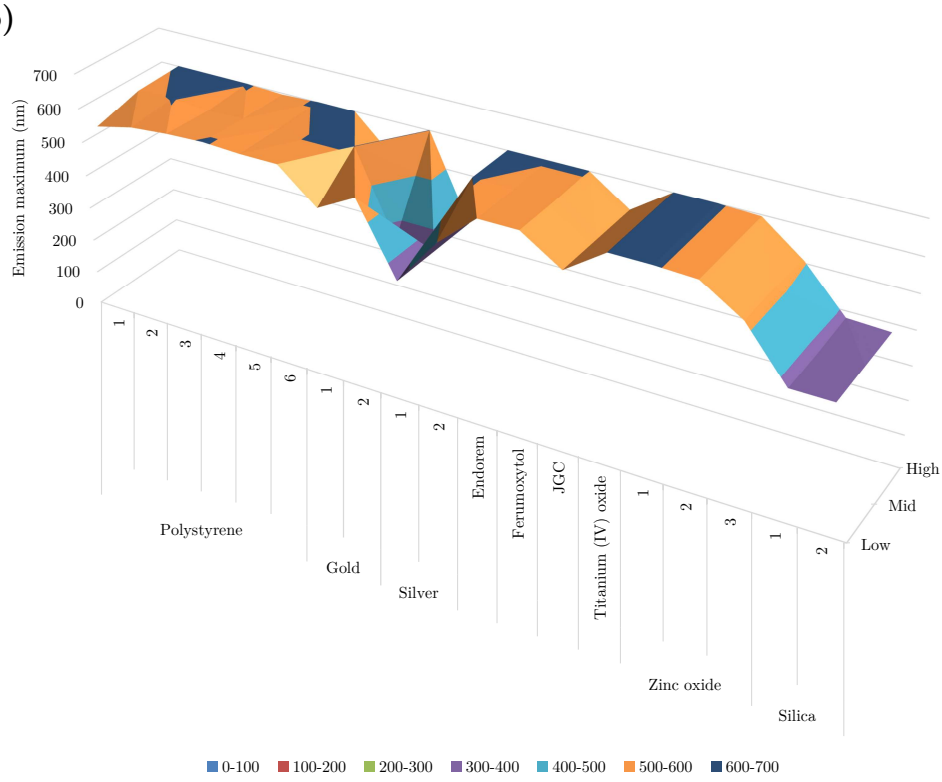

Material	Emission maximum (nm) in RPMI-1640		
	Low	Mid	High
Polystyrene 1	561	596	601
Polystyrene 2	586	601	601
Polystyrene 3	596	591	601
Polystyrene 4	601	596	596
Polystyrene 5	596	596	601
Polystyrene 6	596	601	601
Gold 1	501	601	496
Gold 2	561	356	601
Silver 1	356	356	356
Silver 2	496	601	601
Endorem	596	596	601
Ferumoxytol	596	596	601
JGC	521	521	521
Titanium (IV) oxide	601	601	601
Zinc oxide 1	601	601	601
Zinc oxide 2	596	596	596
Zinc oxide 3	521	521	506
Silica 1	376	376	381
Silica 2	376	376	376

(c)

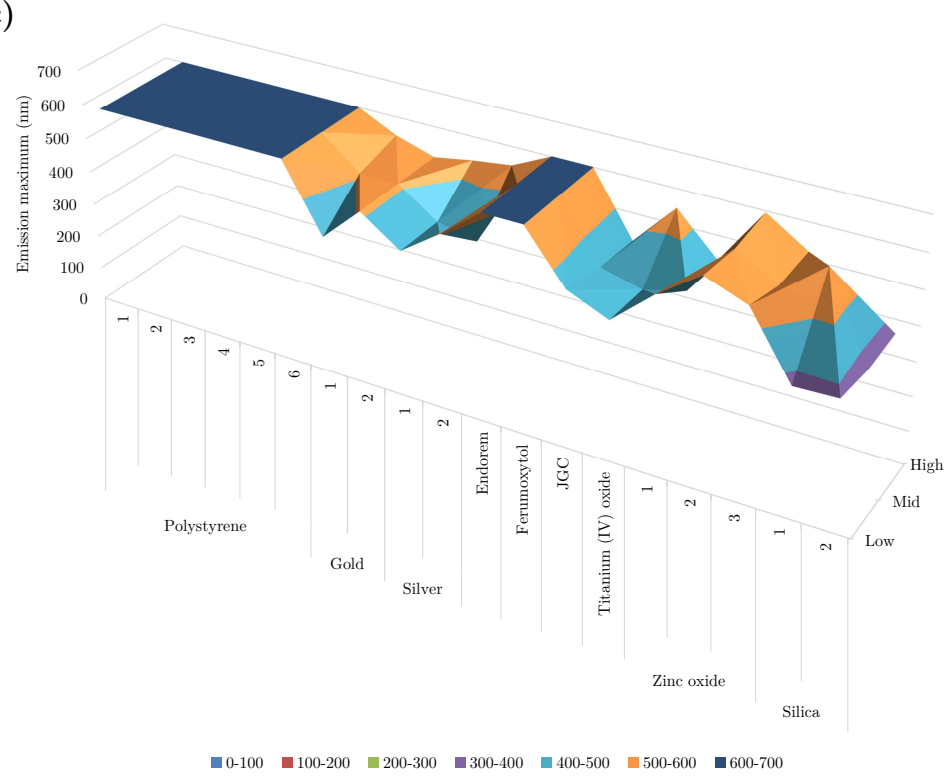

Material	Emission maximum (nm) in RPMI-1640 10% FBS		
	Low	Mid	High
Polystyrene 1	601	601	601
Polystyrene 2	601	601	601
Polystyrene 3	601	601	601
Polystyrene 4	601	601	601
Polystyrene 5	601	601	601
Polystyrene 6	601	601	601
Gold 1	406	511	546
Gold 2	511	511	511
Silver 1	431	431	531
Silver 2	511	406	546
Endorem	601	601	601
Ferumoxytol	601	601	601
JGC	456	431	421
Titanium (IV) oxide	406	401	546
Zinc oxide 1	511	431	431
Zinc oxide 2	596	581	596
Zinc oxide 3	551	516	521
Silica 1	371	601	376
Silica 2	376	356	361

(d)

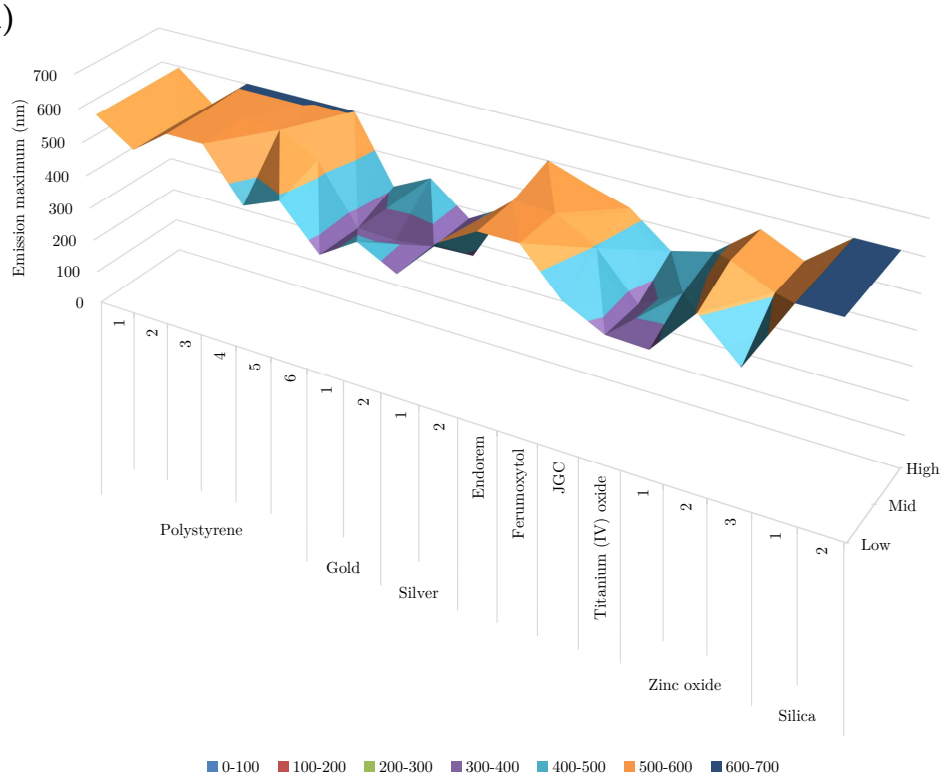

Material	Emission maximum (nm) in DMEM Low	Mid	High
Polystyrene 1	596	596	596
Polystyrene 2	521	521	506
Polystyrene 3	596	596	601
Polystyrene 4	596	596	601
Polystyrene 5	446	591	601
Polystyrene 6	491	531	601
Gold 1	366	361	406
Gold 2	436	356	461
Silver 1	376	371	371
Silver 2	496	376	436
Endorem	561	566	601
Ferumoxytol	561	561	561
JGC	436	496	526
Titanium (IV) oxide	376	371	436
Zinc oxide 1	371	436	466
Zinc oxide 2	506	561	561
Zinc oxide 3	396	506	506
Silica 1	601	601	601
Silica 2	601	601	601

(e)

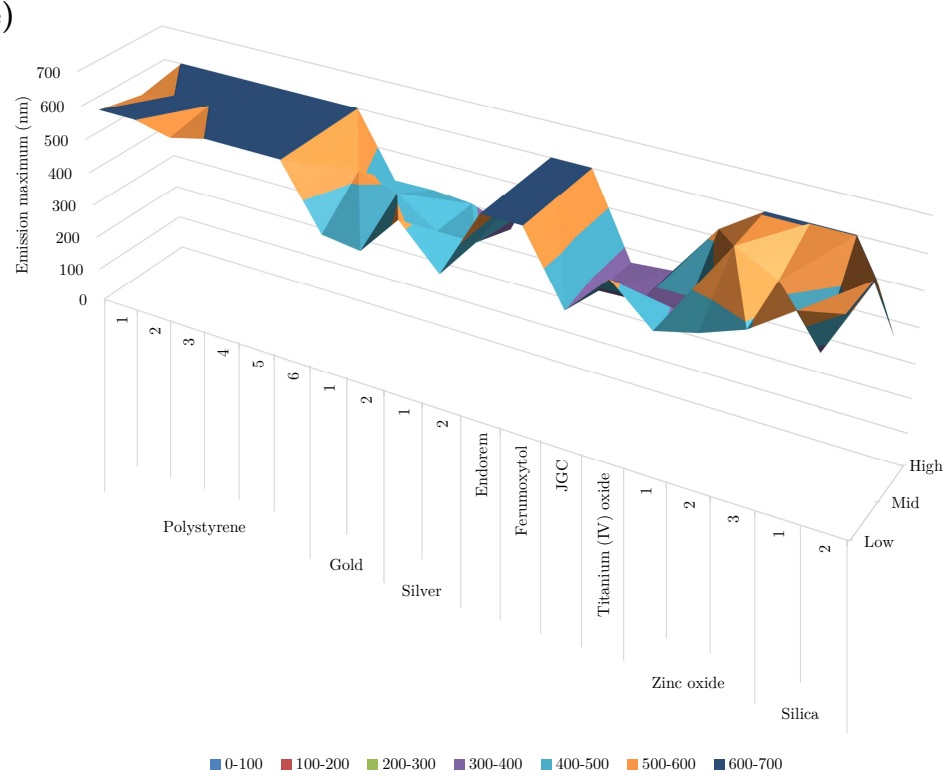

Material	Emission maximum (nm) in DMEM 10% FBS		
	Low	Mid	High
Polystyrene 1	601	576	601
Polystyrene 2	601	601	601
Polystyrene 3	576	601	601
Polystyrene 4	601	601	601
Polystyrene 5	601	601	601
Polystyrene 6	601	601	601
Gold 1	416	521	406
Gold 2	401	486	416
Silver 1	521	406	406
Silver 2	401	406	361
Endorem	601	601	601
Ferumoxytol	601	601	601
JGC	401	366	361
Titanium (IV) oxide	521	371	371
Zinc oxide 1	416	371	521
Zinc oxide 2	446	591	601
Zinc oxide 3	491	531	601
Silica 1	576	371	601
Silica 2	601	601	356

Figure 2.4: Graphical representations of maximum emission wavelengths, and associated wavelengths (nm), of nanomaterials suspended in (a) Deionized water. (b) RPMI-1640. (c) RPMI-1640 supplemented with FBS to 10% final volume. (d) DMEM. (e) DMEM supplemented with FBS to 10% final volume.

2.4 Discussion

Biological contamination is a potential source of false positives in a number of assays examining toxicity and biocompatibility. The materials included in the present study were demonstrated to show no bacterial growth suggesting a lack of viable microbial contamination. However, it is also necessary to confirm the absence of bacterial based contaminants, specifically endotoxin, in the test materials. Presence of such contaminants in nanoparticle preparations could result in the outcomes highlighted in Section 1.6.1.

As has been described previously by others (Yang et al., 2012), some materials demonstrated interference with the ELISA-based assay which was utilised here. This was observed in polystyrenes 2, 3, and 4, gold 2, silver 2, JGC, and silicas 1 and 2 as highlighted in Table 2.4. However, following further dilution, these effects were mitigated thereby providing a reliable determination of endotoxin concentration as evidenced by the spike recovery. A further limitation of this method was the limit of quantification; manufacturer-stated measurement range of 0.05 - 500 EU/ml (Hyglos GmbH, 2017). To complement the results of this assay, and to avoid misleading results due to overlooked interference, the ELISA could be used side by side with another detection method such as a chromogenic LAL-based assay (Neun and Dobrovolskaia, 2011) which does not succumb to the same limitations as the ELISA or gel clot assay mentioned previously. These methodologies were, however, unavailable at the time. The data presented here demonstrates that there are detectable concentrations of endotoxin within some test materials, notably JGC (107.80 EU/ml at a material concentration of 100 µg/ml) and liposome (18.44 EU/ml at a material dilution of 1/10 from stock). This is to be expected as not all commercially available nanomaterials are intended for biological use and are not therefore necessarily guaranteed to be pyrogen free. To ensure that any activation of immune cells that may be observed

in subsequent immunotoxicological assays is not a result of the presence of endotoxin; it is possible to include LPS from *R. sphaeroides*, a potent antagonist of TLR4 signalling, to negate any possible endotoxin effect (InvivoGen, 2007) and therefore ensure effects are nanoparticle dependent.

There are several options for measuring particle sizes (Bootz et al., 2004). The most direct of these are by TEM (Stratton et al., 2013). The crux of this method, and others like it, is that the materials must be fixed in a manner removing them from their intended medium, as well as treated via coating to confer conductivity to the sample surface (Höflinger, 2013). Another limitation is that particles must be measured individually within a frame of limited size, so any measurements are only representative of that population. By utilizing dynamic light scattering over TEM the hydrodynamic diameter of the nanoparticle can be measured. Along with this, a vastly greater number of particles can be assessed simultaneously providing information about the population.

Sizing of nanoparticles in the appropriate buffer is associated to physicochemical characteristics (Sabuncu et al., 2012). The same can be said for measuring the zeta potential as well as optical properties. Data presented in this work has shown that considerable changes arise in the measurable properties of the nanomaterials by suspending nanomaterials in buffer relevant to biological systems, which corresponds to *in vitro* assays performed in subsequent chapters. This is exemplified by nanoparticles such as polystyrene 1, the size of which increased to 1169.93 nm in RPMI-1640 supplemented 10% with FBS compared to its measured size of 208.10 nm in deionised water. ISO 13321:1996 specifies reporting of mean z-average diameter and mean polydispersity index (International Organization for Standardization, 1996). Z-average provides the intensity weighted mean hydrodynamic size but can be skewed by polydispersity caused by aggregates or protein supplementation within a sample (Malvern Instruments Ltd, 2014). Size distribution by intensity overcomes these limitations. This measurement provides

the hydrodynamic diameter of nanoparticles within modes of a multimodal distribution. Using suitable sample preparation the nanoparticles should present the mode of the highest intensity. The size calculated from this, termed "peak mean intensity" in this work, provides the best representation of the nanoparticle size in conditions increasing distribution complexity. For this reason it was found that the peak mean intensity size provided the most accurate representation of the hydrodynamic diameter of the nanomaterials in biologically relevant media. Estimation and extrapolation of properties from values gained in water are evidently not sufficient, and it should always be questioned the method by which the manufacturer stated size was determined. It is possible that alternative methodologies should be included in this type of analysis. Although sensitive to technical limitations including low throughput, extensive optimisation, pore size thresholds which can lead to clogging resultant from heterogeneity in samples (Maas et al., 2015), tunable resistive pulse sensing (TRPS) measurement has been shown to yield additional data for size and charge of nanoparticles and would complement DLS data (Pal et al., 2014). The lower threshold of 40 nm limits the suitability of TRPS to certain size distributions of nanomaterials. Beneficially this renders TRPS insensitive to the presence of protein in media, meaning further undesired distributions are not recorded. Indeed may regulatory agencies now require physicochemical characteristic data using differential techniques to show consistency in measurement (U.S. Food and Drug Administration, 2012b). However, researchers do not necessarily have access to all of these technologies, and their acquisition can be cost limited. The development of alternative, cheaper methodologies is therefore required. Previous work within our group has demonstrated the utility of flow cytometry for the characterisation of changes in nanoparticle size in various matrices as well as simultaneous measurement of protein interaction (Liptrott et al., 2015). Many research groups have access to a flow cytometer, and these techniques may be adapted for use as an additional source of characteri-

sation however this methodology is not a standard in the field and is in its relative infancy for characterisation requiring additional validation, which is ongoing.

Zeta potential has proven to be a highly useful tool to accompany DLS measurements. As mentioned in Section 2.1, there are characteristic magnitudes of charge which provide a guide for the stability of nanoparticle suspensions. Charge stabilization of materials in water is a common practice for metallic nanoparticles e.g. citrate-stabilized gold nanoparticles. This reduces the likelihood of aggregation and allows greater shelf-life of the material. As already known, and further shown here, colloidal stability is not always carried across into more complex buffers. In conjunction with the results of DLS, one gains a greater insight into the reasons behind any buffer related differences in measurements. When the nanoparticles are introduced into a biologically relevant matrix they may undergo changes in their surface chemistry. These changes include, but are not limited to; the adhesion of proteins, ion exchange with the buffer, and salt-induced aggregation.

Zinc oxide and titanium dioxide nanoparticles both displayed low colloidal stability in RPMI-1640 and DMEM, to a point of aggregation and non-viability. This effect has been described regarding titanium dioxide previously (Allouni et al., 2009). This observation is an important one in demonstrating upon introduction to biologically relevant matrices, nanoparticles may no longer remain in the nanoscale. This is crucial when attempting to build quantitative structure-activity relationship (QSAR) models, incorporating physicochemical characteristic data as relationships may not be valid without robust physicochemical characterisation. Furthermore, when considering biological outcomes it would be questionable whether associating properties linked to the nanoscale are valid when aggregates are micro-sized.

The optical properties which some nanoparticles exhibit at the nanoscale are something which tends to be exploited for novel uses. This intrinsic property

creates difficulties when combined with fluorescent molecules in biological assays. Interference can occur if the nanoparticle absorbs or emits at a corresponding wavelength to what is being used to excite or detect the fluorophore (Gonzales et al., 2010).

Particular materials such as gold and iron oxide have characteristic spectral regions at which they have a surface plasmon resonance or absorption peak. This, however, is not always the point of highest absorption across the entire spectrum. In the case of gold nanoparticles, the surface plasmon peak wavelength is in the region of 520 nm (Link and El-Sayed, 1999), the intensity of which directly relates to the concentration of material present. What our assessment has determined is that the absorption maximum at 300 nm in deionised water is minimally affected by material concentration. The convention in biological sciences when presenting absorption spectra of plasmonic nanomaterials is to focus and display data roughly ±100 nm of the plasmon peak. This narrow window does not necessarily provide a true representation of the material's optical properties. Publications focussed toward chemistry and engineering, however, do display spectral data across a wider range and support the observations described here (Amendola and Meneghetti, 2009; Uppal et al., 2010). It can be argued that this style of generating and presenting data should be adopted in biological sciences to provide more complete insight from which better informed conclusions can be drawn.

Similar concentration independent effects were seen in other materials like polystyrene, which do not have a particular maximal absorption wavelength, they absorb across the entire spectrum with only minor fluctuations. If this general absorption is relatively low, then interference, for this reason, can be minimal. Any interference observed can then be attributed to other factors such as turbidity.

The buffer in which the materials are suspended can affect their absorption spectrum. Components of more complex buffers can physically influence the material as mentioned earlier regarding their size and charge. Particular buffers

can have inherent regions of higher absorption which can then be exacerbate those of nanomaterials. Vetten et al. highlights this effect in the case of gold nanoparticles suspended in culture media. The work attributes absorbance peak broadening to the composition and refractive index of the medium (Vetten et al., 2013). Blank correction of these samples, where the medium itself is treated as a baseline, can somewhat alleviate the additive effect, but it is far from a perfect solution, and may reduce the sensitivity of the assay. For this to be a complete solution, the combined absorption of the material and buffer must be additive. As this is not always the case, a compromise must be made, and that blank correction should be applied but not relied on to provide a perfect result. Direct interference controls offer some solution to this, where nanoparticle-containing preparations in the absence of cells are assessed in tandem to the cell-based assay (Petersen, 2015). Further to this, the use of inhibition/enhancement controls provide a means by which these effects may be further visualised. The addition of nanomaterials to a treatment generating a known response would confirm observations from direct interference controls, or reveal assay interference generated following biological processes such as binding of assay targets to the nanoparticle surface.

The work outlined in this chapter has demonstrated that we have been able to determine successfully the levels, or absence, of endotoxin in the materials chosen for analysis, alongside an assessment of microbial contamination. The optical properties of the nanomaterials have been assessed. In doing so, the likelihood of optical interference with assays has been evaluated and has been shown to be minimal. This is a result of there being either no overlap in wavelengths or that the absorption or emission at interfering wavelengths being of low intensity to have little effect.

Chapter 3

Investigating the association between nanoparticle characteristics and blood compatibility

Contents

3.1 Introduction 91

3.2 Methods 96

3.2.1 Materials 96

3.2.2 Plasma coagulation 96

3.2.2.1 Blood collection 96

3.2.2.2 Experimental protocol 96

3.2.3 Haemolysis 99

3.2.3.1 Blood collection 99

3.2.3.2 Determining plasma free haemoglobin 99

3.2.3.3 Calculations 99

3.2.3.4 Experimental procedure 100

3.2.4 Complement activation 101

3.2.4.1 Blood collection 101

3.2.4.2 Experimental procedure 101

3.2.4.3 Calculations 102

3.2.5 Statistical analysis 103

3.3 Results 104

3.3.1 Plasma coagulation 104

3.3.2 Haemolysis 107

3.3.3 Complement activation 110

3.4 Discussion 112

3.1 Introduction

The intended administration route dictates the design of nanoparticle drug carriers (Yildirimer et al., 2011). Nanomedicines administered intravenously come into direct and immediate contact with the blood. As discussed in Section 1.4, evaluation of haemocompatibility, therefore, is vital in the preclinical assessment of nanomedicines (Ilinskaya and Dobrovolskaia, 2013).

Coagulation is critical in haemostasis and is subdivided into three main pathways; intrinsic, extrinsic, and the common pathway. The extrinsic coagulation pathway is initiated through vascular injury which exposes of tissue factor (TF, also identified as factor III) to plasma coagulants, Factor VII, and calcium, promoting conversion of Factor X to Xa (Owens and Mackman, 2010). Tissue factor, a cell-surface glycoprotein, is expressed in the subendothelial tissue (Lasne et al., 2006). However, expression may be induced in monocytes and endothelial cells following injury or pathological stimuli (Rao and Pendurthi, 2012). Activation of the intrinsic cascade is initiated by binding of Factor XII to anionic or hydrophilic surfaces (Vogler and Siedlecki, 2009) such as cellular RNA and polyphosphates released through necrosis, and endotoxin (Esmon et al., 2011). The common pathway is ubiquitous through stimulation of either the extrinsic or intrinsic pathways (Troy, 1988). Thrombin, through enzymatic cleavage by Factor Xa (Krishnaswamy, 2013), converts circulating fibrinogen to fibrin monomer, induces morphological changes in platelets, and mobilises platelet aggregation mediators (Coughlin, 2000).

Each pathway utilises numerous coagulation factors, some of which display commonality between pathways. The intrinsic pathway is assessed using the activated partial thromboplastin time (APTT) assay, and looks at coagulation factors XII, XI, IX, VIII, X, V, and II (prothrombin). Prothrombin time (PT) is used to measure coagulation time via the extrinsic pathway which involves

factors VII, X, V and II. Lastly thrombin time (TT) is used to assess the common pathway. Each of these tests measure the generation time of fibrin following the activation of the coagulation cascade at specific points, via the conversion of coagulation factors from their zymogen to active forms, as can be seen in Figure 3.1.

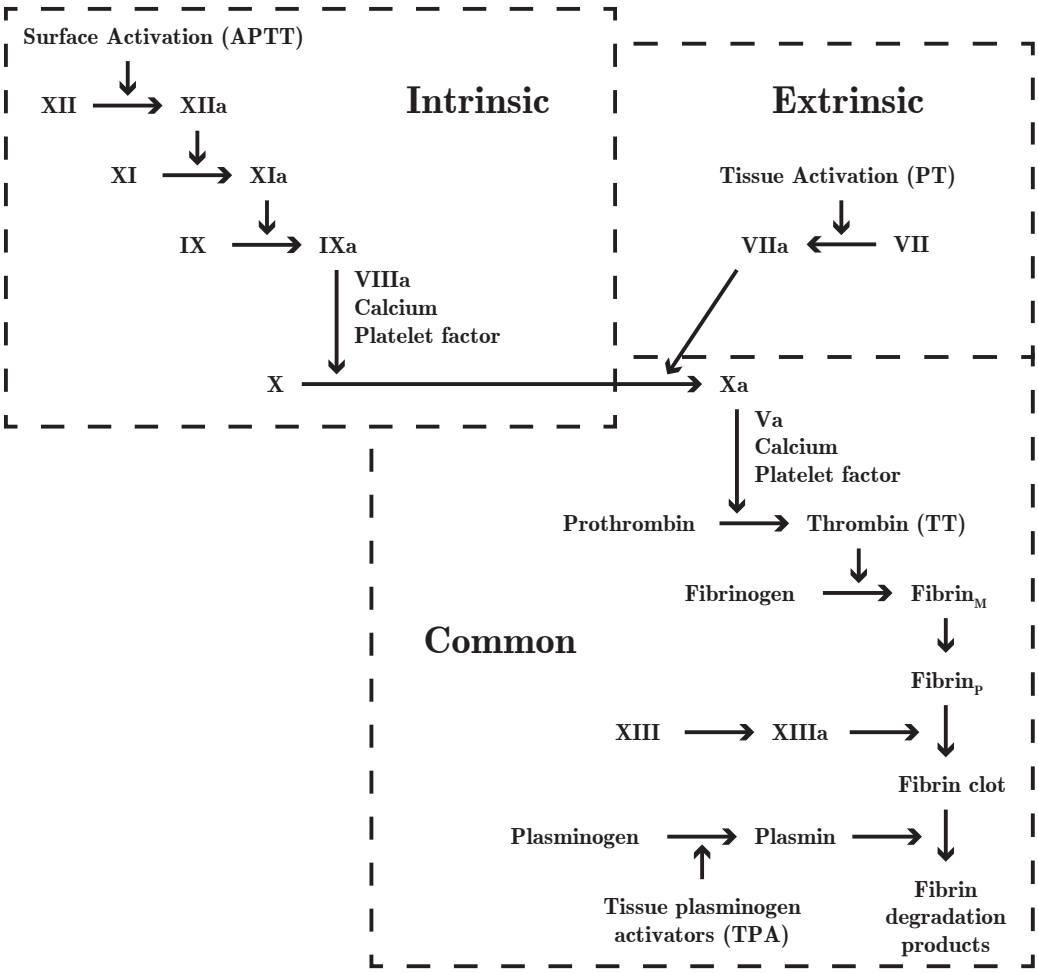

Figure 3.1: Pathways comprising the blood coagulation cascade. Factors displayed; XII - Hageman factor, XI - plasma thromboplastin, IX - Christmas factor, X - Stuart-Prower factor, VII - stable factor, II - prothrombin, XIII - fibrin stabilising factor. Lower-case a denotes active form, Fibrin_M and Fibrin_P represent fibrin monomer and fibrin polymer respectively. Adapted from "Coagulation Tests," by M. N. Raber, in H. K. Walker, W. D. Hall, J. W. Hurst (Eds.), *Clinical Methods: The History, Physical, and Laboratory Examinations* (3rd edition, p. 740), 1990, Boston, MA: Butterworths. Copyright 1990 by Elsevier. Adapted with permission.

Erythrocytes have a haematocrit (blood volume percentage) of 42-47% under

normal conditions. When damaged, they release their intracellular content to the plasma; termed haemolysis. Haptoglobin, a plasma protein, binds the released haemoglobin for removal via the reticuloendothelial system. If this release of haemoglobin is on a larger scale, as a result of a haemolytic anaemia, the effects can be detrimental to the individual displaying this pathology. Fragmentation haemolysis, a form of mechanical destruction of red blood cells, is know to occur via the action of drugs under normal dosing strategies, termed drug-induced thrombotic microangiopathy (DITMA) (Al-Nouri et al., 2015). Haemoglobin is toxic and may affect vascular, myocardial, renal and central nervous system tissues. Concentrations of free haemoglobin greater than 100 nM can result in deleterious effects (Tracz et al., 2007) via oxidative damage under acute exposure, or chronic pathologies affecting vascular, hepatic, splenic, and renal systems (Schaer et al., 2013). For these reasons it is necessary for all medical devices and drugs which come in contact with blood to be tested for potential haemolytic properties (Desai and Lister, 2011).

As mentioned in Section 1.5.2, the complement system is comprised of a number of plasma proteases and cell surface components. Cleavage of the zymogen protease precursors initiate activation of this multicomponent system, whose functions within innate immunity include directing immune responses, pathogen recognition, and involvement in homeostasis (Dunkelberger and Song, 2010). Being a vital *in vivo* system, involvement of the complement system in the biological interactions of nanomaterials is a consideration which cannot be overlooked (Boraschi et al., 2012). The physicochemical characteristics of nanoparticles can share likeness with those of pathogenic microorganisms, including size, charge, and surface modifications (Moghimi et al., 2015). Polymers such as PEG have been exploited for nanoparticle surface functionalization due to their ability to create a steric barrier which reduces the ability of proteins to bind the surface and subsequently reducing complement activation and macrophage uptake (Vonar-

bourg et al., 2006). While some of these properties have been applied in the design of nanoparticles to evade rapid clearance by macrophages, they do not offer a complete solution to overcoming innate immune recognition, and the potential for adverse effects. The formation of anti-PEG antibodies has been shown to occur in healthy volunteers (Garay et al., 2012), where PEG has been shown to behave as a hapten to elicit this response (Ishida and Kiwada, 2013). A small number of studies have shown this to result in enhanced clearance (Ishida and Kiwada, 2013), further reducing nanoparticle circulation time through complement activation (Dams et al., 2000; Ishida et al., 2003).

Binding of complement factors to the surface of nanoparticles can mark them for recognition and clearance by monocytes and macrophages (Peter and Moghimi, 2012). Activation of complement by nanomaterials can also induce adverse reactions (Peter and Moghimi, 2012). Doxil, doxorubicin-containing PEGylated liposomes, have been reported to generate hypersensitivity reactions (Szebeni et al., 2011). Evidence suggests that this effect is mediated by complement activation (Chanan-Khan et al., 2003).

The link between complement activation and platelet activation with regard to pro-coagulant activity (Andersen et al., 2009), as well as complement mediated red blood cell destruction (Suankratay et al., 1999; Freedman, 1987) have been previously documented. The latter has shown involvement in the pathology of subtypes of autoimmune haemolytic anaemia (AIHA) (Berentsen, 2015). Coating of the red blood cell with antibodies IgG1, IgG3 or IgM, can activate complement leading to insertion of complexes C5, 6, 7, 8 and 9 into the cell membrane which disturb osmotic balance resulting in intravascular haemolysis (Garratty, 2008). Extravascular haemolysis occurs through interaction of hepatic and splenic macrophages with C3b/iC3b coated red blood cells (Garratty, 2008).

The aim of this chapter was to observe effects of treatment with nanomaterials outlined in Table 2.1 on plasma coagulation, as well as the potential haemolytic

activity, and influence on complement activation by selected materials.

3.2 Methods

3.2.1 Materials

Sodium citrate, lithium heparin, and K2EDTA coated Vacuettes were purchased from VWR (Pennsylvania, USA). Neoplastine Cl, thrombin, $CaCl_2$ (0.025 M), Owren-Koller buffer, PTTA, CoagControl N+ABN, metal balls, and cuvettes were purchased from Diagnostica Stago (Reading, UK). Haemoglobin Reagent Set was purchased from Teco Diagnostics (California, USA). Dulbecco's phosphate-buffered saline (DPBS), Triton X-100 were purchased from Sigma-Aldrich (Dorset, UK). The MicroVue iC3b EIA was purchased from Quidel (California, USA), and cobra venom factor was purchased from Quidel (Ohio, USA).

Approval for the sampling and storage of human blood samples for biomedical research was gained from the University of Liverpool Committee in Research Ethics (Ref: RETH000563).

3.2.2 Plasma coagulation

3.2.2.1 Blood collection

Blood from healthy volunteers was obtained by venipuncture (3 volunteers) into vacutainers anticoagulated with sodium citrate and used within 30 minutes of being drawn.

3.2.2.2 Experimental protocol

Whole blood was centrifuged for 10 minutes at 2500 × g at room temperature. Plasma inspected for haemolysis, collected, and pooled. Nanomaterials were added to microcentrifuge tubes at sufficient volume to provide final treated concentrations displayed in Table 3.1. Concentrations were chosen in order to

assess the effect of greatest material concentration and carrier, consistent with assays throughout the thesis. Pooled plasma was added to achieve total volumes of 1 ml. Treatments were incubated for 30 minutes at 37°C. During this time; normal and abnormal control plasmas, neoplastine, PTTA reagent, and thrombin were reconstituted in deionized water as indicated on the product packaging, and allowed to stand at room temperature for 30 minutes prior to use. The Merlin MC4 plus coagulometer (ABW Medizin und Technik GmbH, Lemgo, Germany) was turned on 15 minutes prior to use to allow the heating block to reach 37°C. Reagents were transferred to test tubes and placed in the heating block of the coagulometer prior to use. Cuvettes were loaded in the test rows of the coagulometer, a metal ball was placed inside each, and allowed to warm for three minutes.

Specific details of the PT, APTT, and TT assays are outlined below.

As per the protocol established by the NCI-NCL for the analysis of nanoparticle effects on plasma coagulation times *in vitro* (Neun et al., 2015b); samples were run in duplicate, and following coagulation of samples, the time and coefficient of variation (%CV) were recorded. The acceptance criteria for samples was a %CV below 5%. For values greater than this, samples were re-analysed.

Prothrombin time

100 µl of plasma (normal control, abnormal control, untreated, and nanomaterial treated) was added to the cuvette and incubated for 120 seconds. 100 µl of neoplastine (ISI ~ 1.7) was added to trigger coagulation.

Activated partial thromboplastin time

50 µl of plasma (normal control, abnormal control, untreated, and nanomaterial treated), and 50 µl of PTTA reagent were added to the cuvette and incubated for 180 seconds. 50 µl of $CaCl_2$ (0.025 M) was added to trigger coagulation.

Material	Final concentraion/dilution
Polystyrene 1	100 µg/ml
Polystyrene 2	100 µg/ml
Polystyrene 3	100 µg/ml
Polystyrene 4	100 µg/ml
Polystyrene 5	100 µg/ml
Polystyrene 6	100 µg/ml
Gold 1	500 pg/ml
Gold 2	500 pg/ml
Silver 1	100 µg/ml
Silver 2	5 µg/ml
Endorem	100 µg/ml
Ferumoxytol	100 µg/ml
JGC	100 µg/ml
Titanium (IV) oxide	100 µg/ml
Zinc 1	100 µg/ml
Zinc 2	100 µg/ml
Zinc 3	100 µg/ml
Silica 1	100 µg/ml
Silica 2	100 µg/ml
Silica 3	100 µg/ml
Liposome	1/20
Emulsion	1/20

Table 3.1: Final concentrations/dilution factors of nanomaterials used to assess effects on plasma coagulation.

Thrombin time

100 µl of plasma (normal control, abnormal control, untreated, and nanomaterial treated) was added to the cuvette and incubated for 60 seconds. 100 µl of thrombin (1.5 NIH units/ml) was added to trigger coagulation.

3.2.3 Haemolysis

3.2.3.1 Blood collection

Healthy volunteer blood was obtained by venipuncture (3 volunteers) into vacutainers anticoagulated with lithium heparin. The first 10 ml from each donor was discarded to minimise the level of haemolysis in collected samples generated by veinal trauma from puncture (Bush, 2003).

3.2.3.2 Determining plasma free haemoglobin

3 ml of blood from each volunteer was centrifuged at 800 × g for 15 minutes. The plasma was collected and stored at room temperature while 2 ml of haemoglobin reagent was dispensed into microcentrifuge tubes corresponding to "blank" and each volunteer. 10 µl of plasma was added to respective tubes, and incubated at room temperature for 3 minutes. 200 µl of blank and volunteer samples were transferred to a 96 well plate in quadruplicate. 200 µl of methemoglobin standard was added to the plate in triplicate and the absorbance of all samples was measured at 540 nm using a CLARIOstar plate reader (BMG Labtech). The absorbance values were then converted to haemoglobin concentration using the calculation shown in Section 3.2.3.3. Remaining blood from volunteers was diluted to a plasma free haemoglobin concentration of 10 g/dl using DPBS.

3.2.3.3 Calculations

As outlined in the manufacturer's protocol, the calculation used to determine haemoglobin presence is as follows;

$$\frac{\text{Abs. of unknown}}{\text{Abs. of standard}} \times \text{Conc. of standard (g/dl)} = \text{Value (g/dl)}$$

The 60 mg/dl methemoglobin standard produces an absorption equivalent to that of 15 mg/ml of haemoglobin.

3.2.3.4 Experimental procedure

Nanoparticles were prepared at eight times final concentration displayed in Table 3.2 in DPBS. 792 µl of diluted blood from each volunteer was transferred to microcentrifuge tubes in replicates corresponding to negative control, nanomaterial treated, positive control, and inhibition/enhancement controls. To the negative control 8 µl of DPBS was added, 8 µl of eight times concentrated nanomaterials were added to nanomaterial treated, and 8 µl of 1% triton X-100 was added to positive control and designated inhibition/enhancement control wells. Incubation was performed at 37°C for 3 hours and samples were mixed every 30 minutes throughout the duration. Following incubation, 8 µl of eight times concentrated nanomaterials were added to inhibition/enhancement samples, and all preparations were centrifuged at 800 × g for 15 minutes. 100 µl of supernatant was transferred to a 96 well microplate for all samples in triplicate, to which 100 µl of haemoglobin reagent was added. 200 µl of methemoglobin standard was added to the plate in triplicate, and the absorbance of all samples was measured at 540 nm. Calculations were performed as outlined in Section 3.2.3.3, and recorded as percentage haemolysis.

Material	Final concentration/dilution
Polystyrene 2	10 µg/ml
Silica 1	10 µg/ml
Silica 2	10 µg/ml
Silica 3	10 µg/ml
Emulsion	1/200

Table 3.2: Final concentrations and dilution factors used to assess haemolytic potential of chosen nanomaterials.

3.2.4 Complement activation

3.2.4.1 Blood collection

Healthy volunteer blood was obtained by venipuncture (3 volunteers) into vacutainers anticoagulated with K2EDTA. The first 10 ml from each donor was discarded.

3.2.4.2 Experimental procedure

Blood was centrifuged at 2500 × g for 10 minutes. Plasma was evaluated for haemolysis, and pooled.

In microcentrifuge tubes, equal volumes (100 µl) of veronal buffer, plasma, and test-samples (final concentrations displayed in Table 3.3), negative control (DPBS), or positive control (cobra venom factor with functional titer of 628 units/ml) were combined. All samples were prepared in triplicate. Tubes were vortexed to mix components and spun briefly in a microcentrifuge to collect total volume. Treatments were then incubated for 30 minutes at 37°C.

All reagents were provided with the MicroVue iC3b EIA kit. Wash buffer was prepared, and standards and controls were reconstituted using hydrating reagent and allowed to sit for 15 minutes and mixed prior to use.

Cobra venom factor treated samples were diluted 1:40 using iC3b specimen diluent and loaded to the plate at a volume of 100 µl. All other samples and standards were loaded at neat concentration.

The plate was incubated for 30 minutes at room temperature, and washed using the following procedure; well contents were aspirated, 300 µl of wash solution was added and incubated for 1 minute, then aspirated. This was repeated 5 times, and following the final cycle the plate was tapped onto absorbent paper. 50 µl of iC3b conjugate was added to all wells and incubated for 30 minutes at room

temperature. The wash procedure was repeated. 100 µl of substrate solution was added to all wells and incubated for 30 minutes at room temperature. 5 µl of stop solution was added to all wells and the plate gently tapped to ensure even dispersion of colour. Absorbance at 405 nm was measured immediately using a CLARIOstar plate reader. Concentrations of iC3b were determined as described in Section 3.2.4.3, and validated using the high and low iC3b controls included with the kit.

Material	Low	High
Silver 1	1 µg/ml	100 µg/ml
Silver 2	0.01 µg/ml	1 µg/ml
Endorem	1 µg/ml	100 µg/ml
Ferumoxytol	1 µg/ml	100 µg/ml
JGC	1 µg/ml	100 µg/ml
Titanium (IV) oxide	1 µg/ml	100 µg/ml
Zinc oxide 1	1 µg/ml	100 µg/ml
Zinc oxide 2	1 µg/ml	100 µg/ml
Zinc oxide 3	1 µg/ml	100 µg/ml
Silica 1	1 µg/ml	100 µg/ml
Silica 2	1 µg/ml	100 µg/ml
Silica 3	1 µg/ml	100 µg/ml
Liposome	1/10000	1/100

Table 3.3: Concentrations and dilution factors used to assess complement activation in human plasma.

3.2.4.3 Calculations

Concentration of iC3b was calculated using a linear trendline generated from a semi-log curve produced from the MicroVue iC3b EIA kit standards using Microsoft Excel (2013) (Figure 3.4). Dilution corrections of 1:3 were made for all treated samples, and a further 1:40 for the positive control.

3.2.5 Statistical analysis

Statistical analysis was performed using GraphPad Prism 6. Statistical differences were determined using one-way analysis of variance (ANOVA) and Dunnett's multiple comparison tests. A p-value <0.05 was considered as statistically significant. Correlation analysis was performed using GraphPad Prism 6 via non-parametric Spearman correlation. A p-value <0.05 was considered as statistically significant.

3.3 Results

3.3.1 Plasma coagulation

Of all nanomaterials tested, treatment of plasma with titanium (IV) oxide produced the most pronounced reduction in coagulation time, compared to that of the normal (1.95 s), and untreated (2.05 s) controls in the PT assay (Figure 3.2a). Prolongation of coagulation beyond the set limit of 60 seconds was observed in treatment with the emulsion. Prolongation of 2.25 seconds was observed by treatment with silver 1 compared to the untreated control in the PT assay, but a more pronounced prolongation by this material was found in the APTT (27.95 s, Figure 3.2b) and TT (20.95 s, Figure 3.2c) assays, being the only material to generate marked change in the latter. Treatment with zinc oxide nanoparticles demonstrated highly differential effects in the APTT assay where zinc 1 prolonged coagulation beyond the time limit, while zinc 3 reduced coagulation time by 11 seconds compared to untreated plasma (Figure 3.2b). Prolongation was also exhibited by Endorem, JGC, titanium (IV) oxide, and emulsion, beyond the acceptable coagulation time range for the normal control in the APTT assay. Conversely, treatment with zinc 3 reduced the coagulation time by 10.95 seconds compared to untreated plasma.

(a)

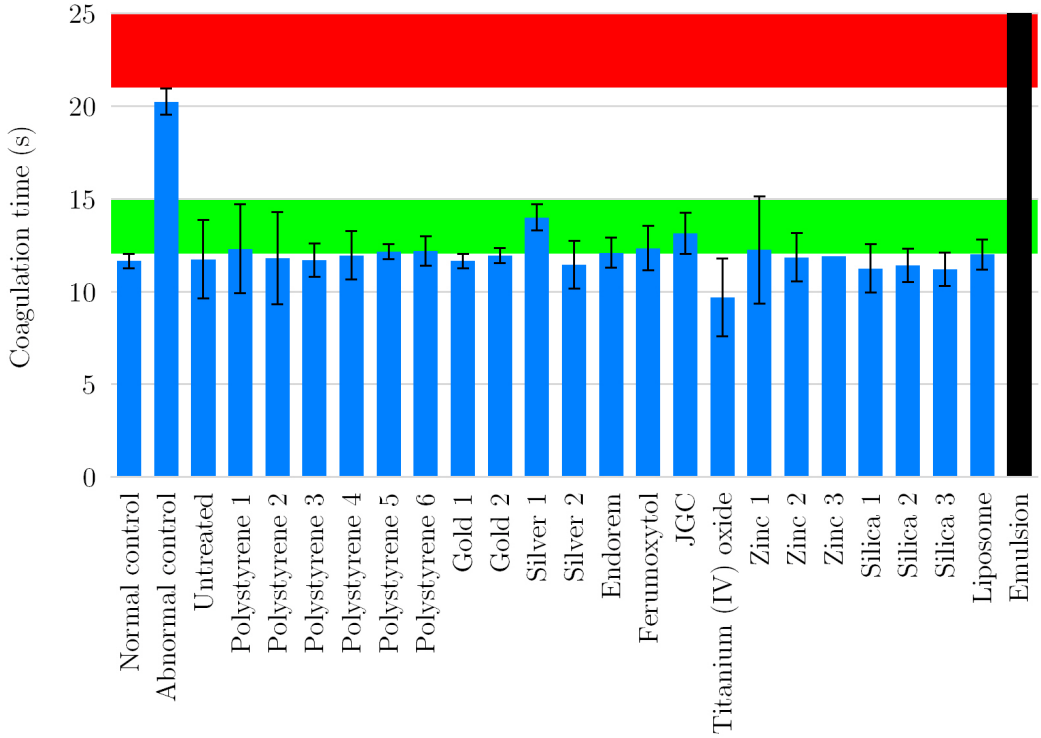
Coagulation time (s)
0
5
10
15
20
25
Normal control
Abnormal control
Untreated
Polystyrene 1
Polystyrene 2
Polystyrene 3
Polystyrene 4
Polystyrene 5
Polystyrene 6
Gold 1
Gold 2
Silver 1
Silver 2
Endorem
Ferumoxytol
JGC
Titanium (IV) oxide
Zinc 1
Zinc 2
Zinc 3
Silica 1
Silica 2
Silica 3
Liposome
Emulsion

(b)

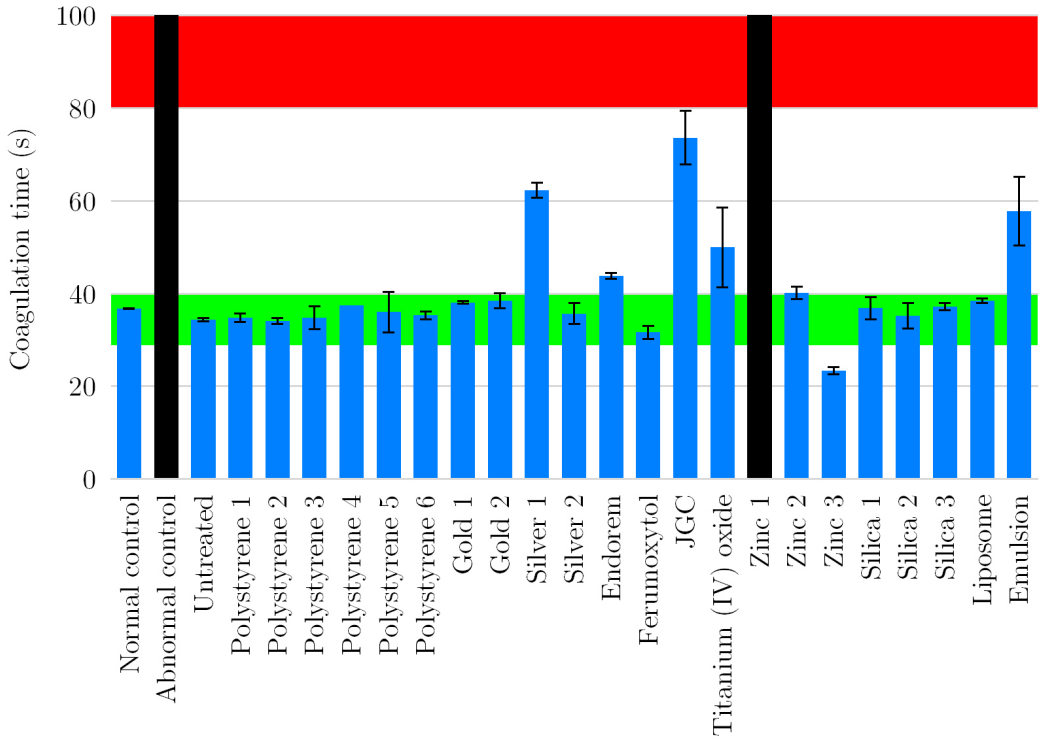
Coagulation time (s)
0
20
40
60
80
100
Normal control
Abnormal control
Untreated
Polystyrene 1
Polystyrene 2
Polystyrene 3
Polystyrene 4
Polystyrene 5
Polystyrene 6
Gold 1
Gold 2
Silver 1
Silver 2
Endorem
Ferumoxytol
JGC
Titanium (IV) oxide
Zinc 1
Zinc 2
Zinc 3
Silica 1
Silica 2
Silica 3
Liposome
Emulsion

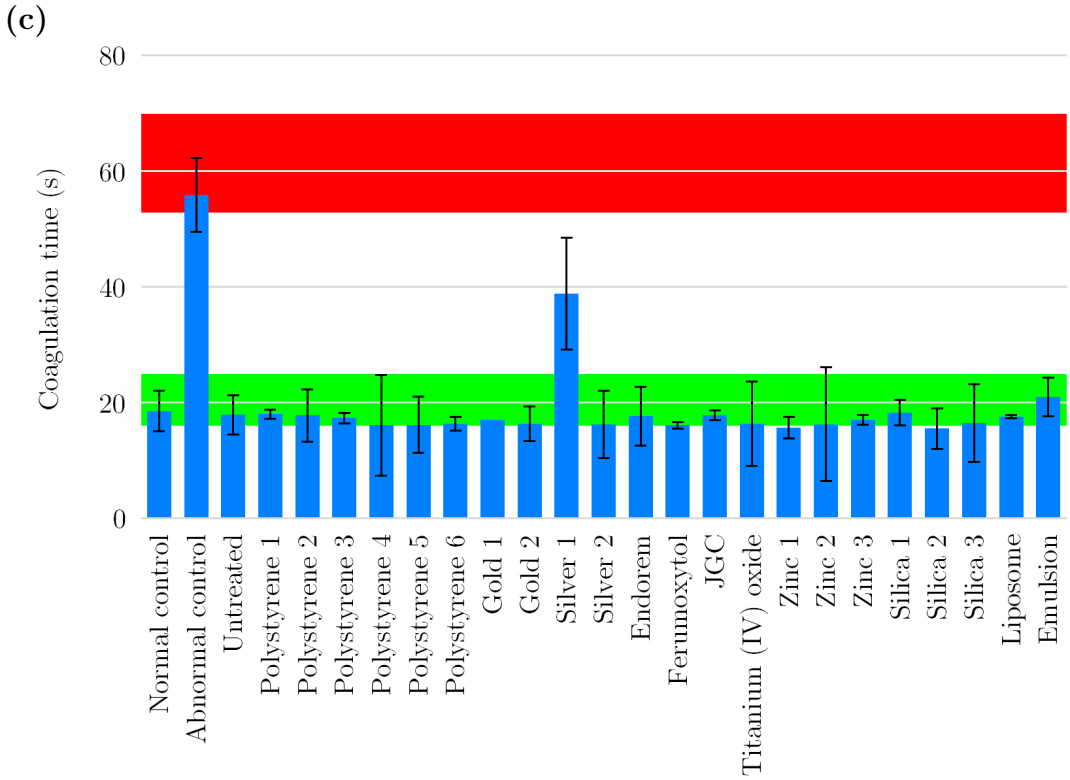

Figure 3.2: Coagulation times for nanoparticle treated plasma via the (a) Extrinsic pathway. (b) Intrinsic pathway. (c) Common pathway. Black bars denote samples which did not coagulate within the time limit. Green, and red highlighted areas indicate expected ranges of coagulation time for normal and abnormal control plasmas respectively, as stated in the manufacturer's product information. Data displayed as average (n = 2) ± %CV.

3.3.2 Haemolysis

Resource availability at the time of assessment limited the number of materials tested. Silica was chosen following indications in the literature of being a material having haemolytic potential. The testing of emulsion was determined by the effects generated in Section 3.3.1.

The American Society for Testing and Materials have set out guidelines for the assessment of haemolysis; <2% is deemed non-haemolytic, 2-5% slightly haemolytic, and >5% haemolytic (American Society for Testing and Materials, 2000).

Two materials demonstrated slightly haemolytic effect; treatment with silica 1 generated an average 2.42% haemolysis in individual 3, and silica 2 caused an average 3.12% haemolysis in individual 1 (Figure 3.3a). No haemolytic activity >5% was observed for any of the nanomaterial treatments.

Negative percentages of haemolysis displayed in Figure 3.3a were attributed to assay variation resulting from percentages being calculated from 10 g/dl plasma free haemoglobin. Similarly, percentages of haemolysis greater than 100% shown in Figure 3.3b are the result of nanomaterial-related absorbance enhancement, as treatment with Triton X-100 generated complete haemolysis of samples.

The calculated percentage haemolysis of silica 1 treated inhibition/enhancement control was 11% less than that of the positive control in individual 2, while being 16.40% and 7.64% higher in individuals 1 and 3 respectively (Figure 3.3b). Inhibition/enhancement did not follow any observable material-associated trend.

(a)

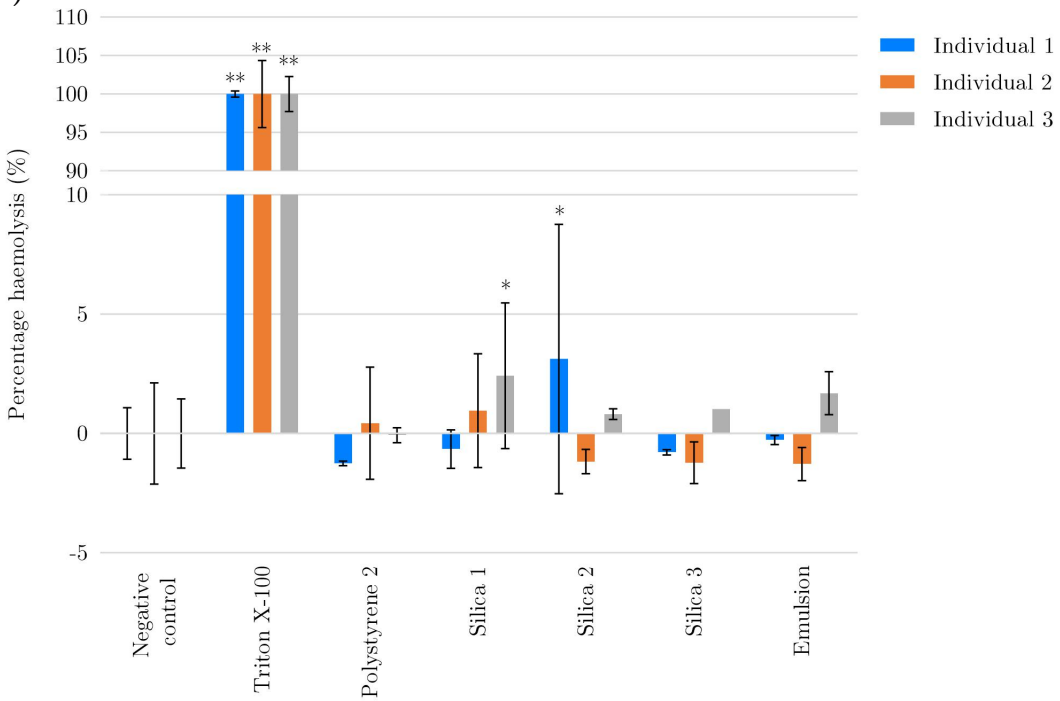
Percentage haemolysis (%)
110
105
100
95
90
10
5
0
-5
**
**
**
*
*
Individual 1
Individual 2
Individual 3
Negative control
Triton X-100
Polystyrene 2
Silica 1
Silica 2
Silica 3
Emulsion

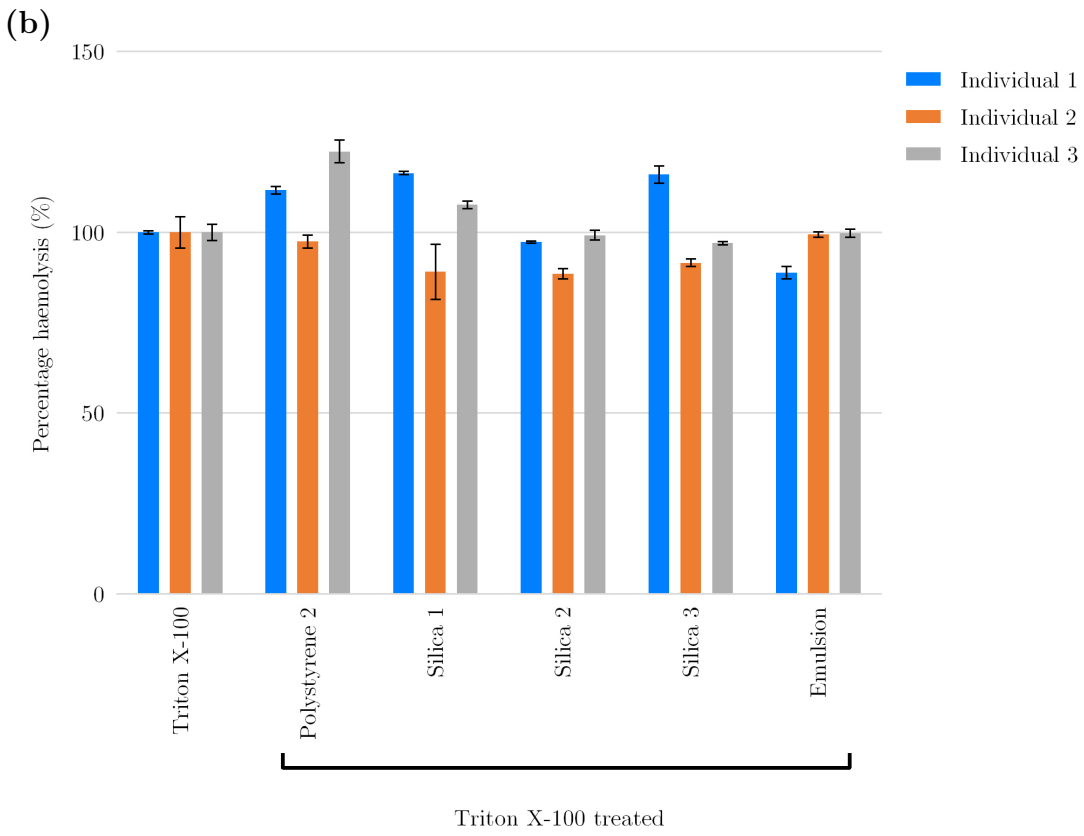

Figure 3.3: Percentage haemolysis, relative to controls, generated by (a) Treatment with stated nanomaterials. * denotes 2-5% haemolysis. ** denotes haemolysis >5%. (b) Nanomaterials following treatment with Triton X-100 to assess inhibition/enhancement. Data displayed as average (n = 3) ± standard deviation.

3.3.3 Complement activation

Figure 3.4 displays the standard curve used to calculate the iC3b concentrations in treated samples as described in Section 3.2.4.3. The standard curve was validated by the calculated concentrations of high and low standards included with the kit falling within the ranges stated by the kit protocol.

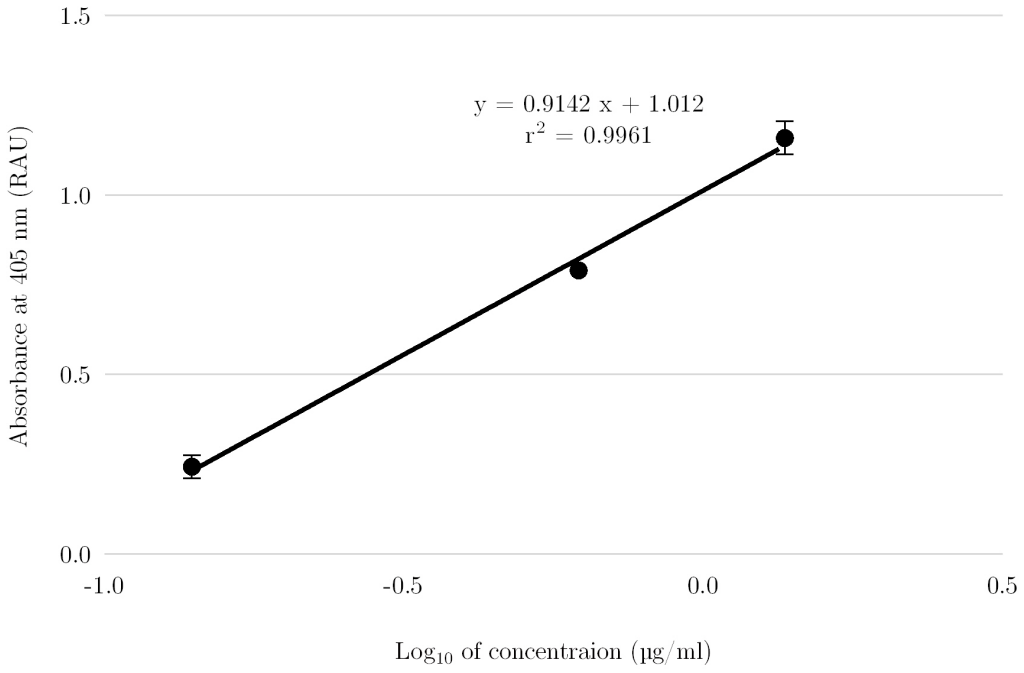

Figure 3.4: Standard curve prepared from standards provided with the iC3b EIA kit, used to calculate iC3b concentrations. Data displayed as average (n = 3) ± standard deviation.

Pooled plasma treated with the positive control, cobra venom factor, demonstrated an iC3b concentration 132.7-fold (p = <0.0001) more than that of the negative control (Figure 3.5).

No nanomaterial treatments, under the experimental conditions described, resulted in iC3b concentrations significantly different than that of the negative control (p = <0.05).

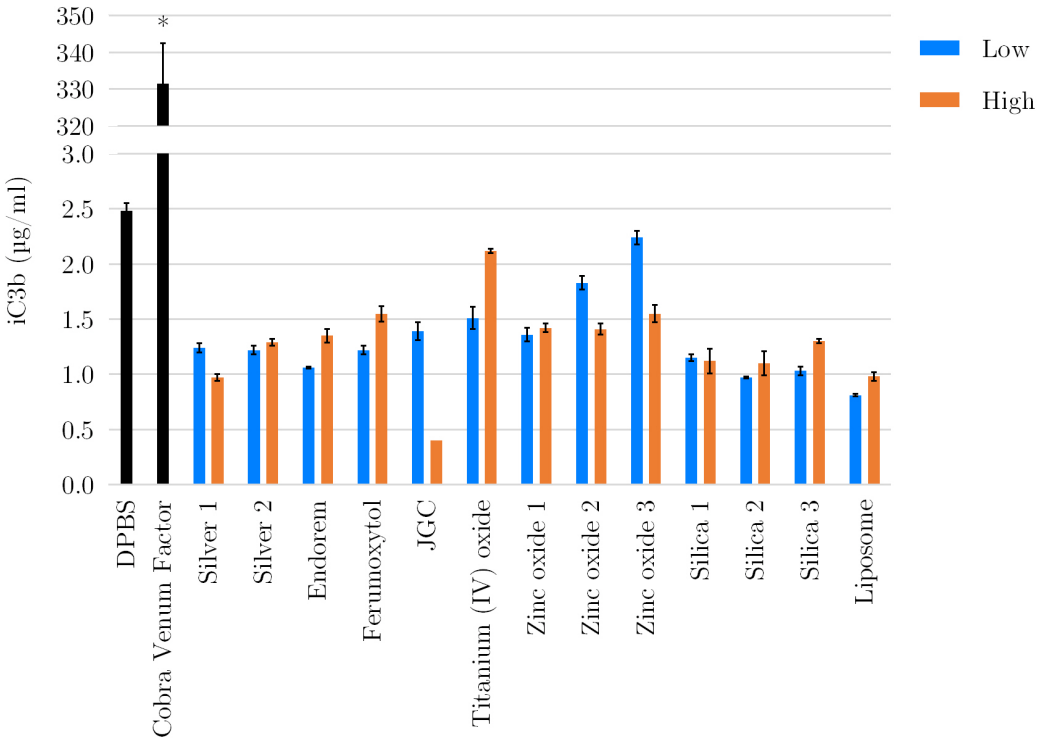

Figure 3.5: iC3b concentrations generated by treatments with negative and positive controls, and stated nanomaterials. Data displayed as average (n = 3) ± standard deviation. * p-value <0.05.

3.4 Discussion

Haematological compatibility is a property of utmost importance when considering nanomaterials being developed for *in vivo* use. For this reason, stringent preclinical assessment is a necessity to evaluate, characterise, and inform the development of nanomaterials for use as nanomedicines and nanotherapeutics.

Plasma coagulation in the presence of excessive endotoxin, through the generation of tissue factor, has been well documented (Pernerstorfer et al., 1999). JGC was found to contain the highest quantity of endotoxin of all materials tested in this work, 107.80 EU/ml at a tested concentration of 100 µg/ml. Treatment of plasma with JGC, however, demonstrated a prolongation in coagulation time of 1.4 seconds via the extrinsic pathway. The endotoxin-related effect is the result of tissue factor expression by monocytes (Pernerstorfer et al., 1999), not present in the cell-free methodology used in this work.

Zinc oxides 1, 2, and 3 each demonstrated highly different impact on coagulation times via the intrinsic pathway. Zinc oxide 2 prolonged coagulation time by 5.8 seconds compared to that of untreated plasma. Zinc 3 displayed procoagulant activity resulting in a coagulation time of 23.4 seconds, outside the accepted range for normal plasma of between 29 and 40 seconds (Diagnostica Stago, 2002). Zinc 1 prolonged coagulation beyond the assay maximum of 120 seconds. Zeta potentials of these materials displayed a high degree of similarity in FBS-supplemented media. Zinc 3 was found to be the largest in these media, while zinc 1 had the smallest size. Without characterisation of these parameters in plasma it cannot be stated with confidence which of these characteristics most influenced the observed effects.

Huang et al. have shown that sodium citrate coated silver nanoparticles did not affect coagulation (Huang et al., 2016). This is corroborated by the assessment of sodium citrate-coated silver 2 in this chapter. Laloy et al. described silver

nanoparticles stabilized by polyvinyl pyrolidone (PVP) as having procoagulant activity (Laloy et al., 2014). No existing literature has been found describing the effects of sodium polyacrylate stabilized nanoparticles on coagulation with which to compare the anticoagulant properties exhibited by silver 1, but it is intuitive that the surface functionalization is a key factor in determining coagulatory effect.

Emulsion treated plasma displayed prolongation of coagulation in the extrinsic, and intrinsic pathways. This was not the case in the common pathway. It could be argued that this is a result of the emulsion having some effect on factor VIII or X, but without further in-depth evaluation cannot be confirmed.

In vitro assessments of plasma coagulation demonstrate good correlation with *in vivo* effects (Dobrovolskaia, 2015; Dobrovolskaia and McNeil, 2013). The metric that is used in these assessments is change in coagulation time from a range that is accepted to be normal in healthy plasma (Neun et al., 2015b). As has been highlighted in Figure 3.2, accepted ranges are used to validate control plasmas used in these assays. While nanomaterial treatments may impact the plasma coagulation time under *in vitro* conditions, these responses should be taken as a preliminary guide for identifying possible cases of cause for concern when considering *in vivo* testing. If a change in coagulation time is found to be statistically significant *in vitro* this may have no bearing on the effect in an animal model. As such, this form of data handling is not applied (Neun et al., 2015b). Similarly *in vitro* assessments of haemolysis conform to a convention where haemolytic activity is scrutinised by percentage-ranges of haemolysis (Malinauskas, 1997; Neun et al., 2015a). As stated in Section 3.3.2 these guideline ranges, set by the American Society for Testing and Materials, are as such; <2% is deemed non-haemolytic, 2-5% slightly haemolytic, and >5% haemolytic (American Society for Testing and Materials, 2000). This allows a clear determinant of the potential for a nanomaterial to generate potentially detrimental effects when applied to *in vivo* models.

Red blood cells, due to the presence of sialylated glycoproteins on the cell surface, demonstrate a negative zeta potential (Fernandes et al., 2011), and it is well known that cationic nanoparticles have a greater tendency for permeation and disruption (Clogston and Patri, 2011). Nanomaterials displaying a zeta potential of between the range of -10 to +10 mV are considered to be neutral, whereas those greater than +30 mV or more negatively than -30 mV are considered to be strongly cationic and anionic, respectively (Clogston and Patri, 2011). A number of the nanomaterials assessed in this work displayed zeta potentials greater than ±30 mV when measured in deionised water namely; polystyrenes 1, 3, 4, 5, 6, silver 1 and 2, and JGC. Further shown in Chapter 2 protein binding to the nanoparticle confers a zeta potential tending toward neutrality. As such, no haemolytic action could be attributed to strong surface charge, corroborated by a number of sources describing negation of the haemolytic potential of nanomaterials following establishment of a protein corona (Martinez et al., 2015; Paula et al., 2012; Tenzer et al., 2013).

The haemolytic potential of silica nanoparticles has been extensively reviewed (Tang and Cheng, 2013), and while it is know that the action of mesoporous silica is a function of the porosity of the material, the information surrounding nonporous silica nanoparticles is comparatively lacking. One instance where nonporous silica has been assessed described the effect of nonporous silica to be less than that of mesoporous at the same particle size (Yu et al., 2011). It was also shown that when the particle surface had been amine-modified, the amount of haemolysis was relative to the concentration (Yu et al., 2011). The effects described by Yu et al. followed an experimental design consistent with others who report haemolysis prior to establishment of a corona (Barshtein et al., 2011). Conversely it has been shown elsewhere that nonporous silica nanoparticles generate a higher lever of haemolysis compared to mesoporous silica, while surface modification with PEG-silane reduced this effect (Lin and Haynes, 2010).

Again, no significant and consistent effect was observed in the three types of silica nanoparticles evaluated in this work.

In recent years there has been an increase in the design of emulsion carriers to reduce the haemolytic effects of drugs. The mechanism through which this is thought to occur is by decreasing the potential contact between erythrocytes and the haemolytic agent (Jumaa and Muller, 2000). Interestingly, Bruxel et al. describe an instance where the loading of oligonucleotides reduce the haemolytic potential of their cationic lipid emulsion carrier (Bruxel et al., 2011). The unloaded nanoemulsion tested in this work showed no evidence of significant influence over erythrocyte stability, and it can be argued that any effects resulting from treatment with emulsion-based materials will be heavily based on their constituents.

Inhibition and enhancement of the calculated percentage of haemolysis was observed. While no material specific trends were observed in these, such an effect should still be considered when assessing other materials, particularly those whose optical characteristics overlap the absorption wavelength used in this assay methodology. As was shown in Chapter 2, none of the materials tested would demonstrate cause for concern in this manner.

The inclusion of inhibition/enhancement controls in this assay was informed by accounts in the literature of nanomaterial interactions with assessments of haemolysis, as discussed in Section 1.6.2. The absorbance spectrum of gold nanoparticles is known to overlap the 540 nm wavelength used to quantify free haemoglobin, potentially resulting in overestimation (Dobrovolskaia et al., 2008b). This control also estimates interaction between nanoparticles and haemoglobin through adsorption to the nanoparticle surface (Neun et al., 2015a). Furthermore, coagulation on the surface of nanoparticles has been described, which limits their surface exposure and modulates their haemolytic potential (Dobrovolskaia and McNeil, 2007).

The positive control, cobra venom factor, resulted in an iC3b concentration 133-times greater than that of the negative control. The mechanism by which this compound activates the complement system is via the alternative pathway. Generation of such a pronounced effect was expected (Vogel et al., 2004) and validates the assay.

Nanomaterial selection was limited by the number of samples able to be loaded to the plate with sufficient replicates. Under the tested conditions it was found that no nanomaterial treatments generated concentrations of iC3b statistically different from that of the untreated control. As a preliminary screen this has indicated that none of the tested nanomaterials activated complement under the assay conditions. This observation could potentially be a result of the binding of this fragment to the nanomaterial surface which would reduce the concentration of free iC3b available to bind the plate. Subsequently during the wash procedure of this assay, the nanoparticles and associated iC3b would have been washed away. This is a consideration which should be taken when applying similar assays to nanomaterials. In this case any complement activation would have needed to be magnitudes higher to overcome this effect, providing sufficient amount of the unbound iC3b fragment to be bind the plate and subsequently detected and quantified. While the methodology utilised here allowed higher throughput and reduction of time compared more laborious methodologies such as single component activities or haemolytic assays (Kirschfink and Mollnes, 2003), additional/further assessment would prove invaluable in confirming this result, either by assessing nanomaterials in cobra venom factor-stimulated plasma, or by assessing via alternative techniques.

While it is well established in the literature that nanoparticles possessing strong charge ($>\pm 30$ mV) have the potential to generate greater, and more detrimental, effect than those tending towards neutral charge (Clogston and Patri, 2011; Ilinskaya and Dobrovolskaia, 2013), the observations made here were lim-

ited by the nanomaterials chosen for use in this work possessing neutral charge in biologically relevant, protein containing, media. With the exception of certain materials affecting coagulation pathways, the lack of any highly aberrant results is supported by pre-existing trends in the literature although to conclusively confirm this, the inclusion of highly charged materials under biologically relevant conditions would have proved beneficial. It can be inferred, however, that surface functionalization, and material specific effects may play a role in the observations made throughout this chapter.

Chapter 4

Nanoparticle physicochemical characteristics and their potential immunogenicity

Contents

4.1 Introduction 120
4.2 Methods 122
4.2.1 Materials 122
4.2.2 Peripheral blood mononuclear cell isolation and culture . . 122
4.2.3 Cytokine secretion determined via multiplex assay 123
4.2.4 IL-1β ELISA 125
4.2.4.1 Assay protocol 126
4.2.4.2 Calculations 127
4.2.5 Inhibition of caspase-1 127
4.2.6 Leukocyte proliferation 128
4.2.6.1 Calculations 129
4.2.7 Statistical analysis 130
4.3 Results 131
4.3.1 Cytokine secretion determined via multiplex assay 131
4.3.2 IL-1β ELISA 136
4.3.3 Inhibition of caspase-1 140
4.3.4 Leukocyte proliferation 141
4.4 Discussion 143

4.1 Introduction

The ideal design of a preclinical assessment is a simple, reliable, robust methodology with good *in vitro* to *in vivo* correlation. Determination of immunotoxicity is a vital aspect prior to the translation of, but not limited to, nanomedicines (Dobrovolskaia et al., 2009; Giannakou et al., 2016). The complex nature of nanoparticles in terms of their physicochemical characteristics lends to the need for rigorous determination of said characteristics in order to establish those which may contribute to adverse immune effects (Dobrovolskaia and McNeil, 2013). In order to perform this on a viable scale, high throughput is a necessity. As such, the development of *in vitro* assays which are able to generate translatable results to further *in vivo* testing is becoming a necessity. In order to achieve this, the use of primary cells in preclinical *in vitro* analysis is becoming more widespread.

As discussed in Section 1.3.1, cytokines as biomarkers of nanoparticle immunomodulatory properties demonstrate good correlation to that to that observed *in vivo* (Dobrovolskaia and McNeil, 2013). Four cytokines, namely IFNγ, TNFα, IL-1β, and IL-10, were chosen for assessment. This selection was based on the inter-related roles these cytokines play, and allowing observation of the influence nanoparticles have on the generation of these inflammatory (TNFα, IL-1β), anti-inflammatory (IL-10), and pleotropic (IFNγ) cytokines. For these reasons the study of cytokine secretion is a pertinent choice relating to the focus of this chapter.

Highlighted in Chapter 1.3.1, nanoparticles, including silica and titanium dioxide, have been shown to interact with inflammasomes (Baron et al., 2015) which are involved in the maturation of pro-inflammatory cytokines IL-1β and IL-18 (Guo et al., 2015). NLRP3 inflammasome activation by endogenous and exogenous danger signals leads to the release of mature IL-1β via the action of caspase-1 (Franchi et al., 2009). Activation of caspase-1 is known to be the rate-limiting

step in inflammation due to IL-1β or IL-18 (Jo et al., 2016). Being such a key component in the regulation and generation of IL-1β, the potential for nanoparticle interference was assessed.

The proliferative response of leukocytes to stimulators and cytokine production is vital in the normal generation of an immune response. The utility of assessing this process *in vitro* can evaluate the potential of nanomaterials for being immunostimulatory or immunosuppressive (Dobrovolskaia and McNeil, 2013). The latter involves the use of a known mitogen/antigen to determine the extent of potential suppression of proliferation. Strong correlation has been shown between *in vitro* and *in vivo* mitogen responses and subsequent immunosuppression by nanomaterial (Moon et al., 2011).

The aim of this chapter was to evaluate the cytokine secretion by primary human peripheral blood mononuclear cells in response to nanoparticles. This was performed by direct quantification, as well as observing the influence of nanomaterials over caspase-1 activity, and inflammasome activation. The impact on proliferation of primary human leukocytes was also assessed.

4.2 Methods

4.2.1 Materials

Chloroquine, Hanks' balanced salt solution (HBSS), penicillin-streptomycin, heat-inactivated human AB serum, HEPES solution, L-glutamine solution, Phytohemagglutinin-M (PHA), rapamycin, and transferrin were purchased from Sigma-Aldrich (Dorset, UK). Lipopolysaccharide (LPS), monosodium urate (MSU), wortmannin, and VX-765 were purchased from Invivogen (San Diego, USA). Ficoll-Paque was purchased from Fisher Scientific (Loughborough, UK). Bio-Plex Pro reagent kit containing antibody-coupled detection beads for human IFNγ, TNFα, IL-1β, IL-10 was purchased from Bio-Rad Laboratories (Hemel Hempstead, UK). Human IL-1 beta ELISA Kit, and Caspase 1 Inhibitor Drug Detection Kit were purchased from ABCAM (Cambridge, UK). Efavirenz powder (>98% pure) was purchased from LGM Pharma (Boca Raton, USA). Lopinavir powder (>98% pure) was purchased from LGC Pharma (London, UK). Buffy coats were obtained from the National Health Service Blood and Transplant Special Health Authority (Liverpool, UK).

Approval for the sampling and storage of human blood samples for biomedical research was gained from the University of Liverpool Committee in Research Ethics (Ref: RETH000563).

4.2.2 Peripheral blood mononuclear cell isolation and culture

Peripheral blood mononuclear cells (PBMCs) were isolated from healthy volunteer blood using Ficoll-Paque separation. Blood was layered over Ficoll-Paque separation medium at a 2:1 ratio respectively in 50 ml falcon tubes. These were

centrifuged for 30 minutes at 2000 rpm without brake. The PBMC layer was transferred to fresh falcon tubes using transfer pipettes. HBSS was added to each PBMC fraction to a total volume of 50 ml, and then centrifuged for 5 minutes at 2000 rpm. The supernatant was discarded and the cell pellet suspended in RPMI-1640 supplemented 10% with FBS. PBMC suspensions were transferred to relevant culture plates prior to experimentation.

4.2.3 Cytokine secretion determined via multiplex assay

PBMCs were isolated from buffy coats (n = 3) as described in Section 4.2.2. Cells were seeded at a density of 2.5×10^5 per well in 1 ml of culture medium in 48-well microplates. PBMCs were then treated with LPS at concentrations of 10, 20, 30, or 40 ng/ml, nanomaterials at the concentrations stated in Table 4.2, or combined treatments of nanomaterials with 20 ng/ml of LPS. Untreated PBMC controls were included, and each condition was prepared in triplicate. Cultures were incubated for 24 hours at 37°C and 5% CO_2. Following incubation; plates were centrifuged for 5 minutes at 2000 rpm, replicate 100 µl aliquots of the supernatants were transferred to fresh 96-well microplates, and stored at -80°C until analysis.

The Bio-Plex Pro assay was used to quantify the concentration of cytokines IFNγ, TNFα, IL-1β, and IL-10 present in the cell culture supernatants, following the manufacturer's guidelines.

Initial preparation involved the Bio-Plex 200 Luminex system (Bio-Rad Laboratories, Hemel Hempstead, UK) being started up to reach the working temperature. Assay buffer, wash buffer, and sample diluent were allowed to equilibrate to room temperature. The lyophilised standard included with the kit was reconstituted in 500 µl of Bio-Plex sample diluent, vortexed, and incubated on ice for 30 minutes. Calibration of the system was performed daily, and validation monthly.

Analyte	Minimum	Maximum
IFNγ	6.93 pg/ml	28395 pg/ml
TNFα	15.40 pg/ml	63082 pg/ml
IL-1β	3.85 pg/ml	8212 pg/ml
IL-10	8.42 pg/ml	34472 pg/ml

Table 4.1: Maximum concentration of standards provided by the manufacturer, and lower limit of quantification (minimum concentration within the 8-point standard curve) for analytes IFNγ, TNFα, IL-1β, and IL-10.

A 5-point logistic curve was prepared following the assay protocol. Maximum standard concentrations of analytes, and lower limits of quantification of analytes of interest are displayed in Table 4.1.

Culture supernatants were allowed to thaw and equilibrate to room temperature, while 50 µl of the coupled beads were added to each well of the assay plate, and subsequently washed twice with 100 µl of Bio-Plex wash buffer using a Bio-Plex Pro Wash Station with magnetic plate carrier (Bio-Rad Laboratories, Hemel Hempstead, UK). Thawed samples were diluted 1:4 using Bio-Plex sample diluent prior to loading to the plate at a volume of 50 µl. Standards and blank (sample diluent) were also loaded at the same volume.

The plate was covered with sealing tape and protected from light using aluminium foil prior to incubation at room temperature for 30 minutes with shaking (850 rpm).

The plate was washed three times with 100 µl of wash buffer, and 25 µl of detection antibodies was added to each well. Sealing and protection from light, and incubation was repeated. During this time the Bio-Plex 200 Luminex was calibrated, and standard values (bead regions, and analyte concentrations) were submitted to the Bio-Plex software.

The plate was again washed three times with 100 µl of wash buffer, and 50 µl of of SA-PE was added to each well before being sealed, covered in aluminium foil, and incubated for 10 minutes at room temperature.

A final washing, three times with 100 µl of wash buffer, was performed and the beads resuspended in 125 µl of assay buffer. The plate was sealed, shaken at 850 rpm for 30 seconds, and then analysed using the Bio-Plex 200 Luminex using the low PMT, RP1 settings, as recommended in the protocol.

Material	Final concentraion
Polystyrene 1	100 µg/ml
Polystyrene 2	100 µg/ml
Polystyrene 3	100 µg/ml
Polystyrene 4	100 µg/ml
Silver 1	100 µg/ml
Silver 2	1 µg/ml
Endorem	10 µg/ml
Ferumoxytol	10 µg/ml
JGC	1 µg/ml
Titanium (IV) oxide	100 µg/ml
Silica 1	100 µg/ml
Silica 2	100 µg/ml
Silica 3	100 µg/ml

Table 4.2: Final concentrations of nanomaterials used to assess cytokine secretion via multiplex assay.

4.2.4 IL-1β ELISA

PBMCs were isolated from Buffy Coats as described in Section 4.2.2 and seeded at a density of 1×10^6/ml in 1 ml of media in 24 well culture plates.

Assay 1 - Wells were designated for untreated cells, and treatments with LPS (20 ng/ml), MSU (100 µg/ml), LPS (20 ng/ml) and MSU (100 µg/ml) designated hereon as "combined positive control", combined positive control and chloroquine (50 µg/ml), combined positive control and wortmannin (100 µg/ml), all of which were prepared in triplicate.

Assay 2 - Wells were designated for untreated cells, and treatments with LPS (20 ng/ml), MSU (100 µg/ml), combined positive control, combined positive control and rapamycin (40 µg/ml), all of which were prepared in triplicate.

Assay 3 - Wells were designated for untreated cells, and treatments with LPS (20 ng/ml), combined positive control, combined positive control and silicas 1, 2, and 3 (100 µg/ml), all of which were prepared in triplicate.

All conditions containing LPS were treated with LPS for 2 hours prior to the addition of further materials. Treatments were incubated for 24 hours at 37°C and 5% CO_2.

4.2.4.1 Assay protocol

IL-1β was quantified using the Human IL-1 beta ELISA Kit following the manufacturer's protocol. Briefly, standard diluent buffer, and wash buffer were diluted to working concentrations using deionized water. IL-1β standard and control were reconstituted as indicated on the product packaging. A 7-point standard curve was prepared, the maximum and minimum concentrations being 500 pg/ml and 15.6 pg/ml respectively.

Cell suspensions were transferred to microcentrifuge tubes and centrifuged at 1000 × g for 10 minutes. 100 µl of supernatant from each sample was transferred to the ELISA plate (n = 3) accompanied by the standards, control, and appropriate blanks included in the kit (n = 2).

Following a three hour incubation the plate was washed three times in 300 µL of wash buffer. 100 µl of Streptavidin-HRP was added to all wells and incubated for 30 minutes. The wash procedure was repeated before adding 100 µL of Chromogen TMB solution for 15 minuted while protected from light.

100 µl of stop reagent was added and the absorbance of each well was imme-

diately measured at 450 nm using a CLARIOstar plate reader. All incubations were performed at room temperature.

4.2.4.2 Calculations

A linear trendline was generated from the standard curve, and validated using control IL-1β of known concentration included with the kit. Concentrations of IL-1β present in samples were interpolated from the trendline (Figure 4.4) using Microsoft Excel (2013).

4.2.5 Inhibition of caspase-1

Assessment of the inhibition of caspase-1 was performed using the Caspase 1 Inhibitor Drug Detection Kit following the manufacturer's protocol. VX-765, Efavirenz, and Lopinavir were prepared at concentrations of 10 µM, and polystyrenes 1-6 were prepared at concentrations of 100 µl/ml, in deionized water. 50 µl of each was added in triplicate to a 96-well microplate. Active caspase-1 was reconstituted in reaction buffer following the kit protocol, 5 µl of which added to each of these wells.

Assay controls were added to the plate as follows; 50 µl of deionized water as background control, caspase-1 control of 50 µl of deionized water and 5 µl active caspase-1, and positive inhibition control comprised of 50 µl of deionized water, 5 µl active caspase-1 and 1 µl of caspase-1 inhibitor.

"Master Mix" was prepared following the assay protocol. DTT was added to the 2× reaction buffer to a final concentration of 10 mM. To this; 1 mM YVAD-AFC substrate was added at 10% total volume. 50 µl of Master Mix was added to each well and incubated at 37°C for 1 hour.

Fluorescence of each well was measured using a CLARIOstar plate reader

with excitation and emission wavelengths of 440 nm and 505 nm respectively.

Average fluorescence values of background control wells were subtracted from all sample wells. Caspase-1 activity in treated samples was calculated as a percentage of the activity present in negative control wells.

4.2.6 Leukocyte proliferation

Culture medium to be used throughout this assay, here-on referred to as leukocyte proliferation (LP) medium, was prepared; RPMI-1640 was supplemented with pooled heat-inactivated human AB serum to 10% final volume, 25 mM HEPES, 2 mM L-glutamine, 25 µg/ml transferrin, 100 µg/ml streptomycin and 100 U/ml penicillin.

Nanomaterials were prepared in LP medium at four times the final concentration displayed in Table 4.3 to allow for the dilution when added to the cell culture. PHA was prepared in LP medium at final concentrations of 2.5, 5, 10, 20, and 40 µg/ml.

PBMCs were isolated from buffy coats (n = 6) as described in Section 4.2.2. PBMC cultures were centrifuged for 5 minutes at 2000 rpm. and culture medium was replaced with LP medium. Cell suspensions were adjusted to a density of 2.5×10^6 cells/ml and plated at a volume of 100 µl/well in 96-well round-bottomed plates.

PBMCs were treated as follows; 100 µl of LP medium was added to the negative "unstimulated" control, 50 µl of 2.5, 5, 10, 20, or 40 µg/ml PHA and 50 µl of LP medium were added as PHA stimulated samples where 20 µg/ml PHA is designated as the "stimulated" control. 50 µl of nanoparticle preparations and 50 µl of LP medium were added to nanoparticle treated wells, and 50 µl of nanoparticle preparations and 50 µl of 20 µg/ml PHA were added to "stimulated" nanoparticle treated wells. All conditions were prepared in triplicate.

Plates were incubated for a total of 48 hours at 37°C, 5% CO_2. For the final 16 hours; 1 µCi of [^{3}H]-thymidine was added to each well.

Cells were harvested onto a filtermat using a Tomtec Harvester 96 (Tomtec, Connecticut, USA), and sealed in a sample bag with melt on scint.

Incorporated radioactivity was measured on a Perkin-Elmer MicroBeta detector (Perkin Elmer, Ohio, USA).

Material	Final concentraion
Polystyrene 1	100 µg/ml
Polystyrene 2	100 µg/ml
Polystyrene 3	100 µg/ml
Polystyrene 4	100 µg/ml
Polystyrene 5	100 µg/ml
Polystyrene 6	100 µg/ml
Silver 1	100 µg/ml
Endorem	10 µg/ml
Ferumoxytol	10 µg/ml
JGC	1 µg/ml
Silica 1	100 µg/ml
Silica 2	100 µg/ml
Silica 3	100 µg/ml

Table 4.3: Final concentrations of nanomaterials used to assess leukocyte proliferation.

4.2.6.1 Calculations

Change in proliferation was calculated using the following equation, where incorporated reactivity in unstimulated control was used relative to unstimulated nanomaterial treatments, and PHA 20 µg/ml was used for stimulated nanomaterial treatments. CPM - counts per minute.

$$\text{Proliferation} = \frac{\text{Incorporated radioactivity}_{\text{sample}}\ \text{(CPM)}}{\text{Incorporated radioactivity}_{\text{control}}\ \text{(CPM)}} \times 100\%$$

4.2.7 Statistical analysis

Statistical analysis was performed using GraphPad Prism 6. Statistical differences were determined using one-way analysis of variance (ANOVA) and Dunnett's multiple comparison tests. A p-value <0.05 was considered as statistically significant.

4.3 Results

4.3.1 Cytokine secretion determined via multiplex assay

No samples were found to have generated IFNγ at a concentration greater than the lower limit of detection for the assay (6.93 pg/ml). Furthermore, as the levels of TNFα, IL-1β, and IL-10 were below the detectable limit of the assay (15.40 pg/ml, 3.85 pg/ml, 8.42 pg/ml respectively) in untreated controls it was not possible to calculate fold difference or perform statistical analysis on these samples.

Detectable concentrations of TNFα were generated in response to all tested concentrations of LPS for all three individuals (Figure 4.1a). The concentrations of TNFα in LPS treatments demonstrated a high degree of similarity in individuals 2 and 3. The concentrations generated in PBMCs from individual 1 were approximately 2.5-times less at all LPS concentrations. JGC and silica 3 generated TNFα is PBMCs from all three individuals. Treatment with silica 2 resulted in TNFα generation in PBMCs from individuals 1 (261.95 pg/ml) and 2 (44.35 pg/ml), but not 3. Only individual 2 was found to have produced TNFα in response to polystyrene 2 (21.86 pg/ml).

Consistent reductions of TNFα concentrations (0.8-, 1-, and 0.3-fold within individuals 1, 2, and 3 respectively) were observed in combined treatments with LPS and all polystyrene nanoparticles, compared to positive controls (Figure 4.1b). Endorem- and Ferumoxytol-combinded LPS treatments also resulted in lower cocentrations of TNFα than solely LPS (20 ng/ml) treated PBMCs. Combined LPS and Silicas 2 and 3, however, resulted in higher concentrations of TNFα in samples from individuals 1 and 2.

Treatment with LPS at all tested concentrations, JGC, and silica 3 resulted in detectable quantities of IL-1β from individuals 1, 2, and 3. The most marked

of these was that of individual 1 in response to treatment with 100 µg/ml of silica 3, being 18-times that of individual 3, and 36-times greater than individual 1 (Figure 4.2a). Silica 3 generated an IL-1β concentration of 11.99 pg/ml in the sample from individual 1, the only one to do so in response to this nanomaterial.

Combined treatment with LPS and silica 3 resulted in the highest concentration of IL-1β generated in response to all tested conditions in PBMCs from all individuals (Figure 4.2b).

LPS treatment across all concentrations, and JGC, resulted in the secretion of IL-10 in PBMCs from all individuals, the most pronounced effect being observed from individual 3 (Figure 4.3a). Silica 3 was found to have stimulated IL-10 secretion in individuals 1 (37.84 pg/ml) and 3 (8.69 pg/ml), while only individual 3 produced a quantifiable concentration of this cytokine in response to titanium (IV) oxide (5.85 pg/ml).

All LPS-combined nanomaterial treatments resulted in less IL-10 than treatment solely with 20 ng/ml LPS in PBMCs from individual 3 (Figure 4.3b). Combined treatments of silver 2, Ferumoxytol, titanium (IV) oxide, silica 2 and silica 3 with LPS generated more IL-10 than LPS-only treatments by individual 1. This increased production was observed in individual 2 from LPS with JGC, and silicas 2 and 3.

Combined treatment with LPS and silver 1 abolished generation of TNFα, IL-1β and IL-10 in all individuals.

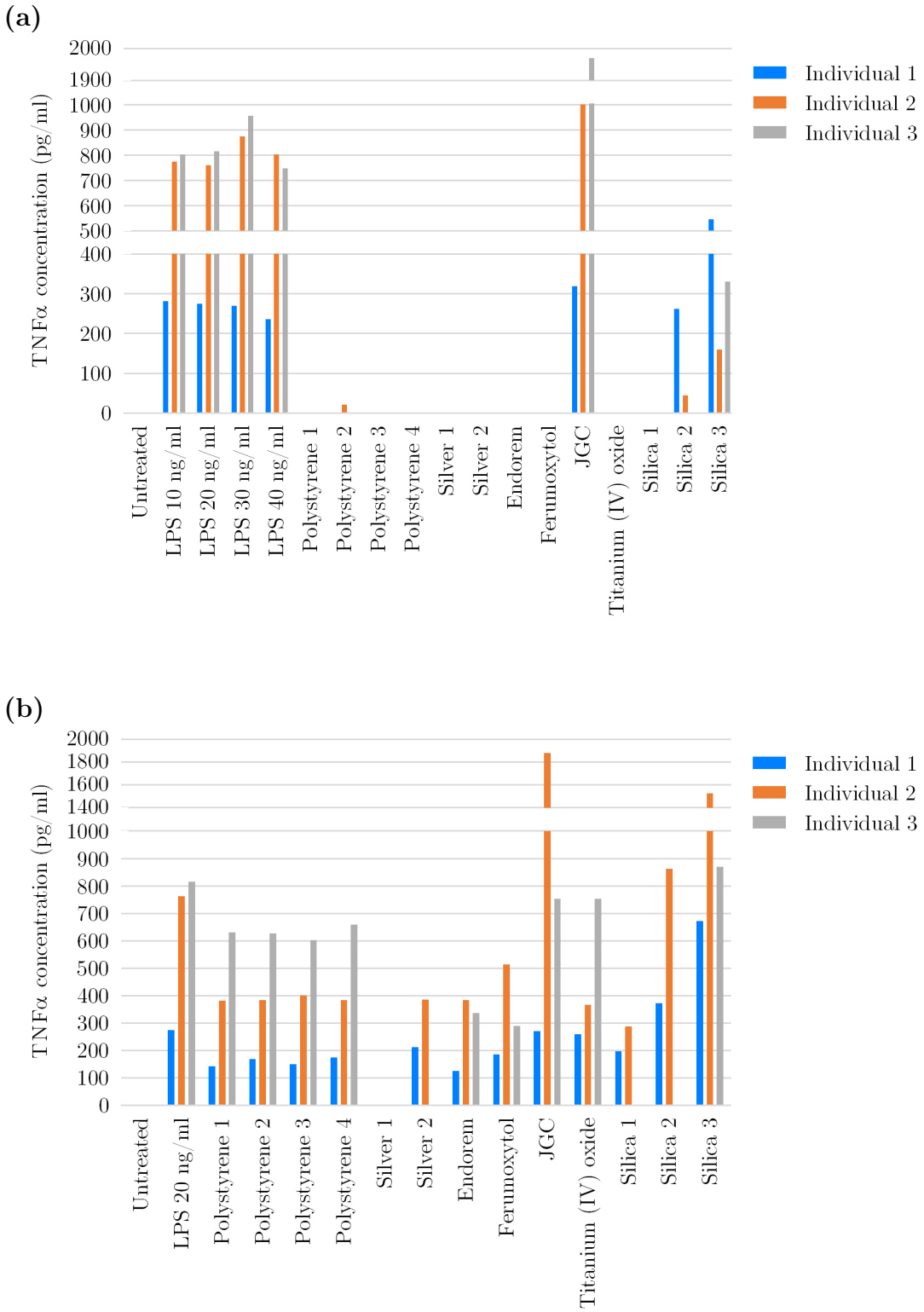

Figure 4.1: Concentrations of cytokine TNFα secreted by peripheral blood mononuclear cells in response to (a) Treatment with LPS, or stated nanomaterials. (b) Combined LPS treatment with stated nanomaterials. Data displayed as average (n = 2).

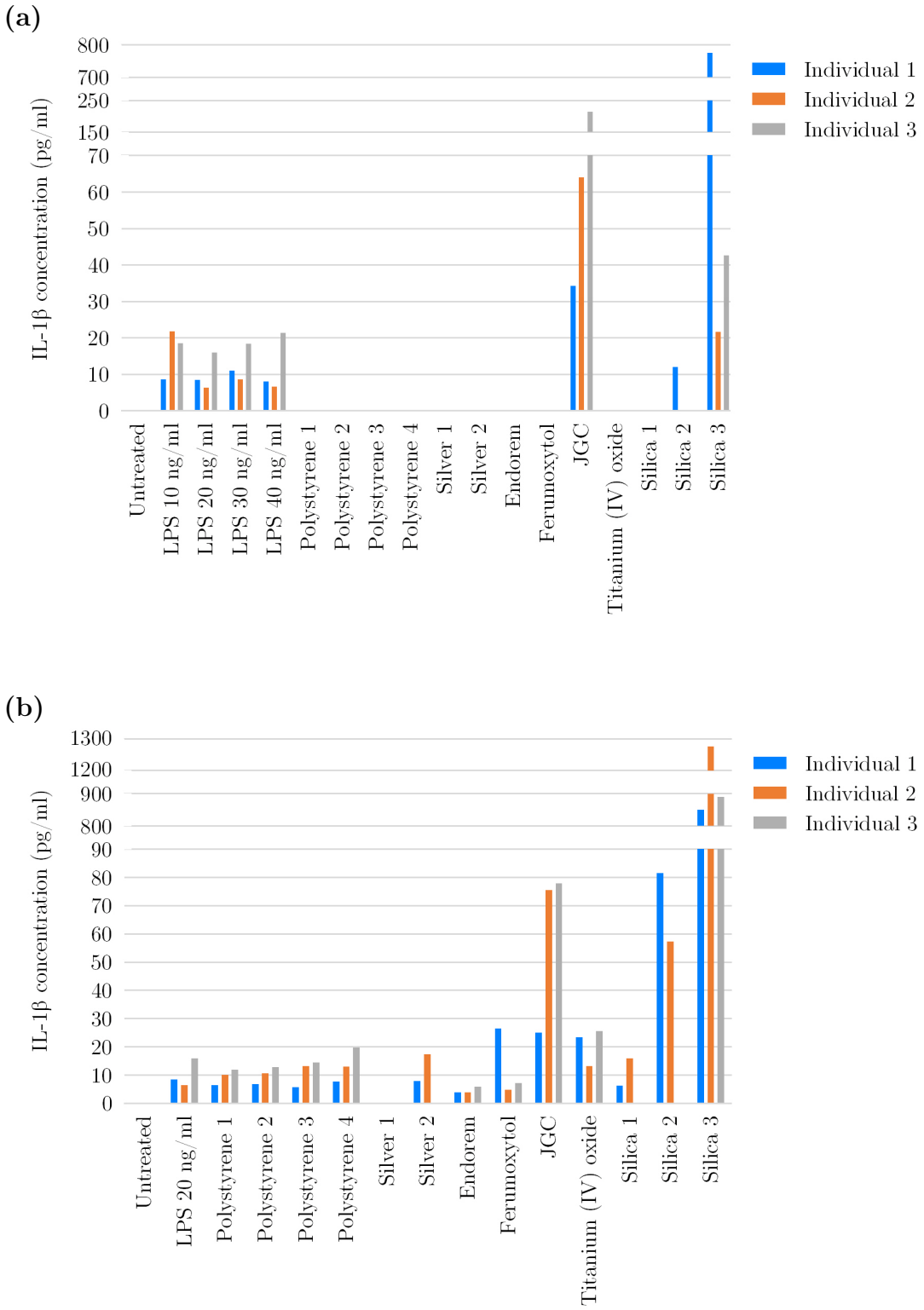

Figure 4.2: Concentrations of cytokine IL-1β secreted by peripheral blood mononuclear cells in response to (a) Treatment with LPS, or stated nanomaterials. (b) Combined LPS treatment with stated nanomaterials. Data displayed as average (n = 2).

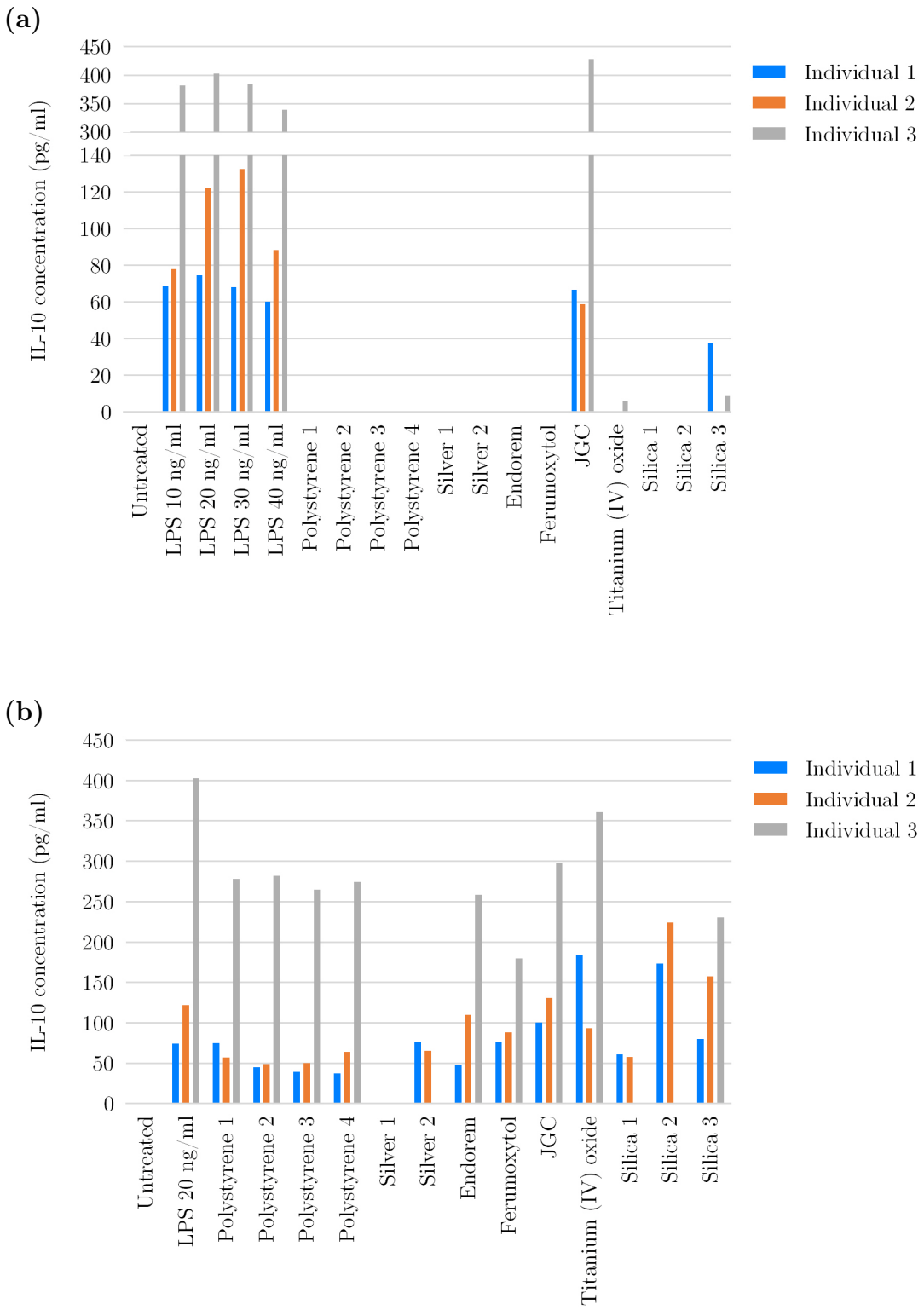

Figure 4.3: Concentrations of cytokine IL-10 secreted by peripheral blood mononuclear cells in response to (a) Treatment with LPS, or stated nanomaterials. (b) Combined LPS treatment with stated nanomaterials. Data displayed as average (n = 2).

4.3.2 IL-1β ELISA

Figure 4.4 displays the standard curve used to calculate the IL-1β concentrations in treated samples as described in Section 4.2.4.2. The standard curve was validated by the calculated concentration of IL-1β control included with the kit falling within the range stated by the kit protocol.

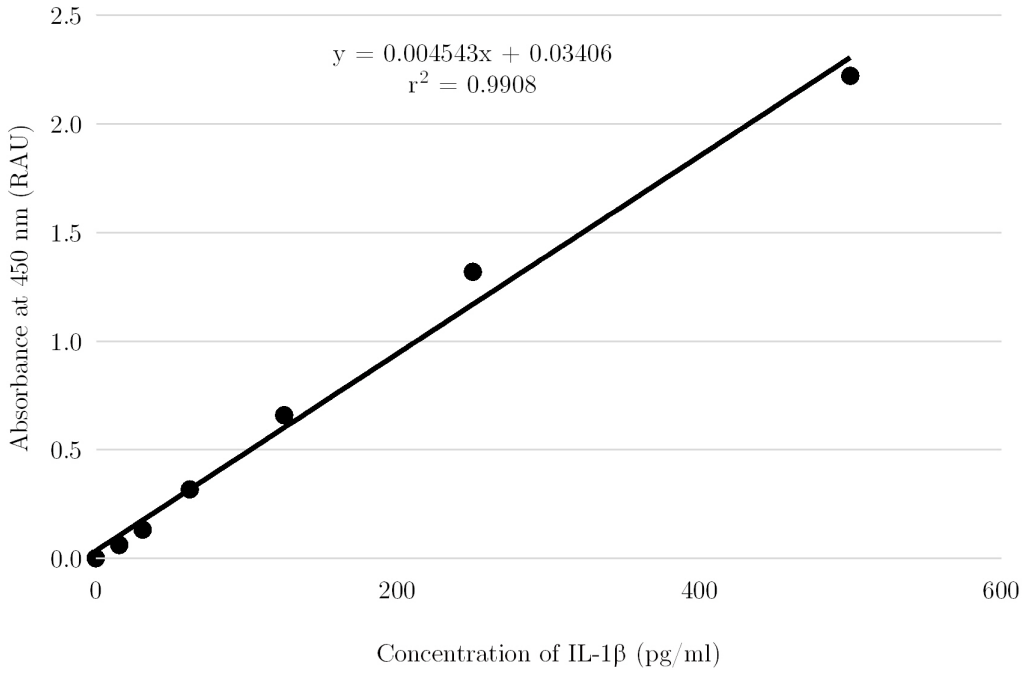

Figure 4.4: Standard curve prepared from standards provided with the Human IL-1 beta ELISA Kit, used to calculate IL-1β concentrations. Data displayed as average (n = 2).

Treatment of PBMCs from all individuals with either LPS or MSU resulted in significantly more IL-1β ($p = <0.0001$) than that of the untreated control (Figure 4.5a). Furthermore, LPS-primed PBMCs treated with MSU generated IL-1β concentrations greater than that by LPS or MSU in isolation.

The untreated controls of the assay represented in Figure 4.5c did not contain a quantifiable concentration of IL-1β. As such it was not possible to calculate fold difference or perform statistical analysis on these samples.

The response of individual 4, as shown in Figure 4.5b, to treatments with solely LPS and MSU would indicate a pre-existing sensitivity potentially due to immune priming or TLR4 activation. Similar was observed in the LPS treatment of individuals 1 and 2 in the subsequent assay (Figure 4.5c)

Chloroquine and wortmannin treatment of LPS-primed PBMCs in individual 1 resulted in near-identical concentrations of IL-1β; 414.96 pg/ml and 413.61 pg/ml respectively (Figure 4.5a). Chloroquine-treatment in individual 2 produced 15 pg/ml more IL-1β than in the combined positive control. Treatment with wortmannin resulted in all individuals displaying concentrations less than that of the combined positive control.

An average four-times lower IL-1β concentration ($p = <0.0001$) was found in treatment with LPS, MSU, and rapamycin, compared to that of LPS and MSU (Figure 4.5b).

The IL-1β concentrations generated in response to silica 3 demonstrated a high degree of similarity to that of the combined control in all individuals (Figure 4.5c). Treatment with silica 2 of LPS-primed PBMCs resulted in comparable IL-1β concentrations generated by individuals 1, 2, and 3, however individual 4 generated a concentration 5-fold less than that of the corresponding combined positive control. Silica 1 treatment generated IL-1β concentrations similar to that of treatment solely with LPS in all individuals.

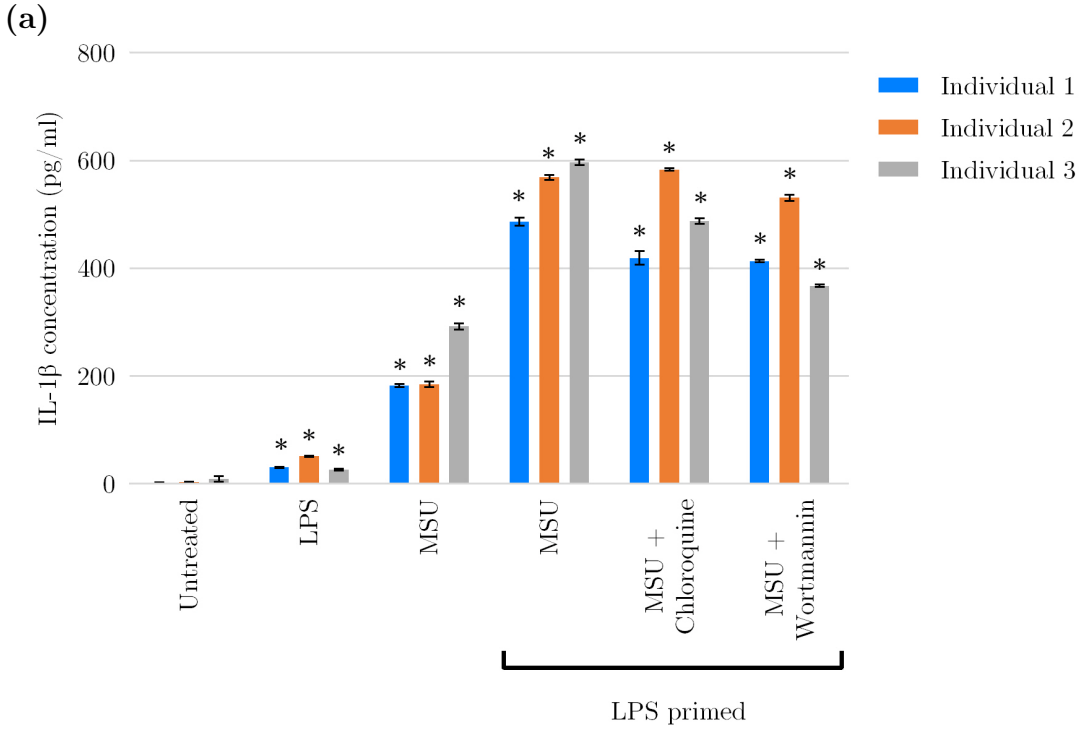
(a)
IL-1β concentration (pg/ml)
800
600
400
200
0
Individual 1
Individual 2
Individual 3
Untreated
LPS
MSU
MSU
MSU + Chloroquine
MSU + Wortmannin
LPS primed

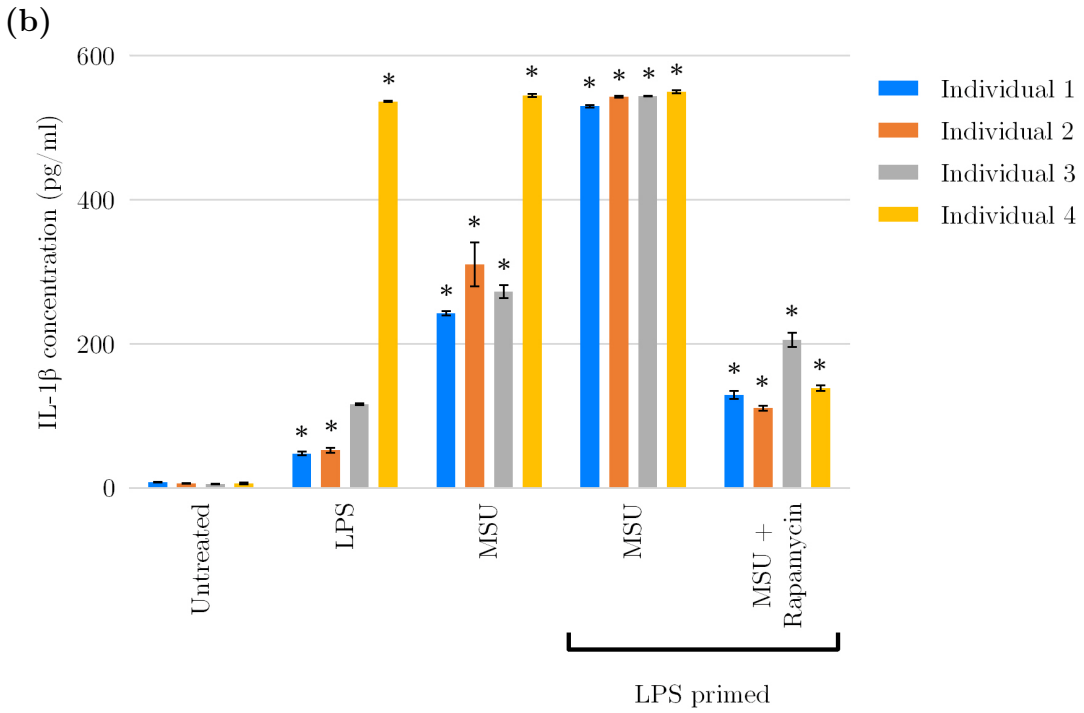
(b)
IL-1β concentration (pg/ml)
600
400
200
0
Individual 1
Individual 2
Individual 3
Individual 4
Untreated
LPS
MSU
MSU
MSU + Rapamycin
LPS primed

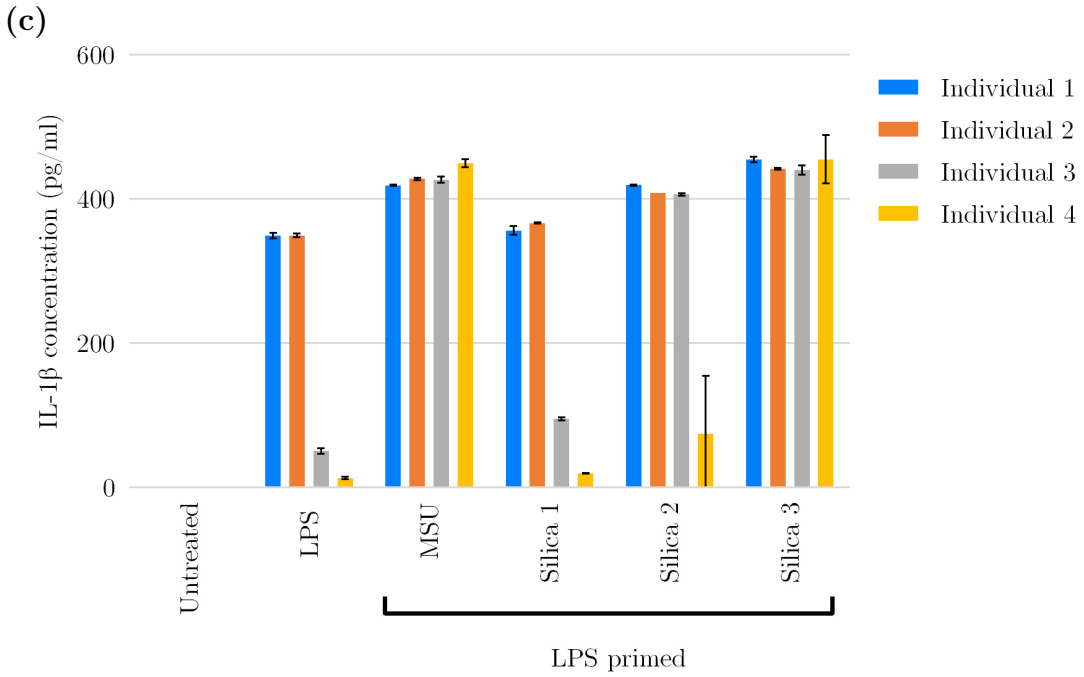

Figure 4.5: IL-1β concentrations generated by treatments with positive controls, and stated nanomaterials. LPS-primed samples were treated with 20ng/ml for 2 hours prior to the addition of further materials. Data displayed as average (n = 3) ± standard deviation. * p-value <0.05.

4.3.3 Inhibition of caspase-1

The caspase-1 inhibitor (Z-VAD-FMK), provided with the kit as a positive control, reduced caspase-1 function by 92.5% (p = <0.0001).

All treatments demonstrated significant inhibition of caspase-1 (p = <0.0001) with the exception of VX765, which had no effect on caspase-1 activity compared to the untreated control. Efavirenz and Lopinavir inhibited caspase-1 activity by 35.3% (p = 0.0130) and 27% (p = 0.0013) respectively. Negatively charged sulphonate-functionalized polystyrenes 2, 4, and 6 demonstrated increasing inhibition of caspase-1 (23%, 28.6%, and 38%) consistent with their increasing size. This trend was absent, however, in quaternary amine-functionalized polystyrenes 1, 3, and 5 (Figure 4.6). Of these materials the greatest effect was demonstrated by polystyrene 3 (275 nm manufacturer provided size) inhibiting caspase-1 by 34.4%. No significant difference between the effects of Efavirenz or Lopinavir and those of the polystyrene nanoparticles was found.

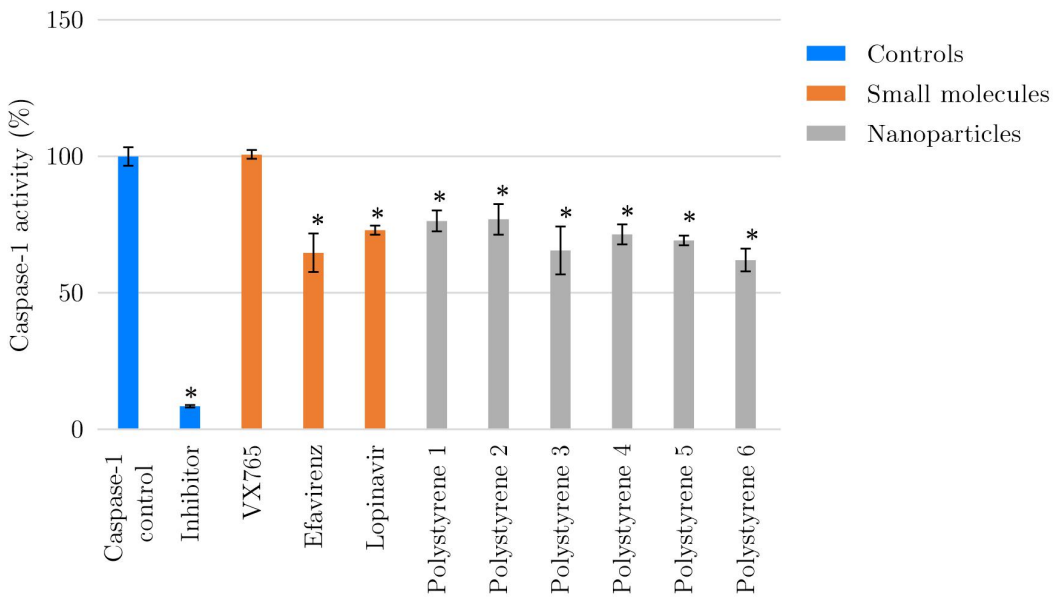

Figure 4.6: Caspase-1 activity displayed as a percentage of total activity in caspase-1 control, following treatments with small molecules, and stated nanomaterials. Data displayed as average (n = 3) ± standard deviation. * p-value <0.05.

4.3.4 Leukocyte proliferation

Silica 2, the largest sized silica nanoparticle at 310 nm (manufacturer's provided size), resulted in a 93% increase in proliferation compared to the untreated control ($p = <0.01$). No other nanomaterial treatments resulted in significant change ($p < 0.05$) from that of the unstimulated control (Figure 4.7a).

Significant change in proliferation of PHA-stimulated nanomaterial treatments was only observed for silver 1 where no viable cellular presence was found ($p < 0.0001$). No other nanomaterial treatments of PHA-stimulated PBMCs resulted in significant change ($p < 0.05$) from that of the PHA-stimulated control (Figure 4.7b).

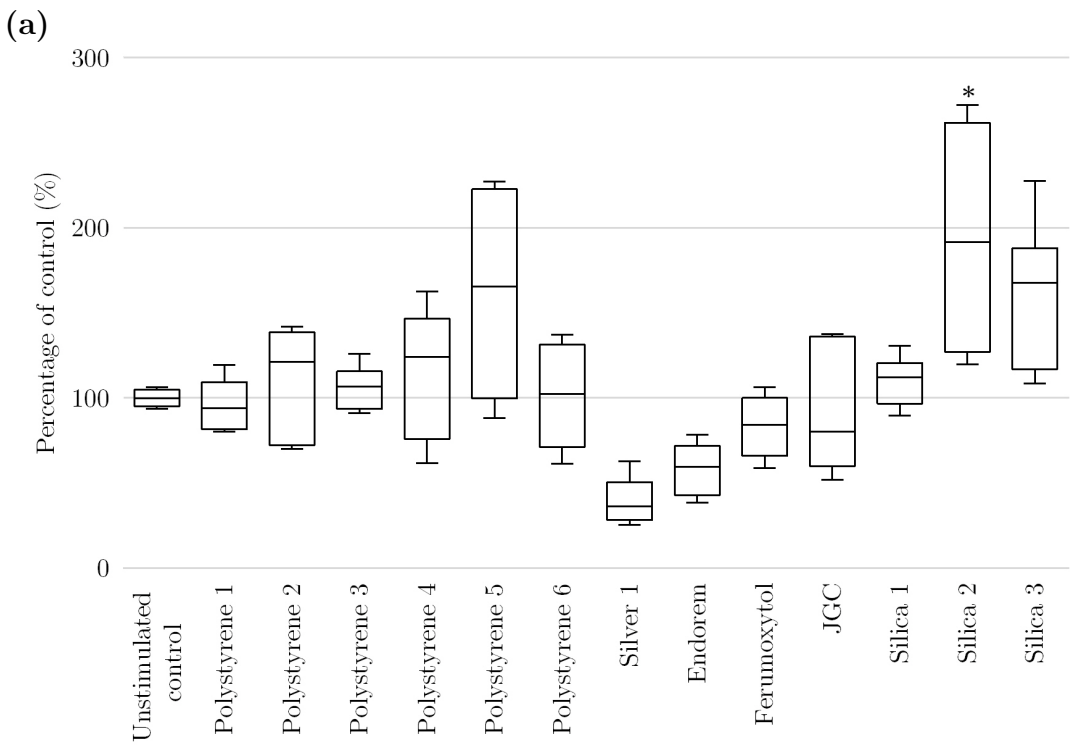

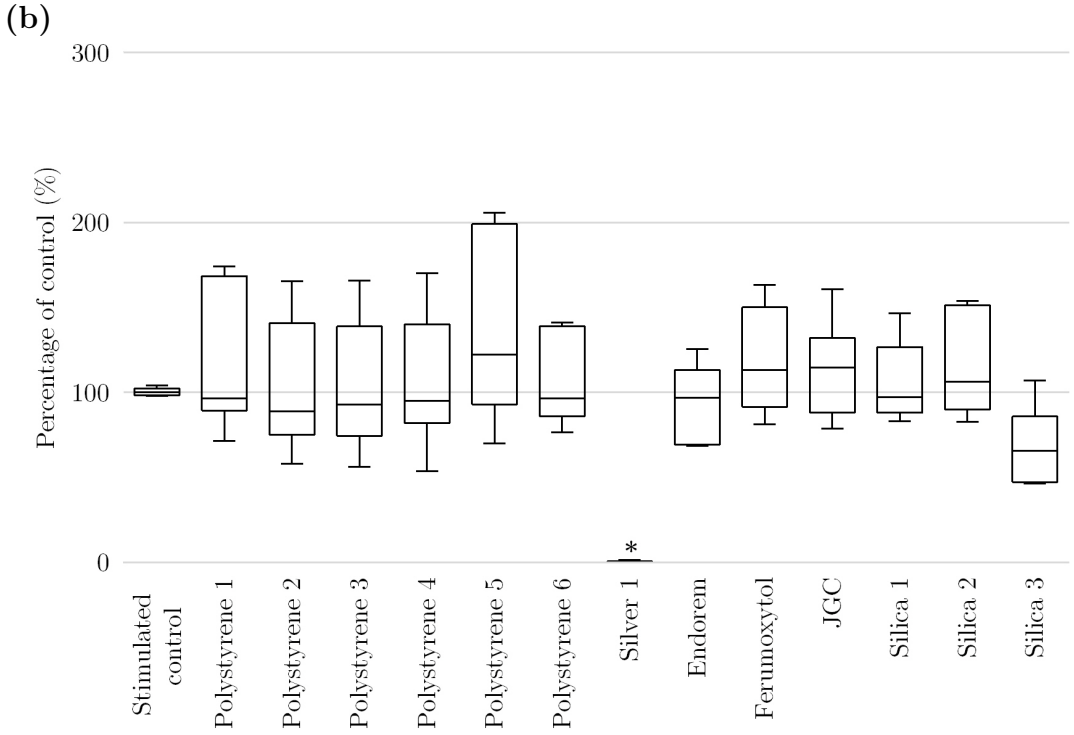

Figure 4.7: Proliferation of peripheral blood mononuclear cells, as a percentage of controls, following treatment with (a) Stated nanomaterials. (b) Combined treatment with PHA and stated nanomaterials. Data displayed as box and whisker plots showing average, maximum, and minimum (n = 6) ± standard deviation. * p-value <0.05.

4.4 Discussion

The interplay of cytokines *in vivo* involves a highly complex, multicomponent system, in which secretion of cytokines from various cells can generate, suppress, or recruit further cell types to the site of inflammation. Dysregulation of cytokine balance is a hallmark of numerous diseased states (Elenkov et al., 2005), but also a source of opportunity for exploitation in the rational design of nanoparticles for nanomedicine.

Thorough assessment of the potential modulation of cytokine profiles by new drugs and therapies has been highlighted by the outcomes of the phase 1 clinical trial of TGN1412, an anti-CD23 monoclonal antibody. Six volunteers received a dose 0.1 mg of TGN1412 per kilogram of body weight (Suntharalingam et al., 2006), 500 times smaller than that deemed safe by preclinical animal studies (Attarwala, 2010). Following infusion, a series of adverse effects involving multiple organ failure were elicited by unexpected cytokine release (Attarwala, 2010). The "cytokine storm", a term coined by Aikawa (1996), is the elevation of both proinflammatory and anti-inflammatory cytokines leading to the deleterious effects observed in the trial. It is important to note that the systemic inflammatory response generated by TGN1412 was in the absence of contaminating organic factors (MHRA, 2006). The cytokine storm to this drug was not observed in the preclinical studies performed in rats and cynomolgus monkeys (Suntharalingam et al., 2006), but would have been detected using an *in vitro* cytokine release assay in primary human blood (Stebbings et al., 2007).

IL-1β is a marker for pyrogenic response and the intentional design of materials to stimulate its production *in vivo* is of great interest for vaccine development (Xiang et al., 2012). Iron oxide nanoparticles have been demonstrated as having great potential in this area. Pusic et al. have described murine dendritic cells treated with <20 nm carboxyl-functionalized nanoparticles resulted in the gener-

ation of a range of cytokines including IL-1β, TNFα, and IFNγ (Pusic et al., 2013). Ferumoxytol, a 30 nm (manufacturer provided size) carboxyl-functionalized iron oxide nanoparticle, was not found to generate secretion of any tested cytokines under the experimental conditions described in this work. Ferumoxytol possesses a negative zeta potential which is still present in complex media (-10.8 mV in RPMI-1640 supplemented 10% with FBS). While it can be assumed that the iron oxide nanoparticles assessed by Pusic et al. were also of negative charge, their qualitative determination of charge by gel electrophoresis does not provide sufficient evidence for comparison. The only iron oxide nanoparticle from the chosen panel which resulted in an increased production of cytokines, without LPS stimulation, was JGC (diethylaminoethyl dextran coated, 52.3 nm manufacturer provided hydrodynamic size). Similar to the observations in the study by Pusic et al., JGC was found to increase IL-1β and TNFα compared to untreated control. Unlike the described study, treatment with JGC did not generate IFNγ to a concentration detectable via the multiplex methodology used (>6.93 pg/ml).

As discussed in Section 1.5.3, proinflammatory cytokines IL-1β and TNFα are known to induce coagulation via the extrinsic pathway via thrombin (FIIa) generation (Chu, 2011) by induction of tissue factor on endothelial cells and monocytes (Johnson et al., 1996). Only two of the tested materials demonstrated elevation in the concentration of secretion of both IL-1β and TNFα in PBMCs from all three individuals, namely JGC and silica 3. No notable change was observed in coagulation time via this pathway for silica. JGC was found to have the opposite effect on this pathway, generating a 1.4 second increase in coagulation time (Figure 3.2a). The assessment of nanomaterial impact on coagulation described in Section 3.2.2.2 was performed under cell-free conditions. Cellular presence is required for the generation of cytokines and, furthermore, the extrinsic coagulation pathway is initiated via damage to red blood cells. The cell-free method used for assessing plasma coagulation should, therefore, not be sensitive to such

an effect. Further assessment of this property in a cell-based coagulation assay would be of interest in future work. While JGC has generated a similar cytokine response to those described by observations of Johnson et al., their data was generated in response to LPS (Johnson et al., 1996). Combined nanomaterial and LPS treatment demonstrated generation of IL-1β and TNFα by all materials, with the exception of silver 1. It would be interesting in further study to observe the effects of combined nanomaterial and LPS treatment on coagulation times in the PT assay to determine the extent of influence that nanomaterial presence would have.

TNFα, IL-1β, and IL-10 are known to be stimulated by LPS in PBMCs (Jansky et al., 2003). Our data supports this observation while also confirming the lack of influence over IFNγ. In order to thoroughly assess the potential inhibitory effects of nanomaterials on the type II interferon IFNγ, use of a different stimulator would be invaluable. PHA is a known IFNγ stimulator (Dobrovolskaia, 2015), in addition to IL-2, and GM-CSF (De Groote et al., 1992). In this work, however, PHA was utilised for its action as a mitogen. When comparing the mitogenic potential of PHA to that of tested nanomaterials it must be noted that its rate, and mode of action is different, involving binding to T cell membranes (Movafagh et al., 2011). Additionally PHA increases membrane permeability (Segel et al., 1979) and while it's commonplace use to assess nanoparticle-related proliferation inhibition (Dobrovolskaia, 2015) in the co-incubation manner utilised here, this effect may alter the rate and/or mechanism of nanoparticle uptake, compared to that in cells not been stimulated with PHA. No literature has been found to investigate the potential for this effect in comparison it to other mitogenic compounds.

Silver 1 generated cytotoxic effect in PHA-stimulated PBMCs at the 48 hour time point, being the only material to do so. Cytotoxicity testing performed in Section 5.2.3 did not highlight any cause for concern in the THP1 or CEM cell

lines following 24 hours exposure. In order to better understand this mechanism, similar testing should be performed in PBMCs at the time point used in this assay. Furthermore, the synergistic action of PHA with silver 1 warrants further evaluation as toxicity at a significant level was not observed in unstimulated PBMCs treated with this nanomaterial.

In order to perform a valid statistical analysis of the impact of nanomaterials on the generation of cytokines measured via multiplex assay (Section 4.3.1) further replicates would be needed. Material availability at the time of assessment limited analysis to duplicate measurements. Increased replicates and a higher number of donor samples would provide a deeper understanding of the effects generated by the tested nanomaterials, as well as provide deeper insight into interindividual variability in responses.

NLRP3 inflammasome induction is indicated by secretion of IL-1β (Franchi et al., 2009). This process requires two distinct signals; a priming signal which leads to the transcriptional upregulation and synthesis of pro-IL-1β, and a second signal activating the NLRP3 inflammasome resulting in IL-1β maturation and secretion (Jo et al., 2016; Latz et al., 2013). This is well exemplified by the IL-1β concentration generated in response to the combined positive control, when compared to solely LPS and MSU treatments.

Silica nanoparticles have been associated with the activation of the NLRP3 inflammasome (Dostert et al., 2008; Hornung et al., 2008; Yazdi et al., 2010). Treatment of LPS-primed PBMCs with silica 3 was found to generate IL-1β concentrations highly similar to that observed in the combined positive control in all individuals. It has been shown previously that sub-micron sized silica particles induce higher levels of IL-1β production as a result of lysosomal dysfunction than those of larger sizes (Kusaka et al., 2014). Silica 3 is known to be the largest of the three tested silica nanoparticles (1062.60 nm). The contradictory result obtained here compared to that described by Kusaka et al. would imply that size

is not the only determinant in this effect. All three silica nanoparticles displayed near-identical zeta potential in RPMI-1640 supplemented 10% with FBS. Silicas 1 and 2 are known to be stabilised with L-arginine, however the stabilisation applied to silica 3 is unknown.

Recently the link between autophagy and regulation of the inflammasome has been established (Yuk and Jo, 2013). IL-1β induces autophagy (Harris, 2011), which in turn regulates endogenous inflammasome activators, inflammasome components, and pro-IL-1β (Harris, 2013; Harris et al., 2011).

The observation that the combined positive controls of LPS and MSU when further treated with the autophagy inducer rapamycin led to a lower concentration of IL-1β than that of solely the combined control is supported by observations by Harris et al., where induction of autophagy in mice with rapamycin reduced serum levels of IL-1β in response to challenge with LPS (Harris et al., 2011).

Chloroquine, an autophagy inhibitor and inducer of lysosomal damage, has been shown previously to activate caspase-1 in an *in vivo* LPS-stimulated mouse model (Shin et al., 2013). Such an effect was not observed in this work, wherein samples from two out of three individuals demonstrated less IL-1β concentration than the combined positive control. Furthermore, the PI3K autophagy inhibitor wortmannin has been evidenced to not affect inflammasome activation (Ghonime et al., 2014). The highly similar response to treatment with wortmannin as with chloroquine, under the tested conditions in this work, would contradict this. This difference may be due to the use of MSU as a confirmatory signal here, while the study by Ghonime et al. utilised ATP for this purpose (Ghonime et al., 2014).

VX-765 is a prodrug requiring conversion by plasma and liver esterases to the active VRT-043198, a potent caspase-1 inhibitor (Stack et al., 2005). The lack of enzymatic conversion validates the absence of observable caspase-1 activity in the chosen cell-free assay.

Efavirenz, a non-nucleoside reverse-transcriptase inhibitor, has been shown to

prevent activation of caspase-1 and caspase-3 in CD4 T cells (Doitsh et al., 2014). The inhibition of cell-free caspase-1 activity observed here demonstrates direct influence of Efavirenz on the enzyme.

Lopinavir, an antiretroviral protease inhibitor, is known to induce apoptosis via suppression of NF-κB (Kariya et al., 2014). NF-κB plays a role in coordinating innate and adaptive immunity, and controls the expression of several proinflammatory cytokines and upregulation of costimulatory molecules on dendritic cells, which are required for T cells activation (Elsabahy and Wooley, 2013). Caspase-1 has been shown to play a role in the activation of NF-κB (Lamkanfi et al., 2004). The apoptotic mechanism of Lopinavir described by Kariya et al. was shown to be caspase-dependent (Kariya et al., 2014). The inhibition of caspase-1 described in this chapter would support this mechanism, however further evaluation of the apoptotic potential of lopinavir under the conditions utilised are required.

Lunov et al. have described 100 nm amino-functionalized polystyrene nanoparticles, but not carboxy- or non-functionalized of the same size, to activate caspase-1 through ROS generation following lysosomal destabilisation (Lunov et al., 2011). The quaternary ammonium- (polystyrenes 1, 3, 5) and sulphonate- (polystyrenes 2, 4, 6) functionalized polystyrene nanoparticles, of varying sizes, assessed in this chapter all demonstrated a highly similar inhibitory effect toward caspase-1. The cell-free nature of the assay design shows that inhibition of caspase-1 by polystyrene nanoparticles is a direct interaction of the material, and not the result of further nanoparticle-related effects. This too may be the case but would require further investigation. By utilising this methodology, it can be elucidated whether inhibition of caspase-1 is a result of nanomaterials directly on caspase-1, or whether there is an interaction with the mechanisms required for its generation.

In addition to consistency with examples in the literature (Liptrott et al., 2014), the decision to utilise uptake of radioactive thymidine over other colourimetric methodologies was to negate any potential interference effects that nano-

materials may pose on the assays without excess wash steps, as highlighted in Section 1.6.2.

Being able to assess the potential recruitment of other cell types which may modulate an inflammatory response to nanoparticles *in vivo* would be of great advantage in current and future perspectives in order to extrapolate *in vitro* observations to *in vivo* outcomes. As mentioned previously, the ability to assess new nanomaterials in a high throughput manner is of great interest, not only to the scientific community, but also to those developing these materials with intent to bring them to commercial market by reducing potential bottlenecks which occur as a result of lengthy assessment procedures.

The use of cell lines for *in vitro* assays is built on a number of advantages including their cost effectiveness, ease of amplification, they do not raise the same ethical concerns as using human or animal tissue, and they reasonably simulate the function of their primary, non-immortalised counterparts. It is well known that through genetic manipulation, the phenotype of cell lines may be altered, including their functionality and responsiveness to stimuli (Kaur and Dufour, 2012). Increasing time in culture and passage number can exacerbate this effect, as well as introducing heterogeneity within cultures.

While there is an ever increasing number of strategies to try to overcome these issues (Luebke, 2012), the use of freshly isolated primary cells provides the most accurate representation of the *in vivo* response that may be generated toward nanoparticles. Such an advantage does exist parallel to the main limitation of using such a strategy, namely interindividual variability (Pfaller et al., 2010) as demonstrated by the data presented in this chapter. Although often described as a limitation, this variability is important to try to identify specific interactions in individuals. The interindividual variability of PBMC cultures is known to be higher than that of whole blood (De Groote et al., 1992). The authors also point out that the potential for cytokine production is highest in whole blood, or PBMC

cultures where the cell density matches that of whole blood. While simulating such physiological conditions may be the ideal scenario, it lends further technical complications *in vitro*, and when considering working with precious nanomaterials where only limited quantities are available. This kind of assay design would be best suited to materials which have a known *in vivo* dosage. However, this information is not readily available for nanomaterials not intended for clinical use, or unloaded nanocarriers whose dosage would be determined by the loading efficiency of the associated drug.

Accounting for this interindividual variability is a concern which has two main proposed solutions. The first of which is to increasing sample size, through which greater statistical power may be achieved, and variability will be inherently reduced. The crux of this approach is summarised by the question; how large a cohort is necessary to alleviate interindividual variability? Additionally, this method adds to the ethical concerns, difficulty in finding sufficient numbers of volunteers, as well as the cost of materials for collection and processing. This is the case for any clinical study and a great deal of guidance in the literature exists to inform researchers in their calculations of sample size (Charan and Biswas, 2013).

It is well known that factors including time of sampling (chrono-immunology) (Geiger et al., 2015), age (Weiskopf et al., 2009), gender (Klein and Flanagan, 2016), diet (Marcos et al., 2003), medications and pre-existing conditions, all affect the immune system. These in turn may modulate the manner, and magnitude, of any immune responses toward challenge by nanomaterials. The alternative, without performing a large scale clinical study in which all environmental factors can be observed and potentially controlled, is to perform immunophenotypic, and potentially genotypic, analysis on donors in addition to the assays of interest. The advantages of this would not only be limited to the interpretation of data generated, but in the subsequent dissemination of results to the scientific

community.

Already there exist calls from researchers and governing bodies for minimum reports of physicochemical details and experimental conditions (Hendren et al., 2015). Further demographics of the sources of primary samples would only aid in the efforts to create truly transferable datasets (Rösslein et al., 2016). Efforts to catalogue existing information to databases, such as caNanoLab (https://cananolab.nci.nih.gov/caNanoLab/), exemplify the need for standardisation in the presentation of information surrounding generated data, which is commonly excluded in order to comply with the conventions of publication. While this is necessary in the current scientific climate, the outlook for high powered computation of the associations between physicochemical characteristics and immunological effects requires these considerations to be taken sooner rather than later.

Chapter 5

Development and optimisation of *in vitro* cellular health and cytotoxicity protocols

Contents

5.1 Introduction 155

5.2 Methods 158

5.2.1 Materials 158

5.2.2 Routine cell culture 158

5.2.3 Cytotoxicity of nanomaterials 159

5.2.3.1 MTT assay 159

5.2.3.2 LDH assay 160

5.2.3.3 Calculations 162

5.2.4 Assessment of cellular health 163

5.2.4.1 Reactive oxygen species generation 163

5.2.4.2 Measurement of reduced glutathione 163

5.2.4.3 Autophagy 165

5.2.5 Development of kinetic assessment assays for cellular health 166

5.2.5.1 Kinetic application of ROS and glutathione fluorescent probes 166

5.2.5.2 Calculations 167

5.2.6 Statistical analysis 167

5.3 Results 169

5.3.1 Cytotoxicity of nanomaterials 169

5.3.1.1 MTT assay 169

5.3.1.2 LDH assay 175

5.3.2 Assessment of cellular health 176

5.3.2.1 Reactive oxygen species generation 176

5.3.2.2 Measurement of reduced glutathione 181

5.3.2.3 Autophagy 185

5.3.3 Development of kinetic assessment assays for cellular health 191

5.3.3.1 Kinetic assessment of reactive oxygen species . . 191

5.3.3.2 Kinetic measurement of reduced glutathione . . . 195

5.4 Discussion 196

5.1 Introduction

Engineered nanomaterials can be composed of substances which, at the macro scale, are well characterised. It should not be assumed, however, that if the components of the nanoparticle are deemed safe in bulk that they will not be subject to quantum size effects which may impart them with greater reactivity or potential toxicity (De Jong and Borm, 2008). Gold is a commonly used example for illustrating this point; where at the bulk scale it is chemically inert, but at the nano-scale has potential for reactivity and cytotoxicity (Alkilany and Murphy, 2010).

Commonly evaluated measures of cellular health *in vitro* focus on metabolic function. Intrinsically linked to this is the oxidative balance which most simply is divided into prooxidant and antioxidant mechanisms. Prooxidant mechanisms relate to the generation of reactive oxygen species which, under normal circumstances, are endogenously generated through processes such as mitochondrial function, and are vital in homeostasis, cell signalling (Ray et al., 2012), and inflammatory function of phagocytes (Robinson, 2008). Cellular antioxidants are comprised of low molecular weight free radical scavengers; reduced glutathione, α-tocopherol, thioredoxins, and ascorbic acid, as well as enzymatic defences; superoxide dismutase, catalase, and glutathione peroxidase (El-Ansary et al., 2014).

Overproduction of ROS and/or a deficiency of antioxidants can result in disturbance to the equilibrium leading to deleterious outcomes, termed oxidative stress (Burton and Jauniaux, 2011).

Excessive ROS can cause damage to proteins, nucleic acids, cellular lipids, and other macromolecules inhibiting their normal functions (El-Ansary et al., 2014). Production of reactive oxygen species is one of the primary hallmarks of inflammation and has been shown to be a principal mechanism for nanoparticle incompatibility (Manke et al., 2013), and has been attributed to a range of

nanoparticle physicochemical characteristics including size, shape, surface functionalization/stabilisation, oxidation status, and aggregation state (Fu et al., 2014). Literature associates high surface charge, as well as smaller nanoparticle size, to the induction of higher levels of ROS (Manke et al., 2013).

While increased production of ROS is of concern, impaired elimination of free radicals leads to increased oxidative stress (Anreddy et al., 2013). Glutathione plays a highly important role as an intracellular defence mechanism against the damaging effects related to ROS (Mytilineou et al., 2002). In aerobic cells it is the most abundant antioxidant; present in micromolar and millimolar concentrations in bodily fluids and tissue respectively (Owen and Butterfield, 2010), and displays even subcellular distribution (Ault and Lawrence, 2003). The ratio of oxidized glutathione (GSSG) to the reduced form (GSH) has been established as a dynamic indicator of oxidative stress (Jones, 2002). Silver (Piao et al., 2011) and gold nanoparticles (Khan et al., 2012) have been shown to influence glutathione based antioxidant mechanisms resulting in oxidative stress via lipid peroxidation (Khan et al., 2012).

The link between ROS and autophagy has gained interest in recent years (Azad et al., 2009; Filomeni et al., 2015; Gibson, 2013). Autophagy is a lysosomal degradation pathway which plays a role in maintaining homeostasis within the cell accomplished by degrading cytoplasmic components such as damaged organelles or unused/misfolded/aggregated proteins, balancing and recycling sources of energy when cells experience nutrient starvation and or stress, and eliminating intracellular pathogens (Meijer and Codogno, 2004). Reactive oxygen species have been found to induce autophagy via mTOR activation, Beclin-1 upregulation, p53, p62, and oxidation of Atg4 (Gibson, 2013). ROS-induced autophagy has also been shown to be repressed by NF-κB by regulating TNFα-induced macroautophagy (Djavaheri-Mergny et al., 2007). Cell death can be caused when autophagy becomes dysregulated (He and Klionsky, 2009). This can result

from either excessive/chronic autophagy, or by insufficient/defective autophagy (Levine and Kroemer, 2008). Nanoparticle-induced autophagy has been associated with a growing number of nanomaterials, while disruption of the autophagic process has been described via mechanisms including cytoskeleton disruption by multiwalled-carbon nanotubes, copper oxide, silver, and silica nanoparticles, and lysosomal dysfunction through defects and modulation of pH by single-walled carbon nanotubes, graphene oxide, and gold nanoparticles in cell lines including THP1, A549, and human umbilical vein endothelial cells (Cohignac et al., 2014; Stern et al., 2012).

The aims of this chapter were to assess the cytotoxicity of test materials in human cell lines, specifically models of T-lymphocytes (CEM) and monocytes (THP-1). Cytotoxicity values (CC_{50}) are particularly important for subsequent analysis to ensure cell death is not a major confounding factor in functional assays. This was achieved using two assays; the outcome of which provided a measure of cytotoxicity, but each via a differing mechanism. These assays, namely MTT and LDH, provide measures of mitochondrial function and cell membrane integrity, respectively. The impact of the nanomaterial library on cellular health; in particular reactive oxygen species generation, reduced glutathione content, and autophagy was investigated. Associations between physicochemical characteristics and the observed effects were evaluated. The final objective was to assess the suitability of commercially available fluorogenic probes for, and to demonstrate the utility of kinetic measurement of oxidative stress in nanotoxicological assay development.

5.2 Methods

5.2.1 Materials

Phenol red-free RPMI-1640, Thiazolyl blue tetrazolium bromide (MTT) powder, Cytotoxicity Detection KitPLUS (LDH), dimethyl sulfoxide (DMSO), and double-distilled water (DDH_2O) were purchased from Sigma-Aldrich (Dorset, UK). CellROX Green Reagent and ThiolTracker Violet were purchased from Thermo Fisher (Cheshire, UK). CYTO-ID Autophagy Detection Kit was purchased from Enzo Life Sciences (Exeter, UK). MACSQuant running buffer was purchased from Miltenyi Biotec GmbH (Bergisch Gladbach, Germany). CEM, Raji, and THP-1 cell lines were purchased from ECACC (European collection of cell cultures) via Public Health England (Salisbury, UK).

5.2.2 Routine cell culture

CEM, Raji, and THP-1 cell lines were cultured in RPMI-1640 supplemented with FBS to 10% final volume, at 37°C with 5% CO_2.

Medium renewal protocol was identical for all three cell lines; cell suspensions were transferred to 50 ml universal tubes and centrifuged for 5 minutes at 2000 rpm. Supernatant was discarded, and cells suspended in 30 ml of pre-warmed (37°C) culture medium.

Viable cell counts were performed using a NucleoCounter NC-100 (ChemoMetec, Allerod, Denmark) following the manufacturer's guidelines. Total cell count was performed by combining equal volumes of cell suspension, Reagent A100 (ChemoMetec), and Reagent B (ChemoMetec) in a microcentrifuge tube. This was mixed by vortex for 5 seconds prior to loading to a NucleoCassette (ChemoMetec). The 1:3 dilution was accounted for when determining final cell count. Cell count of non-viable cells was performed by directly the loading cell suspension to

a NucleoCassette. Viable cell count was calculated by subtracting the non-viable cell count from the total cell count.

THP-1 and CEM, cell cultures were corrected to a density of 2×10^5 viable cells/ml and subcultured when density reached 8×10^5 cells/ml. Raji cell cultures were corrected to a density of 4×10^5 viable cells/ml and subcultured when density reached 1×10^6 cells/ml. Medium renewal/subculturing was performed every 2-3 days.

5.2.3 Cytotoxicity of nanomaterials

5.2.3.1 MTT assay

MTT assay was performed on THP-1 and CEM cell lines. Cells were seeded in 96 well microplates at a density of 5×10^4 per well in 100 µl medium. Blank (RPMI-1640 supplemented with FBS to 10% final volume), and negative control wells of untreated cells were prepared. In test wells; nanomaterials or the positive control vinblastine were added at the maximum concentrations listed in Table 5.1, followed by eight subsequent 1:2 serial dilutions across the plate. All conditions were prepared to a total of eight replicates. Plates were incubated at 37°C, 5% CO_2 for 24 hours. 20% well volume of MTT reagent (5 mg/ml in DPBS) was added to all wells and incubated for two hours. An equal volume of lysis buffer (20% SDS in 50:50 water:DMF) was added to all wells and incubated for 18 hours (37°C, 5% CO_2). Lysis was performed to solubilise the crystalline formazan produced within cells to provide a homogeneous solution within each well. Prior to reading, plates were subjected to orbital shaking for 60 seconds to ensure even distribution of colour throughout samples. Absorbance was measured on a plate reader (CLARIOstar, BMG Labtech, Ortenberg, Germany) at 560 nm wavelength.

To assess nanomaterial interference with the MTT assay, cell-free preparations

were performed under identical conditions to those described above. Material choices for this test were informed by data from the cell-based assay.

5.2.3.2 LDH assay

LDH assay was performed in the THP-1 cell line. Plate layout for this assay was designed following the protocol of the Cytotoxicity Detection KitPLUS (LDH). Cells were seeded in 96 well microplates at a density of 5×10^4 per well in 100 µl medium. Blank control wells of 100 µl of culture medium corresponding to each cell-containing well were prepared.

Nanomaterials were added at the maximum concentrations listed in Table 5.1 followed by eight subsequent 1:2 serial dilutions across the plate in cell and cell-free wells, prepared in triplicate. Wells allocated for untreated (Low control) and treatments with either Triton X-100 or lysis buffer (High control) were included. Following 24 hours incubation at 37°C and 5% CO_2, plates were centrifuged for 5 minutes at 2000 rpm. The supernatants of wells to be treated with Triton X-100 were aspirated and replaced with 200 µl of Triton X-100 (1% in culture medium). 100 µl of fresh culture media was added to all nanomaterial-treated wells, controls, and cell-free preparations. All wells were gently resuspended using a multichannel pipette. 5 µl of lysis buffer, provided with the kit, was added to the wells designated High control. This was to demonstrate the maximum LDH activity in the cell cultures. Untreated cells corresponding to the Low control show LDH activity released by cells in untreated conditions. The plate was incubated for 15 minutes (37°C and 5% CO_2), and then centrifuged for 5 minutes at 2000 rpm. In this time the catalyst, included with the kit, was reconstituted in DDH_2O, and mixed thoroughly after 10 minutes. 100 µl of supernatant from each well was transferred to a fresh 96-well microplate. Reaction mixture was prepared by combining 250 µl of catalyst with 11.25 ml of dye solution, 100 µl of which was added to each well and incubated for 20 minutes. 50 µl of stop solution

was added to each well. Prior to reading, plates were subjected to orbital shaking for 60 seconds. Absorbance was measured on a plate reader (CLARIOstar, BMG Labtech, Ortenberg, Germany) at 492 nm wavelength. Cell-free absorbance values were evaluated for inhibition/enhancement by nanomaterials, and subtracted from their corresponding cell-containing wells.

Material	Maximum concentration/dilution
Polystyrene 1	5000 µg/ml
Polystyrene 2	5000 µg/ml
Polystyrene 3	5000 µg/ml
Polystyrene 4	5000 µg/ml
Polystyrene 5	5000 µg/ml
Polystyrene 6	5000 µg/ml
Gold 1	1000 pg/ml
Gold 2	1000 pg/ml
Silver 1	1500 µg/ml
Silver 2	2 µg/ml
Endorem	3000 µg/ml
Ferumoxytol	1100 µg/ml
JGC	121 µg/ml
Titanium (IV) oxide	1000 µg/ml
Zinc oxide 1	1000 µg/ml
Zinc oxide 2	1000 µg/ml
Zinc oxide 3	1000 µg/ml
Silica 1	5000 µg/ml
Silica 2	5000 µg/ml
Silica 3	1000 µg/ml
Liposome	1/10
Emulsion	1/10

Table 5.1: Maximum concentrations and dilution factors of nanomaterials used to assess cytotoxicity.

5.2.3.3 Calculations

CC_{50} (Cytotoxic Concentration 50 - nanoparticle concentration inducing 50% cell mortality) values were determined via nonlinear regression (sigmoidal dose-response curve) using GraphPad Prism 6.

The criteria used to determine a valid concentration-response curve was that the curve followed a sigmoidal shape from which a CC_{50} concentration was able to be generated, and this concentration was below the stock (greatest possible) concentration of the nanomaterial.

5.2.4 Assessment of cellular health

5.2.4.1 Reactive oxygen species generation

THP-1 cells were seeded at 5×10^5 per well in 100 µl of culture medium in 96-well microplates. Untreated control wells were designated, and treatments with nanomaterials at the final concentrations displayed in Table 5.2, and positive control camptothecin (10 µM) were prepared (n = 4). Following 24 hours incubation (37°C, 5% CO_2), staining was performed using CellROX Green. The probe was added to all wells (with the exception of background untreated cells) at a final concentration of 5 µM, and incubated for 30 minutes (37°C, 5% CO_2). The plate was centrifuged at 2000 rpm for 5 minutes, and supernatant removed. Cells were washed in 100 µl DPBS followed by centrifugation, repeated three times. Following the final aspiration, cells were suspended in 100 µl of MACSQuant running buffer (Miltenyi Biotec, Germany) and transferred to a deep well 96-well microplate. Quantification was performed by flow cytometry (MACSQuant, Miltenyi Biotec) using the FITC channel.

5.2.4.2 Measurement of reduced glutathione

THP-1 cells were seeded at 5×10^5 per well in 100 µl of culture medium in 96-well microplates. Untreated control wells were designated, and treatments with nanomaterials at the final concentrations displayed in Table 5.2, and positive control menadione (10 µM) were prepared (n = 4). Following 24 hours incubation (37°C, 5% CO_2), the plate was centrifuged at 2000 rpm for 5 minutes, and supernatant removed. Cells were washed in 100 µl DPBS followed by centrifugation, repeated twice. During the wash procedure ThiolTracker Violet dye was prepared to 20 mM in DMSO, and subsequently to the working concentration of 20 µM in DPBS and warmed. 100 µl of the dye was added to each well and incubated for 30 min-

utes at 37°C and 5% CO_2. The plate was centrifuged at 2000 rpm for 5 minutes, and supernatant removed. Cells were washed in 100 µl DPBS followed by centrifugation, and finally suspended in 100 µl of MACSQuant running buffer. Cell suspensions were transferred to a deep well 96-well microplate. Quantification was performed by flow cytometry (MACSQuant) using the FITC channel.

Material	Final concentration/dilution			
Polystyrene 1	0.1 µg/ml	1 µg/ml	10 µg/ml	100 µg/ml
Polystyrene 2	0.1 µg/ml	1 µg/ml	10 µg/ml	100 µg/ml
Polystyrene 3	0.1 µg/ml	1 µg/ml	10 µg/ml	100 µg/ml
Polystyrene 4	0.1 µg/ml	1 µg/ml	10 µg/ml	100 µg/ml
Polystyrene 5	0.1 µg/ml	1 µg/ml	10 µg/ml	100 µg/ml
Polystyrene 6	0.1 µg/ml	1 µg/ml	10 µg/ml	100 µg/ml
Gold 1	1 pg/ml	10 pg/ml	100 pg/ml	1000 pg/ml
Gold 2	1 pg/ml	10 pg/ml	100 pg/ml	1000 pg/ml
Silver 1	0.1 µg/ml	1 µg/ml	10 µg/ml	100 µg/ml
Silver 2	1 ng/ml	10 ng/ml	100 ng/ml	1000 ng/ml
Endorem	0.1 µg/ml	1 µg/ml	10 µg/ml	100 µg/ml
Ferumoxytol	0.1 µg/ml	1 µg/ml	10 µg/ml	100 µg/ml
JGC	0.1 µg/ml	1 µg/ml	10 µg/ml	100 µg/ml
Titanium (IV) oxide	0.1 µg/ml	1 µg/ml	10 µg/ml	100 µg/ml
Zinc oxide 1	0.1 µg/ml	1 µg/ml	10 µg/ml	100 µg/ml
Zinc oxide 2	0.1 µg/ml	1 µg/ml	10 µg/ml	100 µg/ml
Zinc oxide 3	0.1 µg/ml	1 µg/ml	10 µg/ml	100 µg/ml
Silica 1	0.1 µg/ml	1 µg/ml	10 µg/ml	100 µg/ml
Silica 2	0.1 µg/ml	1 µg/ml	10 µg/ml	100 µg/ml
Silica 3	0.1 µg/ml	1 µg/ml	10 µg/ml	100 µg/ml
Liposome	1/20000	1/2000	1/200	1/20
Emulsion	1/20000	1/2000	1/200	1/20

Table 5.2: Concentrations and dilution factors used to assess reactive oxygen species generation, reduced glutathione, and autophagy.

5.2.4.3 Autophagy

Determination of optimal time points in three cell lines

CEM, Raji, and THP-1 cells were seeded at 5×10^5 cells/well in 100 µl of culture medium (RPMI-1640 supplemented with FBS to 10% final volume) in 96-well microplates. Untreated background, untreated control wells were designated, and experimental wells were treated with rapamycin (0.5 µM), chloroquine (10 µM), or combined rapamycin and chloroquine (0.5 µM and 10 µM respectively). Positive controls were provided with the Cyto-ID Autophagy Detection Kit, and concentrations were chosen in line with recommendation from the assay protocol.

Treatments were performed reverse-chronologically at 30 minutes, 1, 2, 4, 6, and 8 hours in order that staining procedures were identical, and flow cytometric analysis could be performed in the same run to ensure sample comparability. An additional time point of 24 hours was performed in the THP-1 cell line to attain suitable cellular response. During these incubations, cells were maintained at 37°C, 5% CO_2.

Effect of nanomaterial treatments on autophagy

THP-1 cells were seeded at 5×10^5 per well in 100 µl of culture medium in 96-well microplates. Untreated background, and untreated control wells were designated, and treatments with nanomaterials at the final concentrations displayed in Table 5.2, and positive controls; rapamycin (0.5 µM), chloroquine (10 µM), and combined rapamycin and chloroquine were prepared (n = 4). Preparations were incubated for 24 hours at 37°C, 5% CO_2.

Assay procedure

Following incubations; autophagy was assessed using the Cyto-ID Autophagy Detection Kit following the flow cytometry analysis protocol. Plates were centrifuged (5 minutes, 2000 rpm) and washed in 250 µl of assay buffer (prepared by

diluting the concentrate 1:10 with deionized water). Following centrifugation and aspiration of the supernatants, cells were resuspended in 250 µl of assay buffer. CYTO-ID Green Detection Reagent was prepared by diluting 1:1000 in assay buffer. 250 µl of the diluted reagent was added to all wells with the exception of untreated background. Following incubation for 30 minutes (37°C, 5% CO_2), cells were washed once with 250 µl of assay buffer, and resuspended in 500 µl of assay buffer.

Quantification was performed via flow cytometry using a MACSQuant flow cytometer using the FL1 channel.

5.2.5 Development of kinetic assessment assays for cellular health

Medium, designated "kinetic assay medium", was prepared as follows; RPMI-1640 without phenol red indicator was supplemented to 10% final volume with FBS.

The atmospheric control unit (ACU) of the CLARIOstar plate reader was set to 37°C and 5% CO_2 prior to assay preparation to allow conditions to stabilise.

5.2.5.1 Kinetic application of ROS and glutathione fluorescent probes

THP-1 cell culture was transferred to 50 ml universal tubes and centrifuged at 2000 rpm for 5 minutes. The cells were washed in 50 ml of warm HBSS to remove any residual culture medium. The cell pellet was finally resuspended in kinetic assay medium and the cell density brought to 1×10^5 cells/ml as described in Section 5.2.2.

100 µl of this cell suspension was transferred to a 96 well plate in sufficient replicates for untreated control, as well as treatment with menadione at final

concentrations of 2.5, 5, 10, 20, and 40 µM (n = 4). Blank wells containing 100 µl of kinetic assay medium were also prepared.

Reactive oxygen species generation

CellROX Green fluorescent probe was added to all wells at a concentration of 5 µM.

Quantification was performed using a CLARIOstar monochromatic plate reader (BMG Labtech) reading at 485/520 nm Ex/Em every 30 minutes for time courses of 12 and 24 hours.

A further 12-hour assessment following the preparation protocol outlined in Section 5.2.5 was performed where kinetic assay medium was substituted for RPMI-1640 containing phenol red, supplemented to 10% final volume with FBS.

Measurement of reduced glutathione

ThiolTracker Violet fluorescent probe was added to all wells at a concentration of 20 µM.

Quantification was performed using a CLARIOstar monochromatic plate reader (BMG Labtech) reading at 404/526 nm Ex/Em every 30 minutes for 12 hours.

5.2.5.2 Calculations

AUC (area under the curve) in units of fluorescence per litre per hour, C_{max} (maximum fluorescence at each concentration), and T_{max} (time taken to reach maximum signal) were calculated for the 12 hour kinetic assessment of ROS using Microsoft Excel (2013).

5.2.6 Statistical analysis

Statistical analysis was performed using Stats Direct software (Stats Direct Ltd, Cheshire, UK). Distribution of the data was assessed using the Shapiro-Wilk test,

and statistical significance was evaluated by unpaired t-test. Correlation analysis was performed via nonparametric Spearman correlation using GraphPad Prism 6. A p-value <0.05 was considered as statistically significant.

5.3 Results

5.3.1 Cytotoxicity of nanomaterials

5.3.1.1 MTT assay

Of the nanomaterials tested, only zinc oxides 1 and 2 generated valid CC_{50} values under the described conditions in the MTT assay, given the criteria outlined in Section 5.2.3.3. This was true of both CEM (Figures 5.1a and 5.1b) and THP-1 (Figures 5.2a and 5.2b) cell lines. Zinc 1, the smallest (489.33 nm) and most highly charged (-9.64 mV) of the tested zinc oxide nanoparticles in RPMI-1640 10% FBS, demonstrated CC_{50} concentrations 15.7- and 5.4-times less than that of zinc oxide 2 (611.67 nm, -7.04 mV) in CEM and THP-1 cell lines, respectively.

The CC_{50} concentration of zinc 1 determined in CEM (Table 5.3a) was found to be 2.5-fold less than that in THP-1 (Table 5.3b), and zinc 2 being 0.2-fold less. This indicates that the T lymphocyte cell line (CEM) has a greater cytotoxic sensitivity than the human monocytic cell line (THP1).

The positive control vinblastine resulted in a CC_{50} concentration 0.2-fold higher in THP-1 than CEM (Table 5.3), suggesting that the cytotoxic sensitivity of the CEM cell line applies to small molecules in addition to nanomaterials.

Vinblastine, at its greatest impact in THP1 (Figure 5.2c) led to a ~30% reduction in cell viability, compared to 55% in the CEM cell line. In contrast zincs 1 and 2 reduced cell viability by 95% and 85% in CEM, and 94% and 68% in THP1, respectively. The cytotoxic impact of these zinc nanoparticles was, therefore, greater than vinblastine under the conditions assessed in this assay.

An example of a material which did not produce a valid concentration-response curve in either tested cell line is shown in Figures 5.1d and 5.2d where gold 2 (16.71 nm, -12.4 mV) did not generate overt cytotoxicity within the concentration range tested.

(a)

Material	Calculated CC_{50}
Zinc oxide 1	12.63 µg/ml
Zinc oxide 2	198.20 µg/ml
Vinblastine	27.40 ng/ml

(b)

Material	Calculated CC_{50}
Zinc oxide 1	44.45 µg/ml
Zinc oxide 2	240.50 µg/ml
Vinblastine	33.37 ng/ml

Table 5.3: CC_{50} concentrations generated from MTT assay concentration-response curves following 24 hour treatment with stated nanomaterials in (a) CEM cell line. (b) THP-1 cell line.

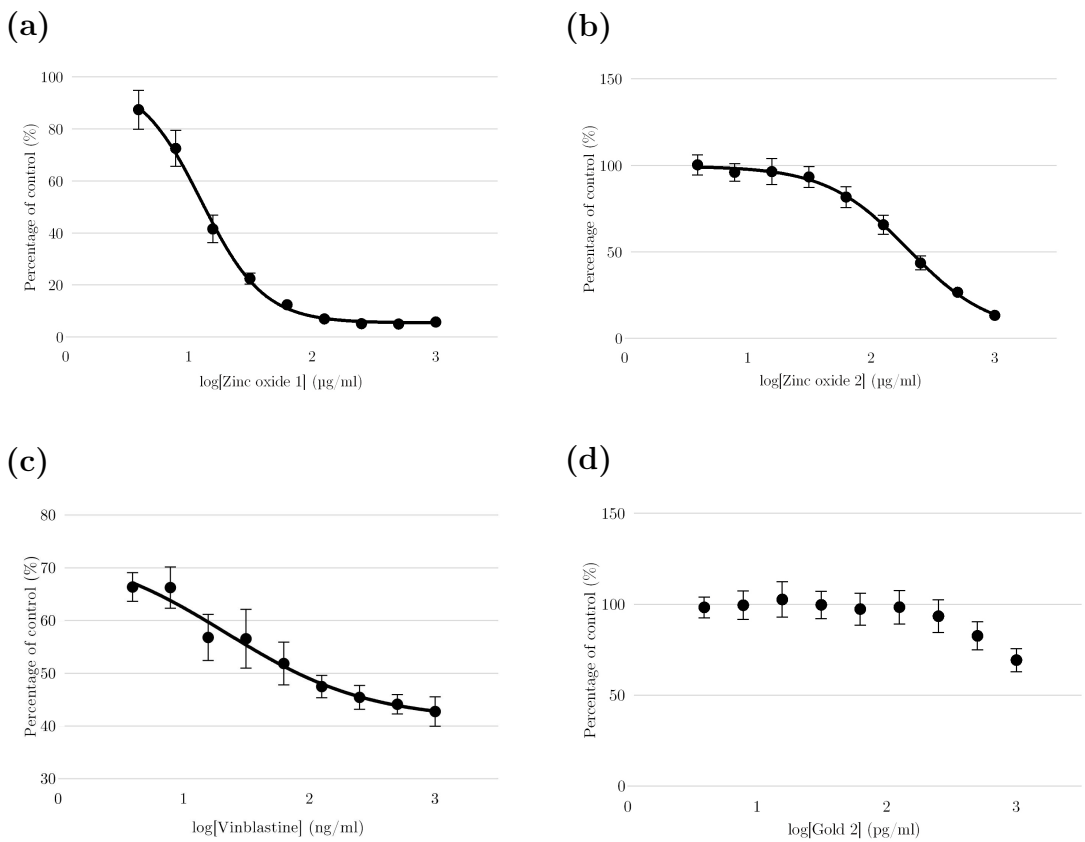

Figure 5.1: MTT assay concentration-response curves generated following 24 hour treatment of CEM cell line with (a) zinc oxide 1. (b) zinc oxide 2. (c) vinblastine. (d) gold 2. Data displayed as average (n = 8) ± standard deviation.

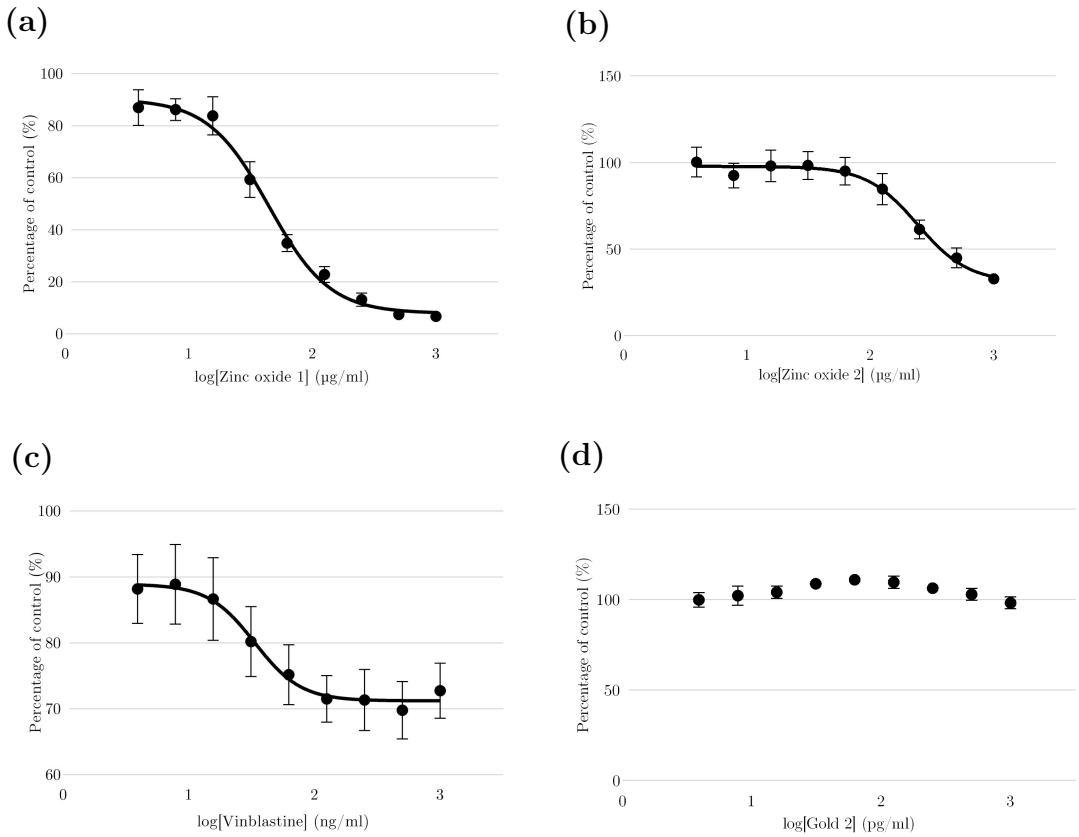

Figure 5.2: MTT assay concentration-response curves generated following 24 hour treatment of THP-1 cell line with (a) zinc oxide 1. (b) zinc oxide 2. (c) vinblastine. (d) gold 2. Data displayed as average (n = 8) ± standard deviation.

Assay interference was observed in a number of treatments. Absorbance values higher than those of untreated control wells were observed in treatments of both CEM and THP-1 with polystyrenes 1-6, in a concentration-dependent manner (Figure 5.3a). Visual inspection of the samples confirmed this not to be a proliferative effect given the absence of the characteristic purple colour change, rather an artefact resulting from the turbidity of the preparations resulting in a nonspecific absorbance overlapping the detection wavelength of the assay.

Under cell-free conditions; silver 1, Endorem, Ferumoxytol (Figure 5.3b), and JGC displayed optical absorption at 560 nm without conversion of the MTT reagent. Silica 3 was found to catalyse the conversion of MTT reagent under cell-free conditions as shown in Figure 5.3c.

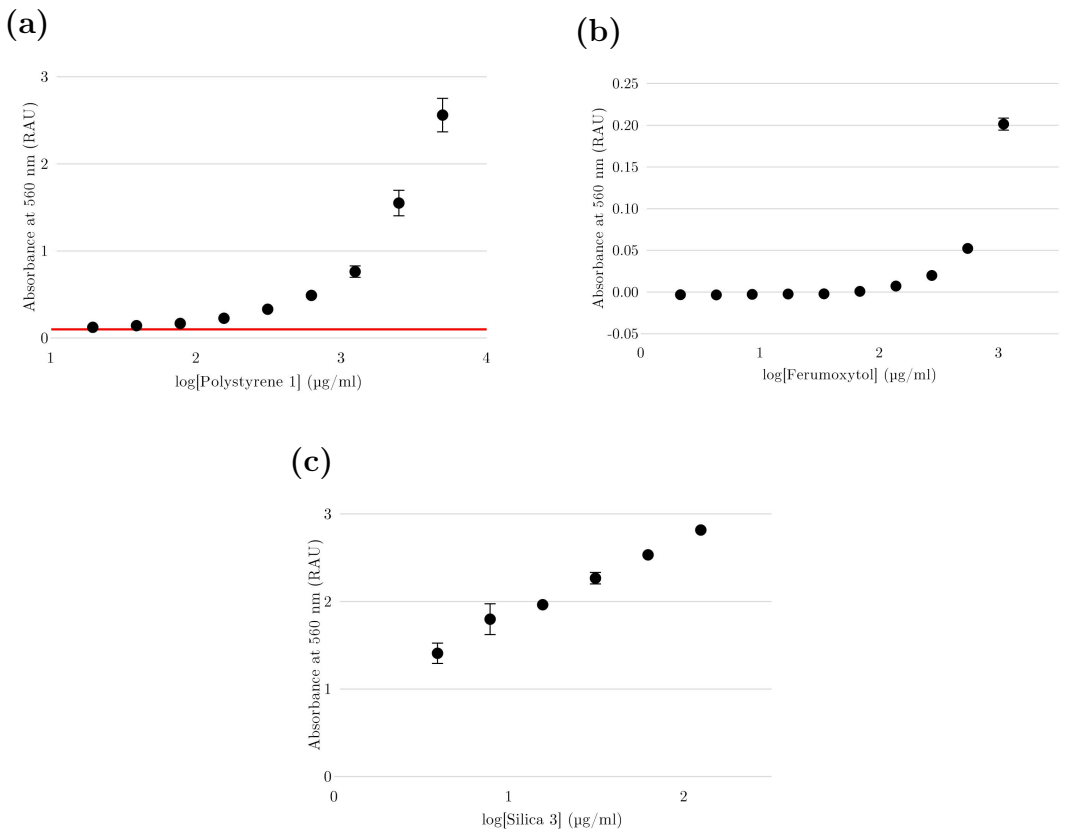

Figure 5.3: MTT assay concentration-response curve generated following 24 hour treatment of THP1 cell line with (a) polystyrene 1. Red horizontal line signifies absorbance of untreated control. MTT assay concentration-response curves generated under cell-free conditions by (b) Ferumoxytol. (c) silica 3. Data displayed as average (n = 8) ± standard deviation.

5.3.1.2 LDH assay

JGC and zinc oxide 1 were the only materials of those tested to generate a valid concentration-response curve, from which CC_{50} values of 75.24 µg/ml and 110.1 µg/ml, respectively, were calculated (Figures 5.4a and 5.4b). No overt toxicity was observed following treatment of THP-1 cells with any other materials under the described conditions when assessed by the LDH assay as exemplified by the concentration-response curve generated by polystyrene 4 (Figure 5.4c). As such, CC_{50} values were unable to be generated from the resulting concentration-response curves.

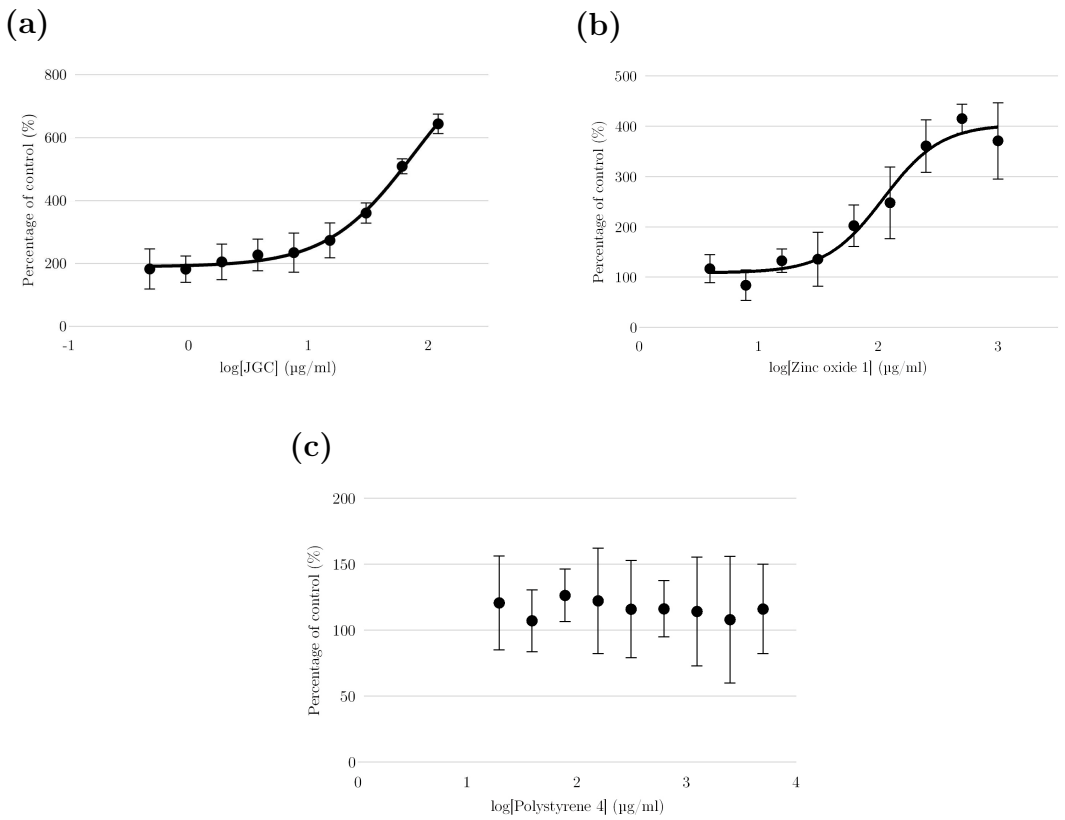

Figure 5.4: LDH assay concentration-response curves generated following 24 hour treatment of THP-1 cells with (a) JGC. (b) zinc oxide 1. (c) polystyrene 4. Data displayed as average (n = 3) ± standard deviation.

5.3.2 Assessment of cellular health

5.3.2.1 Reactive oxygen species generation

Polystyrene 4 at a concentration of 100 µg/ml resulted in the most pronounced effect of all polystyrene nanoparticle treatments, where ROS generation was 48.3% ($p = <0.0001$) that of the untreated control. Polystyrenes 2 (261 nm, -7.02 mV), 4 (453 nm, -7.93 mV), and 6 (497 nm, -6.51 mV), being the smaller and more neutrally charged in RPMI-1640 10% FBS compared to 1 (1169.93 nm, -9.99 mV), 3 (926.93 nm, -8.47 mV), and 5 (802.50 nm, -7.97 mV), resulted in the highest number of significant changes to observed ROS generation within that material class (Figure 5.5a).

Of those tested, the only nanomaterials found to result in an observed level of ROS higher than that of the untreated control were gold 1 and gold 2. At a concentration 100 pg/ml, treatment with both materials resulted in ROS generation significantly higher than untreated THP-1 cells (Figure 5.5b). The condition leading to the greatest induction was that of gold 2 (16.71 nm, -12.4 mV, mix-matrix capped) at 100 pg/ml generated 48.6% ($p = <0.0001$) more compared to 28.3% ($p = 0.0001$) by gold 1 (31.99 nm, -10.97 mV, citrate-stabilised) at the same concentration. Nanomaterials of similar size, charge, or surface stabilisation; Ferumoxytol (33.27 nm, -10.80 mV), JGC (38.42 nm), silver 2 (-11.39 mV, citrate-stabilised), and Endorem (citrate-stabilised), did not exhibit this effect.

Silver 1, the most highly charged nanoparticle tested (-16.27 mV determined in RPMI-1640 10% FBS), resulted in a level of ROS 98.4% ($p = <0.0001$) less than the untreated control at a concentration of 100 µg/ml (Figure 5.5b). Silver 2, possessing different size, charge, and surface stabilisation, generated a similar but less pronounced effect (41.2% less than untreated, $p = <0.0001$). However, the treatment concentration of this material was 1000-times less than that of Silver 1, due to limited concentration of the stock material. Silica 3, a material

demonstrating no known physicochemical similarity, led to a similar observation to that of silver 1 at the same concentration (98.8% less, p = <0.0001). Such an effect was not seen in silicas 1 or 2 (Figure 5.5d). Silica 3 has been shown to have the largest size in RPMI-1640 supplemented with FBS to 10% final volume; 1062.60 nm, compared to 130.80 nm and 400.63 of silicas 1 and 2 respectively, while the zeta potential of all three materials show a high degree of similarity. Whereas silicas 1 and 2 share stabilisation by L-arginine, the stabiliser of silica 3 is unknown.

At 100 µg/ml all zinc oxides displayed a level of ROS ~87% less than untreated (Figure 5.5c). Treatment with emulsion at the highest tested concentration led to a similar effect; 91.9% less, p = <0.0001 (Figure 5.5d). All of these materials vary in their physicochemical properties but have produced similar biological effects. Treatment with the positive control camptothecin, a known inducer of reactive oxygen species, resulted in a level of ROS 86% lower than that of the untreated control (Figure 5.5d).

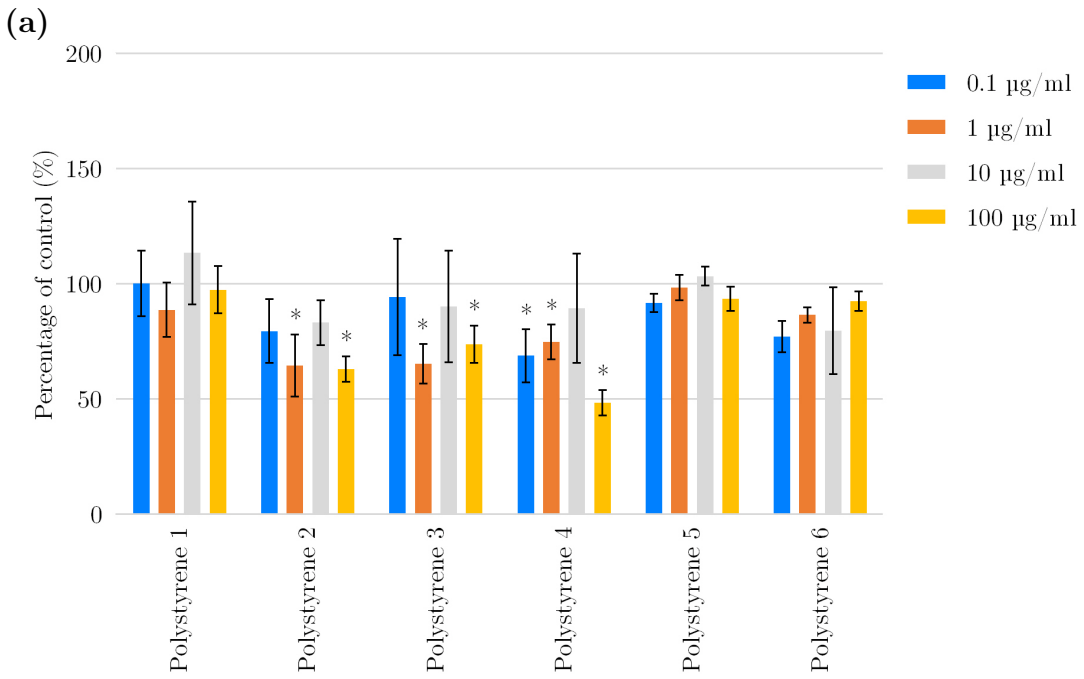

(b)

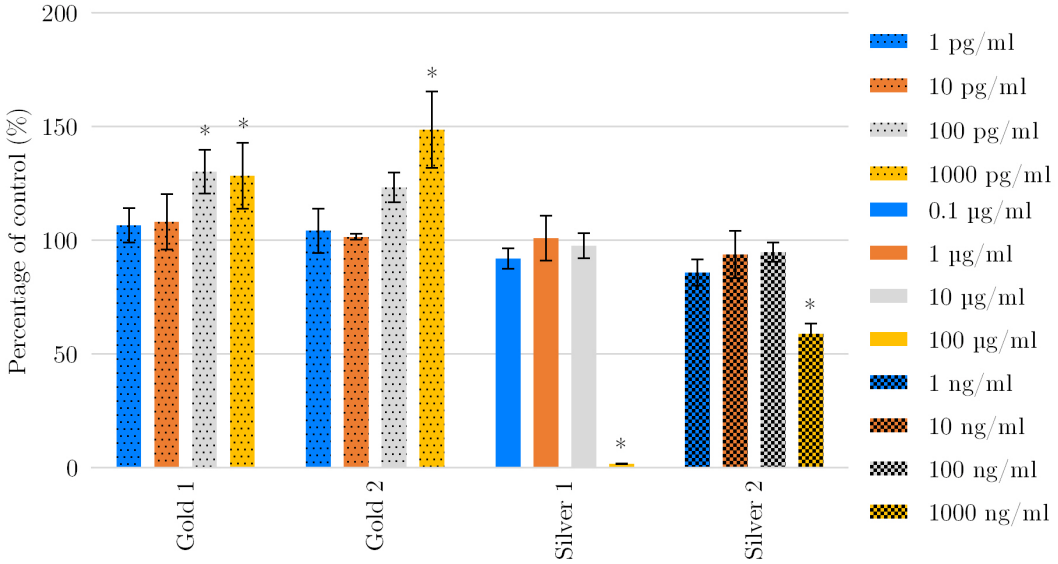
200
150
100
50
0
Percentage of control (%)
Gold 1
Gold 2
Silver 1
Silver 2
1 pg/ml
10 pg/ml
100 pg/ml
1000 pg/ml
0.1 µg/ml
1 µg/ml
10 µg/ml
100 µg/ml
1 ng/ml
10 ng/ml
100 ng/ml
1000 ng/ml

(c)

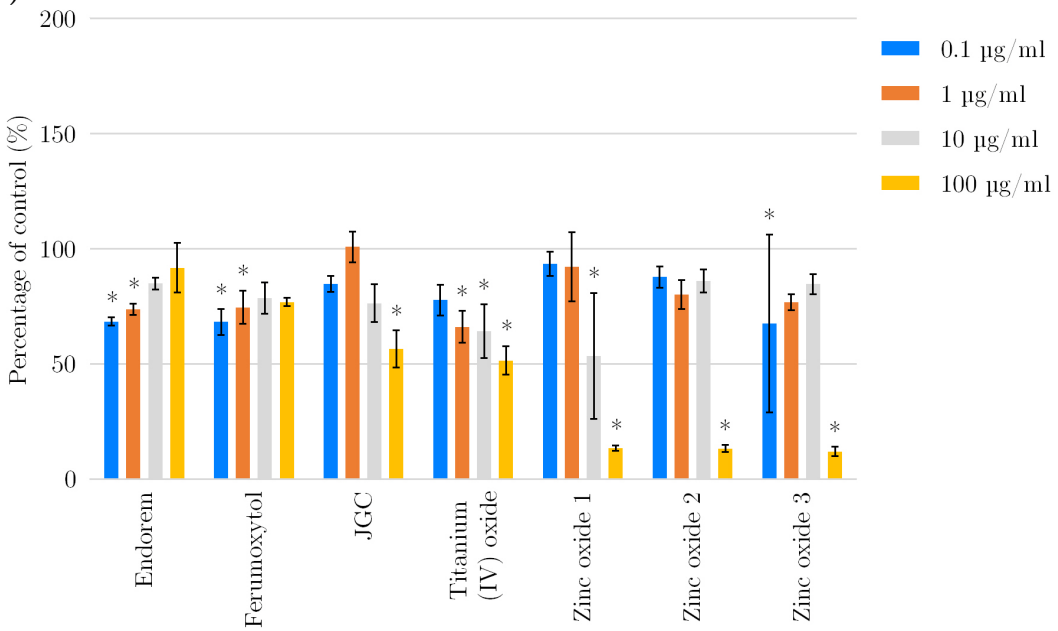
200
150
100
50
0
Percentage of control (%)
Endorem
Ferumoxytol
JGC
Titanium (IV) oxide
Zinc oxide 1
Zinc oxide 2
Zinc oxide 3
0.1 µg/ml
1 µg/ml
10 µg/ml
100 µg/ml

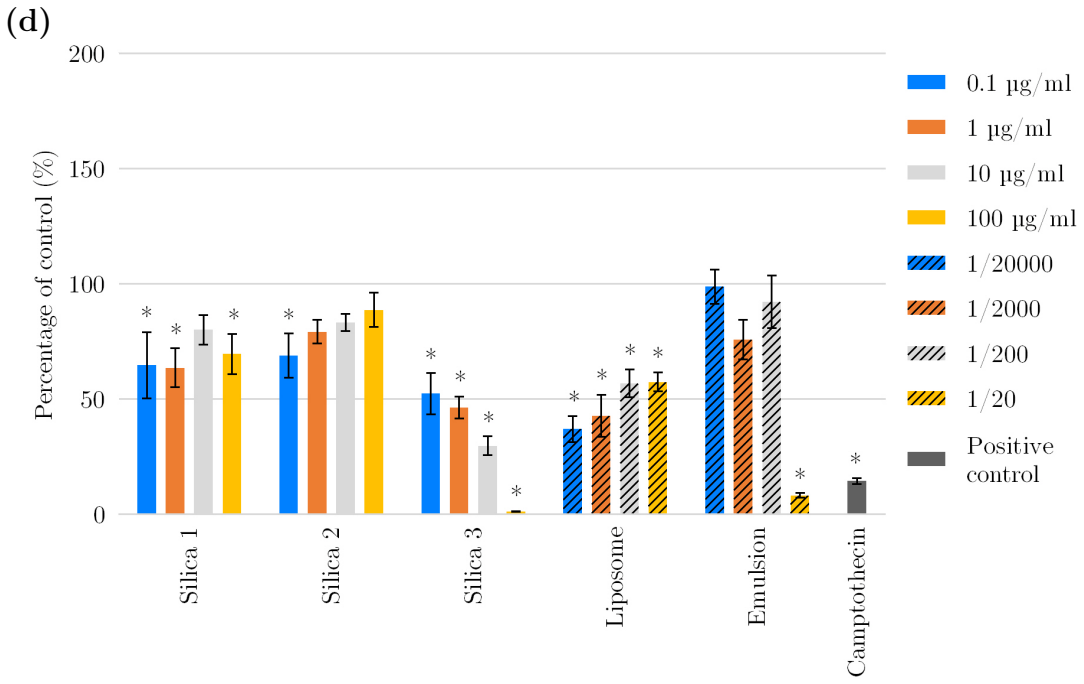

Figure 5.5: Generation of reactive oxygen species in the presence of stated nanomaterials as a percentage of untreated of control. Data displayed as average (n = 4) ± standard deviation. * p-value <0.05.

Significant correlation was found with reactive oxygen species generation at the lowest tested nanomaterial concentrations (0.1 µg/ml, 1 pg/ml, 1 ng/ml, 1/20000 dilution) and zeta potential measured in FBS-supplemented RPMI-1640 ($p = 0.0449$). The trend demonstrates nanomaterials whose zeta potentials tend toward neutrality resulted in less observed ROS than the untreated control. Such correlation was not found in the other treatment conditions.

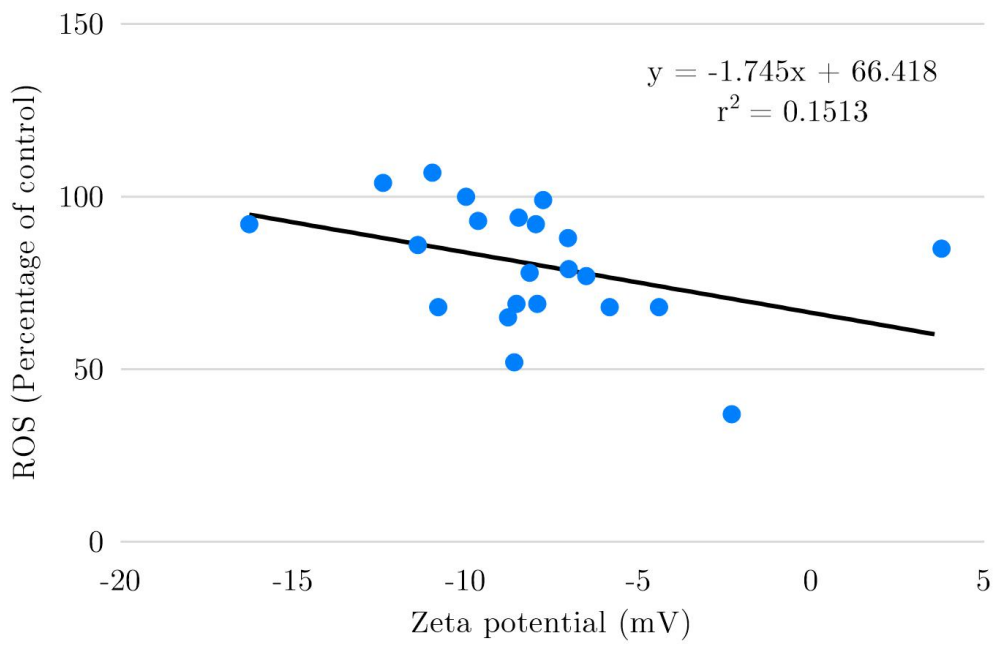

Figure 5.6: Correlation of reactive oxygen species generation at the lowest tested nanomaterial concentrations (0.1 µg/ml, 1 pg/ml, 1 ng/ml, 1/20000 dilution) and zeta potential measured in RPMI-1640 supplemented to 10% final volume with FBS.

5.3.2.2 Measurement of reduced glutathione

At the highest tested concentration, treatment with polystyrenes 1, 3, and 5 resulted in levels of reduced glutathione less than the untreated control (Figure 5.7a). The most pronounced was by polystyrene 5 (97% less, p = <0.0001), followed by polystyrene 3 (39.8% less, p = <0.0001), and then polystyrene 1 (30.2% less, p = 0.01). These three nanomaterials feature quaternary ammonium surface-functionalization, as opposed to the sulphonate-functionalization of polystyrenes 2, 4, and 6 which do not demonstrate this effect.

Treatment of THP-1 cells with Endorem and Ferumoxytol at concentrations of 0.1 µg/ml and 1 µg/ml resulted in significantly higher levels of reduced glutathione than that of untreated cells (Figure 5.7c). Of these materials Ferumoxytol is the most highly charged in RPMI-1640 supplemented with FBS to 10% final volume, while Endorem tends toward neutrality with a zeta potential of -4.40 mV. The response of THP-1 cells to titanium (IV) oxide showed similarity to that of Endorem, where levels of reduced glutathione were nearly identical at 0.1 and 100 µg/ml treatments (Figure 5.7c). Neither of these materials show physicochemical similarity, where titanium (IV) oxide is thirteen-times larger, and its zeta potential is almost double that of Endorem.

All three zinc oxide nanomaterials resulted in significantly more reduced glutathione present than that of untreated THP-1 cells at concentrations of 10 and 100 µg/ml (Figure 5.7c). Significant positive trends were observed where increasing concentration led to greater glutathione in zinc 1 (p = 0.0071), 2 (p = 0.0204) and 3 (p = 0.0164).

Silicas 1 and 2 did not affect the level of reduced glutathione under the described conditions at the highest tested concentration (100 µg/ml), whereas treatment with silica 3 led to a level 60.5% (p = <0.0001) lower than the control. All three of the silica nanoparticles display zeta potentials with a high degree of sim-

ilarity, whereas silica 3 was shown to be 1062.60 nm in RPMI-1640 10% FBS compared to silica 1; 130.80 nm, and silica 2; 400.63 nm.

The positive control menadione generated a 29% ($p = <0.0001$) greater level of glutathione reduction than the untreated control.

No significant correlation ($p = <0.05$) was found between nanomaterial impact on glutathione and the compared parameters of size, zeta potential, or polydispersity.

(a)

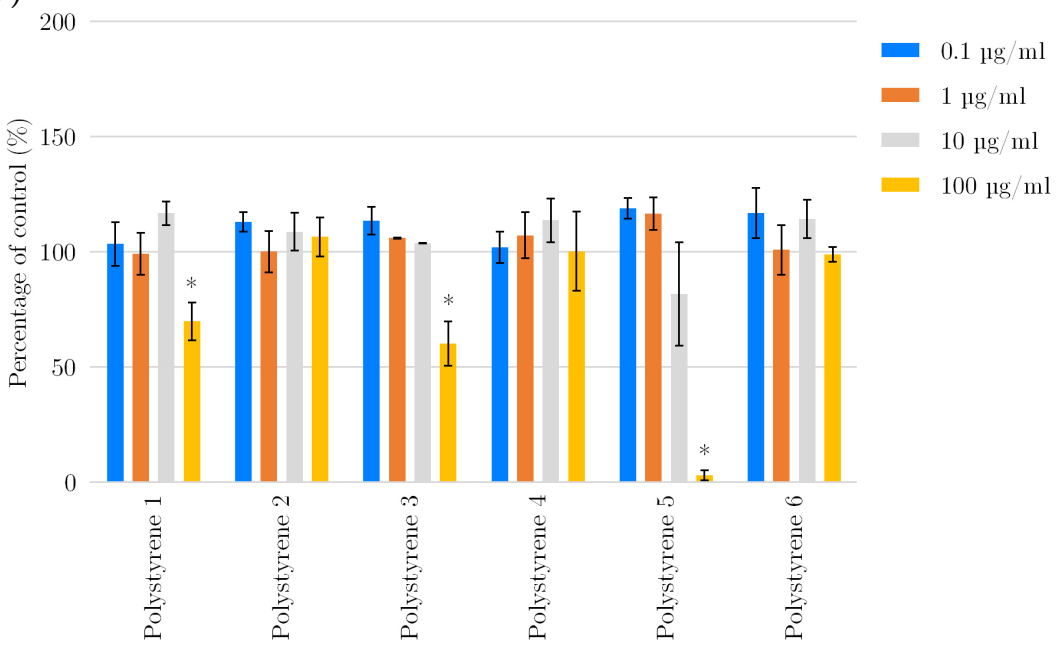

(b)

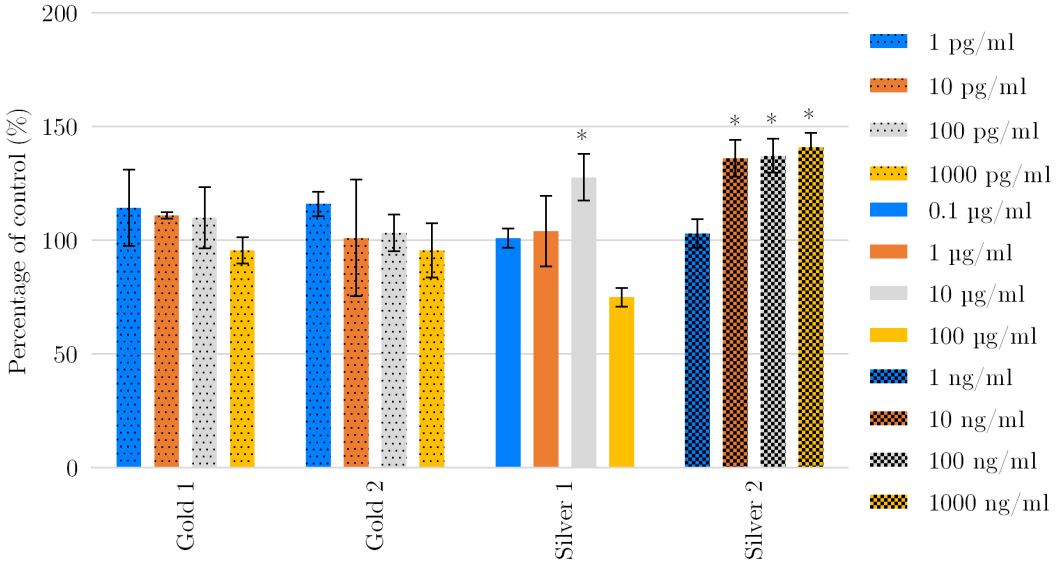
200
150
100
50
0
Percentage of control (%)
Gold 1
Gold 2
Silver 1
Silver 2
1 pg/ml
10 pg/ml
100 pg/ml
1000 pg/ml
0.1 µg/ml
1 µg/ml
10 µg/ml
100 µg/ml
1 ng/ml
10 ng/ml
100 ng/ml
1000 ng/ml

(c)

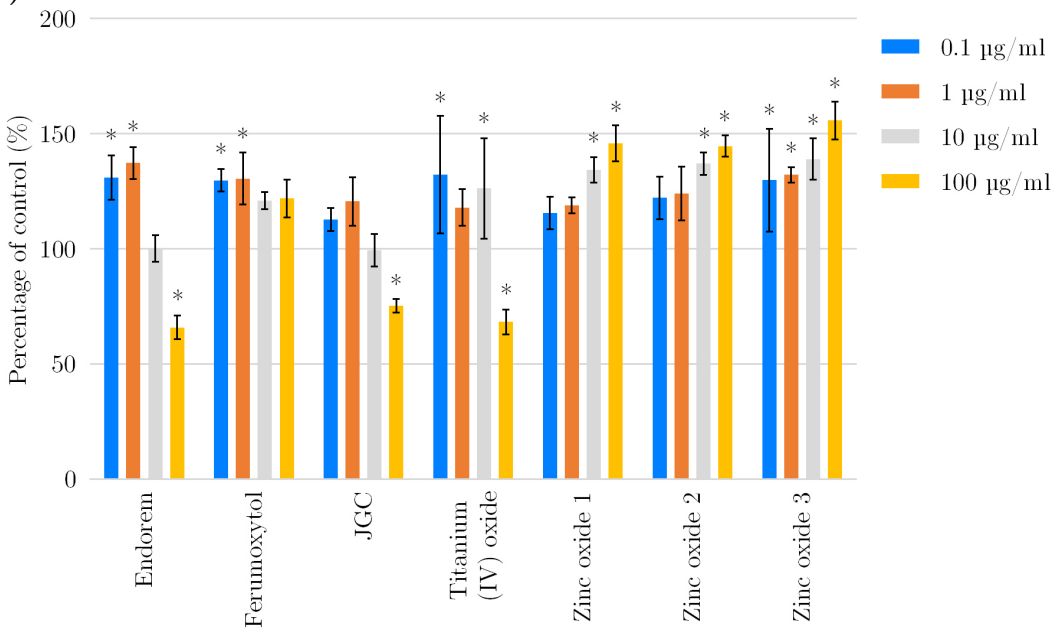
200
150
100
50
0
Percentage of control (%)
Endorem
Ferumoxytol
JGC
Titanium (IV) oxide
Zinc oxide 1
Zinc oxide 2
Zinc oxide 3
0.1 µg/ml
1 µg/ml
10 µg/ml
100 µg/ml

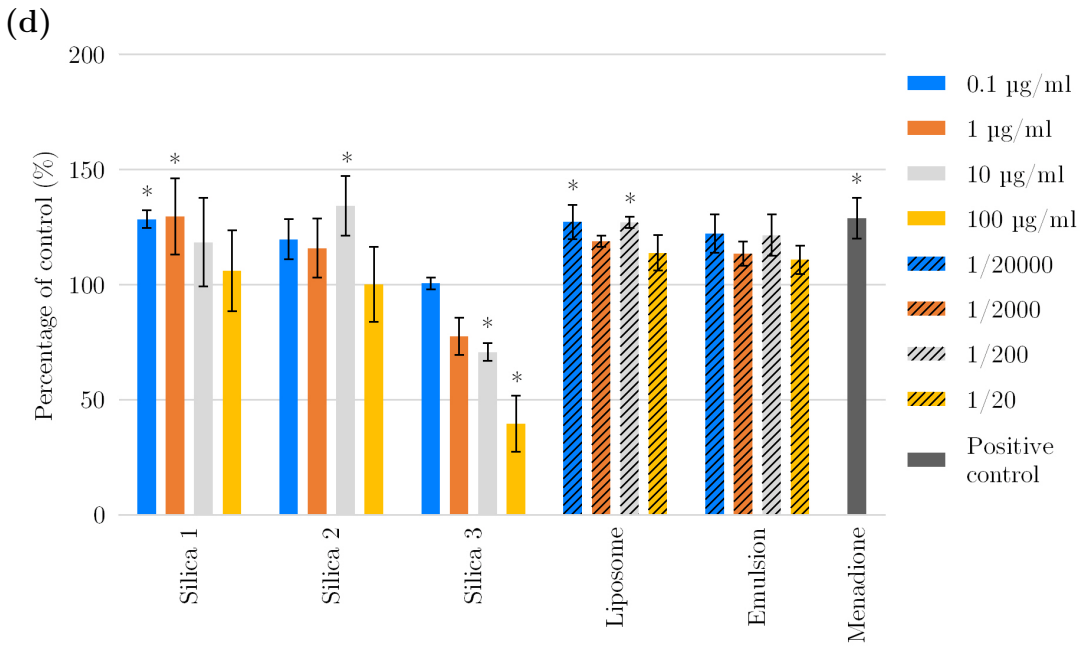

Figure 5.7: Reduced glutathione in the presence of stated nanomaterials as a percentage of untreated control. Data displayed as average (n = 4) ± standard deviation. * p-value <0.05.

5.3.2.3 Autophagy

A time course of autophagic induction (Figure 5.8a, b, c) was performed to establish optimum durations of incubation to gain maximum observable effects. It has been determined here that for this particular experimental design incubation for 8 hours for CEM, 6 hours for Raji, and 24 hours for THP-1 are necessary to reach the desired outcome.

When compared to example data (Figure 5.8d) generated in Jurkat (human T lymphocyte), the magnitude of responses are quite different. Although under different conditions, Jurkat produced a maximum increase of 116.6% under exposure to rapamycin and chloroquine. The maximum autophagic induction in CEM and Raji (Figures 5.8a, and 5.8b) was produced by the combination of rapamycin and chloroquine (105% and 446% respectively). THP-1 demonstrated a 148.7% increase under the combination while chloroquine alone resulted in a 160% induction (Figure 5.8c).

All nanomaterial treatments, with the exception of zinc oxide 1 at 10 µg/ml ($p = 0.9914$), resulted in a significantly lower ($p = <0.0001$) level of autophagy in the THP-1 cell line at 24 hours, compared to the untreated control. The level of autophagy was found to be lowest following treatment with the highest concentration of silver 1, being 22.7% ($p = <0.0001$) that of the untreated control (Figure 5.9b). Liposome resulted in the greatest impact across all treatments with an average 70% less than untreated THP-1 cells (Figure 5.9d).

JGC, titanium (IV) oxide, zinc oxide 2, and zinc oxide 3 all demonstrate greater impact at decreasing concentration (Figure 5.9c). This trend was only found to be statistically significant in titanium (IV) oxide ($p = 0.0499$) and zinc oxide 3 ($p = 0.0061$).

Treatment of THP-1 cells with positive controls rapamycin and chloroquine produced levels of autophagy 32% lower ($p = <0.0001$), and 68% ($p = <0.0001$)

higher than that of the untreated control. Combined treatment with rapamycin and chloroquine caused autophagy to be 40% (p = <0.0001) greater than in untreated cells.

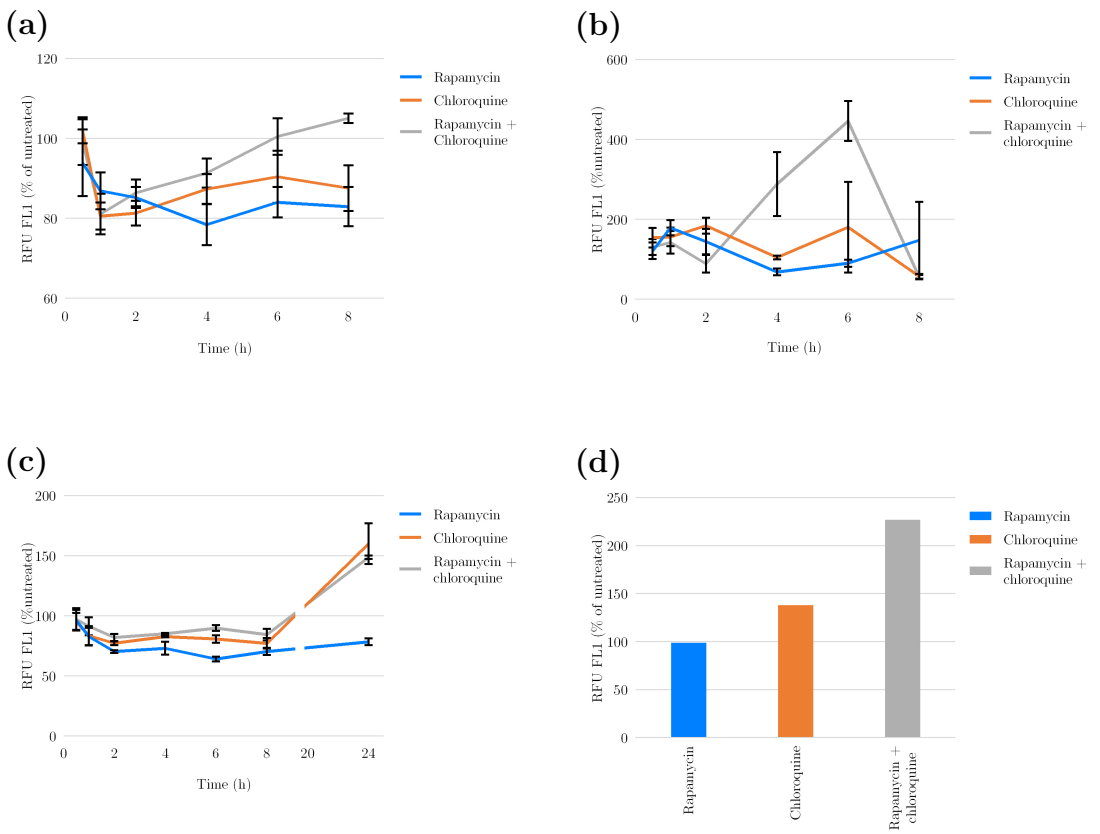

Figure 5.8: Autophagic responses, as a percentage of untreated of control, at stated time points following treatment with 0.5 µM rapamycin, 10 µM chloroquine or combined rapamycin and chloroquine in cell lines (a) CEM. (b) Raji. (c) THP-1. Data displayed as average (n = 4) ± standard deviation. (d) Example response in Jurkat cells treated with 0.5 mM rapamycin, 10 mM chloroquine or combined rapamycin and chloroquine at 18 hours (Enzo Life Sciences, 2016).

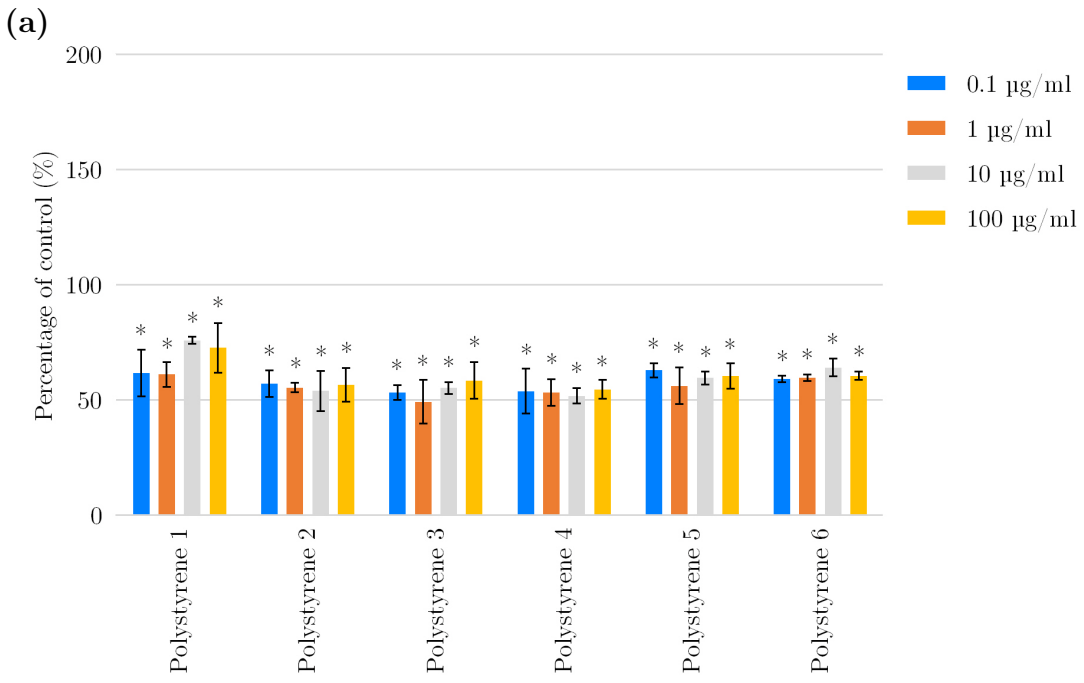
(a)
Percentage of control (%)
200
150
100
50
0
Polystyrene 1
Polystyrene 2
Polystyrene 3
Polystyrene 4
Polystyrene 5
Polystyrene 6
0.1 µg/ml
1 µg/ml
10 µg/ml
100 µg/ml

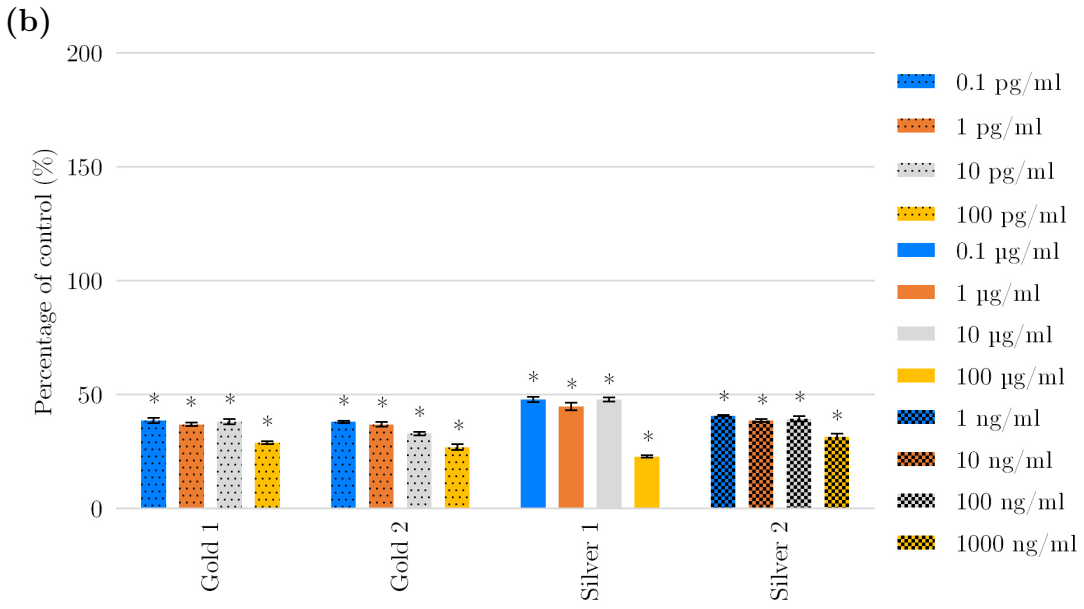
(b)
Percentage of control (%)
200
150
100
50
0
Gold 1
Gold 2
Silver 1
Silver 2
0.1 pg/ml
1 pg/ml
10 pg/ml
100 pg/ml
0.1 µg/ml
1 µg/ml
10 µg/ml
100 µg/ml
1 ng/ml
10 ng/ml
100 ng/ml
1000 ng/ml

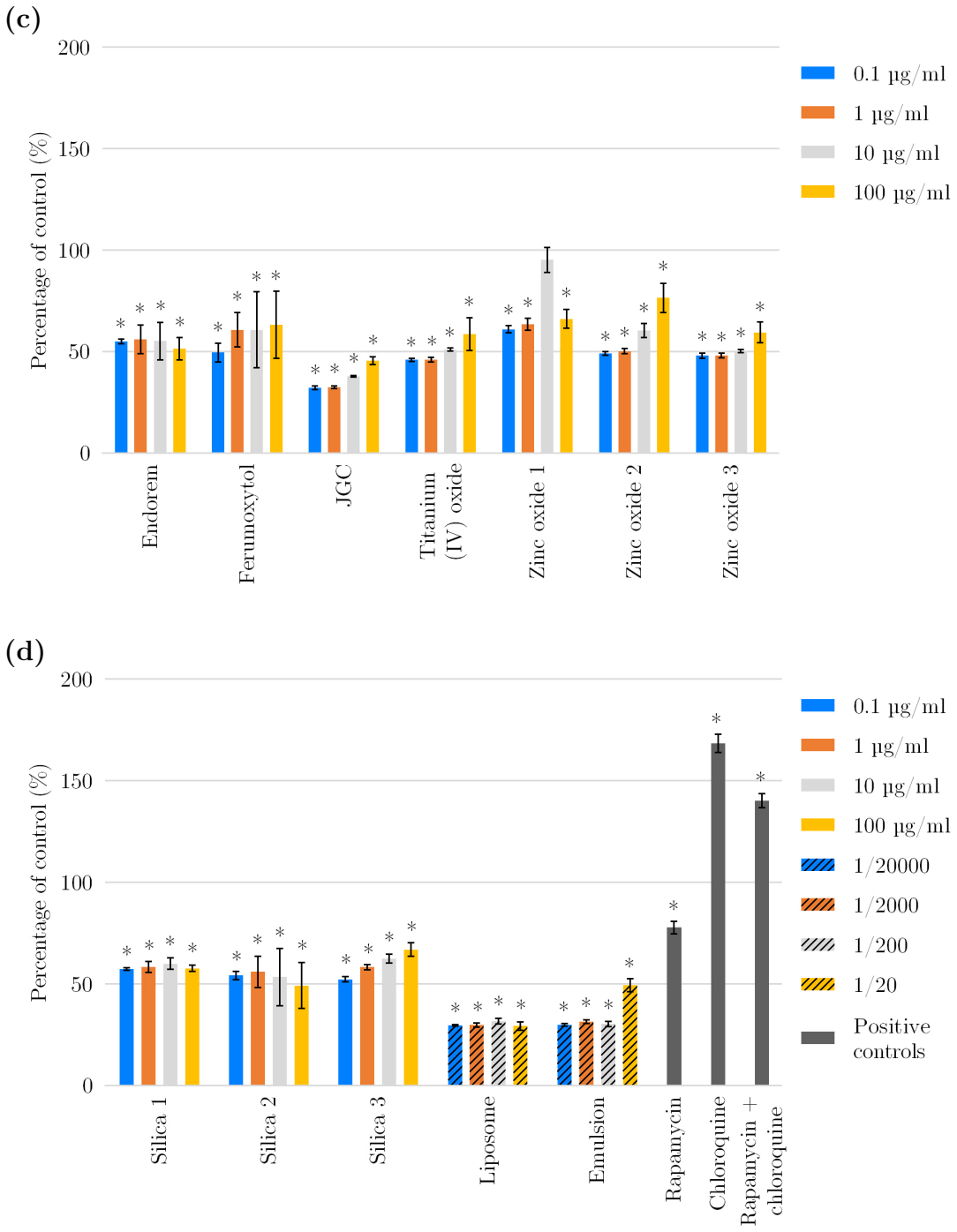

Figure 5.9: Effect on autophagy in THP1 cell line resulting from treatment with the stated nanomaterials for 24 hours as a percentage of untreated of control. Data displayed as average (n = 4) ± standard deviation. * p-value <0.05.

Significant correlation was found with autophagy at the highest tested nanomaterial concentrations (100 µg/ml, 1000 pg/ml, 1000 ng/ml, 1/20 dilution) and Z-average ($p = 0.0060$, Figure 5.10a), as well as peak mean intensity size ($p = 0.0042$, Figure 5.10b). Peak mean intensity size also showed significant correlation ($p = 0.0461$, Figure 5.10c) with the second highest nanomaterial concentrations (10 µg/ml, 100 pg/ml, 100 ng/ml, 1/200 dilution). The observed trend demonstrated by these correlations is that nanoparticles of smaller size resulted in a lower level of autophagy than those of larger size.

(a)

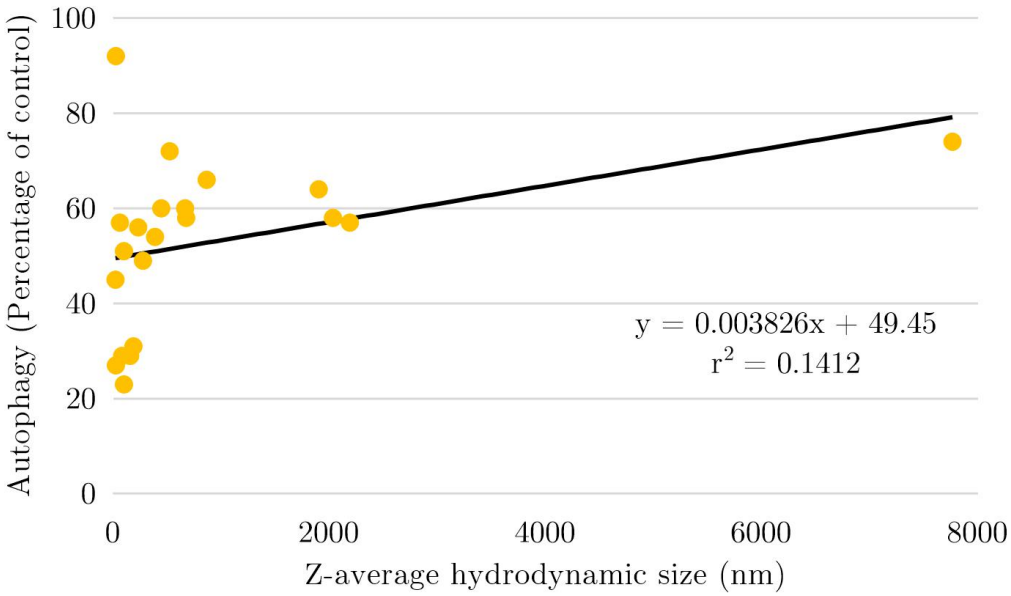

(b)

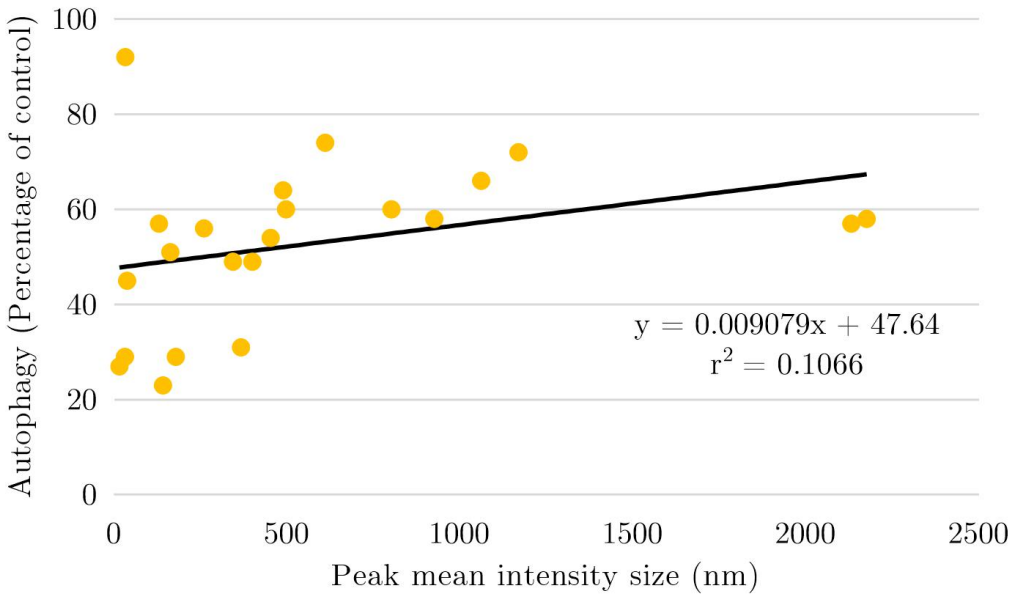

(c)

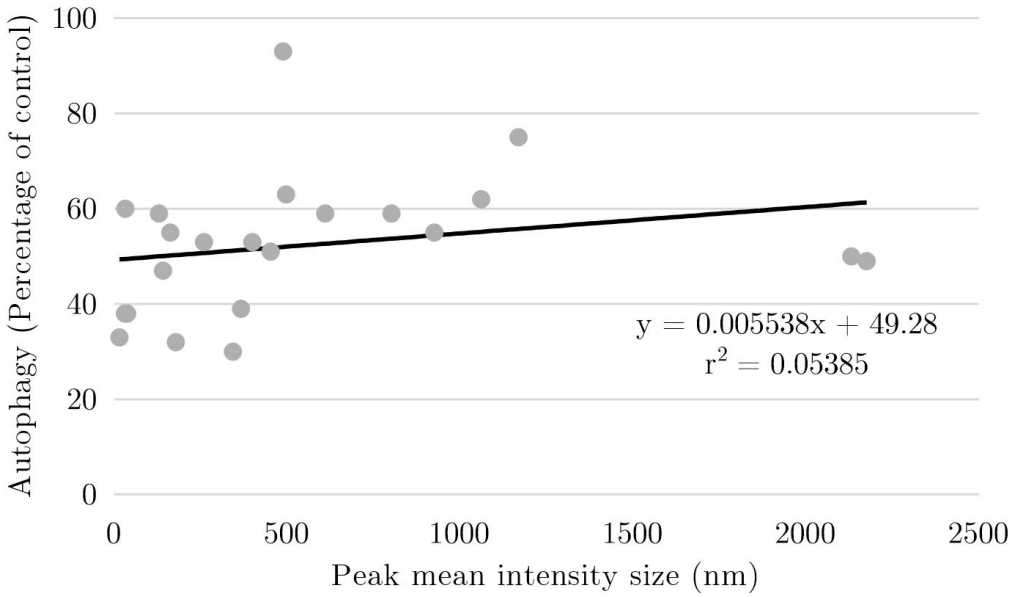

Figure 5.10: Correlation of autophagy at the highest tested nanomaterial concentrations (100 µg/ml, 1000 pg/ml, 1000 ng/ml, 1/20 dilution) and (a) Z-average hydrodynamic size. (b) peak mean intensity size. Correlation of autophagy at the second highest nanomaterial concentrations (10 µg/ml, 100 pg/ml, 100 ng/ml, 1/200 dilution) and (c) peak mean intensity size. All sizes refer to those measured in RPMI-1640 supplemented to 10% final volume with FBS.

5.3.3 Development of kinetic assessment assays for cellular health

5.3.3.1 Kinetic assessment of reactive oxygen species

Amplification of the fluorescent signal produced by 40 µg/ml menadione when measured in media containing phenol red, displayed in Figure 5.11, was attributed to the presence of the indicator. This amplification was not observed at other concentrations when compared to data generated in kinetic assay medium (Figure 5.12a). Such an effect would lead to an overestimation in reactive oxygen species generation, for which reason the use of phenol red-free RPMI-1640 was justified.

The AUC of all menadione treatments over 12 hours were significantly higher than that of untreated cells, the greatest being 1.6-fold ($p = 0.0067$) by 40 µM (Figure 5.12b).

The time to maximum fluorescence was also markedly different between untreated and treated cells, where T_{max} for untreated cells was 270 minutes but 720 minutes for cells treated with 40 µg/ml menadione (Figure 5.12d).

A convergence of the in the fluorescent signal generated by treatments with 20 and 40 µg/ml menadione was observed (Figure 5.13a) as exemplified by the near-identical C_{max} calculated for these treatments (Figure 5.13b). With the exception of these concentrations, the static assessment at 24 hours (Figure 5.13c) showed similar trend to the C_{max} of the kinetic assay. Differences between the two methodologies such as the accumulated signal by the kinetic assay could be associated with the higher fluorescence found in the kinetic C_{max}.

The higher fluorescence values produced by samples treated with higher concentrations of menadione would indicate a higher level of reactive oxygen species in these conditions compared to those treated with lower concentrations.

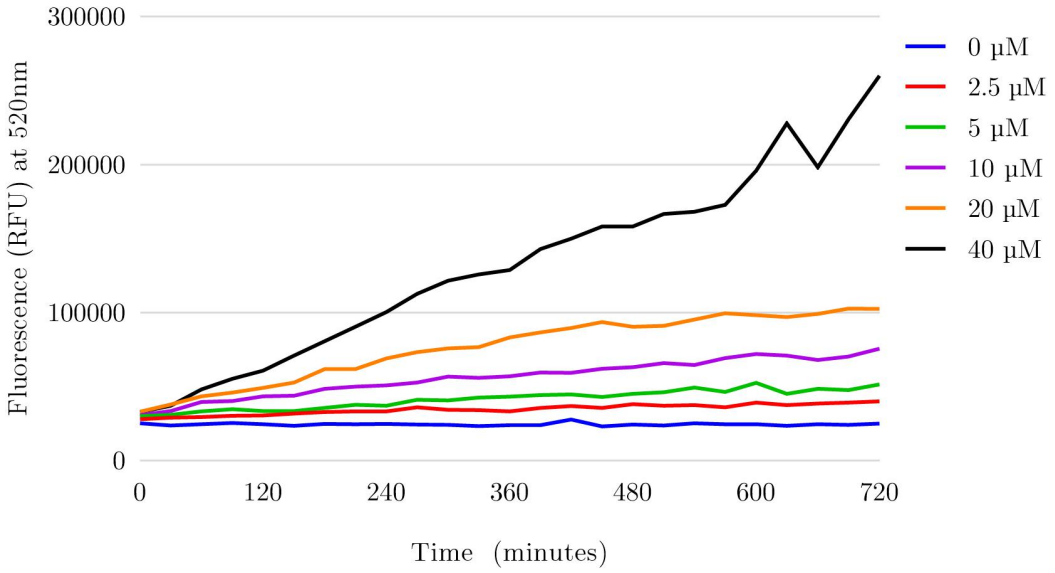

Figure 5.11: Kinetic measurement of reactive oxygen species generation in response to stated concentrations of menadione over 12 hours performed in RPMI-1640 supplemented 10% with FBS containing phenol red. Data representative of mean fluorescence values (n = 3).

(a)

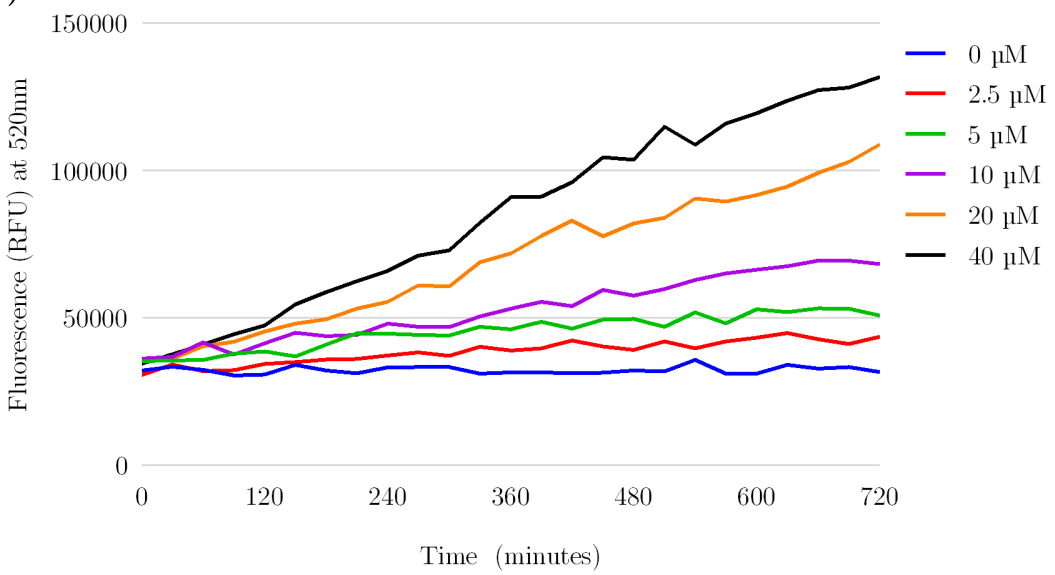

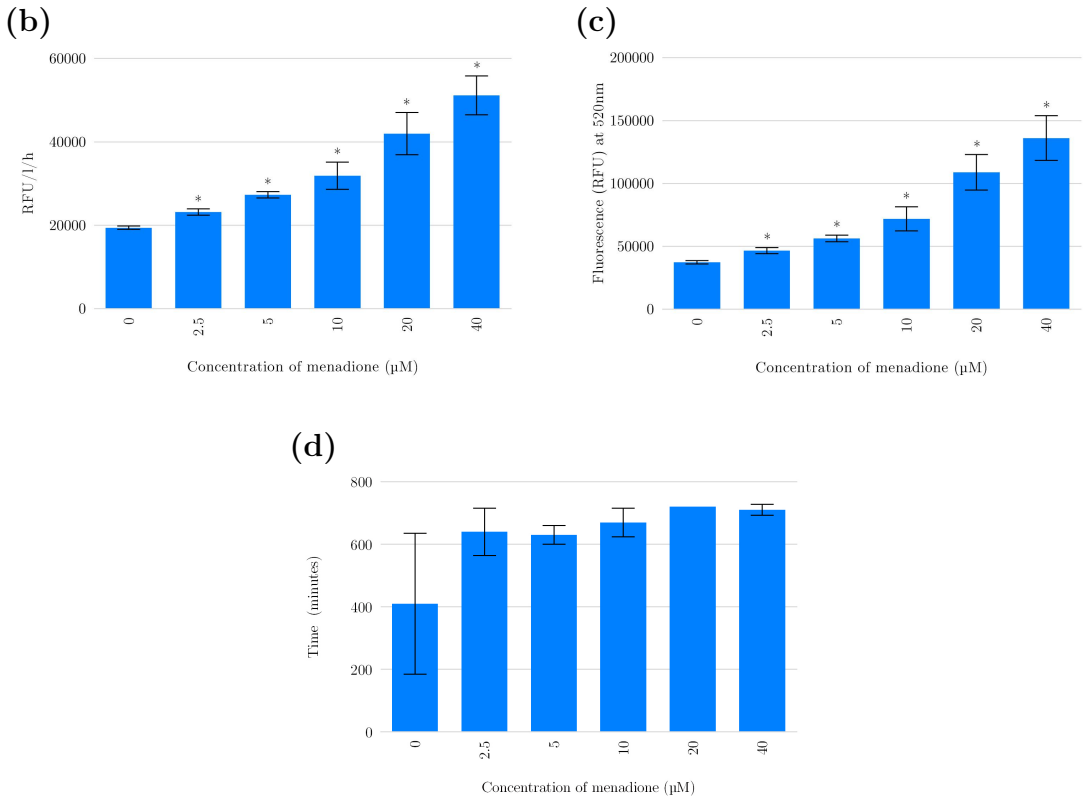

Figure 5.12: (a) Kinetic measurement of reactive oxygen species generation in response to stated concentrations of menadione over 12 hours performed in "kinetic assay medium". Data representative of mean fluorescence values (n = 3). (b) AUC of 12 hour kinetic measurement of ROS generation in response to menadione at stated concentrations, as a function of fluorescence per litre per hour. Data shown is average (n = 3) ± standard deviation. (c) C_{max} maximum fluorescence generated in response to menadione at stated concentrations for 12 hour kinetic measurement of ROS generation. Data shown is average (n = 3) ± standard deviation. (d) T_{max} time taken to achieve maximum fluorescence signal relating to ROS generation in response to menadione at stated concentrations over 12 hours. Data shown is average (n = 3) ± standard deviation. * p-value <0.05.

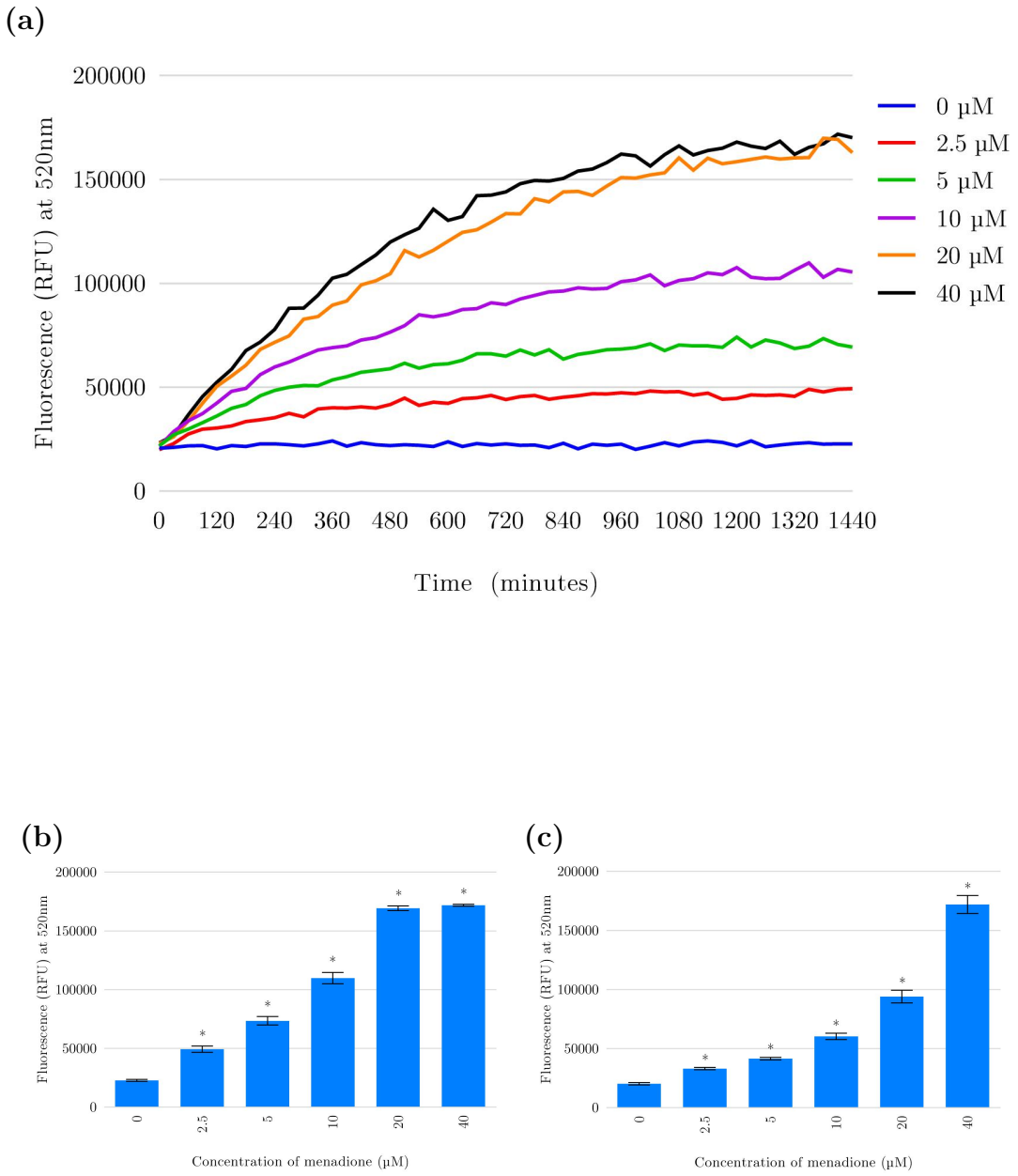

Figure 5.13: (a) Kinetic measurement of reactive oxygen species generation in response to stated concentrations of menadione over 24 hours performed in "kinetic assay medium". Data representative of mean fluorescence values (n = 4). (b) C_{max} maximum fluorescence generated in response to menadione at stated concentrations for 24 hour kinetic measurement of ROS generation. Data shown is average (n = 3) ± standard deviation. (c) Static measurement of ROS generation under stated treatments at 24 hours performed in "kinetic assay medium". Data shown is average (n = 4) ± standard deviation. * p-value <0.05.

5.3.3.2 Kinetic measurement of reduced glutathione

Kinetic measurement of reduced glutathione resulted in detector saturation by the untreated control at 480 minutes (Figure 5.14).

All concentrations of menadione tested resulted in a lower fluorescence than that of the untreated control across the 12 hour period.

THP1 cells treated with higher concentrations of menadione were found to have lower fluorescence intensity at all time points than those treated with lower concentrations, with the exception of some overlap between 2.5 µM and 5 µM treatments 5.14). This would imply that there was less cellular reduced glutathione present in samples treated with greater concentrations of the free radical inducing compound.

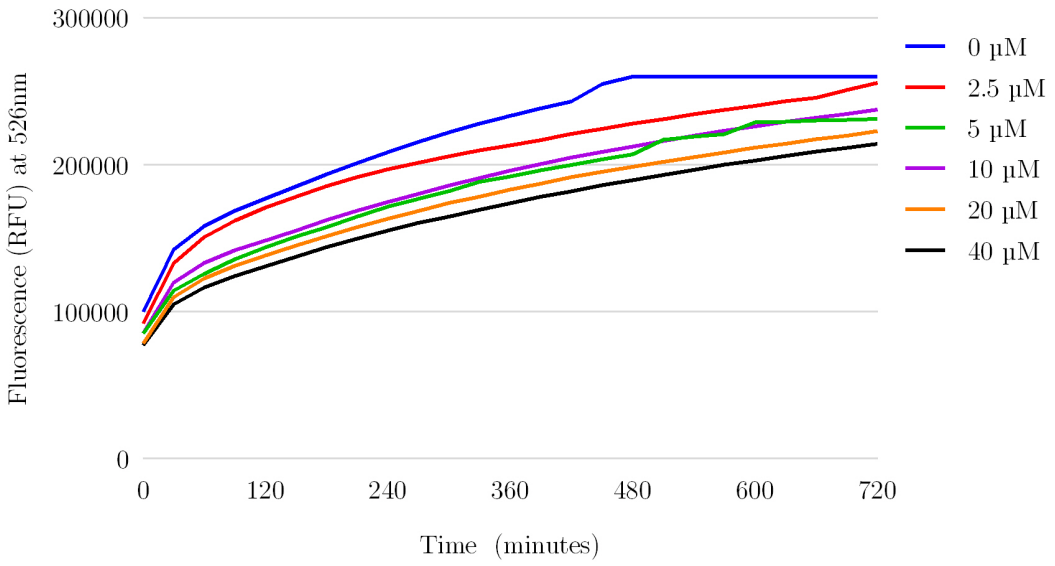

Figure 5.14: Kinetic measurement of glutathione reduction in response to stated concentrations of menadione over 12 hours performed in "kinetic assay medium". Data representative of mean fluorescence values (n = 4).

5.4 Discussion

Cytotoxic assessment of nanomaterials *in vitro* using organotypic cell models can yield a valuable understanding of the mechanisms of nanoparticle toxicity and has the advantage over *in vivo* assessment in terms of cost and logistics (Dobrovolskaia and McNeil, 2013; Lewinski et al., 2008). However, careful consideration must be given when trying to extrapolate *in vitro* cytotoxicity data to *in vivo* doses (Sayes et al., 2007). It is well known that *in vitro* cytotoxicity assessments and *in vivo* acute toxicity, under most conditions, demonstrate little correlation (Garle et al., 1994). The review by McKim highlights the main limitations which exist in using *in vitro* cytotoxicity assays to predict *in vivo* toxicity; central to which is the inability of single endpoint assays to provide quantitative information required to extrapolate the *in vitro* effects to relevant *in vivo* toxicity reference values such as a plasma concentration (McKim, 2010).

As a means to inform nanomaterial concentrations for subsequent assays, measures of cytotoxicity prove useful. Following cytotoxic assessment of the nanomaterial library, choices of treatment concentrations were informed for investigation of the impact of these materials on cellular oxidative balance. This subsequent assessment was carried out via direct determination of ROS generation, and measurement of cellular glutathione. In doing so, observations are drawn on the effects of the nanomaterials, and not artefacts generated due to cell death (Dobrovolskaia, 2015). The adoption of standard cytotoxicity tests for use with nanoparticles has been called into question (Hirsch et al., 2011), due to the complexity of the materials and their likelihood to interfere with assays and produce misleading results (Holder et al., 2012; Kroll et al., 2012). This consideration was at the forefront when choosing and designing the assays performed in this chapter. Of those routinely described in the literature, the MTT and LDH assays were utilised due to their predominance (Love et al., 2012a; Pfaller et al., 2010),

and the mechanisms by which nanoparticle-based interference may be accounted for.

The use of cell lines for such assessment provide benefits including cost effectiveness, ease of amplification, homogeneous response, but are inherently limited compared to primary cells. The sensitivities of cell lines to stimulation differs to that of the primary counterparts as a result of the genetic changes undergone in the immortalisation process, and phenotypic changes over time in culture (ATCC, 2010; Dobrovolskaia, 2015). Use of the THP-1 cell line for *in vitro* assessments of cytotoxicity and modulation of cellular health was informed by their extensive presence in the literature as a model of human monocytes (Chanput et al., 2014), providing a pertinent representation of a cellular subset encountered by nanoparticles in the peripheral blood. CEM cell line was utilised in a comparative capacity in the MTT assay to observe any differences in the sensitivities of these immune cell lines to the positive control and nanomaterial library.

The MTT assay is used a measure of cell viability by determining metabolic function. MTT (3-(4,5-Dimethylthiazol-2-yl)-2,5-Diphenyltetrazolium Bromide), a soluble yellow compound, is reduced to insoluble purple formazan in the presence of actively respiring cells by cleavage of the tetrazolium ring by dehydrogenase enzymes (Slater et al., 1963). The autoconversion of MTT is so well known that manufacturers such as Promega have published literature highlighting this fact (Riss, 2014). Nanoparticles have the capacity to facilitate electron transfer (Kovacic and Somanathan, 2013) and in doing so enable cell free conversion of MTT. Catalysis of MTT under cell free conditions has been described for combustion-generated carbon nanoparticles, and titanium dioxide (Holder et al., 2012), and was observed here for silica 1. In such cases blank correction using cell free preparations of materials could potentially lead to an underestimation of cell viability if the effect is not simply additive.

As an absorbance based assay, the MTT assay is susceptible to interference due

to inherent optical properties of nanomaterials and their preparations. This effect has been highlighted by numerous sources in the literature (Casey et al., 2007; Monteiro-Riviere et al., 2009). The optical properties relating to the absorbance maxima of the tested nanomaterials was assessed in Chapter 2 with no cause for concern regarding incompatibility of the nanomaterials with the MTT assay. However, in practice this did not hold true following the observations of signal generation by preparations in the absence of dye conversion, as well as false positives produced by turbid samples.

Of all the nanomaterials tested in this work; zinc oxides 1 and 2 were the only ones to generate valid CC_{50} values. 53.6 nm zinc oxide nanoparticles have previously been shown to generate toxicity in THP-1 cells, following 24 hours exposure, as determined via the MTT assay (Lanone et al., 2009). Of these, zinc 1 was the only nanomaterial to produce CC_{50} concentrations in both the MTT and LDH assays. This would observation suggests that zinc 1 does have a cytotoxic effect, and not just affecting either mitochondrial function or cell membrane integrity in isolation.

Extracellular quantification of lactate dehydrogenase (LDH) is achieved following the release of the cytoplasmic enzyme from the cell as a result of a reduction in membrane integrity. It is this principal which makes LDH a primary biomarker of haemolysis and erythrocyte damage (Kato et al., 2006).

The LDH protocol chosen for use in this work is based on a colourimetric endpoint. LDH activity catalyses the oxidation of lactate to pyruvate, via the reduction of NAD^+ to $NADH^+/H^+$. The proprietary catalyst then protonates the tetrazolium salt producing the detected formazan product.

The suitability of applying the LDH assay for nanomaterials has been evaluated elsewhere (Han et al., 2011), it can be seen that while it is a useful tool, its application as a one-size-fits-all assay cannot be assumed and must be evaluated on a case by case basis. As highlighted earlier, the preparation of cell free inhi-

bition/enhancement controls were an integral part of the experimental design of the LDH assay. This provided an immediate indicator of nanomaterial suitability for this assay. While these preparations were used as a baseline for cell-based treatments, they were individually scrutinised for material-related interference with the assay (be that catalytic auto-conversion of the reagents, spectral interference, or otherwise). It has been previously described that citrate-capped silver nanoparticles are incompatible with LDH assay due to LDH binding to the nanomaterial surface, and inactivation of LDH by ROS (Oh et al., 2014). While such interference was not observed in the work performed here, interference in this manner would suggest the need for further inhibition/enhancement controls of known quantities of LDH being challenged by nanomaterials.

The increasing human exposure to nanomaterials creates cause for concern with regard to their potential to modulate and affect cellular health. The route of exposure should be a primary consideration for a well informed, mechanistic, approached assessment (Kong et al., 2011). THP-1 as a model of monocytes represent an abundant cellular subset that nanoparticles will encounter in the blood stream, comprising between 10 and 30% of peripheral blood mononuclear cells in healthy individuals (Miyahira, 2012)). THP-1 are a widely utilised *in vitro* model in the literature, and have been validated in their use by numerous sources (Chanput et al., 2014; Garcia et al., 2013; Heil et al., 2002).

The generation of reactive oxygen species has been associated with numerous nanomaterials as a mechanism of nanoparticle-mediated toxicity (Fu et al., 2014). Proposed mechanisms of this include generation of free radicals via Fenton-type reactions (Valko et al., 2006), mitochondrial localisation (Foley et al., 2002), mitochondrial dysfunction via other mechanisms (Manke et al., 2013). Cell-type specific interactions have also been shown, such as frustrated phagocytosis (Bergstrand, 1990) which has been associated with carbon nanotubes (Manke et al., 2013).

Amino-functionalized polystyrene nanoparticles have been found to generate ROS in primary human macrophages, which led to activation of caspase-1, inducing IL-1β (Lunov et al., 2011). Amine-functionalized polystyrene nanoparticles also induced cell death, increased oxidative stress, mitochondrial disruption and release of cytochrome C, indicating apoptotic cell death in primary human alveolar macrophages (Ruenraroengsak and Tetley, 2015). Polystyrenes 1, 3, and 5 possess the most similar surface-functionalization, however did not display any of these effects under the described conditions.

The potential for gold nanoparticles to generate ROS in a detrimental manner has been demonstrated by various sources (Li et al., 2010; Zhang et al., 2003). Here, both citrate- (gold 1) and mix-matrix capped (gold 2) gold nanoparticle treatments resulted in an observed level of ROS higher than that of the untreated control, the only tested materials to do so across all tested concentrations.

Due to their widespread use, a great deal of data exists on the toxicological profile of titanium dioxide nanoparticles (Shi et al., 2013). Titanium dioxide exists in a number of conformations, but its anatase and rutile crystalline forms have been subject to most analysis. Tada-Oikawa et al. have shown that both rutile and anatase titanium dioxide nanoparticles reduced cellular viability of THP-1 cells via MTS assay at 24 hours, as well as increasing the production of ROS (Tada-Oikawa et al., 2016). While the crystalline structure of the titanium (IV) oxide nanoparticles used in this work is unknown, no overt toxicity was observed via MTT or LDH assay. In the aforementioned study; reactive oxygen species assessment was performed via flow cytometry as in this chapter, however the authors used CM-H_2DCFDA staining (Tada-Oikawa et al., 2016). The observed effect of THP-1 treatment with titanium (IV) oxide was a lower level of ROS compared to untreated control, in contrast with the effects described by Tada-Oikawa et al.

Direct quantification of reactive oxygen species poses inherent difficulty as the

presence of these radicals is short-lived, ~10^{-9} seconds, prior to their reaction with cellular components (Fu et al., 2014). Investigation of the level of glutathione, due to its rate limited enzymatic conversion (Tandoğan and Ulusu, 2006), provides an alternative measure for oxidative stress possessing a greater window for observation.

Citrate-stabilised gold nanoparticles have been associated with glutathione depletion in a human liver cell line, HL7702 (Gao et al., 2011). No significant impact was observed following treatment with THP-1 cells with gold 1 (citrate-stabilised) at concentrations of 1000, 100, and 10 pg/ml. Significantly higher glutathione, compared to the untreated control, was found at the lowest treated concentration (1 pg/ml). Mix-matrix capped gold 2 generated effects with a high degree of similarity to those of gold 1 at each concentration tested.

Iron oxide nanoparticles have been implicated with depletion of glutathione by a number of sources (Hohnholt and Dringen, 2011; Radu et al., 2010). Endorem and JGC demonstrated such an effect at a concentration of 100 µg/ml, however, showed the opposite at 0.1 and 1 µg/ml, with no significant change at 10 µg/ml. Reduced glutathione was higher than the untreated control in all tested concentrations of Ferumoxytol.

Nanomaterial toxicity based around their impact towards intracellular processes has led to a large amount of work assessing their influence on inflammation and oxidative stress. Investigation into autophagy, a key homeostatic mechanism, has been comparatively limited. Autophagic dysfunction is becoming widely accepted as an important mechanism of nanomaterial toxicity which requires careful consideration when producing new materials. For this reason it forms part of the standardised assay cascade performed by the NCI-NCL (Stern et al., 2013; Stern and Neun, 2011).

Song et al. have previously shown amino-functionalized negatively charged polystyrene nanoparticles to interfere with autophagosomal degradation by accu-

mulation in lysosomes of fibroblasts over 48 hours (Song et al., 2015). Such effects were not observed for positively or neutrally charged polystyrene nanoparticles (Song et al., 2015). There is some confusion, however, as the authors performed zeta potential measurement in cell culture medium, similarly to work performed in Chapter 2, showing that all tested polystyrene nanoparticles displayed a negative surface charge. It can be ascertained that the "cell culture medium" was DMEM, but it is nowhere stated if the medium was supplemented with FBS. As such the described effects should be attributed to the particular surface functionalization and not to the nanoparticle charge. The polystyrene nanoparticles tested in this work, just as all other materials, resulted in a lower level of autophagy compared to the untreated control. A high degree of similarity was observed in the responses of THP-1 cells to quaternary ammonium (polystyrenes 1, 3, and 5) and sulphonate-functionalized polystyrene nanoparticles (polystyrenes 2, 4, and 6) under the conditions described, as such no comment can be given about the effect of zeta potential or surface functionalization.

The influence of the panel of nanomaterials on autophagy was investigated using a high throughput methodology. Existing techniques to assess autophagy e.g. immunoblot, TEM, GFP-LC3 transfection (Tasdemir et al., 2008), are time and labour intensive, while producing limited amounts of data. The work outlined here incorporates an assay based upon a cationic dye that partitions into cells and accumulates in autophagic vacuoles (pre-autophagosomes, autophagosomes, and autolysosomes (autophagolysosomes)) (Barth et al., 2010). Levels of fluorescence can be quantified using a microplate reader, enabling faster analysis, or flow cytometer enabling multiparameter analysis per sample (used here). Many conditions can be assessed in a relatively short amount of time providing a large dataset which can then be reviewed and individual aspects be further investigated by more traditional means. The ability to perform a high throughput assay like that outlined in this work is invaluable as it provides sufficient data to estab-

lish a material's autophagic impact utilising widely available equipment, or as a preliminary screen from which particular conditions can be further investigated using other established methodologies.

A limitation in the methodology used to assess nanomaterial impact on autophagy is that it is unable to discern whether lower fluorescence is a result of less autophagy, or an increased rate of autophagosome degradation and clearance. Further investigation via associated mechanisms would be required for elucidation of the source of this effect. Additionally, if it was found that the cellular response to these nanoparticles was indeed a reduced level of autophagy, assessment of the biological consequences would be of great interest.

The cell lines relevant to, and available at the time of this work were CEM (T lymphocyte), Raji (B lymphocyte), and THP-1 (human monocytic cell line). In order to generate a detectable and meaningful response, preliminary optimisation of the assay was required. Treatment concentrations of the positive controls rapamycin and chloroquine were informed by the assay protocol (Enzo Life Sciences, 2016). The duration of exposure required to reach the greatest observable effect has been shown to differ greatly between cell types ranging from 6 to 24 hours. The observable effect can differ significantly not only between materials but also in cell types and as such there is no "one size fits all" model available for nanomaterials. The magnitude of autophagic induction at optimal time points has been shown to be cell type dependent, with the greatest response seen in the Raji cell line.

The design of *in vitro* assays to investigate specific biological outcomes is fraught with numerous vital considerations which must be addressed in order to generate valid and meaningful data. Here it was attempted to highlight the importance of informed selection for exposure times with regard to assessments of cellular health. For assays quantifying a secreted entity such as LDH or cytokines, so long as sufficient exposure time has been allowed for the response to

be generated, and the accumulated marker is still stable at the time of assessment, the subsequent measurement will be unaffected (Aziz et al., 2016, 1999). When investigating cellular health using a single time point design in the manner described in this chapter, the time point poses greater impact on the observable outcome. Use of predetermined exposure times, often arbitrarily chosen due to convention or convenience, may not provide a true representation of the maximal effect (Essen BioScience, 2016). Even with optimisation of the assay and preliminary investigation to find the exposure time with positive controls to generate maximum observable effect, the translation of this to other compounds and especially nanomaterials does not necessarily hold true (Kell and Oliver, 2014; Treuel et al., 2013). An assay such as this provides insight into the state of the cell at that particular point in time, providing little indication of what biological changes that it has already undergone which may have reached resolution, or initiated further response. For these reasons; modification of standard static time point protocols allowing kinetic assessment was performed.

A number of factors had to be considered in the development of these kinetic methodologies. Phenol red-free medium was chosen for use informed by fluorescence microplate assessment protocols of assays not requiring wash procedures following labelling/staining of the cells. Furthermore, phenol red-containing medium was observed to generate an amplification in the fluorescent signal of cells treated with 40 µg/ml of menadione, but not present in other treatments. If unobserved this effect would lead to an overestimation of the generated ROS.

Cell density required optimisation in order to generate sufficient detectable signal. Low cell counts are not a limiting factor when utilising flow cytometry, as the staining is measured on a cell by cell basis. In a microplate assay such as this, the optical measurement (absorbance/fluorescence/luminescence) is an average of the entire contents of each well. As is standard practice for microplate-based fluorescence assays; in order to detect potential biological effects a balance must

be met where the cell count is within a range that, following staining, sufficient resolution is found between unstained and stained cells, and between various treatments, with the least additional gain applied. Numerous manufacturers are moving toward the production of dyes generating brighter signal so that fewer cells per treatment is necessary. While such dyes may allow for a lower application of additional gain, this is not necessarily a desirable property for application in this situation. A greater number of cells per treatment serves to reduce variability where averages are being taken from entire well contents. The particular microplate reader used in this work utilises a feature called orbital averaging, where the well is analysed at multiple points within its area and an average is taken (BMG LABTECH, 2016). For a uniformly distributed cell suspension this is not a vital feature, but proves invaluable when applying such methodology to adherent cells. Some inconsistencies in trypsinization or dissociation of adherent cell cultures during sample preparation are inevitable, as is uneven distribution of cells in the well following seeding. Overly vigorous ejection of the cell suspension from the pipette into the well can force the cells to deposit on the edges of the well (as this methodology utilises flat-bottomed microplates). In a worst case scenario; the signal generated following measurement is very low but not as a result of lack of effect, in reality measurement being performed on an area of low cell density.

Important parameters required in the protocol are the setting of gain, and focal height. The CLARIOstar features a function to quickly find the well containing the highest signal. The focal height for measurement is then determined again using a propitiatory function of the equipment. Gain setting parameters allow the user to inform the software of the expected signal at its highest point. This is done as a percentage i.e. the signal generated at time zero is 25% of the maximum, which informs the software to set a lower gain to allow for the increased signal at later time-points so as not to saturate the detector. While

theoretically this is a useful feature it has been found more viable to set multiple reads per time point, each of which having gain settings ranging from low to high. In turn this method produces a greater volume of data, from which the optimal gain-associated dataset can be chosen for subsequent analysis. In the instance of developing a new, or applying an existing protocol to a different cell type, it can serve as a safety net if the response is not as expected either being greater and saturating the detector or not providing sufficient signal strength to differentiate between treatments, both instances providing an unusable dataset requiring the assay to be repeated. Obviously this would be easily rectifiable when performing a single endpoint read, but not so where the problem may develop or highlight itself some hours into a lengthy time-course.

The suitability of dyes is of primary importance. For use in a kinetic application; a fluorescent dye needs to be activated/converted in response to the target effect. Those which display constant signal, relying on partitioning into cells and requiring washing to remove surplus unassociated dye would not prove appropriate as any variation in signal generated would be merely small fluctuations. While a dye may seem to be suitable, in practical application this may not stand true.

Most readily available dyes are irreversibly converted following interaction with the biological target. As long as this is known, appropriate data handling can be performed. A limitation can be derived from this fact, especially in instances of more lengthy assessment times, where depletion of the dye can become a limiting factor. Furthermore, dyes of this type cannot directly allow visualisation of the generation and subsequent reduction of effect. The bioluminescent dye of the Promega RealTime-Glo MT Cell Viability Assay is able to produce such a response (Peters and Worzella, 2015). If this principal were to be applied to other cell health assays such as ROS generation, it would allow antioxidant responses to be observed.

While not yet applied to study the impact of nanoparticles on reactive oxygen species generation or reduced glutathione content, the data presented here shows great promise. With further development this methodology could yield an invaluable platform for monitoring the effects of nanoparticles on cellular health over time with high resolution.

The ability of nanomaterials to interact not only with biological systems but also the methods used to assess these interactions leads to complications with determining the appropriateness of assays as well as the inability to have a one-size-fits-all model for nanoparticle assessment. The necessity to assess nanomaterials on a case-by-case basis limits the suitability of applying existing mechanistic knowledge to new materials. Nanomaterial influence over key aspects of cellular health was assessed. Under the tested conditions lower observed levels of ROS were associated with higher glutathione content. All tested nanomaterial conditions led to a lower level of autophagy compared to untreated controls at 24 hours. The development of, and utility and potential for, kinetic methodologies for the assessment of aspects of cellular health has been demonstrated.

Chapter 6

Preclinical biocompatibility assessment of hyperbranched polydendrons with the potential for drug delivery vehicles

Contents

6.1 Introduction 211

6.2 Methods 213

6.2.1 Materials 213

6.2.2 Physicochemical characterisation 214

6.2.3 Assessment of material contamination 214

6.2.3.1 Determination of endotoxin concentration in nanoparticle samples 214

6.2.3.2 Assessment of possible viable microbial contamination 214

6.2.4 Assessment of cytotoxicity 214

6.2.4.1 MTT assay 214

6.2.4.2 LDH assay 215

6.2.5 Assessment of cellular health 215

6.2.5.1 Reactive oxygen species generation 215

6.2.5.2 Measurement of reduced glutathione 215

6.2.5.3 Autophagy 215

6.2.6 Blood contact properties 216

6.2.6.1 Plasma coagulation 216

6.2.6.2 Haemolysis 216

6.2.7 Immunotoxicological assessment 216

6.2.7.1 Cytokine secretion 216

6.2.7.2 Leukocyte proliferation 216

6.2.8 Statistical analysis 217

6.3 Results 218

6.3.1 Physicochemical characterisation and stability of polydendron materials over time 218
6.3.2 Assessment of endotoxin and possible microbiological contamination 222
6.3.3 Assessment of cytotoxicity 223
6.3.3.1 MTT assay 223
6.3.3.2 LDH assay 225
6.3.4 Assessment of cellular health 226
6.3.4.1 Reactive oxygen species generation 226
6.3.4.2 Measurement of reduced glutathione 227
6.3.4.3 Autophagy 228
6.3.5 Blood contact properties 229
6.3.5.1 Plasma coagulation 229
6.3.5.2 Haemolysis 231
6.3.6 Assessment of potential immunogenicity 234
6.3.6.1 Cytokine secretion 234
6.3.6.2 Leukocyte proliferation 237
6.4 Discussion 238

6.1 Introduction

The aim of the work described in this chapter was to apply the methodologies described, and developed, in previous chapters of this thesis to a class of novel nanomaterials termed hyperbranched polydendrons. The rationale of these dendrimer-like materials was to mimic the surface functionality of dendrimers but at much higher molecular weights and size than conventional dendrimers, whilst maintaining a facile synthesis at low production cost (Hatton, 2015). Currently, dendrimers pose promising candidates as drug nanocarriers for their well-defined structures, loading capacities, and potential for surface functionalization (Madaan et al., 2014), but are hindered by lengthy and costly syntheses (Hatton, 2015).

Polydendrons were produced by mixed initiator polymerizations as described by Hatton (2015). Purified N-(2-Hydroxypropyl) methacrylamide (HPMA) monomers (Figure 6.1c) were polymerised with G2' (Figure 6.1a) and 2000PEG initiator (Figure 6.1b), at 50:50 and 75:25 ratios, to result in 100 monomer unit diblock copolymers. The hyperbranched polymeric architectures were formed by the introduction of ethylene glycol dimethacrylate (EGDMA, Figure 6.1d). Self-assembly of the nanoparticles was achieved by nanoprecipitation of the polymers, dissolved in tetrahydrofuran (THF), into water. This method produced nanoparticles with hydrophobic (G2' initiator) and amphiphilic (2000PEG initiator) domains exposed to the external environment (Figure 6.1e). Steric stabilisation of the nanoparticles was achieved through the combination of hydrophilic surface domains as well as long PEG chain length, improving the stability of the nanoparticles under physiologically-relevant conditions as demonstrated in 0.14 M sodium chloride (Hatton, 2015).

In previous chapters within this thesis, a number of assays have been applied to a panel of nanoparticles with the aim of linking physicochemical characteristics to biological effect. These assays have examined aspects of cellular health, im-

munological and haematological interactions as well as blood contact properties. These assays have previously been demonstrated to provide information on common, acute, toxicities that may hinder translation of these materials to in vivo studies (Dobrovolskaia and McNeil, 2013; Zamboni et al., 2012). In addition to a putative preclinical safety assessment, the work sought to link physicochemical characteristics of these materials with biological impact.

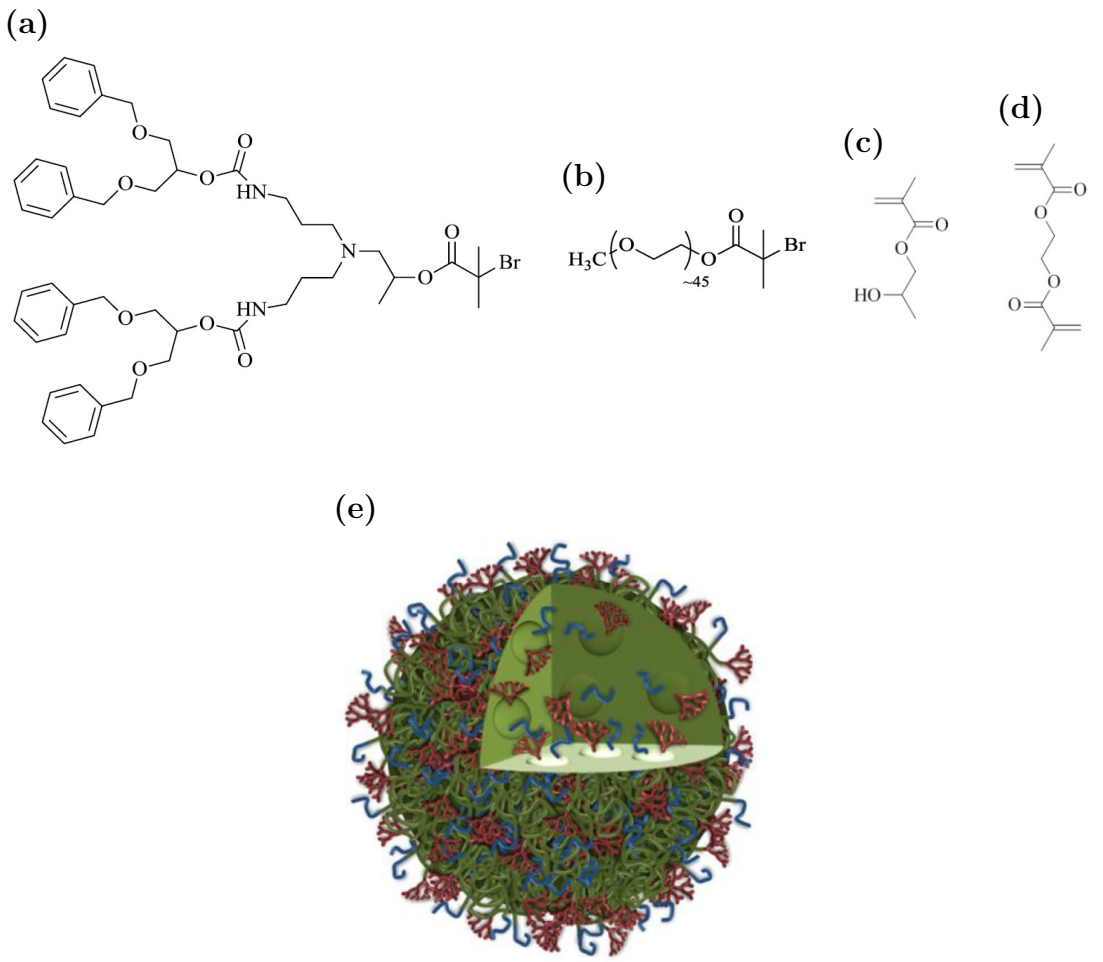

Figure 6.1: Chemical structures of components used in polydendron synthesis (a) G2' initiator. (b) 2000PEG initiator. (c) HPMA. (d) EGDMA. Theoretical structure of the mixed-initiator polydendron nanoparticles (e) Red denotes terminal G2' groups, blue represents 2000PEG groups. Adapted from *Hyperbranched Polydendrons* (p. 105), by F. L. Hatton, 2015, Switzerland: Springer International Publishing. Copyright 2015 by Springer International Publishing Switzerland. Adapted with permission.

6.2 Methods

6.2.1 Materials

Polydendrons composed of G2':2000PEG-pHPMA$_{100}$-EGDMA$_x$ (x = amount of EGDMA present in the polydendron) were provided to us for analysis from the Department of Chemistry at the University of Liverpool (Liverpool, UK) (Hatton, 2015).

The four polydendrons tested were comprised of two ratios (50:50 and 75:25) of dendron initiator (G2') to PEG initiator (2000PEG-pHPMA$_{100}$-EGDMA$_x$, where x = 0.85 for 50:50 and 0.8 for 75:25), and subdivided by size.

Nomenclature of the polydendrons used in this chapter are as follows:

Polydendron (PD) . Ratio of dendron initiator to PEG initiator . Initial Z-average size in deionized water (nm)

where initial Z-average size relates to the Z-average size immediately following production.

Designation	Hydrodynamic size (nm)	PdI
PD.5050.161	160.80	0.07
PD.5050.378	377.80	0.52
PD.7525.157	156.93	0.05
PD.7525.264	264.40	0.00

Table 6.1: Nanomaterials assessed in this chapter including the Z-average hydrodynamic size (nm) and polydispersity index determined by DLS in water at time of production.

Approval for the sampling and storage of human blood samples for biomedical research was gained from the University of Liverpool Committee in Research Ethics (Ref: RETH000563).

6.2.2 Physicochemical characterisation

Stability of polydendrons over time in deionized water was assessed by DLS at 0, 6, 9, and 12 months. Further characterisation of polydendrons in biologically relevant media; RPMI-1640, RPMI-1640 supplemented with FBS to 10% final volume, DMEM, and DMEM supplemented with FBS to 10% final volume, were performed 12 months from production. DLS and zeta potential measurements were performed using a Zetasizer Nano ZS as described in Section 2.2.4.2.

6.2.3 Assessment of material contamination

6.2.3.1 Determination of endotoxin concentration in nanoparticle samples

Endotoxin contamination of polydendrons was assessed using the EndoLISA kit as described in Section 2.2.2. Polydendrons were tested at final concentrations of 100 and 1 µg/ml.

6.2.3.2 Assessment of possible viable microbial contamination

Polydendrons were streaked on plates of LB Agar at neat concentrations. Microbial growth assessment was performed as described in Section 2.2.3.

6.2.4 Assessment of cytotoxicity

6.2.4.1 MTT assay

MTT assay was performed as described in Section 5.2.3.1. THP-1 cells were treated with polydendrons for 24 hours at a maximum concentration of 100 µg/ml, and nine subsequent 1:2 serial dilutions.

6.2.4.2 LDH assay

LDH assay was performed using the Cytotoxicity Detection KitPLUS (LDH) as described in Section 5.2.3.2. THP-1 cells were treated with polydendrons for 24 hours at a maximum concentration of 100 µg/ml, and eight subsequent 1:2 serial dilutions.

6.2.5 Assessment of cellular health

6.2.5.1 Reactive oxygen species generation

Generation of reactive oxygen species was measured via flow cytometry using the CellROX Green fluorogenic probe as described in Section 5.2.4.1. THP-1 cells were treated with polydendrons at concentrations of 0.1, 1, 10, and 100 µg/ml, or camptothecin (10 µM) for 24 hours.

6.2.5.2 Measurement of reduced glutathione

Glutathione reduction was measured via flow cytometry using the ThiolTracker Violet fluorogenic probe as described in Section 5.2.4.2. THP-1 cells were treated with polydendrons at concentrations of 0.1, 1, 10, and 100 µg/ml, or menadione (10 µM) for 24 hours.

6.2.5.3 Autophagy

Effects on autophagy were assessed via flow cytometry using the CYTO-ID Autophagy Detection Kit as described in Section 5.2.4.3. THP-1 cells were treated with polydendrons at concentrations of 0.1, 1, 10, and 100 µg/ml for 24 hours. Positive controls of rapamycin (0.5 µM), chloroquine (10 µM), or combined treatment with rapamycin and chloroquine were included.

6.2.6 Blood contact properties

6.2.6.1 Plasma coagulation

Plasma coagulation via the extrinsic (PT), intrinsic (APTT), and common (TT) pathways was assessed as described in Section 3.2.2.2. Pooled plasma isolated from 3 healthy volunteers was treated with polydendrons at a final concentration of 100 µg/ml for 30 minutes as described in Section 3.2.2.1.

6.2.6.2 Haemolysis

Haemolytic potential of polydendrons was assessed as described in Section 3.2.3. Diluted blood from three healthy volunteers, corrected for plasma free haemoglobin, was treated with polydendrons at a final concentration of 10 µg/ml. Inhibition/enhancement controls of combined 1% Triton-X100 and polydendrons were included.

6.2.7 Immunotoxicological assessment

6.2.7.1 Cytokine secretion

Production of cytokines IFNγ, TNFα, IL-1β, and IL-10 by PBMCs following treatment with polydendrons was assessed via Bio-Plex Pro multiplex assay as described in Section 4.2.3. PBMCs were treated with polydendrons at a final concentration of 100 µg/ml. Combined treatments of polydendrons with LPS (20 ng/ml) were included to assess potential inhibition or enhancement of LPS-mediated stimulation.

6.2.7.2 Leukocyte proliferation

Proliferation was assessed via [^{3}H]-thymidine incorporation as described in Section 4.2.6. PBMCs isolated from buffy coats were treated with polydendrons at

a final concentration of 100 µg/ml. Combined treatments of polydendrons with PHA (20 µg/ml).

6.2.8 Statistical analysis

Statistical analysis was performed using GraphPad Prism 6. Statistical differences were determined using one-way analysis of variance (ANOVA) and Dunnett's multiple comparison tests. A p-value <0.05 was considered as statistically significant.

6.3 Results

6.3.1 Physicochemical characterisation and stability of polydendron materials over time

Size and polydispersity of the polydendrons were monitored over time, as well as visual inspections of the stock solutions, to assess stability of the materials while stored at room temperature. No visible aggregation of the materials was observed and while there were some fluctuations in DLS measured sizes over time (Table 6.2), these were not indicative of aggregation.

Intensity- and volume-weighted size distribution plots of PD.5050.161 displayed unimodal sample distribution in deionized water (Figures 6.2a, 6.2b). Suspension of this polydendron in RPMI-1640 resulted in a greater Z-average size compared to that in deionized water (Figure 6.2c) and the presence of a peak at 5140 nm corresponding to aggregation in one of the replicate measurements. This is exemplified in Figure 6.2d due to its mass. The intensity-weighted distribution of PD.5050.161 suspended in RPMI-1640 supplemented with FBS to 10% final volume displays a multimodal distribution and a skewing of the Z-average size due to peaks at smaller sizes (Figure 6.2e). Figure 6.2f reveals that this is a result of the abundance of protein in the sample generating a peak at 7.66 nm. Similar effect was observed in DMEM supplemented with FBS to 10% final volume. Z-average measurements of polydendrons PD.5050.378, PD.7525.157, and PD.7525.264 were also affected by the presence of protein (Table 6.3).

Peak mean intensity sizes of polydendrons (Table 6.3) overcome the skew generated in the calculations of Z-average. This is exemplified by the consistency of polydendron sizes when measured in complex media compared to that generated in deionized water. For this reason; descriptors of nanoparticle size in complex media throughout this chapter refer to this measure.

With the exception of PD.5050.161, all polydendrons demonstrated positive zeta potential in deionised water (Table 6.3). When introduced to complex culture media, both unsupplemented and supplemented with FBS to 10% final volume, all polydendrons displayed a negative zeta potential tending towards a neutral charge.

	Material	0 months	6 months	9 months	12 months
Z-average	PD.5050.161	160.80	183.80	183.97	188.10
	PD.5050.378	377.80	368.20	352.17	408.33
	PD.7525.157	156.93	155.50	154.50	149.93
	PD.7525.264	264.40	264.07	264.10	394.43
PdI	PD.5050.161	0.07	0.04	0.04	0.09
	PD.5050.378	0.52	0.36	0.45	0.60
	PD.7525.157	0.05	0.06	0.05	0.14
	PD.7525.264	0.00	0.04	0.05	0.27

Table 6.2: Nanoparticle Z-average intensity weighted mean hydrodynamic size (nm) and polydispersity index (PdI) measurements performed at various time points to assess temporal stability of polydendrons in water.

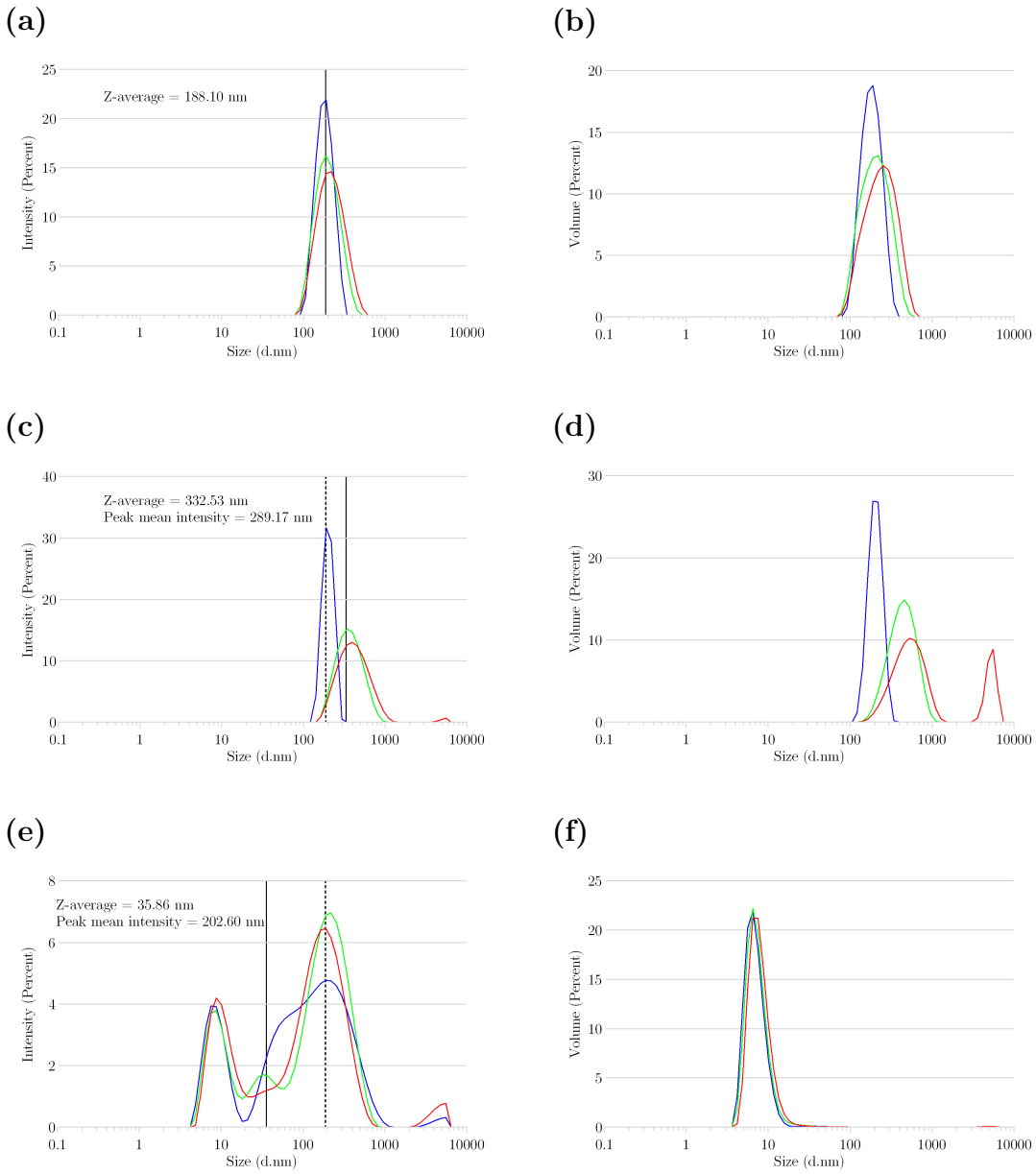

Figure 6.2: Intensity-weighted size distribution plots generated by DLS measurement of PD.5050.161 suspended in (a) deionized water. (c) RPMI-1640. (e) RPMI-1640 supplemented with FBS to 10% final volume. Vertical solid black lines denote preparation specific Z-average nanoparticle size, vertical dashed black lines denote Z-average of PD.5050.161 determined in deionized water. Corresponding volume-weighted size distribution plots generated by DLS measurement of PD.5050.161 suspended in (b) deionized water. (d) RPMI-1640. (f) RPMI-1640 supplemented with FBS to 10% final volume. Red, green, and blue traces represent n=3 sample measurements.

	Material	Deionised water	RPMI-1640	RPMI-1640 10% FBS	DMEM	DMEM 10% FBS
Z-average	PD.5050.161	188.10	332.53	35.86	161.97	106.41
	PD.5050.378	408.33	452.23	27.72	256.30	19.40
	PD.7525.157	149.93	145.33	47.54	109.50	39.49
	PD.7525.264	394.43	361.13	24.84	571.23	69.98
Peak mean intensity	PD.5050.161	207.23	289.17	202.60	181.83	240.00
	PD.5050.378	689.23	831.00	485.10	528.90	437.10
	PD.7525.157	161.30	166.87	134.33	117.73	104.27
	PD.7525.264	392.17	325.43	301.23	208.37	281.10
PdI	PD.5050.161	0.09	0.28	1.00	0.22	0.47
	PD.5050.378	0.60	0.69	0.77	0.68	0.74
	PD.7525.157	0.14	0.16	0.68	0.14	0.65
	PD.7525.264	0.27	0.36	0.88	0.66	0.85
Zeta potential	PD.5050.161	-11.97	-2.01	-2.21	-1.49	0.57
	PD.5050.378	27.17	-1.91	-1.70	-1.14	-1.77
	PD.7525.157	33.77	-1.81	-2.51	-0.99	-0.88
	PD.7525.264	9.73	-0.63	-4.74	-1.33	-1.54

Table 6.3: Nanoparticle Z-average intensity weighted mean hydrodynamic size (nm), peak mean intensity size (nm), polydispersity index (PdI), and zeta potential (mV) determined in deionized water , RPMI-1640, RPMI-1640 supplemented with FBS to 10% final volume, DMEM, and DMEM supplemented with FBS to 10% final volume.

6.3.2 Assessment of endotoxin and possible microbiological contamination

Polydendrons streaked on LB agar did not demonstrate any microbial growth upon visual inspection following 24 hours incubation.

PD.5050.161 at 100 µg/ml was found to contain 0.22 EU/ml of endotoxin (Table 6.4). All other samples fell below the limit of quantification of the assay (0.05 EU/ml). All tested polydendron concentrations generated recoveries within the accepted 50-200% range (Figure 6.3) showing no interference with the assay.

Material	Tested concentration	Endotoxin content	Tested concentration	Endotoxin content
PD.5050.161	100 µg/ml	0.22	1 µg/ml	BLQ
PD.5050.378	100 µg/ml	BLQ	1 µg/ml	BLQ
PD.7525.157	100 µg/ml	BLQ	1 µg/ml	BLQ
PD.7525.264	100 µg/ml	BLQ	1 µg/ml	BLQ

Table 6.4: Endotoxin content (EU/ml) measured from the concentrations stated. BLQ - below limit of quantification (0.05 EU/ml).

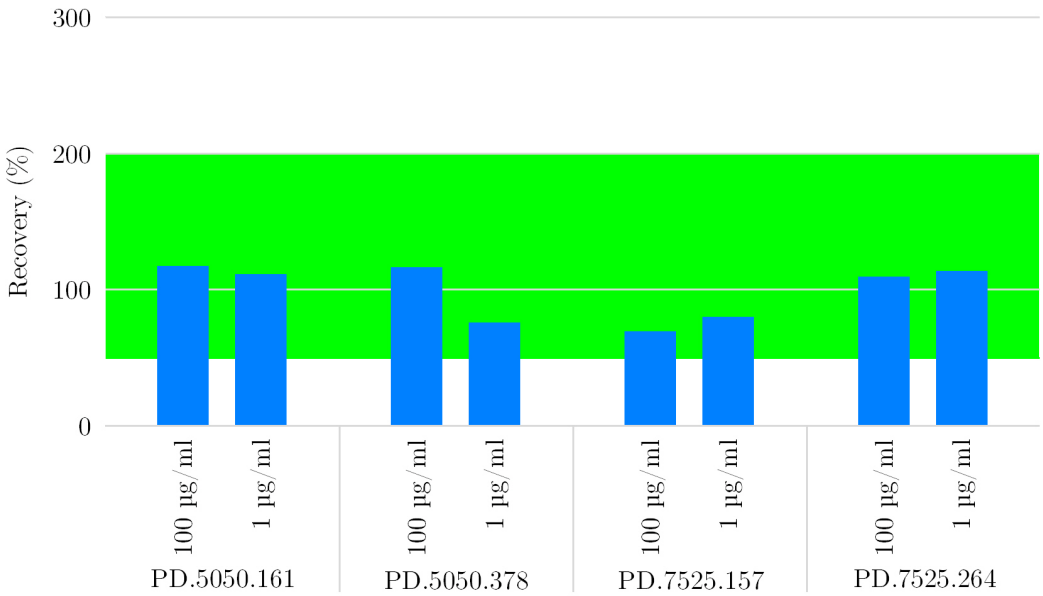

Figure 6.3: Percentage endotoxin recovery from endotoxin spiked nanomaterials at stated concentrations. Green shaded region highlights the acceptable 50-200% range of recovery.

6.3.3 Assessment of cytotoxicity

6.3.3.1 MTT assay

The MTT assay of THP-1 cells treated with polydendrons for 24 hours generated CC_{50} values for PD.5050.161 (67.4 µg/ml, Figure 6.4a), PD.5050.378 (111.4 µg/ml, Figure 6.4b), and PD.7525.264 (26.6 µg/ml, Figure 6.4d). PD.7525.157 did not generate an CC_{50} under the tested conditions (Figure 6.4c).

The greatest cytotoxic impact generated by the polydendrons was observed at the highest tested concentration (100 µg/ml). This resulted in a 35% loss in cell viability following treatment PD.5050.161, however, did not exceed 30% in treatments with PD.5050.378, PD.7525.157, and PD.7525.264, at the 24 hour time point. Incomplete sigmodial concentration-response curves were generate in response to these materials suggesting that at higher concentration, a greater cytotoxic effect may occur. Evaluation of this was not possible due to the limited stock concentrations of the polydendron nanomaterials.

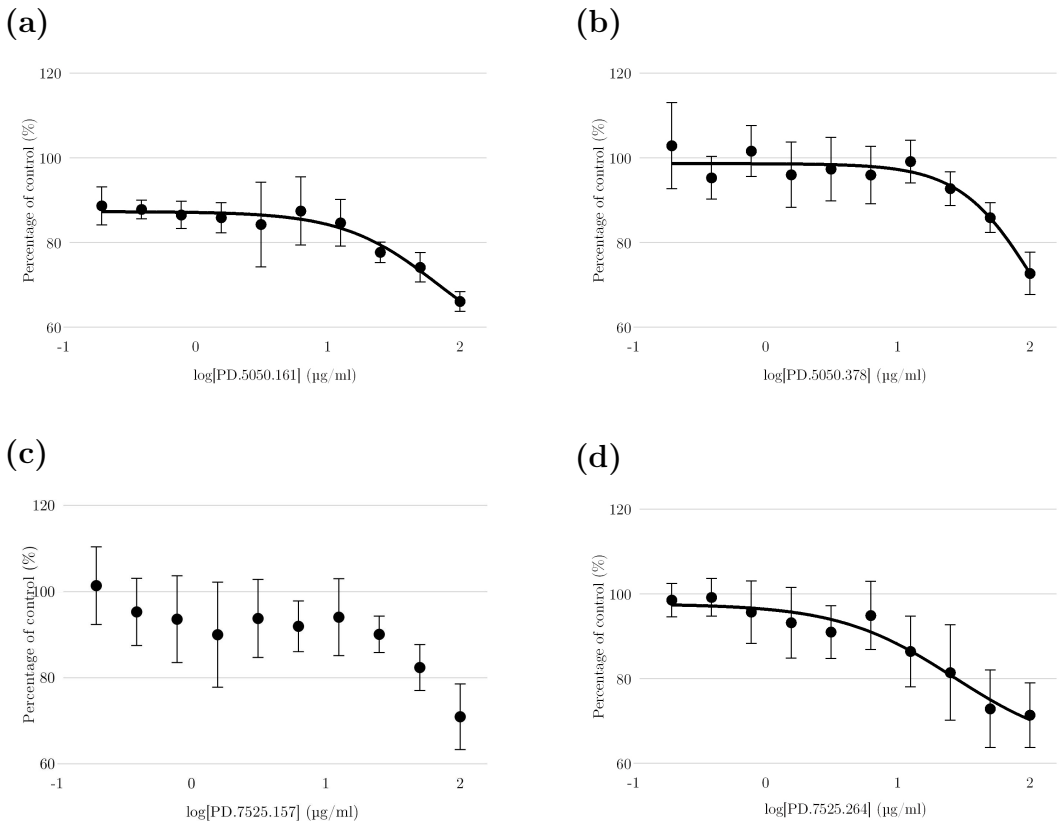

Figure 6.4: MTT assay concentration-response curves generated following 24 hour treatment of THP-1 cells with (a) PD.5050.161. (b) PD.5050.378. (c) PD.7525.157. (d) PD.7525.264. Curves denote treatments which provided calculated CC_{50} concentrations. Data displayed as average (n = 8) ± standard deviation.

6.3.3.2 LDH assay

No overt loss of membrane integrity and release of LDH was observed following treatment of THP-1 cells with polydendrons under the described conditions when assessed by the LDH assay. As such, CC_{50} values were unable to be generated from the resulting concentration-response curves (Figure 6.5).

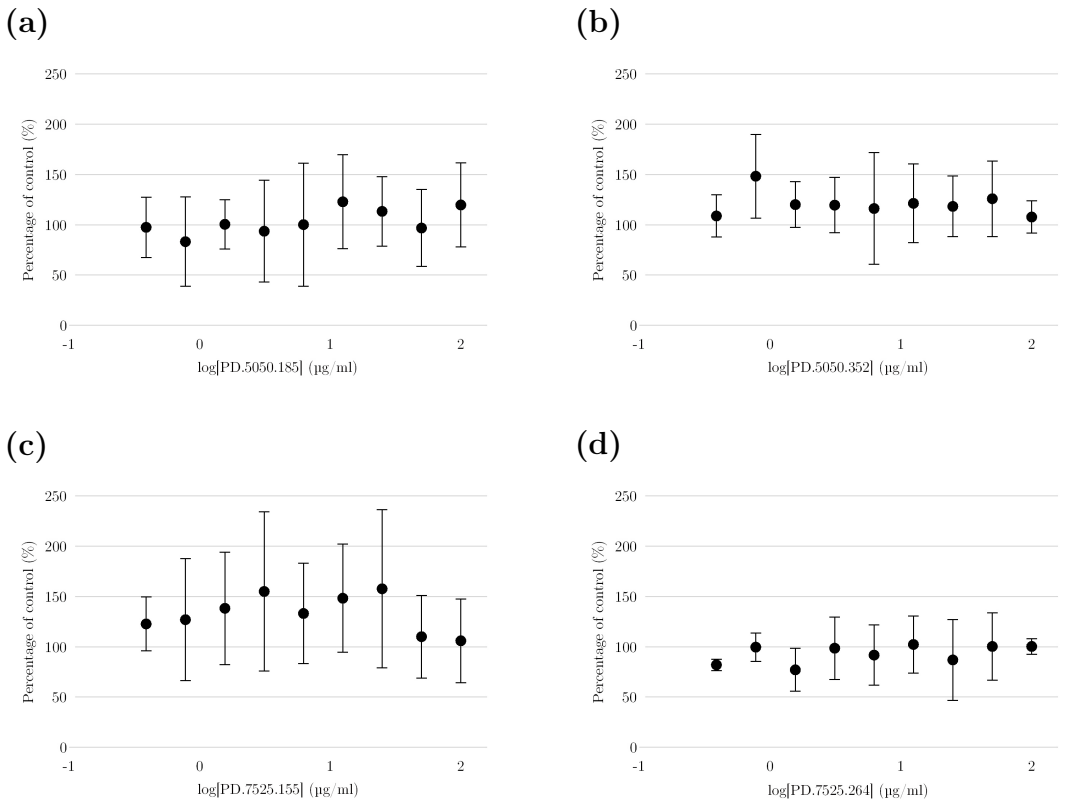

Figure 6.5: LDH assay concentration-response curves generated following 24 hour treatment of THP-1 cells with (a) PD.5050.161. (b) PD.5050.378. (c) PD.7525.157. (d) PD.7525.264. Data displayed as average (n = 3) ± standard deviation.

6.3.4 Assessment of cellular health

6.3.4.1 Reactive oxygen species generation

Overall, significantly lower (p = <0.0001) levels of reactive oxygen species generation were observed across all tested concentrations of polydendrons compared to the control of untreated THP-1 cells at the 24 hour time point (Figure 6.6). The greatest effect was found at the highest treated concentration (100 µg/ml) for each polydendron, where ROS generation was 48% (PD.5050.161), 59% (PD.5050.378), 57% (PD.7525.157), and 39% (PD.7525.264) lower, but concentration-dependent effects were only found in PD.5050.161.

Treatment with the positive control camptothecin, a known inducer of reactive oxygen species, resulted in a level of ROS 86% (p = <0.0001) lower than that of the untreated control.

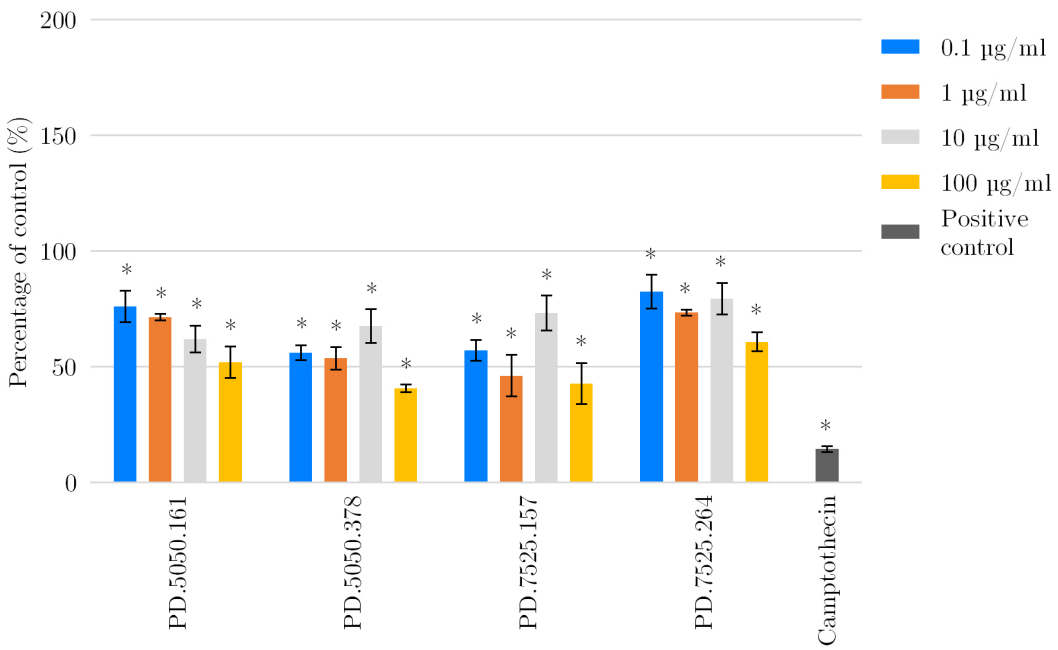

Figure 6.6: Graph displaying the generation of reactive oxygen species in the presence of stated nanomaterials as a percentage of untreated of control. Data displayed as average (n = 4) ± standard deviation. * p-value <0.05.

6.3.4.2 Measurement of reduced glutathione

A 30% greater level of reduced glutathione compared to the untreated control was observed across all treated concentrations of PD.7525.157 (p = <0.0001, Figure 6.7). Similar was observed for 0.1, and 1 µg/ml treatments with PD.5050.378, whereas 10 and 100 µg/ml of this polydendron did not result in significant change. The only polydendron treatment to generate a level of reduced glutathione content lower than that of the untreated control was PD.7525.264 at a concentration of 0.1 µg/ml (14%, p = 0.0195). No further polydendron treatments were found to have significant effect on the level of reduced glutathione under the tested conditions.

Menadione, a compound used to generate free radicals, at a concentration of 10 µM generated a 29% (p = <0.0001) greater level of reduced glutathione than the untreated control.

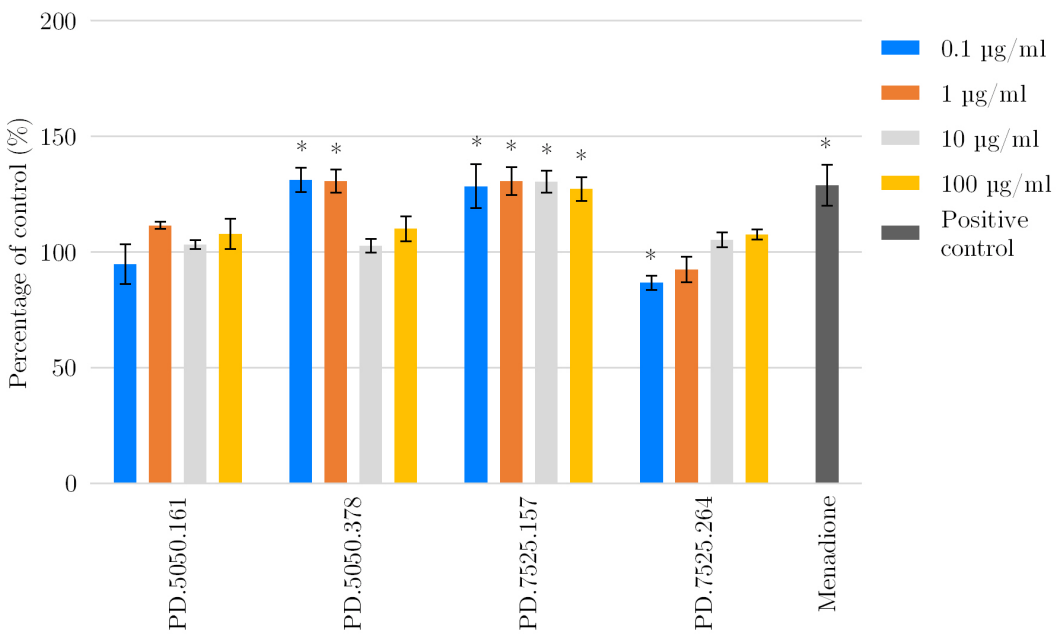

Figure 6.7: Graph displaying reduced glutathione in the presence of stated nanomaterials as a percentage of untreated of control. Data displayed as average (n = 4) ± standard deviation. * p-value <0.05.

6.3.4.3 Autophagy

Levels of autophagy were found to be significantly lower (p = <0.0001) across all polydendron treatments, with the exceptions of 100 µg/ml PD.5050.378 (p = 0.1425) and PD.7525.264 (p = 0.9996), compared to the untreated control after 24 hours. 100 µg/ml was found to generate the least effect across all materials. Treatment with PD.7525.157, possessing the smallest peak mean intensity size in RPMI-1640 10% FBS (134.33 nm), resulted in the lowest observed levels of autophagy compared to the other polydendrons, at each tested concentration.

Treatment of THP-1 cells with positive controls rapamycin and chloroquine produced levels of autophagy 32% (p = <0.0001) lower, and 68% (p = <0.0001) higher than that of the untreated control. Combined treatment with rapamycin and chloroquine caused autophagy to be 40% (p = <0.0001) greater than in untreated cells.

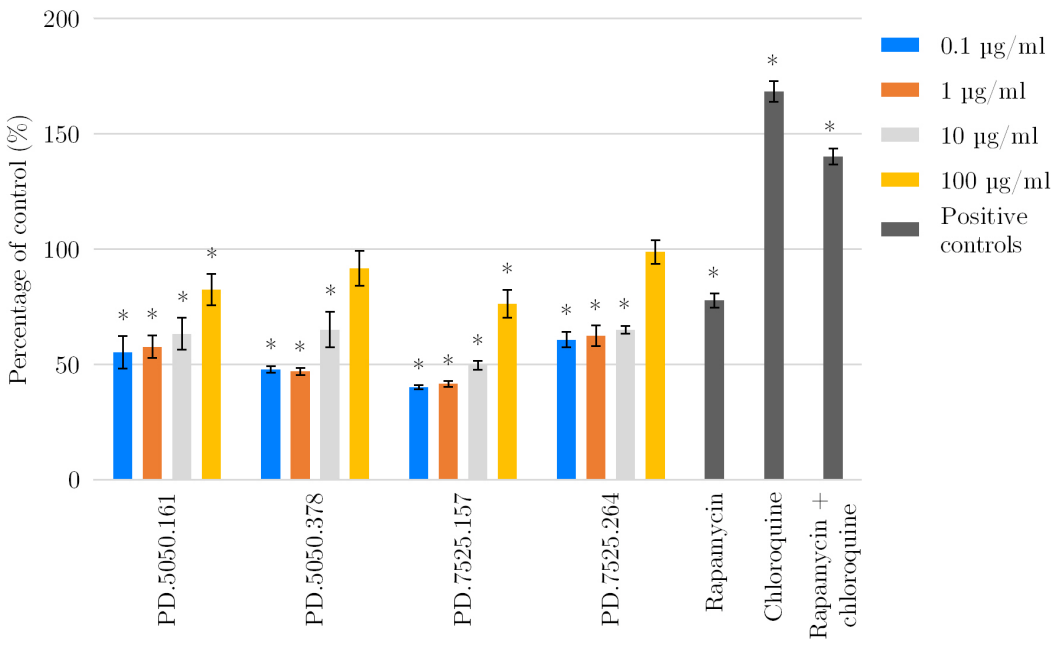

Figure 6.8: Graph displaying the effect on autophagy resulting from treatment with the stated nanomaterials as a percentage of untreated of control. Data displayed as average (n = 4) ± standard deviation. * p-value <0.05.

6.3.5 Blood contact properties

6.3.5.1 Plasma coagulation

Under the tested conditions, the greatest effect was observed in treatment of pooled plasma with PD.7525.157 where coagulation occurred at 11.2 seconds compared to 11.75 for the untreated control (Figure 6.9a).

Untreated plasma and all polydendron treated plasma coagulation times fell within the accepted "normal" range of 12-15 seconds for the intrinsic coagulation pathway. A 1.8 second greater coagulation time resulted from treatment with PD.7525.157 compared to untreated plasma (Figure 6.9b).

Coagulation time via the common coagulation pathway of PD.7525.157-treated plasma was 2.8 seconds faster than that of untreated plasma (Figure 6.9c).

(a)

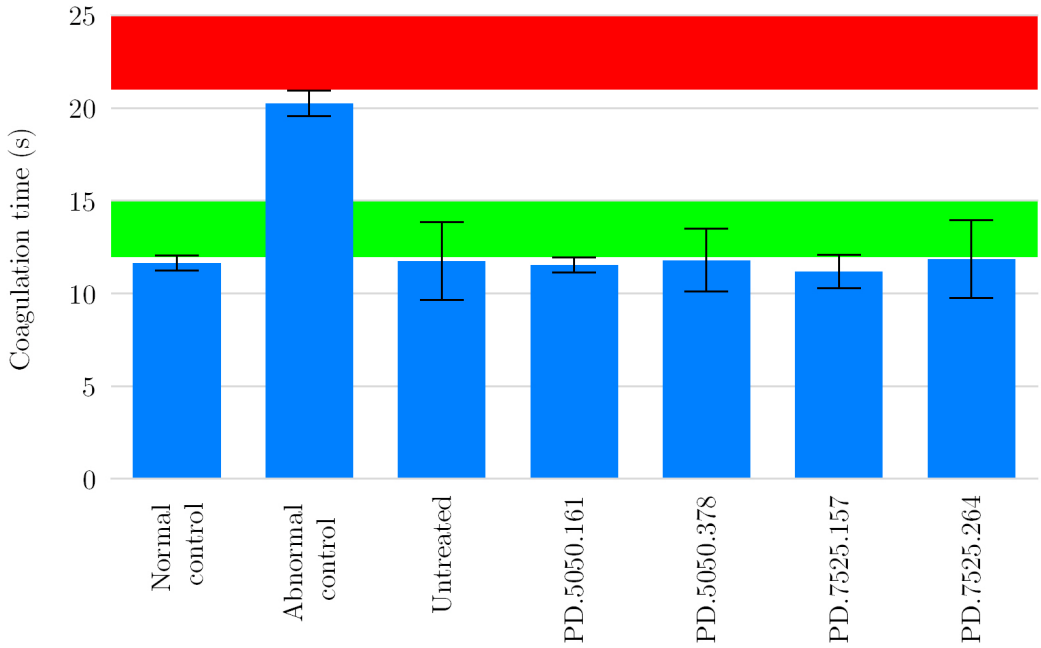

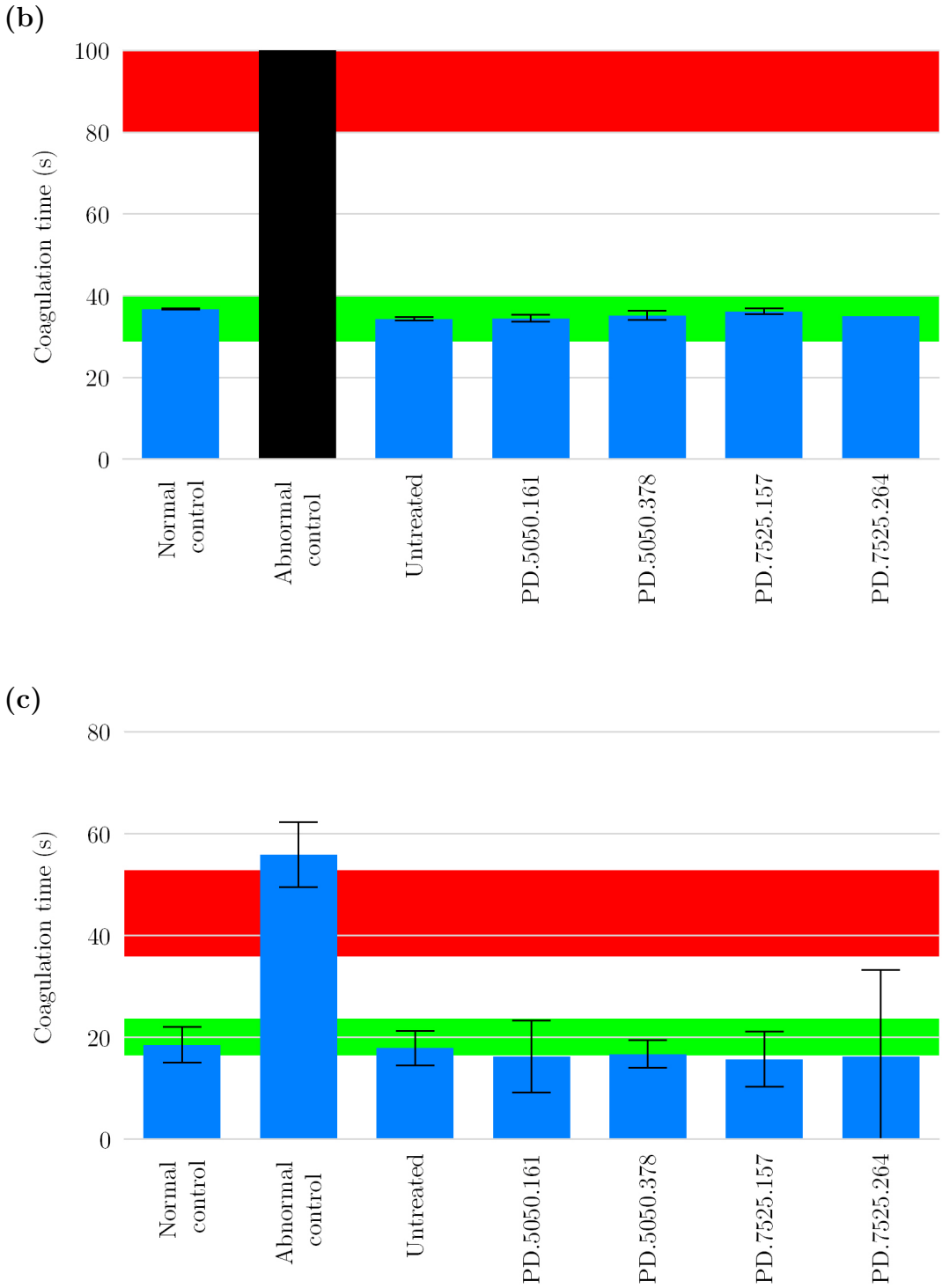

Figure 6.9: Coagulation times for nanoparticle treated plasma via the (a) Extrinsic pathway. (b) Intrinsic pathway. (c) Common pathway. Black bars denote samples which did not coagulate within the time limit. Green, and red highlighted areas indicate expected ranges of coagulation time for normal and abnormal control plasmas respectively, as stated in the manufacturer's product information. Data displayed as average of duplicate measurements ± %CV.

6.3.5.2 Haemolysis

The American Society for Testing and Materials have set out guidelines for the assessment of haemolysis; <2% is deemed non-haemolytic, 2-5% slightly haemolytic, and >5% haemolytic (American Society for Testing and Materials, 2000). Treatment of healthy volunteer whole blood with polydendrons not result in major haemolysis however, treatment with PD.5050.161 in individual 1, and PD.7525.157 in individual 3 demonstrated slight haemolytic activity (3.85% and 2.35% respectively, Figure 6.10a). Interindividual variability was observed regarding the magnitude and effect of polydendron treatment relative to the untreated control. Negative percentages of haemolysis displayed in Figure 6.10a were attributed to assay variation resulting from percentages being calculated from 10 g/dl plasma free haemoglobin as described in Section 3.2.3.

Inhibition (12%) of Triton X-100 induced haemolysis by PD.5050.161 treated samples was observed in blood from individuals 2 and 3. PD.5050.378 and PD.7525.157 also inhibited haemolysis in individual 2 by 11% and 9% respectively. Enhancement of calculated percentage of haemolysis was found by PD.5050.378 (25%) and PD.7525.264 (30%) in blood from individual 1 (Figure 6.10b). This effect is attributed to material presence, as total haemolysis was achieved with Triton X-100 treatment.

(a)

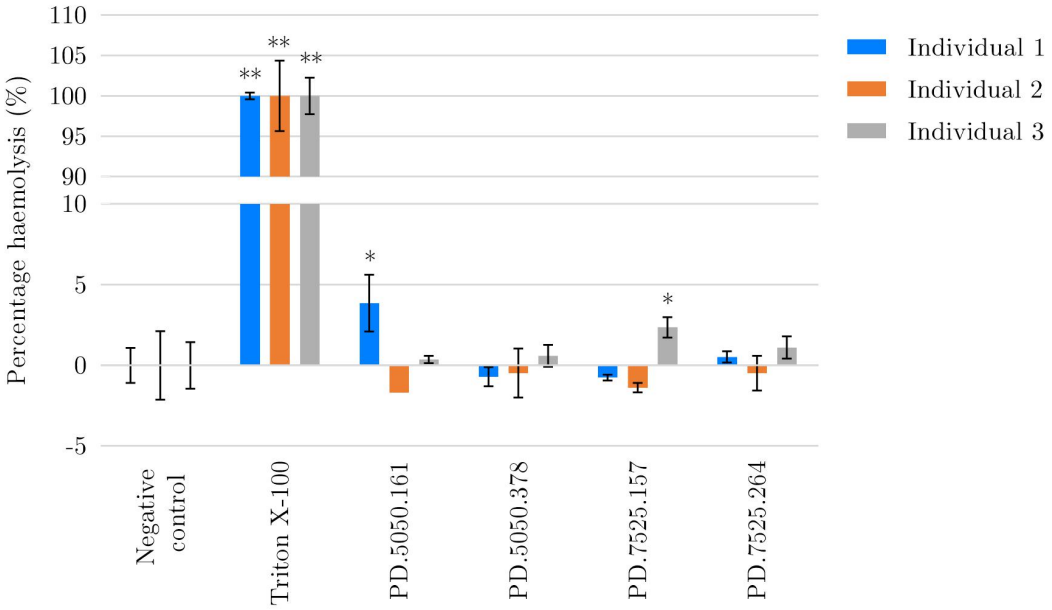
Percentage haemolysis (%)
110
105
100
95
90
10
5
0
-5
**
**
**
*
*
Individual 1
Individual 2
Individual 3
Negative control
Triton X-100
PD.5050.161
PD.5050.378
PD.7525.157
PD.7525.264

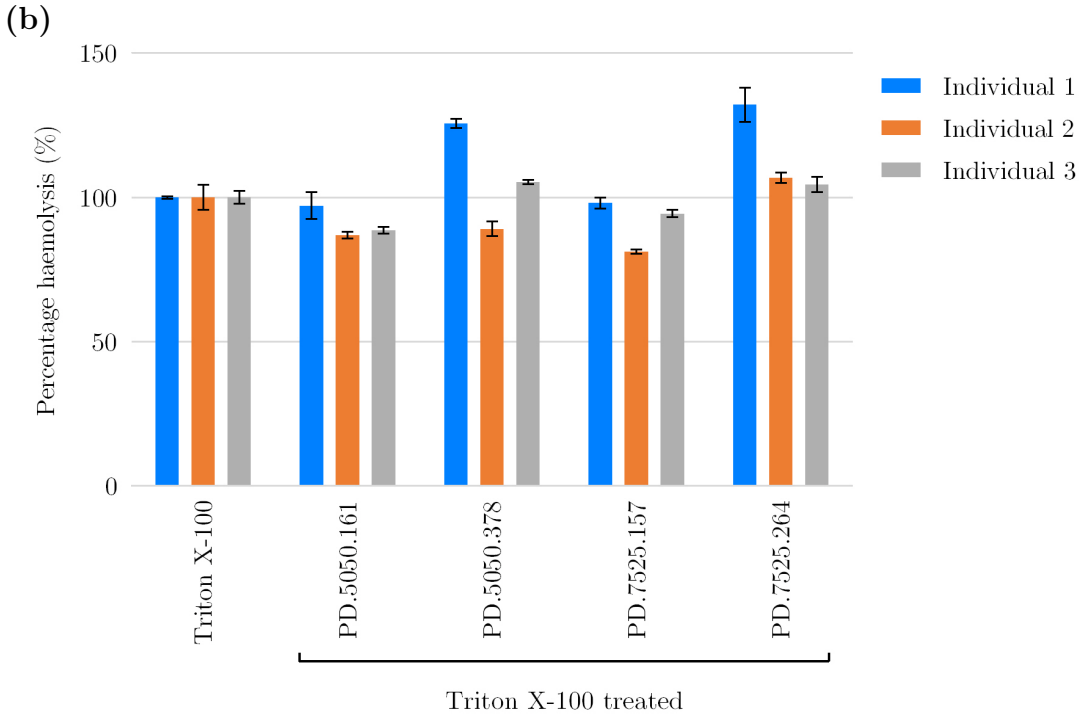

Figure 6.10: Percentage haemolysis, relative to controls, generated by (a) Treatment with stated nanomaterials. * denotes 2-5% haemolysis. ** denotes haemolysis >5%. (b) Nanomaterials following treatment with Triton X-100 to assess inhibition/enhancement. Data displayed as average (n = 3) ± standard deviation.

6.3.6 Assessment of potential immunogenicity

6.3.6.1 Cytokine secretion

No samples were found to have generated IFNγ at a concentration greater than the lower limit of detection for the assay (6.93 pg/ml). Furthermore, as the levels of TNFα, IL-1β, and IL-10, were below the detectable limit of the assay (TNFα - 15.40 pg/ml, IL-1β - 3.85 pg/ml, IL-10 - 8.42 pg/ml) in untreated controls, it was not possible to calculate fold difference or perform statistical analysis on these samples.

Treatment with PD.5050.161 generated 83.43, and 100.27 pg/ml of TNFα in individuals 2, and 3 respectively (Figure 6.11a).

In LPS stimulated samples, all polydendron treatments resulted in inhibition of TNFα compared with the positive control in individuals 1 and 2. PD.5050.378 enhanced the level of TNFα in individual 3 by 18 pg/ml. IL-1β was inhibited in individual 1 and, with the exception of PD.5050.378, individual 3. Enhancement of 48% was observed in individual 2. IL-10 production was inhibited by all polydendrons in LPS stimulated samples, most notably 50% by PD.7525.264 in individual 1, 50% by PD.5050.378 in individual 2, and 69% by PD.7525.157 in individual 3.

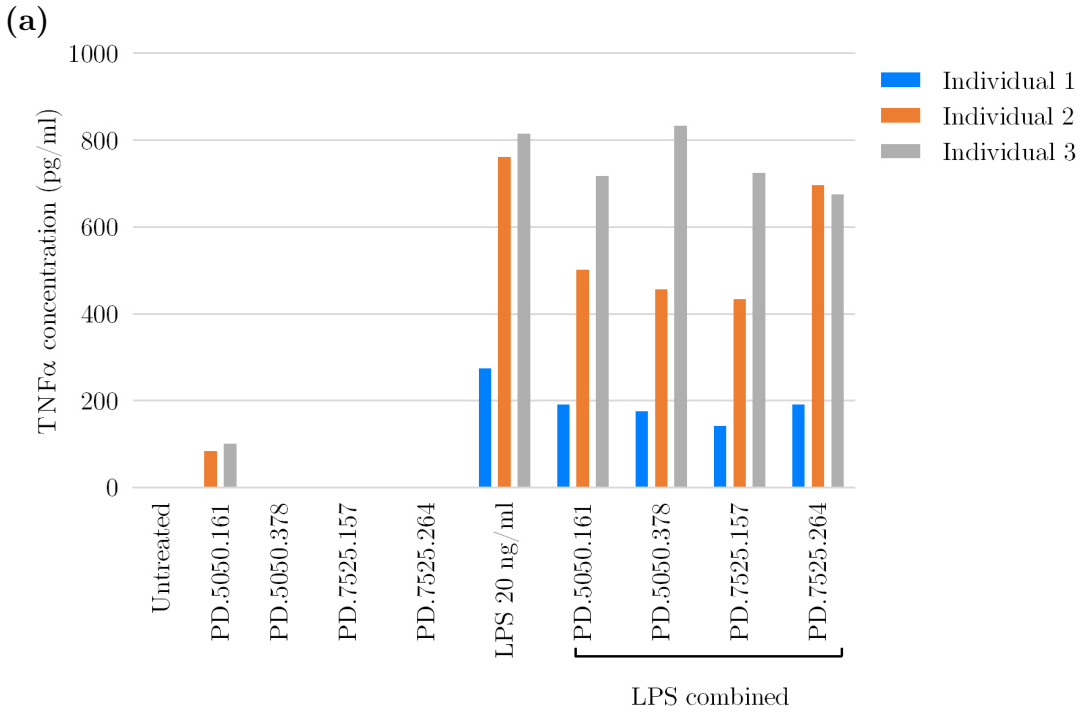
(a)
TNFα concentration (pg/ml)
1000
800
600
400
200
0
Individual 1
Individual 2
Individual 3
Untreated
PD.5050.161
PD.5050.378
PD.7525.157
PD.7525.264
LPS 20 ng/ml
PD.5050.161
PD.5050.378
PD.7525.157
PD.7525.264
LPS combined

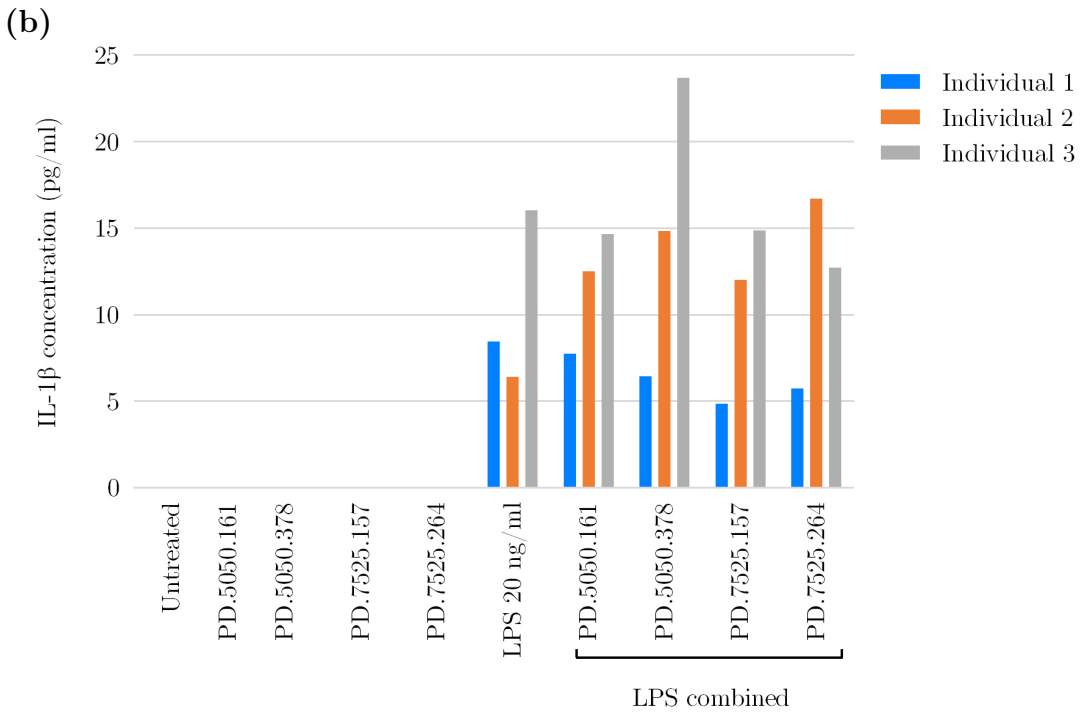
(b)
IL-1β concentration (pg/ml)
25
20
15
10
5
0
Individual 1
Individual 2
Individual 3
Untreated
PD.5050.161
PD.5050.378
PD.7525.157
PD.7525.264
LPS 20 ng/ml
PD.5050.161
PD.5050.378
PD.7525.157
PD.7525.264
LPS combined

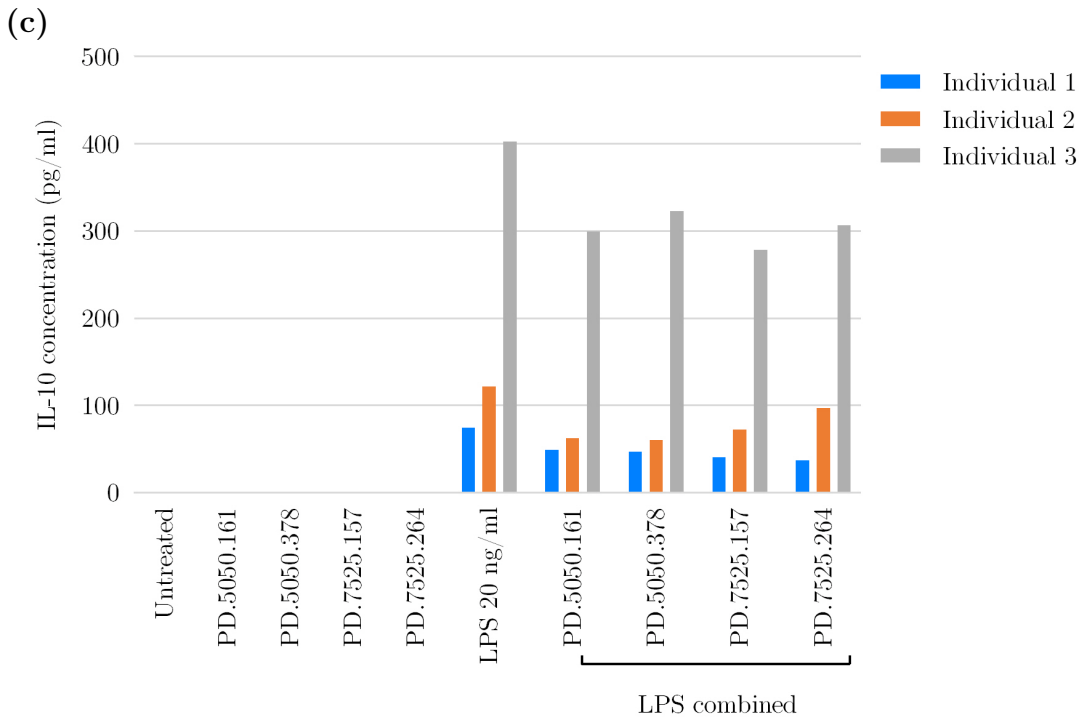

Figure 6.11: Concentrations of cytokines (a) TNFα, (b) IL-1β, (c) IL-10 secreted by peripheral blood mononuclear cells in response to treatment with polydendrons, LPS, or combined LPS treatment with polydendrons. Red horizontal line signifies lower limit of quantification.

6.3.6.2 Leukocyte proliferation

Significantly greater proliferation (62.8%, p = 0.0095) was observed in PBMCs treated with PD.5050.161 compared to the unstimulated control. No further polydendron treatments were found to have generated a statistically significant effect on leukocyte proliferation.

No significant changes were found in leukocyte proliferation between the stimulated control and coincubations of PBMCs with polydendron materials and PHA. Therefore, the polydendron materials did not enhance, or inhibit, PHA stimulated proliferation (Figure 6.12).

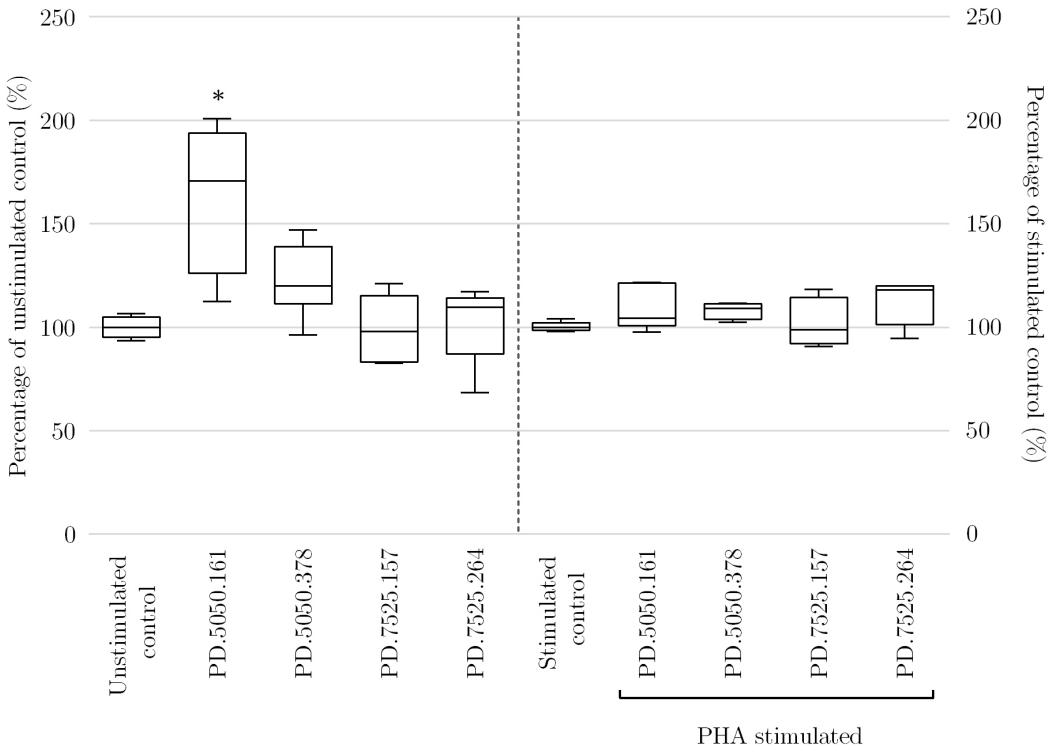

Figure 6.12: Proliferation of peripheral blood mononuclear cells in the presence of polydendrons, and combined treatment with PHA and polydendrons. Data displayed as box and whisker plots showing average, maximum, and minimum (n = 6) ± standard deviation. * p-value <0.05.

6.4 Discussion

The application of routinely used physicochemical characterisation methodologies and assays are not always appropriate to determine material biocompatibility of nanomaterials (Cleland et al., 2016). As outlined in Chapter 2, this can be the result of either direct or indirect interference by the physicochemical and optical characteristics of nanomaterials (Baer, 2011), or their preparation i.e. polydispersity, low or high concentration, turbidity, or the medium which they are suspended in. While for nanomaterials of low complexity e.g. monodisperse spherical solid nanoparticles, an accurate measurement of size and charge can be achieved in water (Dieckmann et al., 2009; Rameshwar et al., 2006) or under vacuum (Stratton et al., 2013). Increasingly complex nanomaterials whose structure and stability relies on remaining in suspension such as dendrimers and emulsions, pose limitations on the characterisation methodologies which can be directly applied (Wang et al., 2012), or require specialised preparation such as cryo-fixation (Klang et al., 2012).

These measurements, however, are not as applicable when the eventual fate of the nanomaterial is to be introduced into a biological system. The complexity of the medium to which the material is introduced can greatly affect the nanoparticle's physical state causing changes in size, charge, and agglomeration state (Lazzari et al., 2012). This is especially pertinent when the nanomaterial under evaluation is of a novel architecture such as hyperbranched polydendrons (Hatton, 2015). Therefore, the need to measure physicochemical characteristics in biologically relevant media becomes increasingly important, especially when attempting to observe trends amongst various formulations.

Stability of the polydendrons over time (as measured by changes in size and PdI) was monitored over a one-year period as a confirmatory measure of the long-term stability described by Hatton (2015). As with any nanomaterial being

assessed, the shelf life is of importance not only for the end product, but in knowing that the physicochemical characteristics maintain consistency over time ensuring data produced is comparable. The parameters monitored in Table 6.2 show high stability for the polydendrons when stored at room temperature for a period of 12 months.

As discussed in Section 2.4, the use of peak mean intensity size was most applicable when the polydendrons were assessed in complex media. For this measure nanoparticle sizes within modes of the sample distribution are generated separately to those of Z-average allowing the peak's source to be distinguished. When considering the Z-average sizes in exclusion of the peak mean intensity sizes it would appear that the nanoparticle sizes are altered significantly following introduction to complex media. Observing this further measure highlights limitations in the methods employed to calculate nanoparticle sizes using this technology. As was the intention of the design of these polydendrons; steric stabilisation imparted a stability and consistency in size following introduction to complex media.

The observation that PD.5050.161 at a concentration of 100 µg/ml was the only preparation to contain a quantity of endotoxin greater than the limit of detection for the assay (0.05 EU/ml), although being formulated from the same reagents as PD.5050.378, is not unexpected as these materials were not prepared to GMP standard. No other polydendron preparations were found to contain quantifiable levels of endotoxin and evaluations of spike recovery showed no cause for concern regarding polydendrons sequestering endotoxin, all being within the accepted range of 50-200% (U.S. Food and Drug Administration, 2012a; European Medicines Agency, 2010).

Use of the THP-1 cell line for *in vitro* assessments of cytotoxicity and modulation of cellular health, as discussed in Chapter 5, was informed by their extensive presence in the literature as a model of human monocytes (Chanput et al., 2014)

providing a pertinent representation of a cellular subset encountered by nanoparticles in the peripheral blood. Previous development and optimisation of assays in this cell line established their continued use in this chapter.

No assay interference was observed by the polydendrons in either the MTT or LDH assays as evidenced by the inclusion of cell free controls within each assay run. Polydendrons PD.5050.161, PD.5050.378, and PD7525.264 generated CC_{50} values in the MTT assay. THF was used as a solvent in the production of polydendrons and is removed by overnight evaporation (Hatton, 2015). While THF has been deemed non-cytotoxic on its own (U.S. Environmental Protection Agency, 2011), any effects resulting from residual THF are unknown. This could be controlled for by using a secondary, earlier, timepoint for assay (~2 hours) where nanomaterials would not yet have accumulated intracellularly but small molecules would. It can be suggested that the polydendrons have some influence over mitochondrial activity, but do not necessarily generate cytotoxicity under the conditions assessed as evidenced by data generated in the LDH assay. The MTT assay relies on mitochondrial dehydrogenases in order to produce the detected formazan product (Berridge and Tan, 1993), whereas the LDH assay measures LDH activity following disruption of cell membrane integrity and release of the enzyme from the cytosol. No overt cytotoxicity was observed in the LDH assay under the conditions tested, supporting the proposed idea and strengthening the arguments set out in Chapter 1 surrounding the need for complementary assays as a confirmative measure. Maximum tested concentrations were limited by the process used to produce the polydendron suspension. As the work outlined here is a preclinical assessment, the concentrations tested could not be based on pharmacokinetic data. Data on the PK of these materials would provide an informed basis for further compatibility assessment.

To further explore the theme of complementary assays, in accordance with the work set out in Chapter 5, the impact of polydendrons on oxidative stress was

assessed by both oxidative and antioxidant mechanisms. As discussed in Chapter 5; the generation of the antioxidant response requires first the propagation of reactive oxygen species. The time-dependant nature of these processes must be considered when monitoring, and relating the observed effect to the biological effect. It has been shown that higher levels of reduced glutathione, most evident in response to PD.5050.378 and PD.7525.157, correspond with lower ROS levels at the same time point compared to untreated cells. Treatments with PD.5050.161 and PD.7525.264 do not display as great a magnitude in effect which may relate to the assay being performed at an earlier point in the generation of the antioxidant response, or a return to homoeostasis. The lower level of reactive oxygen species in response to treatments with PD.5050.161, combined with the lack of influence over reduced glutathione content, would imply that this variant possesses some antioxidant properties. Further assessment would be required to confirm this. An absence in dose-dependent effects raises the question of how the polydendron nanomaterials are affecting pro- and antioxidant mechanisms in the THP1 cell line. This could be the result of concentration-dependent limitation of cellular uptake, which would necessitate differing time points being required to detect maximum observable effect. An kinetic assessment paradigm like that described in Section 5.2.5 would be highly advantageous for such an evaluation.

Similar to the observations described in Chapter 5, polydendron treatments at concentrations of 0.1, 1, and 10 µg/ml exhibited lower levels of autophagy compared to the untreated control in THP-1 cells at 24 hours. It was interesting to observe that at the highest tested concentration (100 µg/ml) there was no significant change from untreated cells in treatments with PD.5050.378, PD.7525.157, and PD.7525.264. This may be the result of a restorative effect, or this concentration affecting the time to onset of the effects found in the other tested concentrations. While the optimal time point for this assay was validated in Chapter 5 using the small molecule controls rapamycin and chloroquine,

the mechanisms by which these enter cells (Kell and Oliver, 2014) differ from that of nanoparticles (Treuel et al., 2013). Small molecules are able to directly reach the cytoplasm which results in a faster generation of biological response compared to that of nanoparticles which is reliant on particle escape from endocytic machinery or release of degradation products. The fluorescent probe used here for measuring autophagy exhibits fluorescence following incorporation into pre-autophagosomes, autophagosomes, and autolysosomes (autophagolysosomes) (Enzo Life Sciences, 2016). Any pH changes resulting from the presence of nanomaterials in autophagosomes could potentially modulate the efficacy of the probe. The potential for this has been shown by Song et al. where the fluorescence intensity of acridine orange (AO) labelled lysosomes was reduced by cationic polystyrene nanoparticles affecting lysosomal pH (Song et al., 2015). Also in a similar manner to the observations described by Song et al.; damage caused to the autophagosomal membrane by nanomaterials could lead to leakage of the probe and reduce the amount available to generate fluorescence. Evidence for this has also been described for single walled carbon nanotubes, graphene oxide, and gold nanoparticles, in murine peritoneal macrophages (Wan et al., 2013). These effects are not assay interference, but biological impacts to which the assays show sensitivity. Increased autophagic flux could also lead to more rapid degradation of autophagosomes reducing the amount which could be labelled. Future assessment of autophagy in this manner could benefit from a complementary assessment such as determining the concentration of LC3B; a microtubule-associated protein recruited to autophagosomal membranes (Tanida et al., 2008), or P62; involved in packing and delivery of polyubiquitinated, misfolded, aggregated proteins and dysfunctional organelles for autophagic degradation (Moscat and Diaz-Meco, 2009).

Analysis of polydendron haemocompatibility revealed that plasma coagulation times via the extrinsic, intrinsic, and common coagulation pathways were

largely unaffected under the conditions described here. Treatment of plasma with PD.7525.157, in each instance, resulted in the greatest average difference in coagulation time from that of untreated plasma. It cannot be stated with certainty whether these changes are biologically relevant without further assessment *in vivo*. Furthermore, the use of pooled plasma in this experimental design proved to be both a benefit and a potential limitation. Coagulation response was normalised by pooling, but also potentially skewed by the interindividual variability in the expression of coagulation factors (Corlan and Ross, 2011) given the relatively small sample size. Haemolytic potential was affected by interindividual variability but no polydendron treatments generated a truly haemolytic (>5%) response (American Society for Testing and Materials, 2000). An enhancement of the calculated percentage haemolysis was found where one individual exceeded the maximum possible, under the treatment conditions. This could be the result of variability in sample preparations, but the potential for this effect to be material-related cannot be ruled out without performing the assay using blood from a greater number of individuals. This enhancement was limited only to the inhibition/enhancement assay preparation and not present the standard assay.

Assessment of the cytokine secretion of PBMCs in response to the polydendron materials revealed that a detectable generation of TNFα was present in two out of three individuals treated with PD.5050.161. Of the four polydendrons, PD.5050.161 was the only one to contain a quantifiable endotoxin content (0.22 EU/ml). While this may have exacerbated the immunogenic properties of the material; no stimulation of IL-10, shown previously to be produced by alveolar macrophages in response to endotoxin (Chanteux et al., 2007), was observed. Significant proliferation was observed following treatment with PD.5050.161 (Figure 6.12). TNFα and IL-1β are well known to induce proliferation in human lymphocytes (Ebert, 1998; Falkoff et al., 1983; Lichtman et al., 1988).

In order to perform a valid statistical analysis of the impact of nanomaterials

on the generation of cytokines measured via multiplex assay (Section 6.3.6.1) further replicates would be needed. Material availability at the time of assessment limited analysis to duplicate measurements. Increased replicates and a higher number of donor samples would provide a deeper understanding of the effects generated by the tested nanomaterials, as well as provide deeper insight into interindividual variability in responses.

The link between generation of these cytokines and the proliferative response is strengthened by PD.5050.378 generating a significant proliferative response in primary human leukocytes. It can be proposed that this effect is formulation dependent as neither of the 75:25 dendron initiator:PEG initiator polydendrons resulted in any change in proliferation, nor the generation of cytokines to a detectable degree. It should be highlighted that while cytokine production was measured at 24 hours, proliferation was assessed at 72 hours. This later time would have allowed further cytokine generation to be realised and subsequent effects to take place such as the observed proliferative effect. Inhibition enhancement controls showed no significant change in proliferation in PHA-stimulated polydendron treatments but interindividual response and magnitude of variability in LPS-combined cytokine analyses. Measured level of IL-1β displayed a ~2-fold increase from the LPS-stimulated control in all polydendron-combined treatments in individual 2. TNFα and IL-10, however, were lower in polydendron-combined treatments. LPS is an activator of the inflammasome, a process which demonstrates a characteristic generation of IL-1β in turn promoting TNFα expression (Guo et al., 2015). While this has not been found at the chosen timepoint, the observation could potentially indicate inflammasome activation but further investigation would be required. Work performed at the NCI-NCL has shown that of the nanoparticles tested to date; ~10% induce cytokines, of which 63% induced IL-8 and of that population 53% did so exclusively, without inducing TNFα and IL-1β (Dobrovolskaia, 2015). Typically the materials found to behave in this

manner were liposomes, micelles, and nanoemulsions, with a highlighted example of Cremophor-EL micelles (Dobrovolskaia, 2015). The use of this excipient has been further studied by comparing the cytokine generation in response to Taxol (Cremophor-EL vehicle) and Abraxane (Cremophor-free albumin-bound paclitaxel) resulting in observations that human PBMCs produce IL-8 in the absence of TNFα and IL-1β in response to Taxol while no inflammatory cytokines are induced by Abraxane (Ilinskaya et al., 2015). Further work into the influence of polydendrons on cytokine generation would benefit from the inclusion of IL-8 in the panel of tested cytokines.

The two polydendrons composed of a higher ratio of PEG (PD.5050.161 and PD.5050.378) generated more, potentially detrimental effects. Although the surface structure of the polydendrons is not conclusively known, with regard to the presentation of constituent groups to the external environment of the nanoparticle, the greater proportion of dendron initiator in polydendrons PD.7525.157 and PD.7525.264 appears to have conferred greater compatibility with the biological mechanisms assessed in this work. From the observations made throughout this chapter; polydendrons composed of a 75:25 ratio of dendron initiator:PEG initiator would appear to be the most suitable candidates for further development as drug carriers. Specifically, PD.7525.264 showed the least immunomodulatory potential of all tested polydendrons. Choice of a material for widely applicable use as a drug carrier platform necessitates immunocompatibility (Adlakha-Hutcheon et al., 2009). This would need to be ensured throughout development of the material prior to *in vivo* studies.

Further physicochemical characterization of these materials to gather more data on physicochemical characteristics, such as hydrophobicity, may provide a clearer insight into relationships between physicochemical characteristics and biological impact. The work performed here highlights the need for robust, and thorough, analysis of these characteristics in order to build structure-activity

relationships.

Through the assessment described here it has been determined that the polydendron materials appear to be compatible with the biological systems assessed, however, assessments of cytotoxicity at later time points are needed. Physicochemical characterisation has revealed good stability over the tested period, as well as following introduction to complex biologically relevant media. Tests of *in vitro* bio-, immuno-, haemocompatibility showed minimal cause for concern with only minor interactions observed. However, the full impact of these interactions should be carefully observed in subsequent *in vivo* studies. Some associations between physicochemical characteristics were observed. The inclusion of additional variants of these materials may serve to further clarify the associations detailed here.

Chapter 7

General discussion

The aims of this thesis were to assess the associations between nanoparticle physicochemical characteristics and their observed biological effects focussing on aspects of cellular health, immuno- and haemocompatibility using a standardised analytical approach. Additionally, an *in vitro* assay cascade serving as a preclinical assessment for a small library of commercially available as well as in-house nanomaterials was established. Following a thorough analysis of physicochemical characteristics in a range of relevant biological matrices this work was conducted to allow direct comparison of nanomaterials within, and between, assays. This approach in testing showed utility for all tested nanomaterials and proved suitable when applied to polydendrons; a previously uninvestigated novel class of nanomaterials, with the inclusion of suitable controls. The methodologies presented here, with due consideration to the suggestions proposed throughout this thesis, should be widely applicable to classes of nanomaterials not investigated in this current work.

The early developmental process for nanomaterials for biological application can be generally summarised by the workflow depicted in Figure 7.1. Formulation and synthesis of a suitable candidate material is closely followed by two related stages of characterisation. The first of which focusses on assessments of material contamination and physicochemical characteristics. The information generated by these are used to inform the biological and chemical characterisation in a second stage of analysis. By performing these assessments in a sequential format, it allows for "stop points" to be adhered to stopping unsuitable materials from progressing without rectification of issues such as contamination. Each of these criteria are essential to inform the development of earlier stages in an iterative process.

Determination of possible biological contamination of nanomaterial products is important to inform observations of preclinical assessments which may be strongly impacted by such contaminants, as well as for the eventual production

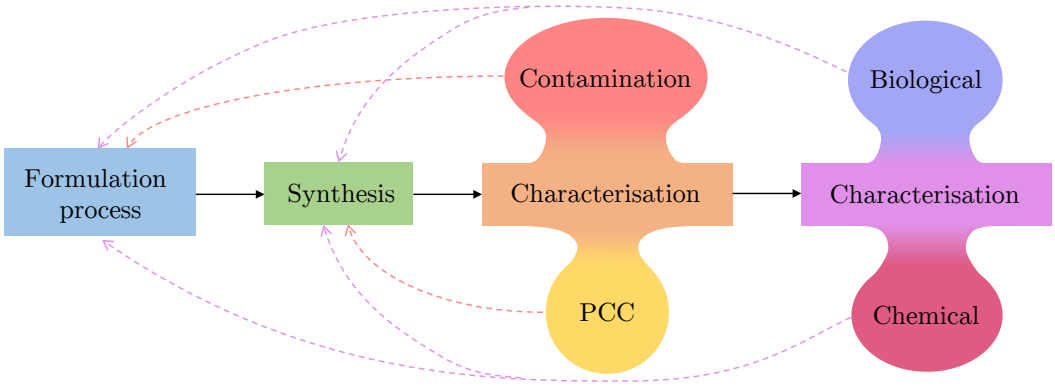

Figure 7.1: Structure of development process for nanomaterials prior to biological assessment. Solid lines denote direction of workflow. Dashed lines denote feedback informing previous steps in the workflow. Acronyms used; PCC - physicochemical characteristics.

of GMP-grade materials for progression to market. This aspect of characterisation poses numerous obstacles which must be addressed prior to implementation. Methods for endotoxin measurement such as LAL testing may require specialised equipment, not necessarily accessible outside specialist institutions. The use of such equipment requires extensive training, or highly experienced staff, for effective operation. Given the complexity of the assessment, it is vital that the investigator be able to recognise and discriminate any potential assay interference. The choice of assay to measure endotoxin will be influenced by the physicochemical characteristics of the material under assessment. Compatibility of nanomaterials with particular methodologies is not guaranteed, as such should be scrutinised prior to the application of such assessment (Neun and Dobrovolskaia, 2011). For this reason the FDA requires validation of the accuracy and reliability of endotoxin measurement by comparing two testing methodologies (USP, 2011). In turn, this makes endotoxin assessment a relatively complex issue that must be treated carefully.

Physicochemical characterisation plays an important role in monitoring batch-to-batch reproducibility in nanomaterial manufacture. This is a vital activity

given that variation, in essence, produces a new nanomaterial which may generate biological effects different from those previously tested thereby rendering the existing information difficult to interpret or use in SAR studies. The growing body of literature relating biological effects to particular nanoparticle physicochemical characteristics further highlights the need for comprehensive characterisation (Gatoo et al., 2014).

Commercially available nanomaterials are routinely provided with information of their size and zeta potential determined in water, and details of surface functionalization. This information is becoming insufficient given the extensive potential biological applications of nanomaterials. It is becoming widely accepted that these measures are not sufficient by themselves when application of these materials in biologically relevant media is known to influence such parameters (Sabuncu et al., 2012). Other physicochemical parameters such as hydrophobicity are not routinely provided, given the class of product within which they are categorised. In the process of drug development; information is generated on parameters such as solubility and hydrophobicity, whereas nanomaterials are not necessarily treated in such a manner. Techniques are available for the analysis of these properties in nanoparticles, but require extensive material-specific optimisation (Mitrano and Ranville, 2014; Murthy and Harivardhan Reddy, 2006). Minimum provided information for nanomaterials would benefit from the inclusion of further physicochemical characteristics so that biological effects may be better related to all, available, PCC.

Combined with the information provided by manufacturers on the nanoparticle surface stabilisation/functionalization, characterisation in water and biologically relevant matrices provided a basis in this work from which comparisons could be drawn from existing literature on the biological impact of nanoparticles.

Cytotoxicity was assessed in order to inform nanomaterial concentrations for subsequent assays. As mentioned previously, without having *in vitro* PK/exposure

data, which is most often the case in novel material development, the rational course of action is to assess a broad range of sub-cytotoxic concentrations.

Assessments of aspects of cellular health, focussing on reactive oxygen species, glutathione, and autophagy, were performed utilising facile flow cytometry-based methodologies permitting relatively high-throughput screening. Such experimental design proves great utility in the generation of a dataset of sufficient statistical power to provide information on nanomaterial effects, while also supporting or forming the basis from which further in-depth mechanistic elucidation may be subsequently performed. Trends observed through these assessments included the observed generation of reactive oxygen species in nanoparticle treatments being less than untreated controls, and association between nanoparticles possessing neutral zeta potential being more pronounced in this effect. Conversely, the literature associates high surface charge, as well as smaller nanoparticle size, to the induction of higher levels or ROS (Manke et al., 2013). However, it is difficult to compare data between literature reports without comprehensive information on how the physicochemical characteristics were determined. These evaluations demonstrated the necessity of assay optimisation for translation in different cellular models, as well as application of the techniques to nanomaterial treatments. The importance of time points on observed biological effect led to the development of micro-plate based kinetic assessments of reactive oxygen species and glutathione. The data generated here showed the potential benefits of these techniques, and further development of these protocols could yield assessment platforms which provide data with high resolution of the changes in these processes over time while being much more efficient in terms of material use. Such a paradigm could alleviate some of the issues which surround standard assay optimisation, allowing for better standardisation.

Cell lines provided a useful platform for *in vitro* assessments, however, they are potentially limited in the ability to suitably extrapolate to *in vivo* models (ATCC,

2010; Dobrovolskaia, 2015), and for this reason immunological assessments were performed in primary human cells. The focus of many arguments is the need for greater characterisation of nanomaterials. It has been proposed that primary samples should also undergo characterisation (Rösslein et al., 2016). Through phenotypic and genotypic assessment, the ability to assess donor background in such a manner would add strength to relationships between physicochemical relationships and biological effects. In addition to characterising the status of volunteer samples used, the utility of mixed immune cell populations in these assessments outweighs initial isolated subset assessments. Assessment of sub-populations in isolation would generate a clearer understanding of direct nanomaterial impact, but simultaneously lose the inter-cell-type interactions which govern responses *in vivo*.

Numerous examples in the literature have associated biological effects with particular physicochemical characteristics. In most circumstances, however, conflicting data exists. This is most often a result of some difference in the experimental design or mode of analysis. Said differences may be inadvertent, or informed by advances in the understanding of particular mechanisms and processes. An example of this, highlighted in Chapter 3, is that of haemolytic potential and strong cationic charge (Barshtein et al., 2011) where the importance of nanoparticle-protein corona formation in biological media has informed more recent studies to perform such assessments not in the absence of protein (Martinez et al., 2015; Paula et al., 2012; Tenzer et al., 2013).

The production of nanomaterials, although existing on an industrial scale for some time, is still in its relative infancy with regard to the biological applications of these materials. Standardisation of safety screening is an ongoing effort which continues to develop with growing understanding of the mechanisms by which nanomaterials behave.

Attempts to draw comparisons between existing literature and work pre-

sented in this thesis further highlighted the need for standardisation in the data generated on nanomaterials, for example the protocols developed by the NCI-NCL for their nanomaterial characterisation assay cascade are freely available (https://nanolab.cancer.gov/working_assay-cascade.asp). This effort provides a source of information from which researchers in the field can use as a reference to inform their own work, however validation is necessary prior to their employment. As much of their work conforms to, or informs regulatory bodies, wider adoption of said protocols would intuitively be encouraged in order to better standardise assessment and more broadly challenge the applicability to other nanomaterials. Adoption of standardised protocols, in itself, does not completely alleviate the problems faced when attempting to draw comparisons of information generated from different sources. Variability between labs in *in vitro* data generated on the same materials using the same methods is a known issue (Lanone et al., 2009). Efforts to alleviate this involve strict adherence to the protocols and stringent quality control checks. This is inherently difficult when considering less controllable sources of variability. These may include sources of reagents, cell line differences, storage conditions and time between collection of primary samples and their use. One, potential, solution to this has already been established elsewhere, in the form of the minimum information about a microarray experiment (MIAME) (Brazma et al., 2001). This system allows presented data to be easily interpreted and that results derived from its analysis can be independently verified. Similar efforts are ongoing to establish a standardised nanoparticle data repository Nanomaterial Data Curation Initiative (NDCI) (Hendren et al., 2015).

Assessments demonstrating nanoparticles to be safe and not exert overt influence do not necessarily reach the wider community. Such information is vitally useful in the rational design of nanoparticles. Databases, such as caNanoLab (https://cananolab.nci.nih.gov/caNanoLab/), acting as repositories for such information pose the ideal platform for dissemination of this type of data. Adop-

tion of these platforms would provide a means for associations to be made by researchers, and providing power to computational analysis potentially leading to better informed structure-activity relationships.

Greater insight into the effect of nanoparticles on the diseased state would benefit from testing in relevant patient samples. Nanomaterials, ideally, should be considered in the final format for which they have been developed. Not only will this aid in determining if the nanoparticle is fit for purpose, but also how its application may affect patient populations in terms of nanomedicine (David et al., 2016). It is hoped that with greater integration and cooperation of various research efforts the development of nanomedicines will gain speed to bring forward these advances in patient care.

The work presented within this thesis adds to the knowledge relating particle characteristics to biological effects relevant to their use clinically. It has been highlighted that robust physicochemical characterisation is vital to that analysis. Additionally, the methodologies used and developed, throughout this thesis will serve future preclinical characterisation of novel nanomaterials.

References

Adlakha-Hutcheon, G., Khaydarov, R., Korenstein, R., Varma, R., Vaseashta, A., Stamm, H., and Abdel-Mottaleb, M. (2009). *Nanomaterials, nanotechnology*, pages 195–207. Springer Netherlands, Dordrecht.

Agashe, H. B., Babbar, A. K., Jain, S., Sharma, R. K., Mishra, A. K., Asthana, A., Garg, M., Dutta, T., and Jain, N. K. (2007). Investigations on biodistribution of technetium-99m-labeled carbohydrate-coated poly(propylene imine) dendrimers. *Nanomedicine (Lond)*, 3(2):120–7.

Aggarwal, P., Hall, J. B., McLeland, C. B., Dobrovolskaia, M. A., and McNeil, S. E. (2009). Nanoparticle interaction with plasma proteins as it relates to particle biodistribution, biocompatibility and therapeutic efficacy. *Adv Drug Deliv Rev*, 61(6):428–37.

Aikawa, N. (1996). Cytokine storm in the pathogenesis of multiple organ dysfunction syndrome associated with surgical insults. *Nihon Geka Gakkai Zasshi*, 97(9):771–7.

Al-Nouri, Z. L., Reese, J. A., Terrell, D. R., Vesely, S. K., and George, J. N. (2015). Drug-induced thrombotic microangiopathy: A systematic review of published reports. *Blood*, 125(4):616–8.

Alexis, F., Pridgen, E., Molnar, L. K., and Farokhzad, O. C. (2008). Factors affecting the clearance and biodistribution of polymeric nanoparticles. *Mol Pharm*, 5(4):505–15.

Alimonti, J. B., Ball, T. B., and Fowke, K. R. (2003). Mechanisms of CD4+ T lymphocyte cell death in human immunodeficiency virus infection and AIDS. *J Gen Virol*, 84(Pt 7):1649–61.

Alkilany, A. M. and Murphy, C. J. (2010). Toxicity and cellular uptake of gold nanoparticles: What we have learned so far? *Journal of Nanoparticle Research*, 12(7):2313–2333.

Allouni, Z. E., Cimpan, M. R., Hol, P. J., Skodvin, T., and Gjerdet, N. R. (2009). Agglomeration and sedimentation of TiO2 nanoparticles in cell culture medium. *Colloids Surf B Biointerfaces*, 68(1):83–7.

Almeida, J. P., Chen, A. L., Foster, A., and Drezek, R. (2011). In vivo biodistribution of nanoparticles. *Nanomedicine (Lond)*, 6(5):815–35.

Alving, C. R. (1991). Liposomes as carriers of antigens and adjuvants. *J Immunol Methods*, 140(1):1–13.

Alving, C. R., Banerji, B., Shiba, T., Kotani, S., Clements, J. D., and Richards, R. L. (1980). Liposomes as vehicles for vaccines. *Prog Clin Biol Res*, 47:339–55.

Amendola, V. and Meneghetti, M. (2009). Size evaluation of gold nanoparticles by UV-vis spectroscopy. *The Journal of Physical Chemistry C*, 113(11):4277–4285.

American Society for Testing and Materials (2000). *Standard practice for assessment of hemolytic properties of materials*. ASTM International, West Conshohocken, PA.

Andersen, A. J., Hashemi, S. H., Andresen, T. L., Hunter, A. C., and Moghimi, S. M. (2009). Complement: Alive and kicking nanomedicines. *J Biomed Nanotechnol*, 5(4):364–72.

Anderson, J. M., Rodriguez, A., and Chang, D. T. (2008). Foreign body reaction to biomaterials. *Semin Immunol*, 20(2):86–100.

Andreakos, E., Sacre, S. M., Smith, C., Lundberg, A., Kiriakidis, S., Stonehouse, T., Monaco, C., Feldmann, M., and Foxwell, B. M. (2004). Distinct pathways of lps-induced nf-kappa b activation and cytokine production in human myeloid and nonmyeloid cells defined by selective utilization of myd88 and mal/tirap. *Blood*, 103(6):2229–37.

Annison, L., Dompreh, A., and Adu-Sarkodie, Y. (2013). The immunological response of HIV-positive patients initiating HAART at the Komfo Anokye Teaching Hospital, Kumasi, Ghana. *Ghana Med J*, 47(4):164–70.

Anreddy, R. N., Yellu, N. R., and Devarakonda, K. R. (2013). Oxidative biomarkers to assess the nanoparticle-induced oxidative stress. *Methods Mol Biol*, 1028:205–19.

Arango Duque, G. and Descoteaux, A. (2014). Macrophage cytokines: involvement in immunity and infectious diseases. *Front Immunol*, 5:491.

Arumugam, T. V., Magnus, T., Woodruff, T. M., Proctor, L. M., Shiels, I. A., and Taylor, S. M. (2006). Complement mediators in ischemia-reperfusion injury. *Clin Chim Acta*, 374(1-2):33–45.

Arvizo, R., Bhattacharya, R., and Mukherjee, P. (2010). Gold nanoparticles: Opportunities and challenges in nanomedicine. *Expert Opin Drug Deliv*, 7(6):753–63.

ATCC (2010). Passage number effects in cell lines. Technical Report 7, American Type Culture Collection, Rockville, MD. Retrieved from https://www.atcc.org/~/media/PDFs/Technical%20Bulletins/tb07.ashx

Attarwala, H. (2010). TGN1412: From discovery to disaster. *J Young Pharm*, 2(3):332–6.

Ault, J. G. and Lawrence, D. A. (2003). Glutathione distribution in normal and oxidatively stressed cells. *Exp Cell Res*, 285(1):9–14.

Azad, M. B., Chen, Y., and Gibson, S. B. (2009). Regulation of autophagy by reactive oxygen species (ROS): Implications for cancer progression and treatment. *Antioxid Redox Signal*, 11(4):777–90.

Aziz, N., Detels, R., Quint, J. J., Li, Q., Gjertson, D., and Butch, A. W. (2016). Stability of cytokines, chemokines and soluble activation markers in unprocessed blood stored under different conditions. *Cytokine*, 84:17–24.

Aziz, N., Nishanian, P., Mitsuyasu, R., Detels, R., and Fahey, J. L. (1999). Variables that affect assays for plasma cytokines and soluble activation markers. *Clin Diagn Lab Immunol*, 6(1):89–95.

Baalousha, M. and Lead, J. R. (2012). Rationalizing nanomaterial sizes measured by atomic force microscopy, flow field-flow fractionation, and dynamic light scattering: Sample preparation, polydispersity, and particle structure. *Environ Sci Technol*, 46(11):6134–42.

Baer, D. R. (2011). Surface characterization of nanoparticles. *J Surf Anal*, 17(3):163–169.

Ballesteros-Tato, A., Stone, S. L., and Lund, F. E. (2014). Innate ifngamma-producing b cells. *Cell Res*, 24(2):135–6.

Baron, L., Gombault, A., Fanny, M., Villeret, B., Savigny, F., Guillou, N., Panek, C., Le Bert, M., Lagente, V., Rassendren, F., Riteau, N., and Couillin, I. (2015). The NLRP3 inflammasome is activated by nanoparticles through ATP, ADP and adenosine. *Cell Death Dis*, 6:e1629.

Barshtein, G., Arbell, D., and Yedgar, S. (2011). Hemolytic effect of polymeric nanoparticles: Role of albumin. *IEEE Trans Nanobioscience*, 10(4):259–61.

Barth, S., Glick, D., and Macleod, K. F. (2010). Autophagy: Assays and artifacts. *J Pathol*, 221(2):117–24.

Bates, S. M. and Weitz, J. I. (2005). Coagulation assays. *Circulation*, 112(4):e53–60.

Baud, V. and Karin, M. (2001). Signal transduction by tumor necrosis factor and its relatives. *Trends Cell Biol*, 11(9):372–7.

Benezra, M., Penate-Medina, O., Zanzonico, P. B., Schaer, D., Ow, H., Burns, A., DeStanchina, E., Longo, V., Herz, E., Iyer, S., Wolchok, J., Larson, S. M., Wiesner, U., and Bradbury, M. S. (2011). Multimodal silica nanoparticles are effective cancer-targeted probes in a model of human melanoma. *J Clin Invest*, 121(7):2768–80.

Benmerah, A. and Lamaze, C. (2007). Clathrin-coated pits: Vive la difference? *Traffic*, 8(8):970–82.

Berentsen, S. (2015). Role of complement in autoimmune hemolytic anemia. *Transfus Med Hemother*, 42(5):303–10.

Bergstrand, H. (1990). The generation of reactive oxygen-derived species by phagocytes. *Agents Actions Suppl*, 30:199–211.

Bermejo, J. F., Ortega, P., Chonco, L., Eritja, R., Samaniego, R., Mullner, M., de Jesus, E., de la Mata, F. J., Flores, J. C., Gomez, R., and Munoz-Fernandez, A. (2007). Water-soluble carbosilane dendrimers: Synthesis biocompatibility and complexation with oligonucleotides; evaluation for medical applications. *Chemistry*, 13(2):483–95.

Berridge, M. V., Herst, P. M., and Tan, A. S. (2005). Tetrazolium dyes as tools in cell biology: New insights into their cellular reduction. *Biotechnol Annu Rev*, 11:127–52.

Berridge, M. V. and Tan, A. S. (1993). Characterization of the cellular reduction of 3-(4,5-dimethylthiazol-2-yl)-2,5-diphenyltetrazolium bromide (MTT): Subcellular localization, substrate dependence, and involvement of mitochondrial electron transport in MTT reduction. *Arch Biochem Biophys*, 303(2):474–82.

Bianchi, M. G., Allegri, M., Costa, A. L., Blosi, M., Gardini, D., Del Pivo, C., Prina-Mello, A., Di Cristo, L., Bussolati, O., and Bergamaschi, E. (2015). Titanium dioxide nanoparticles enhance macrophage activation by LPS through a TLR4-dependent intracellular pathway. *Toxicology Research*, 4(2):385–398.

Billi, F., Benya, P., Kavanaugh, A., Adams, J., McKellop, H., and Ebramzadeh, E. (2012). The john charnley award: an accurate and extremely sensitive method to separate, display, and characterize wear debris: part 2: metal and ceramic particles. *Clin Orthop Relat Res*, 470(2):339–50.

BMG LABTECH (2016). Microplate reading technology: Well scanning. BMG LABTECH, Cary, NC. Retrieved from http://www.bmglabtech.com/en/technology/microplate-reader-technology/well-scanning-obj-51-943.html.

Bootz, A., Vogel, V., Schubert, D., and Kreuter, J. (2004). Comparison of scanning electron microscopy, dynamic light scattering and analytical ultracentrifugation for the sizing of poly(butyl cyanoacrylate) nanoparticles. *Eur J Pharm Biopharm*, 57(2):369–75.

Boraschi, D. (2014). *Nanoparticles and the Immune System*, chapter 5 - Nanoparticles and Immunological Frailty, pages 69–75. Academic Press, San Diego, CA.

Boraschi, D., Costantino, L., and Italiani, P. (2012). Interaction of nanoparticles with immunocompetent cells: Nanosafety considerations. *Nanomedicine (Lond)*, 7(1):121–31.

Bouchard, B. A. and Tracy, P. B. (2003). The participation of leukocytes in coagulant reactions. *J Thromb Haemost*, 1(3):464–9.

Braden, B. C., Goldbaum, F. A., Chen, B. X., Kirschner, A. N., Wilson, S. R., and Erlanger, B. F. (2000). X-ray crystal structure of an anti-Buckminsterfullerene antibody Fab fragment: Biomolecular recognition of C(60). *Proc Natl Acad Sci U S A*, 97(22):12193–7.

Brazma, A., Hingamp, P., Quackenbush, J., Sherlock, G., Spellman, P., Stoeckert, C., Aach, J., Ansorge, W., Ball, C. A., Causton, H. C., Gaasterland, T., Glenisson, P., Holstege, F. C., Kim, I. F., Markowitz, V., Matese, J. C., Parkinson, H., Robinson, A., Sarkans, U., Schulze-Kremer, S., Stewart, J., Taylor, R., Vilo, J., and Vingron, M. (2001). Minimum information about a microarray experiment (MIAME)-toward standards for microarray data. *Nat Genet*, 29(4):365–71.

Brenza, T., Tu, M., Apicella, M., and Fiegel, J. (2011). Evaluation of a nanoparticle delivery vehicle with bacterial targeting ligand for respiratory treatment. In *2011 AIChE Annual Meeting*, Minneapolis Convention Center, Minneapolis.

Breton, G., Chomont, N., Takata, H., Fromentin, R., Ahlers, J., Filali-Mouhim, A., Riou, C., Boulassel, M. R., Routy, J. P., Yassine-Diab, B., and Sekaly, R. P. (2013). Programmed death-1 is a marker for abnormal distribution of naive/memory T cell subsets in HIV-1 infection. *J Immunol*, 191(5):2194–204.

Brown, C., Williams, S., Tipper, J. L., Fisher, J., and Ingham, E. (2007). Characterisation of wear particles produced by metal on metal and ceramic on metal hip prostheses under standard and microseparation simulation. *J Mater Sci Mater Med*, 18(5):819–27.

Bruxel, F., Cojean, S., Bochot, A., Teixeira, H., Bories, C., Loiseau, P. M., and Fattal, E. (2011). Cationic nanoemulsion as a delivery system for oligonucleotides targeting malarial topoisomerase II. *Int J Pharm*, 416(2):402–9.

Bryant, C. E., Spring, D. R., Gangloff, M., and Gay, N. J. (2010). The molecular basis of the host response to lipopolysaccharide. *Nat Rev Microbiol*, 8(1):8–14.

Burton, G. J. and Jauniaux, E. (2011). Oxidative stress. *Best Pract Res Clin Obstet Gynaecol*, 25(3):287–99.

Bush, V. (2003). The hemolyzed specimen: Causes, effects, and reduction. BD Vacutainer Systems, Franklin Lakes, NJ. Retrieved from www.bd.com/vacutainer/labnotes/pdf/Volume13Number1_VS7044.pdf.

Casey, A., Herzog, E., Davoren, M., Lyng, F. M., Byrne, H. J., and Chambers, G. (2007). Spectroscopic analysis confirms the interactions between single walled carbon nanotubes and various dyes commonly used to assess cytotoxicity. *Carbon*, 45(7):1425–1432.

Catelas, I., Bobyn, J. D., Medley, J. B., Krygier, J. J., Zukor, D. J., and Huk, O. L. (2003). Size, shape, and composition of wear particles from metal-metal hip simulator testing: effects of alloy and number of loading cycles. *J Biomed Mater Res A*, 67(1):312–27.

Cedervall, T., Lynch, I., Lindman, S., Berggard, T., Thulin, E., Nilsson, H., Dawson, K. A., and Linse, S. (2007). Understanding the nanoparticle-protein corona using methods to quantify exchange rates and affinities of proteins for nanoparticles. *Proc Natl Acad Sci U S A*, 104(7):2050–5.

Cella, M., Miller, H., and Song, C. (2014). Beyond nk cells: the expanding universe of innate lymphoid cells. *Front Immunol*, 5:282.

Cesta, M. F., Ryman-Rasmussen, J. P., Wallace, D. G., Masinde, T., Hurlburt, G., Taylor, A. J., and Bonner, J. C. (2010). Bacterial lipopolysaccharide enhances PDGF signaling and pulmonary fibrosis in rats exposed to carbon nanotubes. *Am J Respir Cell Mol Biol*, 43(2):142–51.

Chanan-Khan, A., Szebeni, J., Savay, S., Liebes, L., Rafique, N. M., Alving, C. R., and Muggia, F. M. (2003). Complement activation following first exposure to pegylated liposomal doxorubicin (Doxil): Possible role in hypersensitivity reactions. *Ann Oncol*, 14(9):1430–7.

Chang, Y. P., Pinaud, F., Antelman, J., and Weiss, S. (2008). Tracking biomolecules in live cells using quantum dots. *J Biophotonics*, 1(4):287–98.

Chanput, W., Mes, J. J., and Wichers, H. J. (2014). THP-1 cell line: An in vitro cell model for immune modulation approach. *Int Immunopharmacol*, 23(1):37–45.

Chanteux, H., Guisset, A. C., Pilette, C., and Sibille, Y. (2007). LPS induces IL-10 production by human alveolar macrophages via MAPKinases- and Sp1-dependent mechanisms. *Respir Res*, 8:71.

Charan, J. and Biswas, T. (2013). How to calculate sample size for different study designs in medical research? *Indian J Psychol Med*, 35(2):121–6.

Chen, B. X., Wilson, S. R., Das, M., Coughlin, D. J., and Erlanger, B. F. (1998). Antigenicity of fullerenes: Antibodies specific for fullerenes and their characteristics. *Proc Natl Acad Sci U S A*, 95(18):10809–13.

Chen, L. Q., Fang, L., Ling, J., Ding, C. Z., Kang, B., and Huang, C. Z. (2015). Nanotoxicity of silver nanoparticles to red blood cells: Size dependent adsorption, uptake, and hemolytic activity. *Chemical Research in Toxicology*, 28(3):501–509.

Choi, J., Reipa, V., Hitchins, V. M., Goering, P. L., and Malinauskas, R. A. (2011). Physicochemical characterization and in vitro hemolysis evaluation of silver nanoparticles. *Toxicol Sci*, 123(1):133–43.

Chonn, A., Semple, S. C., and Cullis, P. R. (1992). Association of blood proteins with large unilamellar liposomes in vivo. relation to circulation lifetimes. *J Biol Chem*, 267(26):18759–65.

Christen, V. and Fent, K. (2016). Silica nanoparticles induce endoplasmic reticulum stress response and activate mitogen activated kinase (MAPK) signalling. *Toxicology Reports*, 3:832–840.

Chu, A. J. (2011). Tissue factor, blood coagulation, and beyond: An overview. *International Journal of Inflammation*, 2011.

Cleland, A. N., Fraikin, J., Meinhold, P., and Monzon, F. (2016). One size does not fit all: Nanoparticle size analysis for nanomedicine applications. *Drug Development and Delivery*, 16(3):20–26.

Clogston, J. D. and Patri, A. K. (2011). Zeta potential measurement. *Methods Mol Biol*, 697:63–70.

Cohignac, V., Landry, M. J., Boczkowski, J., and Lanone, S. (2014). Autophagy as a possible underlying mechanism of nanomaterial toxicity. *Nanomaterials*, 4(3):548–582.

Collier, A. C. and Pritsos, C. A. (2003). The mitochondrial uncoupler dicumarol disrupts the MTT assay. *Biochem Pharmacol*, 66(2):281–7.

Corlan, A. D. and Ross, J. (2011). Canalization effect in the coagulation cascade and the interindividual variability of oral anticoagulant response. a simulation study. *Theor Biol Med Model*, 8:37.

Coughlin, S. R. (2000). Thrombin signalling and protease-activated receptors. *Nature*, 407(6801):258–64.

Couper, K. N., Blount, D. G., and Riley, E. M. (2008). IL-10: The master regulator of immunity to infection. *J Immunol*, 180(9):5771–7.

Coyne, D. W. (2009). Ferumoxytol for treatment of iron deficiency anemia in patients with chronic kidney disease. *Expert Opin Pharmacother*, 10(15):2563–8.

Crist, R. M., Grossman, J. H., Patri, A. K., Stern, S. T., Dobrovolskaia, M. A., Adiseshaiah, P. P., Clogston, J. D., and McNeil, S. E. (2013). Common pitfalls in nanotechnology: Lessons learned from NCI's Nanotechnology Characterization Laboratory. *Integr Biol (Camb)*, 5(1):66–73.

Crommelin, D. J. and Storm, G. (2003). Liposomes: From the bench to the bed. *J Liposome Res*, 13(1):33–6.

Dams, E. T., Laverman, P., Oyen, W. J., Storm, G., Scherphof, G. L., van Der Meer, J. W., Corstens, F. H., and Boerman, O. C. (2000). Accelerated blood clearance and altered biodistribution of repeated injections of sterically stabilized liposomes. *J Pharmacol Exp Ther*, 292(3):1071–9.

Darwich, L., Coma, G., Pena, R., Bellido, R., Blanco, E. J., Este, J. A., Borras, F. E., Clotet, B., Ruiz, L., Rosell, A., Andreo, F., Parkhouse, R. M., and Bofill, M. (2009). Secretion of interferon-gamma by human macrophages demonstrated at the single-cell level after costimulation with interleukin (il)-12 plus il-18. *Immunology*, 126(3):386–93.

David, C. A., Owen, A., and Liptrott, N. J. (2016). Determining the relationship between nanoparticle characteristics and immunotoxicity: Key challenges and approaches. *Nanomedicine (Lond)*, 11(11):1447–64.

Davis, B. K., Wen, H., and Ting, J. P. (2011). The inflammasome nlrs in immunity, inflammation, and associated diseases. *Annu Rev Immunol*, 29:707–35.

Day, C. L., Kaufmann, D. E., Kiepiela, P., Brown, J. A., Moodley, E. S., Reddy, S., Mackey, E. W., Miller, J. D., Leslie, A. J., DePierres, C., Mncube, Z., Duraiswamy, J., Zhu, B., Eichbaum, Q., Altfeld, M., Wherry, E. J., Coovadia, H. M., Goulder, P. J., Klenerman, P., Ahmed, R., Freeman, G. J., and Walker, B. D. (2006). PD-1 expression on HIV-specific T cells is associated with T-cell exhaustion and disease progression. *Nature*, 443(7109):350–4.

De Groote, D., Zangerle, P. F., Gevaert, Y., Fassotte, M. F., Beguin, Y., Noizat-Pirenne, F., Pirenne, J., Gathy, R., Lopez, M., Dehart, I., and et al. (1992). Direct stimulation of cytokines (IL-1 beta, TNF-alpha, IL-6, IL-2, IFN-gamma and GM-CSF) in whole blood. I. Comparison with isolated PBMC stimulation. *Cytokine*, 4(3):239–48.

De Jong, W. H. and Borm, P. J. (2008). Drug delivery and nanoparticles: Applications and hazards. *Int J Nanomedicine*, 3(2):133–49.

De Paoli Lacerda, S. H., Semberova, J., Holada, K., Simakova, O., Hudson, S. D., and Simak, J. (2011). Carbon nanotubes activate store-operated calcium entry in human blood platelets. *ACS Nano*, 5(7):5808–5813.

Denes, A., Lopez-Castejon, G., and Brough, D. (2012). Caspase-1: Is IL-1 just the tip of the ICEberg? *Cell Death Dis*, 3:e338.

Desai, L. S. and Lister, L. (2011). Biocompatibility safety assessment of medical devices: FDA/ISO and Japanese guidelines. Toxikon Corp., Bedford, MA. Retrieved from http://www.toxikon.com/userfiles/files/biocompatibilityassessmentfdajapaneseguideline.pdf.

Diabate, S., Mulhopt, S., Paur, H. R., Wottrich, R., and Krug, H. F. (2002). In vitro effects of incinerator fly ash on pulmonary macrophages and epithelial cells. *Int J Hyg Environ Health*, 204(5-6):323–6.

Diagnostica Stago (2002). *STA - coag control N + Abn, control plasmas for coagulation tests on STA. Package insert (Cat. No. 00676).* Diagnostica Stago, Parsippany, NJ.

Dieckmann, Y., Colfen, H., Hofmann, H., and Petri-Fink, A. (2009). Particle size distribution measurements of manganese-doped ZnS nanoparticles. *Anal Chem*, 81(10):3889–95.

Dinkins, C., Pilli, M., and Kehrl, J. H. (2014). Roles of autophagy in HIV infection. *Immunol Cell Biol*.

Djavaheri-Mergny, M., Amelotti, M., Mathieu, J., Besancon, F., Bauvy, C., and Codogno, P. (2007). Regulation of autophagy by NFkappaB transcription factor and reactives oxygen species. *Autophagy*, 3(4):390–2.

Dobrovolskaia, M. A. (2015). Pre-clinical immunotoxicity studies of nanotechnology-formulated drugs: Challenges, considerations and strategy. *J Control Release*.

Dobrovolskaia, M. A., Aggarwal, P., Hall, J. B., and McNeil, S. E. (2008a). Preclinical studies to understand nanoparticle interaction with the immune system and its potential effects on nanoparticle biodistribution. *Mol Pharm*, 5(4):487–95.

Dobrovolskaia, M. A., Clogston, J. D., Neun, B. W., Hall, J. B., Patri, A. K., and McNeil, S. E. (2008b). Method for analysis of nanoparticle hemolytic properties in vitro. *Nano Lett*, 8(8):2180–7.

Dobrovolskaia, M. A., Germolec, D. R., and Weaver, J. L. (2009). Evaluation of nanoparticle immunotoxicity. *Nat Nanotechnol*, 4(7):411–4.

Dobrovolskaia, M. A. and McNeil, S. E. (2007). Immunological properties of engineered nanomaterials. *Nat Nanotechnol*, 2(8):469–78.

Dobrovolskaia, M. A. and McNeil, S. E. (2012). *Handbook of immunological properties of engineered nanomaterials*, volume 1, chapter Endotoxin and engineered nanomaterials, pages 77–115. World Scientific.

Dobrovolskaia, M. A. and McNeil, S. E. (2013). Understanding the correlation between in vitro and in vivo immunotoxicity tests for nanomedicines. *J Control Release*, 172(2):456–66.

Dobrovolskaia, M. A., Neun, B. W., Clogston, J. D., Ding, H., Ljubimova, J., and McNeil, S. E. (2010). Ambiguities in applying traditional Limulus amoebocyte lysate tests to quantify endotoxin in nanoparticle formulations. *Nanomedicine (London, England)*, 5(4):555–562.

Dobrovolskaia, M. A., Patri, A. K., Potter, T. M., Rodriguez, J. C., Hall, J. B., and McNeil, S. E. (2012a). Dendrimer-induced leukocyte procoagulant activity depends on particle size and surface charge. *Nanomedicine (Lond)*, 7(2):245–56.

Dobrovolskaia, M. A., Patri, A. K., Simak, J., Hall, J. B., Semberova, J., De Paoli Lacerda, S. H., and McNeil, S. E. (2012b). Nanoparticle size and surface charge determine effects of PAMAM dendrimers on human platelets in vitro. *Mol Pharm*, 9(3):382–93.

Dobrovolskaia, M. A. and Vogel, S. N. (2002). Toll receptors, CD14, and macrophage activation and deactivation by LPS. *Microbes Infect*, 4(9):903–14.

Doitsh, G., Galloway, N. L., Geng, X., Yang, Z., Monroe, K. M., Zepeda, O., Hunt, P. W., Hatano, H., Sowinski, S., Munoz-Arias, I., and Greene, W. C. (2014). Cell death by pyroptosis drives CD4 T-cell depletion in HIV-1 infection. *Nature*, 505(7484):509–14.

Domanski, D. M., Klajnert, B., and Bryszewska, M. (2004). Influence of PAMAM dendrimers on human red blood cells. *Bioelectrochemistry*, 63(1-2):189–91.

Doorn, P. F., Campbell, P. A., Worrall, J., Benya, P. D., McKellop, H. A., and Amstutz, H. C. (1998). Metal wear particle characterization from metal on metal total hip replacements: transmission electron microscopy study of periprosthetic tissues and isolated particles. *J Biomed Mater Res*, 42(1):103–11.

Dostert, C., Petrilli, V., Van Bruggen, R., Steele, C., Mossman, B. T., and Tschopp, J. (2008). Innate immune activation through Nalp3 inflammasome sensing of asbestos and silica. *Science*, 320(5876):674–7.

Duchesne, L., Gentili, D., Comes-Franchini, M., and Fernig, D. G. (2008). Robust ligand shells for biological applications of gold nanoparticles. *Langmuir*, 24(23):13572–80.

Duff, G. W. (1983). Endotoxins and their detection with the Limulus amebocyte lysate test. *The Yale Journal of Biology and Medicine*, 56(1):53–54.

Dunkelberger, J. R. and Song, W. C. (2010). Complement and its role in innate and adaptive immune responses. *Cell Res*, 20(1):34–50.

Dykman, L. A., Sumaroka, M. V., Staroverov, S. A., Zaitseva, I. S., and Bogatyrev, V. A. (2004). Immunogenic properties of the colloidal gold. *Izv Akad Nauk Ser Biol*, (1):86–91.

Ebert, E. C. (1998). Tumour necrosis factor-alpha enhances intraepithelial lymphocyte proliferation and migration. *Gut*, 42(5):650–5.

Eisenbarth, S. C., Colegio, O. R., O'Connor, W., Sutterwala, F. S., and Flavell, R. A. (2008). Crucial role for the Nalp3 inflammasome in the immunostimulatory properties of aluminium adjuvants. *Nature*, 453(7198):1122–6.

El-Ansary, A. K., Kotb, M., Rizk, M. Z., and Siddiqi, N. J. (2014). Prooxidant mechanisms in toxicology. *Biomed Res Int*, 2014:308625.

Elenkov, I. J., Iezzoni, D. G., Daly, A., Harris, A. G., and Chrousos, G. P. (2005). Cytokine dysregulation, inflammation and well-being. *Neuroimmunomodulation*, 12(5):255–69.

Elsabahy, M. and Wooley, K. L. (2013). Cytokines as biomarkers of nanoparticle immunotoxicity. *Chem Soc Rev*, 42(12):5552–76.

Elsayed, M. M. and Cevc, G. (2011). Turbidity spectroscopy for characterization of submicroscopic drug carriers, such as nanoparticles and lipid vesicles: Size determination. *Pharm Res*, 28(9):2204–22.

Enzo Life Sciences (2016). *CYTO-ID autophagy detection kit: Product manual*. Enzo Life Sciences, Farmingdale, NY.

Esmon, C. T., Xu, J., and Lupu, F. (2011). Innate immunity and coagulation. *J Thromb Haemost*, 9 Suppl 1:182–8.

Essen BioScience (2016). IncuCyte cell health & viability assays. Essen BioScience, Ann Arbor, MI. Retrieved from http://www.essenbioscience.com/media/uploads/files/8000-0434-A00_-_Cell_Health_brochure.pdf.

European Medicines Agency (2010). *ICH guideline Q4B annex 14 to note for evaluation and recommendation of pharmacopoeial texts for use in the ICH regions on bacterial endotoxins tests - General chapter step 3*. European Medicines Agency, London.

Falkoff, R. J., Muraguchi, A., Hong, J. X., Butler, J. L., Dinarello, C. A., and Fauci, A. S. (1983). The effects of interleukin 1 on human B cell activation and proliferation. *J Immunol*, 131(2):801–5.

Fernandes, H. P., Cesar, C. L., and de Lourdes Barjas-Castro, M. (2011). Electrical properties of the red blood cell membrane and immunohematological investigation. *Rev Bras Hematol Hemoter*, 33(4):297–301.

Filomeni, G., De Zio, D., and Cecconi, F. (2015). Oxidative stress and autophagy: The clash between damage and metabolic needs. *Cell Death Differ*, 22(3):377–88.

Foley, S., Crowley, C., Smaihi, M., Bonfils, C., Erlanger, B. F., Seta, P., and Larroque, C. (2002). Cellular localisation of a water-soluble fullerene derivative. *Biochem Biophys Res Commun*, 294(1):116–9.

Fraczek, L. A. and Martin, B. K. (2010). Transcriptional control of genes for soluble complement cascade regulatory proteins. *Mol Immunol*, 48(1-3):9–13.

Franca, A., Pelaz, B., Moros, M., Sanchez-Espinel, C., Hernandez, A., Fernandez-Lopez, C., Grazu, V., de la Fuente, J. M., Pastoriza-Santos, I., Liz-Marzan, L. M., and Gonzalez-Fernandez, A. (2010). Sterilization matters: Consequences of different sterilization techniques on gold nanoparticles. *Small*, 6(1):89–95.

Franchi, L., Eigenbrod, T., Munoz-Planillo, R., and Nunez, G. (2009). The inflammasome: A caspase-1-activation platform that regulates immune responses and disease pathogenesis. *Nat Immunol*, 10(3):241–7.

Franco, A. T., Corken, A., and Ware, J. (2015). Platelets at the interface of thrombosis, inflammation, and cancer. *Blood*, 126(5):582–8.

Freedman, J. (1987). The significance of complement on the red cell surface. *Transfus Med Rev*, 1(1):58–70.

Frick, S. U., Bacher, N., Baier, G., Mailander, V., Landfester, K., and Steinbrink, K. (2012). Functionalized polystyrene nanoparticles trigger human dendritic cell maturation resulting in enhanced cd4+ t cell activation. *Macromol Biosci*, 12(12):1637–47.

Frohlich, E. (2012). The role of surface charge in cellular uptake and cytotoxicity of medical nanoparticles. *Int J Nanomedicine*, 7:5577–91.

Fu, P. P., Xia, Q., Hwang, H. M., Ray, P. C., and Yu, H. (2014). Mechanisms of nanotoxicity: Generation of reactive oxygen species. *J Food Drug Anal*, 22(1):64–75.

Game, D. S. and Lechler, R. I. (2002). Pathways of allorecognition: implications for transplantation tolerance. *Transpl Immunol*, 10(2-3):101–8.

Gao, W., Xu, K., Ji, L., and Tang, B. (2011). Effect of gold nanoparticles on glutathione depletion-induced hydrogen peroxide generation and apoptosis in HL7702 cells. *Toxicol Lett*, 205(1):86–95.

Garay, R. P., El-Gewely, R., Armstrong, J. K., Garratty, G., and Richette, P. (2012). Antibodies against polyethylene glycol in healthy subjects and in patients treated with PEG-conjugated agents. *Expert Opin Drug Deliv*, 9(11):1319–23.

Garcia, I., Pouzet, C., Brulas, M., Bauza, E., Botto, J. M., and Domloge, N. (2013). Evaluation of THP-1 cell line as an in vitro model for long-term safety assessment of new molecules. *Int J Cosmet Sci*, 35(6):568–74.

Garlanda, C., Dinarello, C. A., and Mantovani, A. (2013). The interleukin-1 family: Back to the future. *Immunity*, 39(6):1003–18.

Garle, M. J., Fentem, J. H., and Fry, J. R. (1994). In vitro cytotoxicity tests for the prediction of acute toxicity in vivo. *Toxicol In Vitro*, 8(6):1303–12.

Garratty, G. (2008). The James Blundell Award Lecture 2007: Do we really understand immune red cell destruction? *Transfus Med*, 18(6):321–34.

Gatoo, M. A., Naseem, S., Arfat, M. Y., Dar, A. M., Qasim, K., and Zubair, S. (2014). Physicochemical properties of nanomaterials: Implication in associated toxic manifestations. *Biomed Res Int*, 2014:498420.

Ge, L., Li, Q., Wang, M., Ouyang, J., Li, X., and Xing, M. M. (2014). Nanosilver particles in medical applications: synthesis, performance, and toxicity. *Int J Nanomedicine*, 9:2399–407.

Geiger, S. S., Fagundes, C. T., and Siegel, R. M. (2015). Chrono-immunology: Progress and challenges in understanding links between the circadian and immune systems. *Immunology*, 146(3):349–58.

Germain, M. A., Hatton, A., Williams, S., Matthews, J. B., Stone, M. H., Fisher, J., and Ingham, E. (2003). Comparison of the cytotoxicity of clinically relevant cobalt-chromium and alumina ceramic wear particles in vitro. *Biomaterials*, 24(3):469–79.

Ghonime, M. G., Shamaa, O. R., Das, S., Eldomany, R. A., Fernandes-Alnemri, T., Alnemri, E. S., Gavrilin, M. A., and Wewers, M. D. (2014). Inflammasome priming by lipopolysaccharide is dependent upon ERK signaling and proteasome function. *J Immunol*, 192(8):3881–8.

Giannakou, C., Park, M. V., de Jong, W. H., van Loveren, H., Vandebriel, R. J., and Geertsma, R. E. (2016). A comparison of immunotoxic effects of nanomedicinal products with regulatory immunotoxicity testing requirements. *Int J Nanomedicine*, 11:2935–52.

Giardiello, M., Liptrott, N. J., McDonald, T. O., Moss, D., Siccardi, M., Martin, P., Smith, D., Gurjar, R., Rannard, S. P., and Owen, A. (2016). Accelerated oral nanomedicine discovery from miniaturized screening to clinical production exemplified by paediatric HIV nanotherapies. *Nat Commun*, 7:13184.

Gibson, S. B. (2013). Investigating the role of reactive oxygen species in regulating autophagy. *Methods Enzymol*, 528:217–35.

Gilbert, B., Huang, F., Zhang, H., Waychunas, G. A., and Banfield, J. F. (2004). Nanoparticles: Strained and stiff. *Science*, 305(5684):651–4.

Giroux, M., Schmidt, M., and Descoteaux, A. (2003). IFN-gamma-induced MHC class II expression: transactivation of class II transactivator promoter IV by IFN regulatory factor-1 is regulated by protein kinase C-alpha. *J Immunol*, 171(8):4187–94.

Gonzales, M., Mitsumori, L. M., Kushleika, J. V., Rosenfeld, M. E., and Krishnan, K. M. (2010). Cytotoxicity of iron oxide nanoparticles made from the thermal decomposition of organometallics and aqueous phase transfer with Pluronic F127. *Contrast media & molecular imaging*, 5(5):286–293.

Goppert, T. M. and Muller, R. H. (2005). Polysorbate-stabilized solid lipid nanoparticles as colloidal carriers for intravenous targeting of drugs to the brain: Comparison of plasma protein adsorption patterns. *J Drug Target*, 13(3):179–87.

Gunawan, C., Lim, M., Marquis, C. P., and Amal, R. (2014). Nanoparticle-protein corona complexes govern the biological fates and functions of nanoparticles. *Journal of Materials Chemistry B*, 2(15):2060–2083.

Guo, H., Callaway, J. B., and Ting, J. P. (2015). Inflammasomes: Mechanism of action, role in disease, and therapeutics. *Nat Med*, 21(7):677–87.

Gupta, A. K. and Gupta, M. (2005). Synthesis and surface engineering of iron oxide nanoparticles for biomedical applications. *Biomaterials*, 26(18):3995–4021.

Gustafsson, s., Jonasson, S., Sandström, T., Lorentzen, J. C., and Bucht, A. (2014). Genetic variation influences immune responses in sensitive rats following exposure to TiO2 nanoparticles. *Toxicology*, 326:74–85.

Hall, J. B., Dobrovolskaia, M. A., Patri, A. K., and McNeil, S. E. (2007). Characterization of nanoparticles for therapeutics. *Nanomedicine (Lond)*, 2(6):789–803.

Han, X., Gelein, R., Corson, N., Wade-Mercer, P., Jiang, J., Biswas, P., Finkelstein, J. N., Elder, A., and Oberdorster, G. (2011). Validation of an LDH assay for assessing nanoparticle toxicity. *Toxicology*, 287(1-3):99–104.

Hanley, C., Thurber, A., Hanna, C., Punnoose, A., Zhang, J., and Wingett, D. G. (2009). The influences of cell type and ZnO nanoparticle size on immune cell cytotoxicity and cytokine induction. *Nanoscale Res Lett*, 4(12):1409–20.

Harris, J. (2011). Autophagy and cytokines. *Cytokine*, 56(2):140–4.

Harris, J. (2013). Autophagy and IL-1 family cytokines. *Front Immunol*, 4:83.

Harris, J., Hartman, M., Roche, C., Zeng, S. G., O'Shea, A., Sharp, F. A., Lambe, E. M., Creagh, E. M., Golenbock, D. T., Tschopp, J., Kornfeld, H., Fitzgerald, K. A., and Lavelle, E. C. (2011). Autophagy controls IL-1beta secretion by targeting pro-IL-1beta for degradation. *J Biol Chem*, 286(11):9587–97.

Hatton, F. (2015). *Hyperbranched polydendrons: A new macromolecular architecture*. Springer International Publishing, Basel.

He, C. and Klionsky, D. J. (2009). Regulation mechanisms and signaling pathways of autophagy. *Annu Rev Genet*, 43:67–93.

He, X., Young, S. H., Schwegler-Berry, D., Chisholm, W. P., Fernback, J. E., and Ma, Q. (2011). Multiwalled carbon nanotubes induce a fibrogenic response by stimulating reactive oxygen species production, activating NF-kappaB signaling, and promoting fibroblast-to-myofibroblast transformation. *Chem Res Toxicol*, 24(12):2237–48.

Heil, T. L., Volkmann, K. R., Wataha, J. C., and Lockwood, P. E. (2002). Human peripheral blood monocytes versus THP-1 monocytes for in vitro biocompatibility testing of dental material components. *J Oral Rehabil*, 29(5):401–7.

Hendren, C. O., Powers, C. M., Hoover, M. D., and Harper, S. L. (2015). The nanomaterial data curation initiative: A collaborative approach to assessing, evaluating, and advancing the state of the field. *Beilstein J Nanotechnol*, 6:1752–62.

Heneka, M. T., Kummer, M. P., Stutz, A., Delekate, A., Schwartz, S., Vieira-Saecker, A., Griep, A., Axt, D., Remus, A., Tzeng, T. C., Gelpi, E., Halle, A., Korte, M., Latz, E., and Golenbock, D. T. (2013). NLRP3 is activated in Alzheimer's disease and contributes to pathology in APP/PS1 mice. *Nature*, 493(7434):674–8.

Hirsch, C., Roesslein, M., Krug, H. F., and Wick, P. (2011). Nanomaterial cell interactions: Are current in vitro tests reliable? *Nanomedicine (Lond)*, 6(5):837–47.

Hobson, J., Liptrott, N., Rannard, S., and Owen, A. (2013). Immunological safety assessment and viral efficacy of novel pickering stabilised nanoemulsions containing lopinavir and efavirenz. In *European Summit for Clinical Nanomedicine 2013 - 6th CLINAM*, Basel, Switzerland.

Hobson, J., Slater, R., Martin, P., Owen, A., and Rannard, S. P. (2017). Improving intestinal permeation of poorly water soluble drugs using polymer stabilised oil-in-water nanoemulsions. In *Royal Society of Chemistry: Chemical Nanosciences and Nanotechnology Network Meeting*, Keele, UK.

Höflinger, G. (2013). Brief introduction to coating technology for electron microscopy. Leica Microsystems, Vienna. Retrieved from www.leica-microsystems.com/science-lab/brief-introduction-to-coating-technology-for-electron-microscopy/.

Hofmann, S., Blume, R., Wirth, C. T., Cantoro, M., Sharma, R., Ducati, C., Hävecker, M., Zafeiratos, S., Schnoerch, P., Oestereich, A., Teschner, D., Albrecht, M., Knop-Gericke, A., Schlögl, R., and Robertson, J. (2009). State of transition metal catalysts during carbon nanotube growth. *The Journal of Physical Chemistry C*, 113(5):1648–1656.

Hofmann, S., Grasberger, H., Jung, P., Bidlingmaier, M., Vlotides, J., Janssen, O. E., and Landgraf, R. (2002). The tumour necrosis factor-alpha induced vascular permeability is associated with a reduction of VE-cadherin expression. *Eur J Med Res*, 7(4):171–6.

Hohnholt, M. C. and Dringen, R. (2011). Iron-dependent formation of reactive oxygen species and glutathione depletion after accumulation of magnetic iron oxide nanoparticles by oligodendroglial cells. *Journal of Nanoparticle Research*, 13(12):6761–6774.

Holder, A. L., Goth-Goldstein, R., Lucas, D., and Koshland, C. P. (2012). Particle-induced artifacts in the MTT and LDH viability assays. *Chem Res Toxicol*, 25(9):1885–92.

Hollmig, S. T., Ariizumi, K., and Cruz, P. D., J. (2009). Recognition of non-self-polysaccharides by C-type lectin receptors dectin-1 and dectin-2. *Glycobiology*, 19(6):568–75.

Hornung, V., Bauernfeind, F., Halle, A., Samstad, E. O., Kono, H., Rock, K. L., Fitzgerald, K. A., and Latz, E. (2008). Silica crystals and aluminum salts activate the NALP3 inflammasome through phagosomal destabilization. *Nat Immunol*, 9(8):847–56.

Huang, D., Zhou, H., and Gao, J. (2015). Nanoparticles modulate autophagic effect in a dispersity-dependent manner. *Sci Rep*, 5:14361.

Huang, H., Lai, W., Cui, M., Liang, L., Lin, Y., Fang, Q., Liu, Y., and Xie, L. (2016). An evaluation of blood compatibility of silver nanoparticles. *Sci Rep*, 6:25518.

Huang, X., Jain, P. K., El-Sayed, I. H., and El-Sayed, M. A. (2007). Gold nanoparticles: Interesting optical properties and recent applications in cancer diagnostics and therapy. *Nanomedicine (Lond)*, 2(5):681–93.

Hyglos GmbH (2017). *Package Insert EndoLISA*. Hyglos GmbH, Bernried am Starnberger See.

Ilinskaya, A. N., Clogston, J. D., McNeil, S. E., and Dobrovolskaia, M. A. (2015). Induction of oxidative stress by Taxol(R) vehicle Cremophor-EL triggers production of interleukin-8 by peripheral blood mononuclear cells through the mechanism not requiring de novo synthesis of mRNA. *Nanomedicine*, 11(8):1925–38.

Ilinskaya, A. N. and Dobrovolskaia, M. A. (2013). Nanoparticles and the blood coagulation system. Part II: Safety concerns. *Nanomedicine (Lond)*, 8(6):969–81.

Ilinskaya, A. N. and Dobrovolskaia, M. A. (2014). Immunosuppressive and anti-inflammatory properties of engineered nanomaterials. *Br J Pharmacol*, 171(17):3988–4000.

Ingham, B. (2015). X-ray scattering characterisation of nanoparticles. *Crystallography Reviews*, 21(4):229–303.

Ingulli, E. (2010). Mechanism of cellular rejection in transplantation. *Pediatr Nephrol*, 25(1):61–74.

International Organization for Standardization (1996). Iso 13321:1996 particle size analysis - photon correlation spectroscopy. International Organization for Standardization, Geneva. Retrieved from https://www.iso.org/obp/ui/#iso:std:iso:13321:ed-1:v1:en.

InvivoGen (2007). Agonistic and antagonistic effects of LPS on TLR4 - review. InvivoGen, San Diego, CA. Retrieved from http://www.invivogen.com/review-lps-tlr4.

Ishida, T. and Kiwada, H. (2013). Anti-polyethyleneglycol antibody response to PEGylated substances. *Biol Pharm Bull*, 36(6):889–91.

Ishida, T., Maeda, R., Ichihara, M., Irimura, K., and Kiwada, H. (2003). Accelerated clearance of PEGylated liposomes in rats after repeated injections. *J Control Release*, 88(1):35–42.

Ishida, T., Wang, X., Shimizu, T., Nawata, K., and Kiwada, H. (2007). PEGylated liposomes elicit an anti-PEG IgM response in a T cell-independent manner. *J Control Release*, 122(3):349–55.

Izon Science (2015). Tunable resistive pulse sensing. Izon Science, Cambridge, MA. Retrieved from http://www.izon.com/assets/SideColumnPDFs/TRPS-Brochure-April-15.pdf.

Jansky, L., Reymanova, P., and Kopecky, J. (2003). Dynamics of cytokine production in human peripheral blood mononuclear cells stimulated by LPS or infected by Borrelia. *Physiol Res*, 52(5):593–8.

Jo, E. K., Kim, J. K., Shin, D. M., and Sasakawa, C. (2016). Molecular mechanisms regulating NLRP3 inflammasome activation. *Cell Mol Immunol*, 13(2):148–59.

Johnson, K., Aarden, L., Choi, Y., De Groot, E., and Creasey, A. (1996). The proinflammatory cytokine response to coagulation and endotoxin in whole blood. *Blood*, 87(12):5051–60.

Jones, C. F., Campbell, R. A., Franks, Z., Gibson, C. C., Thiagarajan, G., Vieira-de Abreu, A., Sukavaneshvar, S., Mohammad, S. F., Li, D. Y., Ghandehari, H., Weyrich, A. S., Brooks, B. D., and Grainger, D. W. (2012). Cationic PAMAM dendrimers disrupt key platelet functions. *Mol Pharm*, 9(6):1599–611.

Jones, D. P. (2002). Redox potential of GSH/GSSG couple: Assay and biological significance. *Methods Enzymol*, 348:93–112.

Jumaa, M. and Muller, B. W. (2000). Lipid emulsions as a novel system to reduce the hemolytic activity of lytic agents: Mechanism of the protective effect. *Eur J Pharm Sci*, 9(3):285–90.

Jun, E. A., Lim, K. M., Kim, K., Bae, O. N., Noh, J. Y., Chung, K. H., and Chung, J. H. (2011). Silver nanoparticles enhance thrombus formation through increased platelet aggregation and procoagulant activity. *Nanotoxicology*, 5(2):157–67.

Kagan, V. E., Tyurina, Y. Y., Tyurin, V. A., Konduru, N. V., Potapovich, A. I., Osipov, A. N., Kisin, E. R., Schwegler-Berry, D., Mercer, R., Castranova, V., and Shvedova, A. A. (2006). Direct and indirect effects of single walled carbon nanotubes on RAW 264.7 macrophages: Role of iron. *Toxicol Lett*, 165(1):88–100.

Kalkanidis, M., Pietersz, G. A., Xiang, S. D., Mottram, P. L., Crimeen-Irwin, B., Ardipradja, K., and Plebanski, M. (2006). Methods for nano-particle based vaccine formulation and evaluation of their immunogenicity. *Methods*, 40(1):20–9.

Kanno, S., Furuyama, A., and Hirano, S. (2007). A murine scavenger receptor MARCO recognizes polystyrene nanoparticles. *Toxicol Sci*, 97(2):398–406.

Kariya, R., Taura, M., Suzu, S., Kai, H., Katano, H., and Okada, S. (2014). HIV protease inhibitor Lopinavir induces apoptosis of primary effusion lymphoma cells via suppression of NF-kappaB pathway. *Cancer Lett*, 342(1):52–9.

Kato, G. J., McGowan, V., Machado, R. F., Little, J. A., Taylor, J., Morris, C. R., Nichols, J. S., Wang, X., Poljakovic, M., Morris, S. M., and Gladwin, M. T. (2006). Lactate dehydrogenase as a biomarker of hemolysis-associated nitric oxide resistance, priapism, leg ulceration, pulmonary hypertension, and death in patients with sickle cell disease. *Blood*, 107(6):2279–85.

Kato, H., Suzuki, M., Fujita, K., Horie, M., Endoh, S., Yoshida, Y., Iwahashi, H., Takahashi, K., Nakamura, A., and Kinugasa, S. (2009). Reliable size determination of nanoparticles using dynamic light scattering method for in vitro toxicology assessment. *Toxicol In Vitro*, 23(5):927–34.

Kaur, G. and Dufour, J. M. (2012). Cell lines: Valuable tools or useless artifacts. *Spermatogenesis*, 2(1):1–5.

Keijzer, C., Spiering, R., Silva, A. L., van Eden, W., Jiskoot, W., Vervelde, L., and Broere, F. (2013). PLGA nanoparticles enhance the expression of retinaldehyde dehydrogenase enzymes in dendritic cells and induce FoxP3(+) T-cells in vitro. *J Control Release*, 168(1):35–40.

Kell, D. B. and Oliver, S. G. (2014). How drugs get into cells: Tested and testable predictions to help discriminate between transporter-mediated uptake and lipoidal bilayer diffusion. *Front Pharmacol*, 5:231.

Kelly, K. L., Coronado, E., Zhao, L. L., and Schatz, G. C. (2003). The optical properties of metal nanoparticles: The influence of size, shape, and dielectric environment. *The Journal of Physical Chemistry B*, 107(3):668–677.

Kettler, K., Veltman, K., van de Meent, D., van Wezel, A., and Hendriks, A. J. (2014). Cellular uptake of nanoparticles as determined by particle properties, experimental conditions, and cell type. *Environ Toxicol Chem*, 33(3):481–92.

Khaitan, A. and Unutmaz, D. (2011). Revisiting immune exhaustion during HIV infection. *Curr HIV/AIDS Rep*, 8(1):4–11.

Khan, H. A., Abdelhalim, M. A., Al-Ayed, M. S., and Alhomida, A. S. (2012). Effect of gold nanoparticles on glutathione and malondialdehyde levels in liver, lung and heart of rats. *Saudi J Biol Sci*, 19(4):461–4.

Kim, S. H., Lee, K. Y., and Jang, Y. S. (2012). Mucosal immune system and M cell-targeting strategies for oral mucosal vaccination. *Immune Netw*, 12(5):165–75.

King, A., Ndifon, C., Lui, S., Widdows, K., Kotamraju, V. R., Agemy, L., Teesalu, T., Glazier, J. D., Cellesi, F., Tirelli, N., Aplin, J. D., Ruoslahti, E., and Harris, L. K. (2016). Tumor-homing peptides as tools for targeted delivery of payloads to the placenta. *Sci Adv*, 2(5):e1600349.

Kingsbury, S. R., Conaghan, P. G., and McDermott, M. F. (2011). The role of the NLRP3 inflammasome in gout. *J Inflamm Res*, 4:39–49.

Kirkham, M. and Parton, R. G. (2005). Clathrin-independent endocytosis: New insights into caveolae and non-caveolar lipid raft carriers. *Biochim Biophys Acta*, 1745(3):273–86.

Kirschfink, M. and Mollnes, T. E. (2003). Modern complement analysis. *Clin Diagn Lab Immunol*, 10(6):982–9.

Kivisakk, P., Alm, G. V., Fredrikson, S., and Link, H. (2000). Neutralizing and binding anti-interferon-beta (IFN-beta) antibodies. A comparison between IFN-beta-1a and IFN-beta-1b treatment in multiple sclerosis. *Eur J Neurol*, 7(1):27–34.

Klang, V., Matsko, N. B., Valenta, C., and Hofer, F. (2012). Electron microscopy of nanoemulsions: An essential tool for characterisation and stability assessment. *Micron*, 43(2-3):85–103.

Klein, S. L. and Flanagan, K. L. (2016). Sex differences in immune responses. *Nat Rev Immunol*.

Knaapen, A. M., Borm, P. J., Albrecht, C., and Schins, R. P. (2004). Inhaled particles and lung cancer. Part A: Mechanisms. *Int J Cancer*, 109(6):799–809.

Kong, B., Seog, J. H., Graham, L. M., and Lee, S. B. (2011). Experimental considerations on the cytotoxicity of nanoparticles. *Nanomedicine (Lond)*, 6(5):929–41.

Kovacic, P. and Somanathan, R. (2013). Nanoparticles: Toxicity, radicals, electron transfer, and antioxidants. *Methods Mol Biol*, 1028:15–35.

Krishnaswamy, S. (2013). The transition of prothrombin to thrombin. *J Thromb Haemost*, 11 Suppl 1:265–76.

Kroll, A., Pillukat, M. H., Hahn, D., and Schnekenburger, J. (2009). Current in vitro methods in nanoparticle risk assessment: Limitations and challenges. *Eur J Pharm Biopharm*, 72(2):370–7.

Kroll, A., Pillukat, M. H., Hahn, D., and Schnekenburger, J. (2012). Interference of engineered nanoparticles with in vitro toxicity assays. *Arch Toxicol*, 86(7):1123–36.

Krpetic, Z., Anguissola, S., Garry, D., Kelly, P. M., and Dawson, K. A. (2014). Nanomaterials: Impact on cells and cell organelles. *Adv Exp Med Biol*, 811:135–56.

Krug, H. F. and Wick, P. (2011). Nanotoxicology: An interdisciplinary challenge. *Angew Chem Int Ed Engl*, 50(6):1260–78.

Kusaka, T., Nakayama, M., Nakamura, K., Ishimiya, M., Furusawa, E., and Ogasawara, K. (2014). Effect of silica particle size on macrophage inflammatory responses. *PLoS One*, 9(3):e92634.

Laloy, J., Minet, V., Alpan, L., Mullier, F., Beken, S., Toussaint, O., Lucas, S., and Dogn'e, J. M. (2014). Impact of silver nanoparticles on haemolysis, platelet function and coagulation. *Nanobiomedicine*, page 1.

Lamkanfi, M., Kalai, M., Saelens, X., Declercq, W., and Vandenabeele, P. (2004). Caspase-1 activates nuclear factor of the kappa-enhancer in B cells independently of its enzymatic activity. *J Biol Chem*, 279(23):24785–93.

Lanone, S., Rogerieux, F., Geys, J., Dupont, A., Maillot-Marechal, E., Boczkowski, J., Lacroix, G., and Hoet, P. (2009). Comparative toxicity of 24 manufactured nanoparticles in human alveolar epithelial and macrophage cell lines. *Part Fibre Toxicol*, 6:14.

LaRosa, D. F., Rahman, A. H., and Turka, L. A. (2007). The innate immune system in allograft rejection and tolerance. *J Immunol*, 178(12):7503–9.

Larsen, C. P., Morris, P. J., and Austyn, J. M. (1990). Migration of dendritic leukocytes from cardiac allografts into host spleens. a novel pathway for initiation of rejection. *J Exp Med*, 171(1):307–14.

Larsson, M., Hill, A., and Duffy, J. (2012). Suspension stability; why particle size, zeta potential and rheology are important. *Annual Transactions of the Nordic Rheology Society*, 20.

Lasne, D., Jude, B., and Susen, S. (2006). From normal to pathological hemostasis. *Can J Anaesth*, 53(6 Suppl):S2–11.

Latz, E., Xiao, T. S., and Stutz, A. (2013). Activation and regulation of the inflammasomes. *Nat Rev Immunol*, 13(6):397–411.

Lazzari, S., Moscatelli, D., Codari, F., Salmona, M., Morbidelli, M., and Diomede, L. (2012). Colloidal stability of polymeric nanoparticles in biological fluids. *J Nanopart Res*, 14(6):920.

Le Moine, A., Goldman, M., and Abramowicz, D. (2002). Multiple pathways to allograft rejection. *Transplantation*, 73(9):1373–81.

Lee, H., Lee, E., Kim, D. K., Jang, N. K., Jeong, Y. Y., and Jon, S. (2006). Antibiofouling polymer-coated superparamagnetic iron oxide nanoparticles as potential magnetic resonance contrast agents for in vivo cancer imaging. *J Am Chem Soc*, 128(22):7383–9.

Leonaviciene, L., Bradunaite, R., and Astrauskas, V. (2004). Proinflammatory cytokine interleukin-17 and its role in pathogenesis of rheumatoid arthritis. *Medicina (Kaunas)*, 40(5):419–22.

Leonov, A. P., Zheng, J., Clogston, J. D., Stern, S. T., Patri, A. K., and Wei, A. (2008). Detoxification of gold nanorods by treatment with polystyrenesulfonate. *ACS Nano*, 2(12):2481–8.

Leroueil, P. R., Berry, S. A., Duthie, K., Han, G., Rotello, V. M., McNerny, D. Q., Baker, J. R., J., Orr, B. G., and Holl, M. M. (2008). Wide varieties of cationic nanoparticles induce defects in supported lipid bilayers. *Nano Lett*, 8(2):420–4.

Levine, B. and Kroemer, G. (2008). Autophagy in the pathogenesis of disease. *Cell*, 132(1):27–42.

Lewinski, N., Colvin, V., and Drezek, R. (2008). Cytotoxicity of nanoparticles. *Small*, 4(1):26–49.

Li, C., Li, J., Li, Y., Lang, S., Yougbare, I., Zhu, G., Chen, P., and Ni, H. (2012). Crosstalk between platelets and the immune system: Old systems with new discoveries. *Adv Hematol*, 2012:384685.

Li, J. J., Hartono, D., Ong, C. N., Bay, B. H., and Yung, L. Y. (2010). Autophagy and oxidative stress associated with gold nanoparticles. *Biomaterials*, 31(23):5996–6003.

Li, L., Jiang, W., Luo, K., Song, H., Lan, F., Wu, Y., and Gu, Z. (2013). Superparamagnetic iron oxide nanoparticles as mri contrast agents for non-invasive stem cell labeling and tracking. *Theranostics*, 3(8):595–615.

Li, T., Senesi, A. J., and Lee, B. (2016). Small angle X-ray scattering for nanoparticle research. *Chemical Reviews*, 116(18):11128–11180.

Li, Y. and Boraschi, D. (2016). Endotoxin contamination: A key element in the interpretation of nanosafety studies. *Nanomedicine (Lond)*, 11(3):269–87.

Li, Y., Zhang, Y., and Yan, B. (2014). Nanotoxicity overview: Nano-threat to susceptible populations. *Int J Mol Sci*, 15(3):3671–97.

Lichtman, A. H., Chin, J., Schmidt, J. A., and Abbas, A. K. (1988). Role of interleukin 1 in the activation of T lymphocytes. *Proc Natl Acad Sci U S A*, 85(24):9699–703.

Lin, F.-C. and Young, H. A. (2013). The talented interferon-gamma. *Advances in Bioscience and Biotechnology*, 4(7):6–13.

Lin, Y. S. and Haynes, C. L. (2010). Impacts of mesoporous silica nanoparticle size, pore ordering, and pore integrity on hemolytic activity. *J Am Chem Soc*, 132(13):4834–42.

Link, S. and El-Sayed, M. A. (1999). Size and temperature dependence of the plasmon absorption of colloidal gold nanoparticles. *The Journal of Physical Chemistry B*, 103(21):4212–4217.

Liptrott, N. J., Giardiello, M., Hunter, J. W., Tatham, L., Tidbury, L. R., Siccardi, M., Rannard, S., and Owen, A. (2015). Flow cytometric analysis of the physical and protein-binding characteristics of solid drug nanoparticle suspensions. *Nanomedicine (Lond)*, 10(9):1407–21.

Liptrott, N. J., Kendall, E., Nieves, D. J., Farrell, J., Rannard, S., Fernig, D. G., and Owen, A. (2014). Partial mitigation of gold nanoparticle interactions with human lymphocytes by surface functionalization with a 'mixed matrix'. *Nanomedicine (Lond)*, 9(16):2467–79.

Love, S. A., Maurer-Jones, M. A., Thompson, J. W., Lin, Y. S., and Haynes, C. L. (2012a). Assessing nanoparticle toxicity. *Annu Rev Anal Chem (Palo Alto Calif)*, 5:181–205.

Love, S. A., Thompson, J. W., and Haynes, C. L. (2012b). Development of screening assays for nanoparticle toxicity assessment in human blood: Preliminary studies with charged Au nanoparticles. *Nanomedicine (Lond)*, 7(9):1355–64.

Lubberts, E., Joosten, L. A., Oppers, B., van den Bersselaar, L., Coenen-de Roo, C. J., Kolls, J. K., Schwarzenberger, P., van de Loo, F. A., and van den Berg, W. B. (2001). IL-1-independent role of IL-17 in synovial inflammation and joint destruction during collagen-induced arthritis. *J Immunol*, 167(2):1004–13.

Luebke, R. (2012). Immunotoxicant screening and prioritization in the twenty-first century. *Toxicol Pathol*, 40(2):294–9.

Lukacova, M., Barak, I., and Kazar, J. (2008). Role of structural variations of polysaccharide antigens in the pathogenicity of gram-negative bacteria. *Clin Microbiol Infect*, 14(3):200–6.

Lunov, O., Syrovets, T., Loos, C., Nienhaus, G. U., Mailander, V., Landfester, K., Rouis, M., and Simmet, T. (2011). Amino-functionalized polystyrene nanoparticles activate the NLRP3 inflammasome in human macrophages. *ACS Nano*, 5(12):9648–57.

Luzio, J. P., Pryor, P. R., and Bright, N. A. (2007). Lysosomes: Fusion and function. *Nat Rev Mol Cell Biol*, 8(8):622–32.

Maas, S. L., de Vrij, J., van der Vlist, E. J., Geragousian, B., van Bloois, L., Mastrobattista, E., Schiffelers, R. M., Wauben, M. H., Broekman, M. L., and Nolte-'t Hoen, E. N. (2015). Possibilities and limitations of current technologies

for quantification of biological extracellular vesicles and synthetic mimics. *J Control Release*, 200:87–96.

Maccormack, T. J., Clark, R. J., Dang, M. K., Ma, G., Kelly, J. A., Veinot, J. G., and Goss, G. G. (2012). Inhibition of enzyme activity by nanomaterials: Potential mechanisms and implications for nanotoxicity testing. *Nanotoxicology*, 6(5):514–25.

Madaan, K., Kumar, S., Poonia, N., Lather, V., and Pandita, D. (2014). Dendrimers in drug delivery and targeting: Drug-dendrimer interactions and toxicity issues. *J Pharm Bioallied Sci*, 6(3):139–50.

Malinauskas, R. A. (1997). Plasma hemoglobin measurement techniques for the in vitro evaluation of blood damage caused by medical devices. *Artif Organs*, 21(12):1255–67.

Malvern Instruments Ltd (2014). Overview of key principles of dynamic light scattering. Malvern Instruments Ltd, Malvern. Retrieved from http://www.news-medical.net/whitepaper/20141218/Overview-of-Key-Principles-of-Dynamic-Light-Scattering.aspx.

Mamo, T., Moseman, E. A., Kolishetti, N., Salvador-Morales, C., Shi, J., Kuritzkes, D. R., Langer, R., von Andrian, U., and Farokhzad, O. C. (2010). Emerging nanotechnology approaches for HIV/AIDS treatment and prevention. *Nanomedicine (Lond)*, 5(2):269–85.

Manke, A., Wang, L., and Rojanasakul, Y. (2013). Mechanisms of nanoparticle-induced oxidative stress and toxicity. *BioMed Research International*, 2013:15.

Marcos, A., Nova, E., and Montero, A. (2003). Changes in the immune system are conditioned by nutrition. *Eur J Clin Nutr*, 57 Suppl 1:S66–9.

Martinez, D. S. T., Paula, A. J., Fonseca, L. C., Luna, L. A. V., Silveira, C. P., DurÃ¡n, N., and Alves, O. L. (2015). Monitoring the hemolytic effect of mesoporous silica nanoparticles after human blood protein corona formation. *European Journal of Inorganic Chemistry*, 2015(27):4595–4602.

McGuinnes, C., Duffin, R., Brown, S., Mills, L. N., Megson, I. L., Macnee, W., Johnston, S., Lu, S. L., Tran, L., Li, R., Wang, X., Newby, D. E., and Donaldson, K. (2011). Surface derivatization state of polystyrene latex nanoparticles determines both their potency and their mechanism of causing human platelet aggregation in vitro. *Toxicol Sci*, 119(2):359–68.

McKim, J. M., J. (2010). Building a tiered approach to in vitro predictive toxicity screening: A focus on assays with in vivo relevance. *Comb Chem High Throughput Screen*, 13(2):188–206.

McMahon, H. T. and Boucrot, E. (2011). Molecular mechanism and physiological functions of clathrin-mediated endocytosis. *Nat Rev Mol Cell Biol*, 12(8):517–33.

McNeil, S. E. (2009). Nanoparticle therapeutics: A personal perspective. *Wiley Interdiscip Rev Nanomed Nanobiotechnol*, 1(3):264–71.

Medina-Kauwe, L. K. (2007). "Alternative" endocytic mechanisms exploited by pathogens: New avenues for therapeutic delivery? *Adv Drug Deliv Rev*, 59(8):798–809.

Meijer, A. J. and Codogno, P. (2004). Regulation and role of autophagy in mammalian cells. *Int J Biochem Cell Biol*, 36(12):2445–62.

Metselaar, J. M. and Storm, G. (2005). Liposomes in the treatment of inflammatory disorders. *Expert Opin Drug Deliv*, 2(3):465–76.

MHRA (2006). Investigations into adverse incidents during clinical trials of TGN1412. Technical report.

Mikami, Y., Dhakshinamoorthy, A., Alvaro, M., and Garcia, H. (2013). Catalytic activity of unsupported gold nanoparticles. *Catalysis Science & Technology*, 3(1):58–69.

Milosev, I. and Remskar, M. (2009). In vivo production of nanosized metal wear debris formed by tribochemical reaction as confirmed by high-resolution TEM and XPS analyses. *J Biomed Mater Res A*, 91(4):1100–10.

Minko, T., Pakunlu, R. I., Wang, Y., Khandare, J. J., and Saad, M. (2006). New generation of liposomal drugs for cancer. *Anticancer Agents Med Chem*, 6(6):537–52.

Mitrano, D. and Ranville, J. F. (2014). Quantitative evaluation of nanoparticle dissolution kinetics using single particle ICP-MS: A case study with silver nanoparticles. PerkinElmer, Inc., Waltham, MA. Retrieved from https://www.perkinelmer.com/CMSResources/Images/44-158789APP_NexION-350Q-Silver-Nanoparticles-Dissolution-Kinetics_011750_01.pdf.

Miyahira, A. (2012). Types of immune cells present in human pbmc. Sanguine Biosciences, Sherman Oaks, CA. Retrieved from http://technical.sanguinebio.com/types-of-immune-cells-present-in-human-pbmc/.

Mogensen, T. H. (2009). Pathogen recognition and inflammatory signaling in innate immune defenses. *Clin Microbiol Rev*, 22(2):240–73, Table of Contents.

Moghimi, S. M., Wibroe, P. P., Wu, L., and Farhangrazi, Z. S. (2015). Insidious pathogen-mimicking properties of nanoparticles in triggering the lectin pathway of the complement system. *European Journal of Nanomedicine*, 7(3).

Montazer, M., Behzadnia, A., Pakdel, E., Rahimi, M. K., and Moghadam, M. B. (2011). Photo induced silver on nano titanium dioxide as an enhanced antimicrobial agent for wool. *J Photochem Photobiol B*, 103(3):207–14.

Monteiro-Riviere, N. A., Inman, A. O., and Zhang, L. W. (2009). Limitations and relative utility of screening assays to assess engineered nanoparticle toxicity in a human cell line. *Toxicol Appl Pharmacol*, 234(2):222–35.

Moon, E. Y., Yi, G. H., Kang, J. S., Lim, J. S., Kim, H. M., and Pyo, S. (2011). An increase in mouse tumor growth by an in vivo immunomodulating effect of titanium dioxide nanoparticles. *J Immunotoxicol*, 8(1):56–67.

Moon, H., Lee, J., Min, J., and Kang, S. (2014). Developing genetically engineered encapsulin protein cage nanoparticles as a targeted delivery nanoplatform. *Biomacromolecules*, 15(10):3794–801.

Moore, T. L., Rodriguez-Lorenzo, L., Hirsch, V., Balog, S., Urban, D., Jud, C., Rothen-Rutishauser, B., Lattuada, M., and Petri-Fink, A. (2015). Nanoparticle colloidal stability in cell culture media and impact on cellular interactions. *Chemical Society Reviews*, 44(17):6287–6305.

Morgan, B. P. (1999). Regulation of the complement membrane attack pathway. *Crit Rev Immunol*, 19(3):173–98.

Morgan, M. J. and Liu, Z. G. (2011). Crosstalk of reactive oxygen species and nf-kappab signaling. *Cell Res*, 21(1):103–15.

Moscat, J. and Diaz-Meco, M. T. (2009). p62 at the crossroads of autophagy, apoptosis, and cancer. *Cell*, 137(6):1001–4.

Mosmann, T. (1983). Rapid colorimetric assay for cellular growth and survival: application to proliferation and cytotoxicity assays. *J Immunol Methods*, 65(1-2):55–63.

Movafagh, A., Heydary, H., Mortazavi-Tabatabaei, S. A., and Azargashb, E. (2011). The significance application of indigenous phytohemagglutinin (PHA) mitogen on metaphase and cell culture procedure. *Iran J Pharm Res*, 10(4):895–903.

Moyano, D. F., Goldsmith, M., Solfiell, D. J., Landesman-Milo, D., Miranda, O. R., Peer, D., and Rotello, V. M. (2012). Nanoparticle hydrophobicity dictates immune response. *J Am Chem Soc*, 134(9):3965–7.

Mulens-Arias, V., Rojas, J. M., Perez-Yague, S., Morales, M. P., and Barber, D. F. (2015). Polyethylenimine-coated SPIONs trigger macrophage activation through TLR-4 signaling and ROS production and modulate podosome dynamics. *Biomaterials*, 52:494–506.

Murdock, R. C., Braydich-Stolle, L., Schrand, A. M., Schlager, J. J., and Hussain, S. M. (2008). Characterization of nanomaterial dispersion in solution prior to in vitro exposure using dynamic light scattering technique. *Toxicol Sci*, 101(2):239–53.

Murthy, R. S. R. and Harivardhan Reddy, L. (2006). *Poly (alkyl cyanoacrylate) Nanoparticles for Delivery of Anticancer Drugs;*, chapter 15, pages 251–280. CRC Press, Danvers, MA.

Mytilineou, C., Kramer, B. C., and Yabut, J. A. (2002). Glutathione depletion and oxidative stress. *Parkinsonism Relat Disord*, 8(6):385–7.

Nakanishi, T., Kunisawa, J., Hayashi, A., Tsutsumi, Y., Kubo, K., Nakagawa, S., Nakanishi, M., Tanaka, K., and Mayumi, T. (1999). Positively charged liposome functions as an efficient immunoadjuvant in inducing cell-mediated immune response to soluble proteins. *J Control Release*, 61(1-2):233–40.

Nam, H. Y., Kwon, S. M., Chung, H., Lee, S. Y., Kwon, S. H., Jeon, H., Kim, Y., Park, J. H., Kim, J., Her, S., Oh, Y. K., Kwon, I. C., Kim, K., and Jeong, S. Y. (2009). Cellular uptake mechanism and intracellular fate of hydrophobically modified glycol chitosan nanoparticles. *J Control Release*, 135(3):259–67.

Nash, T., Allison, A. C., and Harington, J. S. (1966). Physico-chemical properties of silica in relation to its toxicity. *Nature*, 210(5033):259–61.

National Cancer Institute (2013). *NCL fact sheet*. Retrieved from http://nanolab.cancer.gov/NCL%20Fact%20Sheet.pdf, Frederick, MD.

Nel, A. E., Madler, L., Velegol, D., Xia, T., Hoek, E. M., Somasundaran, P., Klaessig, F., Castranova, V., and Thompson, M. (2009). Understanding biophysicochemical interactions at the nano-bio interface. *Nat Mater*, 8(7):543–57.

Nemmar, A., Yuvaraju, P., Beegam, S., Yasin, J., Dhaheri, R. A., Fahim, M. A., and Ali, B. H. (2015). In vitro platelet aggregation and oxidative stress caused by amorphous silica nanoparticles. *Int J Physiol Pathophysiol Pharmacol*, 7(1):27–33.

Nesargikar, P. N., Spiller, B., and Chavez, R. (2012). The complement system: history, pathways, cascade and inhibitors. *Eur J Microbiol Immunol (Bp)*, 2(2):103–11.

Neuberger, T., SchÃ¶pf, B., Hofmann, H., Hofmann, M., and von Rechenberg, B. (2005). Superparamagnetic nanoparticles for biomedical applications: Possibilities and limitations of a new drug delivery system. *Journal of Magnetism and Magnetic Materials*, 293(1):483–496.

Neubert, J., Wagner, S., Kiwit, J., Brauer, A. U., and Glumm, J. (2015). New findings about iron oxide nanoparticles and their different effects on murine primary brain cells. *Int J Nanomedicine*, 10:2033–49. Neubert, Jenni Wagner, Susanne Kiwit, Jurgen Brauer, Anja U Glumm, Jana eng Research Support, Non-U.S. Gov't New Zealand 2015/03/21 06:00 Int J Nanomedicine. 2015 Mar 13;10:2033-49. doi: 10.2147/IJN.S74404. eCollection 2015.

Neun, B. W. and Dobrovolskaia, M. A. (2011). Detection and quantitative evaluation of endotoxin contamination in nanoparticle formulations by LAL-based assays. *Methods Mol Biol*, 697:121–30.

Neun, B. W., Ilinskaya, A. N., and Dobrovolskaia, M. A. (2015a). *Analysis of hemolytic properties of nanoparticles*. Nanotechnology Characterization Laboratory, Frederick, MD.

Neun, B. W., Rodriguez, J., Ilinskaya, A., and Dobrovolskaia, M. A. (2015b). *Analysis of nanoparticle effects on plasma coagulation times in vitro*. Nanotechnology Characterization Laboratory, Frederick, MD.

Niemetz, J. (1972). Coagulant activity of leukocytes. Tissue factor activity. *J Clin Invest*, 51(2):307–13.

Niemetz, J. and Fani, K. (1971). Role of leukocytes in blood coagulation and the generalized Shwartzman reaction. *Nat New Biol*, 232(34):247–8.

Noguez, C. (2007). Surface plasmons on metal nanoparticles: The influence of shape and physical environment. *The Journal of Physical Chemistry C*, 111(10):3806–3819.

Novak, S., Drobne, D., Valant, J., Pipan-Tkalec, Z., Pelicon, P., Vavpetic, P., Grlj, N., Falnoga, I., Mazej, D., and Remskar, M. (2012). Cell membrane integrity and internalization of ingested TiO(2) nanoparticles by digestive gland cells of a terrestrial isopod. *Environ Toxicol Chem*, 31(5):1083–90.

Oh, S. J., Kim, H., Liu, Y., Han, H. K., Kwon, K., Chang, K. H., Park, K., Kim, Y., Shim, K., An, S. S., and Lee, M. Y. (2014). Incompatibility of silver nanoparticles with lactate dehydrogenase leakage assay for cellular viability test is attributed to protein binding and reactive oxygen species generation. *Toxicol Lett*, 225(3):422–32.

Ong, K. J., MacCormack, T. J., Clark, R. J., Ede, J. D., Ortega, V. A., Felix, L. C., Dang, M. K. M., Ma, G., Fenniri, H., Veinot, J. G. C., and Goss, G. G. (2014). Widespread nanoparticle-assay interference: Implications for nanotoxicity testing. *PLoS ONE*, 9(3):e90650.

Oslakovic, C., Cedervall, T., Linse, S., and Dahlback, B. (2012). Polystyrene nanoparticles affecting blood coagulation. *Nanomedicine*, 8(6):981–6.

Ouyang, W., Rutz, S., Crellin, N. K., Valdez, P. A., and Hymowitz, S. G. (2011). Regulation and functions of the il-10 family of cytokines in inflammation and disease. *Annu Rev Immunol*, 29:71–109.

Ow, H., Larson, D. R., Srivastava, M., Baird, B. A., Webb, W. W., and Wiesner, U. (2005). Bright and stable core-shell fluorescent silica nanoparticles. *Nano Lett*, 5(1):113–7.

Owen, J. B. and Butterfield, D. A. (2010). Measurement of oxidized/reduced glutathione ratio. *Methods Mol Biol*, 648:269–77.

Owens, A. P., r. and Mackman, N. (2010). Tissue factor and thrombosis: The clot starts here. *Thromb Haemost*, 104(3):432–9.

Ozkazanc, D., Yoyen-Ermis, D., Tavukcuoglu, E., Buyukasik, Y., and Esendagli, G. (2016). Functional exhaustion of cd4+ t cells induced by co-stimulatory signals from myeloid leukaemia cells. *Immunology*, 149(4):460–471.

Pal, A. K., Aalaei, I., Gadde, S., Gaines, P., Schmidt, D., Demokritou, P., and Bello, D. (2014). High resolution characterization of engineered nanomaterial dispersions in complex media using tunable resistive pulse sensing technology. *ACS Nano*, 8(9):9003–15.

Panzarini, E., Inguscio, V., Tenuzzo, B. A., Carata, E., and Dini, L. (2013). Nanomaterials and autophagy: New insights in cancer treatment. *Cancers (Basel)*, 5(1):296–319.

Papadakis, K. A. and Targan, S. R. (2000). Tumor necrosis factor: Biology and therapeutic inhibitors. *Gastroenterology*, 119(4):1148–57.

Park, B. S. and Lee, J. O. (2013). Recognition of lipopolysaccharide pattern by TLR4 complexes. *Exp Mol Med*, 45:e66.

Paula, A. J., Martinez, D. S. T., Araujo Júnior, R. T., Souza Filho, A. G., and Alves, O. L. (2012). Suppression of the hemolytic effect of mesoporous silica nanoparticles after protein corona interaction: Independence of the surface microchemical environment. *Journal of the Brazilian Chemical Society*, 23:1807–1814.

Peng, Q., Li, K., Sacks, S. H., and Zhou, W. (2009). The role of anaphylatoxins c3a and c5a in regulating innate and adaptive immune responses. *Inflamm Allergy Drug Targets*, 8(3):236–46.

Pernerstorfer, T., Stohlawetz, P., Hollenstein, U., Dzirlo, L., Eichler, H. G., Kapiotis, S., Jilma, B., and Speiser, W. (1999). Endotoxin-induced activation of the coagulation cascade in humans: Effect of acetylsalicylic acid and acetaminophen. *Arterioscler Thromb Vasc Biol*, 19(10):2517–23.

Peter, P. W. and Moghimi, S. M. (2012). *Complement sensing of nanoparticles and nanomedicines*, volume 1113 of *ACS Symposium Series*, book section 14, pages 365–382. American Chemical Society, Washington, DC.

Peters, C. and Worzella, T. (2015). The new Atmospheric Control Unit (ACU) for the CLARIOstar provides versatility in long term cell-based assays. BMG LABTECH, Cary, NC. Retrieved from http://www.bmglabtech.com/condeon/cdata/media/35216/1370095.pdf.

Petersen, E. J. (2015). *Control experiments to avoid artifacts and misinterpretations in nanoecotoxicology testing.* National Institute of Standards and Technology, Gaithersburg, MD.

Petersen, L. K., Ramer-Tait, A. E., Broderick, S. R., Kong, C. S., Ulery, B. D., Rajan, K., Wannemuehler, M. J., and Narasimhan, B. (2011). Activation of innate immune responses in a pathogen-mimicking manner by amphiphilic polyanhydride nanoparticle adjuvants. *Biomaterials*, 32(28):6815–22.

Pfaller, T., Colognato, R., Nelissen, I., Favilli, F., Casals, E., Ooms, D., Leppens, H., Ponti, J., Stritzinger, R., Puntes, V., Boraschi, D., Duschl, A., and Oostingh, G. J. (2010). The suitability of different cellular in vitro immunotoxicity and genotoxicity methods for the analysis of nanoparticle-induced events. *Nanotoxicology*, 4(1):52–72.

Piao, M. J., Kang, K. A., Lee, I. K., Kim, H. S., Kim, S., Choi, J. Y., Choi, J., and Hyun, J. W. (2011). Silver nanoparticles induce oxidative cell damage in human liver cells through inhibition of reduced glutathione and induction of mitochondria-involved apoptosis. *Toxicol Lett*, 201(1):92–100.

Pitek, A. S., O'Connell, D., Mahon, E., Monopoli, M. P., Baldelli Bombelli, F., and Dawson, K. A. (2012). Transferrin coated nanoparticles: study of the bionano interface in human plasma. *PLoS One*, 7(7):e40685.

Potter, T. M., Nuen, B. W., Rodriguez, J., Ilinskaya, A. N., and Dobrovolskaia, M. (2015). *Preparation of human whole blood and peripheral blood mononuclear cell cultures to analyze nanoparticle potential to induce inflammatory cytokines, chemokines and interferons in vitro.* Nanotechnology Characterization Laboratory, Frederick, MD.

Pourzal, R., Catelas, I., Theissmann, R., Kaddick, C., and Fischer, A. (2011). Characterization of wear particles generated from CoCrMo alloy under sliding wear conditions. *Wear*, 271(9-10):1658–1666.

Pulskamp, K., Diabate, S., and Krug, H. F. (2007). Carbon nanotubes show no sign of acute toxicity but induce intracellular reactive oxygen species in dependence on contaminants. *Toxicol Lett*, 168(1):58–74.

Pusic, K., Aguilar, Z., McLoughlin, J., Kobuch, S., Xu, H., Tsang, M., Wang, A., and Hui, G. (2013). Iron oxide nanoparticles as a clinically acceptable delivery platform for a recombinant blood-stage human malaria vaccine. *FASEB J*, 27(3):1153–66.

Rabolli, V., Thomassen, L. C., Princen, C., Napierska, D., Gonzalez, L., Kirsch-Volders, M., Hoet, P. H., Huaux, F., Kirschhock, C. E., Martens, J. A., and Lison, D. (2010). Influence of size, surface area and microporosity on the in vitro cytotoxic activity of amorphous silica nanoparticles in different cell types. *Nanotoxicology*, 4(3):307–18.

Radomski, A., Jurasz, P., Alonso-Escolano, D., Drews, M., Morandi, M., Malinski, T., and Radomski, M. W. (2005). Nanoparticle-induced platelet aggregation and vascular thrombosis. *Br J Pharmacol*, 146(6):882–93.

Radu, M., Munteanu, M. C., Petrache, S., Serban, A. I., Dinu, D., Hermenean, A., Sima, C., and Dinischiotu, A. (2010). Depletion of intracellular glutathione and increased lipid peroxidation mediate cytotoxicity of hematite nanoparticles in MRC-5 cells. *Acta Biochim Pol*, 57(3):355–60.

Raj, S., Jose, S., Sumod, U. S., and Sabitha, M. (2012). Nanotechnology in cosmetics: Opportunities and challenges. *Journal of Pharmacy & Bioallied Sciences*, 4(3):186–193.

Rajput, N. (2015). Methods of preparation of nanoparticles - a review. *IJAET*, 7(4):1806–1811.

Rameshwar, T., Samal, S., Lee, S., Kim, S., Cho, J., and Kim, I. S. (2006). Determination of the size of water-soluble nanoparticles and quantum dots by field-flow fractionation. *J Nanosci Nanotechnol*, 6(8):2461–7.

Rannard, S. and Owen, A. (2009). Nanomedicine: Not a case of "one size fits all". *Nano Today*, 4(5):382–384.

Rao, L. V. and Pendurthi, U. R. (2012). Regulation of tissue factor coagulant activity on cell surfaces. *J Thromb Haemost*, 10(11):2242–53.

Ray, P. D., Huang, B. W., and Tsuji, Y. (2012). Reactive oxygen species (ROS) homeostasis and redox regulation in cellular signaling. *Cell Signal*, 24(5):981–90.

Razzaboni, B. L. and Bolsaitis, P. (1990). Evidence of an oxidative mechanism for the hemolytic activity of silica particles. *Environ Health Perspect*, 87:337–41.

Reddy, S. T., Swartz, M. A., and Hubbell, J. A. (2006). Targeting dendritic cells with biomaterials: Developing the next generation of vaccines. *Trends Immunol*, 27(12):573–9.

Rego, A. C. and Oliveira, C. R. (2003). Mitochondrial dysfunction and reactive oxygen species in excitotoxicity and apoptosis: Implications for the pathogenesis of neurodegenerative diseases. *Neurochem Res*, 28(10):1563–74.

Reisetter, A. C., Stebounova, L. V., Baltrusaitis, J., Powers, L., Gupta, A., Grassian, V. H., and Monick, M. M. (2011). Induction of inflammasome-dependent pyroptosis by carbon black nanoparticles. *J Biol Chem*, 286(24):21844–52.

Rettig, L., Haen, S. P., Bittermann, A. G., von Boehmer, L., Curioni, A., Kramer, S. D., Knuth, A., and Pascolo, S. (2010). Particle size and activation threshold: A new dimension of danger signaling. *Blood*, 115(22):4533–41.

Riss, T. (2014). Is your MTT assay really the best choice? Promega, Madison, WI. Retrieved from http://www.promega.co.uk/~/pdf/resources/pubhub/is-your-mtt-assay-really-the-best-choice/.

Robinson, J. M. (2008). Reactive oxygen species in phagocytic leukocytes. *Histochem Cell Biol*, 130(2):281–97.

Rojas, J. M., Sanz-Ortega, L., Mulens-Arias, V., Gutierrez, L., Perez-Yague, S., and Barber, D. F. (2016). Superparamagnetic iron oxide nanoparticle uptake alters M2 macrophage phenotype, iron metabolism, migration and invasion. *Nanomedicine*, 12(4):1127–38.

Rösslein, M., Liptrott, N., Owen, A., Boisseau, P., Wick, P., and Herrmann, I. K. (2016). Sound understanding of environmental, health and safety, clinical, and market aspects is imperative to clinical translation of nanomedicines. Manuscript submitted for publication.

Ruenraroengsak, P. and Tetley, T. D. (2015). Differential bioreactivity of neutral, cationic and anionic polystyrene nanoparticles with cells from the human alveolar compartment: Robust response of alveolar type 1 epithelial cells. *Part Fibre Toxicol*, 12:19.

Sabuncu, A. C., Grubbs, J., Qian, S., Abdel-Fattah, T. M., Stacey, M. W., and Beskok, A. (2012). Probing nanoparticle interactions in cell culture media. *Colloids Surf B Biointerfaces*, 95:96–102.

Saha, K., Moyano, D. F., and Rotello, V. M. (2014). Protein coronas suppress the hemolytic activity of hydrophilic and hydrophobic nanoparticles. *Materials Horizons*, 1(1):102–105.

Salatin, S. and Yari Khosroushahi, A. (2017). Overviews on the cellular uptake mechanism of polysaccharide colloidal nanoparticles. *J Cell Mol Med*.

Saraiva, M. and O'Garra, A. (2010). The regulation of il-10 production by immune cells. *Nat Rev Immunol*, 10(3):170–81.

Sarma, J. V. and Ward, P. A. (2011). The complement system. *Cell Tissue Res*, 343(1):227–35.

Saupe, A., McBurney, W., Rades, T., and Hook, S. (2006). Immunostimulatory colloidal delivery systems for cancer vaccines. *Expert Opin Drug Deliv*, 3(3):345–54.

Sayes, C. M., Reed, K. L., and Warheit, D. B. (2007). Assessing toxicity of fine and nanoparticles: Comparing in vitro measurements to in vivo pulmonary toxicity profiles. *Toxicol Sci*, 97(1):163–80.

Schaer, D. J., Buehler, P. W., Alayash, A. I., Belcher, J. D., and Vercellotti, G. M. (2013). Hemolysis and free hemoglobin revisited: Exploring hemoglobin and hemin scavengers as a novel class of therapeutic proteins. *Blood*, 121(8):1276–84.

Schrurs, F. and Lison, D. (2012). Focusing the research efforts. *Nat Nanotechnol*, 7(9):546–8.

Schutze, S., Wiegmann, K., Machleidt, T., and Kronke, M. (1995). Tnf-induced activation of nf-kappa b. *Immunobiology*, 193(2-4):193–203.

Schwenk, M. H. (2010). Ferumoxytol: a new intravenous iron preparation for the treatment of iron deficiency anemia in patients with chronic kidney disease. *Pharmacotherapy*, 30(1):70–9.

Segel, G. B., Simon, W., and Lichtman, M. A. (1979). Regulation of sodium and potassium transport in phytohemagglutinin-stimulated human blood lymphocytes. *J Clin Invest*, 64(3):834–41.

Seong, S. Y. and Matzinger, P. (2004). Hydrophobicity: An ancient damage-associated molecular pattern that initiates innate immune responses. *Nat Rev Immunol*, 4(6):469–78.

Shah, D. S., Sakthivel, T., Toth, I., Florence, A. T., and Wilderspin, A. F. (2000). DNA transfection and transfected cell viability using amphipathic asymmetric dendrimers. *Int J Pharm*, 208(1-2):41–8.

Shah, P., Bhalodia, D., and Shelat, P. (2010). Nanoemulsion: A pharmaceutical review. *Systematic Reviews in Pharmacy*, 1:24–32.

Shang, L., Nienhaus, K., and Nienhaus, G. U. (2014). Engineered nanoparticles interacting with cells: Size matters. *Journal of Nanobiotechnology*, 12:5–5.

Sharkey, J., Starkey Lewis, P. J., Barrow, M., Alwahsh, S. M., Noble, J., Livingstone, E., Lennen, R. J., Jansen, M. A., Carrion, J. G., Liptrott, N., Forbes, S., Adams, D. J., Chadwick, A. E., Forbes, S. J., Murray, P., Rosseinsky, M. J., Goldring, C. E., and Park, B. K. (2017). Functionalized superparamagnetic iron oxide nanoparticles provide highly efficient iron-labeling in macrophages for magnetic resonance-based detection in vivo. *Cytotherapy*, 19(4):555–569.

Sheen, M. R., Lizotte, P. H., Toraya-Brown, S., and Fiering, S. (2014). Stimulating antitumor immunity with nanoparticles. *Wiley Interdiscip Rev Nanomed Nanobiotechnol*, 6(5):496–505.

Sheth, P., Sandhu, H., Singhal, D., Malick, W., Shah, N., and Kislalioglu, M. S. (2012). Nanoparticles in the pharmaceutical industry and the use of supercritical fluid technologies for nanoparticle production. *Curr Drug Deliv*, 9(3):269–84.

Shi, H., Magaye, R., Castranova, V., and Zhao, J. (2013). Titanium dioxide nanoparticles: A review of current toxicological data. *Part Fibre Toxicol*, 10:15.

Shi, Y., Yadav, S., Wang, F., and Wang, H. (2010). Endotoxin promotes adverse effects of amorphous silica nanoparticles on lung epithelial cells in vitro. *J Toxicol Environ Health A*, 73(11):748–56.

Shima, F., Akagi, T., and Akashi, M. (2015). Effect of hydrophobic side chains in the induction of immune responses by nanoparticle adjuvants consisting of amphiphilic poly(γ-glutamic acid). *Bioconjugate Chemistry*, 26(5):890–898.

Shin, J. N., Fattah, E. A., Bhattacharya, A., Ko, S., and Eissa, N. T. (2013). Inflammasome activation by altered proteostasis. *J Biol Chem*, 288(50):35886–95.

Shvedova, A. A., Castranova, V., Kisin, E. R., Schwegler-Berry, D., Murray, A. R., Gandelsman, V. Z., Maynard, A., and Baron, P. (2003). Exposure to carbon nanotube material: Assessment of nanotube cytotoxicity using human keratinocyte cells. *J Toxicol Environ Health A*, 66(20):1909–26.

Simard, J. C., Vallieres, F., de Liz, R., Lavastre, V., and Girard, D. (2015). Silver nanoparticles induce degradation of the endoplasmic reticulum stress sensor activating transcription factor-6 leading to activation of the NLRP-3 inflammasome. *J Biol Chem*, 290(9):5926–39.

Sims, P. J., Wiedmer, T., Esmon, C. T., Weiss, H. J., and Shattil, S. J. (1989). Assembly of the platelet prothrombinase complex is linked to vesiculation of the platelet plasma membrane. Studies in Scott syndrome: An isolated defect in platelet procoagulant activity. *J Biol Chem*, 264(29):17049–57.

Slater, T. F., Sawyer, B., and Straeuli, U. (1963). Studies on succinate-tetrazolium reductase systems: III. Points of coupling of four different tetrazolium salts. *Biochim Biophys Acta*, 77:383–93.

Smulders, S., Kaiser, J. P., Zuin, S., Van Landuyt, K. L., Golanski, L., Vanoirbeek, J., Wick, P., and Hoet, P. H. (2012). Contamination of nanoparticles by endotoxin: Evaluation of different test methods. *Part Fibre Toxicol*, 9:41.

Smyth, E., Solomon, A., Vydyanath, A., Luther, P. K., Pitchford, S., Tetley, T. D., and Emerson, M. (2015). Induction and enhancement of platelet aggregation in vitro and in vivo by model polystyrene nanoparticles. *Nanotoxicology*, 9(3):356–64.

Solaro, R., Chiellini, F., and Battisti, A. (2010). Targeted delivery of protein drugs by nanocarriers. *Materials*, 3(3):1928.

Song, W., Popp, L., Yang, J., Kumar, A., Gangoli, V. S., and Segatori, L. (2015). The autophagic response to polystyrene nanoparticles is mediated by transcription factor EB and depends on surface charge. *J Nanobiotechnology*, 13:87.

Song, W. C., Sarrias, M. R., and Lambris, J. D. (2000). Complement and innate immunity. *Immunopharmacology*, 49(1-2):187–98.

Sorbara, M. T. and Girardin, S. E. (2011). Mitochondrial ROS fuel the inflammasome. *Cell Res*, 21(4):558–60.

Speth, C., Loffler, J., Krappmann, S., Lass-Florl, C., and Rambach, G. (2013). Platelets as immune cells in infectious diseases. *Future Microbiol*, 8(11):1431–51.

Srivastava, V., Gusain, D., and Sharma, Y. C. (2015). Critical review on the toxicity of some widely used engineered nanoparticles. *Industrial & Engineering Chemistry Research*, 54(24):6209–6233.

Stack, J. H., Beaumont, K., Larsen, P. D., Straley, K. S., Henkel, G. W., Randle, J. C., and Hoffman, H. M. (2005). IL-converting enzyme/caspase-1 inhibitor VX-765 blocks the hypersensitive response to an inflammatory stimulus in monocytes from familial cold autoinflammatory syndrome patients. *J Immunol*, 175(4):2630–4.

Stadtländer, C. T. K. H. (2007). Scanning electron microscopy and transmission electron microscopy of mollicutes: Challenges and opportunities. In Méndez-Vilas, A. and Díaz, J., editors, *Modern Research and Educational Topics in Microscopy*, volume 1, pages 122–131. FORMATEX, Badajoz.

Stark, W. J., Stoessel, P. R., Wohlleben, W., and Hafner, A. (2015). Industrial applications of nanoparticles. *Chemical Society Reviews*.

Stebbings, R., Findlay, L., Edwards, C., Eastwood, D., Bird, C., North, D., Mistry, Y., Dilger, P., Liefooghe, E., Cludts, I., Fox, B., Tarrant, G., Robinson, J., Meager, T., Dolman, C., Thorpe, S. J., Bristow, A., Wadhwa, M., Thorpe, R., and Poole, S. (2007). "Cytokine storm" in the phase I trial of monoclonal antibody TGN1412: Better understanding the causes to improve preclinical testing of immunotherapeutics. *J Immunol*, 179(5):3325–31.

Stern, S. T., Adiseshaiah, P. P., and Crist, R. M. (2012). Autophagy and lysosomal dysfunction as emerging mechanisms of nanomaterial toxicity. *Part Fibre Toxicol*, 9:20.

Stern, S. T., McLeland, C., and Rodriguez, J. (2013). *Autophagic dysfunction assay: Qualitative analysis of MAP LC3I to LC3-II conversion by Western blot*. Nanotechnology Characterization Laboratory, Frederick, MD.

Stern, S. T. and Neun, B. W. (2011). *Autophagic dysfunction in LLC-PK1 cells*. Nanotechnology Characterization Laboratory, Frederick, MD.

Stieneker, F., Kreuter, J., and Lower, J. (1991). High antibody titres in mice with polymethylmethacrylate nanoparticles as adjuvant for HIV vaccines. *AIDS*, 5(4):431–5.

Stratton, W., Buckett, M., and McKernan, S. (2013). Procedure for TEM measurement of nanoparticles. *Microscopy and Microanalysis*, 19(2):1098–1099.

Su, X., Yu, Y., Zhong, Y., Giannopoulou, E. G., Hu, X., Liu, H., Cross, J. R., Ratsch, G., Rice, C. M., and Ivashkiv, L. B. (2015). Interferon-gamma regulates cellular metabolism and mRNA translation to potentiate macrophage activation. *Nat Immunol*, 16(8):838–49.

Suankratay, C., Mold, C., Zhang, Y., Lint, T. F., and Gewurz, H. (1999). Mechanism of complement-dependent haemolysis via the lectin pathway: Role of the complement regulatory proteins. *Clin Exp Immunol*, 117(3):442–8.

Subbarao, N. (2012). *Handbook of immunological properties of engineered nanomaterials*, volume 1, chapter Impact of Nanoparticle Sterilization on Analytical Characterization, pages 53–75. World Scientific.

Sumbayev, V. V., Yasinska, I. M., Garcia, C. P., Gilliland, D., Lall, G. S., Gibbs, B. F., Bonsall, D. R., Varani, L., Rossi, F., and Calzolai, L. (2013). Gold nanoparticles downregulate interleukin-1beta-induced pro-inflammatory responses. *Small*, 9(3):472–7.

Suntharalingam, G., Perry, M. R., Ward, S., Brett, S. J., Castello-Cortes, A., Brunner, M. D., and Panoskaltsis, N. (2006). Cytokine storm in a phase 1 trial of the anti-CD28 monoclonal antibody TGN1412. *N Engl J Med*, 355(10):1018–28.

Svenson, S. and Tomalia, D. A. (2005). Dendrimers in biomedical applications–reflections on the field. *Adv Drug Deliv Rev*, 57(15):2106–29.

Swanson, S. J., Ferbas, J., Mayeux, P., and Casadevall, N. (2004). Evaluation of methods to detect and characterize antibodies against recombinant human erythropoietin. *Nephron Clin Pract*, 96(3):c88–95.

Szabo, P. and Zelko, R. (2015). Formulation and stability aspects of nanosized solid drug delivery systems. *Curr Pharm Des*, 21(22):3148–57.

Szacilowski, K., Macyk, W., Drzewiecka-Matuszek, A., Brindell, M., and Stochel, G. (2005). Bioinorganic photochemistry: frontiers and mechanisms. *Chem Rev*, 105(6):2647–94.

Szebeni, J., Muggia, F., Gabizon, A., and Barenholz, Y. (2011). Activation of complement by therapeutic liposomes and other lipid excipient-based therapeutic products: prediction and prevention. *Adv Drug Deliv Rev*, 63(12):1020–30.

Tada-Oikawa, S., Ichihara, G., Fukatsu, H., Shimanuki, Y., Tanaka, N., Watanabe, E., Suzuki, Y., Murakami, M., Izuoka, K., Chang, J., Wu, W., Yamada, Y., and Ichihara, S. (2016). Titanium dioxide particle type and concentration influence the inflammatory response in Caco-2 cells. *Int J Mol Sci*, 17(4):576.

Tandoğan, B. and Ulusu, N. N. (2006). Kinetic mechanism and molecular properties of glutathione reductase. *FABAD J Pharm Sci*, 31:230–237.

Tang, L. and Cheng, J. (2013). Nonporous silica nanoparticles for nanomedicine application. *Nano Today*, 8(3):290–312.

Tanida, I., Ueno, T., and Kominami, E. (2008). LC3 and autophagy. *Methods Mol Biol*, 445:77–88.

Tasdemir, E., Maiuri, M. C., Galluzzi, L., Vitale, I., Djavaheri-Mergny, M., D'Amelio, M., Criollo, A., Morselli, E., Zhu, C., Harper, F., Nannmark, U., Samara, C., Pinton, P., Vicencio, J. M., Carnuccio, R., Moll, U. M., Madeo, F., Paterlini-Brechot, P., Rizzuto, R., Szabadkai, G., Pierron, G., Blomgren, K., Tavernarakis, N., Codogno, P., Cecconi, F., and Kroemer, G. (2008). Regulation of autophagy by cytoplasmic p53. *Nat Cell Biol*, 10(6):676–87.

Tatham, L. M., Rannard, S. P., and Owen, A. (2015). Nanoformulation strategies for the enhanced oral bioavailability of antiretroviral therapeutics. *Ther Deliv*, 6(4):469–90.

Teixeira, L. K., Fonseca, B. P., Barboza, B. A., and Viola, J. P. (2005). The role of interferon-gamma on immune and allergic responses. *Mem Inst Oswaldo Cruz*, 100 Suppl 1:137–44.

Tenzer, S., Docter, D., Kuharev, J., Musyanovych, A., Fetz, V., Hecht, R., Schlenk, F., Fischer, D., Kiouptsi, K., Reinhardt, C., Landfester, K., Schild, H., Maskos, M., Knauer, S. K., and Stauber, R. H. (2013). Rapid formation of plasma protein corona critically affects nanoparticle pathophysiology. *Nat Nanotechnol*, 8(10):772–81.

Thompson, M. (2010). The characterisation of nanoparticles. Analytical Methods Committee, Royal Society of Chemistry, Cambridge. Retrieved from http://www.rsc.org/images/characterisation-nanoparticles-technical-brief-48_tcm18-214815.pdf.

Tipper, J. L., Galvin, A. L., Williams, S., McEwen, H. M., Stone, M. H., Ingham, E., and Fisher, J. (2006). Isolation and characterization of UHMWPE wear particles down to ten nanometers in size from in vitro hip and knee joint simulators. *J Biomed Mater Res A*, 78(3):473–80.

Totani, L. and Evangelista, V. (2010). Platelet-leukocyte interactions in cardiovascular disease and beyond. *Arterioscler Thromb Vasc Biol*, 30(12):2357–61.

Tough, D. F., Sun, S., and Sprent, J. (1997). T cell stimulation in vivo by lipopolysaccharide (LPS). *J Exp Med*, 185(12):2089–94.

Tracz, M. J., Alam, J., and Nath, K. A. (2007). Physiology and pathophysiology of heme: Implications for kidney disease. *J Am Soc Nephrol*, 18(2):414–20.

Treuel, L., Eslahian, K. A., Docter, D., Lang, T., Zellner, R., Nienhaus, K., Nienhaus, G. U., Stauber, R. H., and Maskos, M. (2014). Physicochemical characterization of nanoparticles and their behavior in the biological environment. *Phys Chem Chem Phys*, 16(29):15053–67.

Treuel, L., Jiang, X., and Nienhaus, G. U. (2013). New views on cellular uptake and trafficking of manufactured nanoparticles. *J R Soc Interface*, 10(82):20120939.

Troy, G. C. (1988). An overview of hemostasis. *Vet Clin North Am Small Anim Pract*, 18(1):5–20.

Tsai, C. Y., Lu, S. L., Hu, C. W., Yeh, C. S., Lee, G. B., and Lei, H. Y. (2012). Size-dependent attenuation of TLR9 signaling by gold nanoparticles in macrophages. *J Immunol*, 188(1):68–76.

Uppal, M. A., Kafizas, A., Ewing, M. B., and Parkin, I. P. (2010). The effect of initiation method on the size, monodispersity and shape of gold nanoparticles formed by the Turkevich method. *New Journal of Chemistry*, 34(12):2906–2914.

U.S. Environmental Protection Agency (2011). *IRIS toxicological review of tetrahydrofuran (THF) (interagency science discussion draft).* U.S. Environmental Protection Agency, Washington, DC.

U.S. Food and Drug Administration (2012a). *Guidance for industry: Pyrogen and endotoxins testing: Questions and answers.* U.S. Department of Health and Human Services, Silver Spring, MD.

U.S. Food and Drug Administration (2012b). *S2(R1) genotoxicity testing and data interpretation for pharmaceuticals intended for human use.* U.S. Department of Health and Human Services, Silver Spring, MD.

U.S. Food and Drug Administration (2015). *FDA's approach to regulation of nanotechnology products.* Retrieved from http://www.fda.gov/ScienceResearch/SpecialTopics/Nanotechnology/ucm301114, Silver Spring, MD.

USP (2011). 1225 validation of compendial procedures. U.S. Pharmacopeial Convention, Rockville, MD. Retrieved from https://hmc.usp.org/sites/default/files/documents/HMC/GCs-Pdfs/c1225.pdf.

Valko, M., Rhodes, C. J., Moncol, J., Izakovic, M., and Mazur, M. (2006). Free radicals, metals and antioxidants in oxidative stress-induced cancer. *Chem Biol Interact*, 160(1):1–40.

Vallhov, H., Qin, J., Johansson, S. M., Ahlborg, N., Muhammed, M. A., Scheynius, A., and Gabrielsson, S. (2006). The importance of an endotoxin-free environment during the production of nanoparticles used in medical applications. *Nano Lett*, 6(8):1682–6.

Vasconcelos, D. M., Santos, S. G., Lamghari, M., and Barbosa, M. A. (2016). The two faces of metal ions: From implants rejection to tissue repair/regeneration. *Biomaterials*, 84:262–75.

Vauthier, C. (2012). *Formulating nanoparticles to achieve oral and intravenous delivery of challenging drugs*, pages 1–19. The Royal Society of Chemistry.

Venkitanarayanan, K. S., Ezeike, G. O., Hung, Y. C., and Doyle, M. P. (1999). Efficacy of electrolyzed oxidizing water for inactivating Escherichia coli O157:H7, Salmonella enteritidis, and Listeria monocytogenes. *Applied and Environmental Microbiology*, 65(9):4276–4279.

Vertegel, A. A., Siegel, R. W., and Dordick, J. S. (2004). Silica nanoparticle size influences the structure and enzymatic activity of adsorbed lysozyme. *Langmuir*, 20(16):6800–7.

Vescovo, T., Refolo, G., Romagnoli, A., Ciccosanti, F., Corazzari, M., Alonzi, T., and Fimia, G. M. (2014). Autophagy in HCV infection: Keeping fat and inflammation at bay. *Biomed Res Int*, 2014:265353.

Vetten, M. A., Tlotleng, N., Tanner Rascher, D., Skepu, A., Keter, F. K., Boodhia, K., Koekemoer, L. A., Andraos, C., Tshikhudo, R., and Gulumian, M. (2013). Label-free in vitro toxicity and uptake assessment of citrate stabilised gold nanoparticles in three cell lines. *Part Fibre Toxicol*, 10:50.

Voelkel, K., Krug, H. F., and Diabate, S. (2003). Formation of reactive oxygen species in rat epithelial cells upon stimulation with fly ash. *J Biosci*, 28(1):51–5.

Vogel, C. W., Fritzinger, D. C., Hew, B. E., Thorne, M., and Bammert, H. (2004). Recombinant cobra venom factor. *Mol Immunol*, 41(2-3):191–9.

Vogler, E. A. and Siedlecki, C. A. (2009). Contact activation of blood-plasma coagulation. *Biomaterials*, 30(10):1857–69.

von Bruhl, M. L., Stark, K., Steinhart, A., Chandraratne, S., Konrad, I., Lorenz, M., Khandoga, A., Tirniceriu, A., Coletti, R., Kollnberger, M., Byrne, R. A., Laitinen, I., Walch, A., Brill, A., Pfeiler, S., Manukyan, D., Braun, S., Lange, P., Riegger, J., Ware, J., Eckart, A., Haidari, S., Rudelius, M., Schulz, C., Echtler, K., Brinkmann, V., Schwaiger, M., Preissner, K. T., Wagner, D. D., Mackman, N., Engelmann, B., and Massberg, S. (2012). Monocytes, neutrophils, and platelets cooperate to initiate and propagate venous thrombosis in mice in vivo. *J Exp Med*, 209(4):819–35.

Vonarbourg, A., Passirani, C., Saulnier, P., Simard, P., Leroux, J. C., and Benoit, J. P. (2006). Evaluation of pegylated lipid nanocapsules versus complement system activation and macrophage uptake. *J Biomed Mater Res A*, 78(3):620–8.

Vroman, L., Adams, A. L., Fischer, G. C., and Munoz, P. C. (1980). Interaction of high molecular weight kininogen, factor XII, and fibrinogen in plasma at interfaces. *Blood*, 55(1):156–9.

Wajant, H., Pfizenmaier, K., and Scheurich, P. (2003). Tumor necrosis factor signaling. *Cell Death Differ*, 10(1):45–65.

Walczyk, D., Bombelli, F. B., Monopoli, M. P., Lynch, I., and Dawson, K. A. (2010). What the cell "sees" in bionanoscience. *J Am Chem Soc*, 132(16):5761–8.

Walenga, J. M. and Hoppensteadt, D. A. (2004). Monitoring the new antithrombotic drugs. *Semin Thromb Hemost*, 30(6):683–95.

Wan, B., Wang, Z. X., Lv, Q. Y., Dong, P. X., Zhao, L. X., Yang, Y., and Guo, L. H. (2013). Single-walled carbon nanotubes and graphene oxides induce autophagosome accumulation and lysosome impairment in primarily cultured murine peritoneal macrophages. *Toxicol Lett*, 221(2):118–27.

Wandee, R., Florence, S., and Ornlaksana, P. (2009). *Disperse systems*, book section 11, pages 357–421. Drugs and the Pharmaceutical Sciences. CRC Press, Boca Raton, FL.

Wang, P., Henning, S. M., and Heber, D. (2010). Limitations of MTT and MTS-based assays for measurement of antiproliferative activity of green tea polyphenols. *PLoS One*, 5(4):e10202.

Wang, X., Guerrand, L., Wu, B., Li, X., Boldon, L., Chen, W., and Liu, L. (2012). Characterizations of polyamidoamine dendrimers with scattering techniques. *Polymers*, 4:600–616.

Wang, X., Ishida, T., and Kiwada, H. (2007). Anti-PEG IgM elicited by injection of liposomes is involved in the enhanced blood clearance of a subsequent dose of PEGylated liposomes. *J Control Release*, 119(2):236–44.

Wang, Y. X. (2011). Superparamagnetic iron oxide based mri contrast agents: Current status of clinical application. *Quant Imaging Med Surg*, 1(1):35–40.

Wei, X., Jiang, W., Yu, J., Ding, L., Hu, J., and Jiang, G. (2015). Effects of SiO2 nanoparticles on phospholipid membrane integrity and fluidity. *J Hazard Mater*, 287:217–24.

Weiskopf, D., Weinberger, B., and Grubeck-Loebenstein, B. (2009). The aging of the immune system. *Transpl Int*, 22(11):1041–50.

Wiesenthal, A., Hunter, L., Wang, S., Wickliffe, J., and Wilkerson, M. (2011). Nanoparticles: Small and mighty. *Int J Dermatol*, 50(3):247–54.

Wraith, D. (2016). Autoimmunity: Antigen-specific immunotherapy. *Nature*, 530(7591):422–3.

Wree, A., Eguchi, A., McGeough, M. D., Pena, C. A., Johnson, C. D., Canbay, A., Hoffman, H. M., and Feldstein, A. E. (2014). NLRP3 inflammasome activation results in hepatocyte pyroptosis, liver inflammation, and fibrosis in mice. *Hepatology*, 59(3):898–910.

Xia, T., Kovochich, M., Liong, M., Madler, L., Gilbert, B., Shi, H., Yeh, J. I., Zink, J. I., and Nel, A. E. (2008). Comparison of the mechanism of toxicity of zinc oxide and cerium oxide nanoparticles based on dissolution and oxidative stress properties. *ACS Nano*, 2(10):2121–34.

Xiang, S., Fuchsberger, M., Karlson, T. D. L., Hardy, C. L., Selomulya, C., and Plebanski, M. (2012). *Nanoparticles, immune modulation and vaccine delivery*, book section 15, pages 449–475. World Scientific, Singapore.

Xiong, H. M. (2013). ZnO nanoparticles applied to bioimaging and drug delivery. *Adv Mater*, 25(37):5329–35.

Xu, H., Liew, L. N., Kuo, I. C., Huang, C. H., Goh, D. L., and Chua, K. Y. (2008). The modulatory effects of lipopolysaccharide-stimulated b cells on differential t-cell polarization. *Immunology*, 125(2):218–28.

Xue, Y., Xiao, H., and Zhang, Y. (2015). Antimicrobial polymeric materials with quaternary ammonium and phosphonium salts. *Int J Mol Sci*, 16(2):3626–55.

Yah, C. S., Simate, G. S., and Iyuke, S. E. (2012). Nanoparticles toxicity and their routes of exposures. *Pak J Pharm Sci*, 25(2):477–91.

Yang, D., Zhao, Y., Guo, H., Li, Y., Tewary, P., Xing, G., Hou, W., Oppenheim, J. J., and Zhang, N. (2010). [Gd@C(82)(OH)(22)](n) nanoparticles induce dendritic cell maturation and activate Th1 immune responses. *ACS Nano*, 4(2):1178–86.

Yang, E. J., Jang, J., Lim, D. H., and Choi, I. H. (2012). Enzyme-linked immunosorbent assay of IL-8 production in response to silver nanoparticles. *Methods Mol. Biol.*, 926:131–9.

Yao, M., He, L., McClements, D. J., and Xiao, H. (2015). Uptake of gold nanoparticles by intestinal epithelial cells: Impact of particle size on their absorption, accumulation, and toxicity. *Journal of Agricultural and Food Chemistry*, 63(36):8044–8049.

Yazdi, A. S., Guarda, G., Riteau, N., Drexler, S. K., Tardivel, A., Couillin, I., and Tschopp, J. (2010). Nanoparticles activate the NLR pyrin domain containing 3 (Nlrp3) inflammasome and cause pulmonary inflammation through release of IL-1alpha and IL-1beta. *Proc Natl Acad Sci U S A*, 107(45):19449–54.

Yi, J. S., Cox, M. A., and Zajac, A. J. (2010). T-cell exhaustion: characteristics, causes and conversion. *Immunology*, 129(4):474–81.

Yildirimer, L., Thanh, N. T., Loizidou, M., and Seifalian, A. M. (2011). Toxicology and clinical potential of nanoparticles. *Nano Today*, 6(6):585–607.

Yu, T., Malugin, A., and Ghandehari, H. (2011). Impact of silica nanoparticle design on cellular toxicity and hemolytic activity. *ACS Nano*, 5(7):5717–28.

Yuan, Y., Ding, J., Xu, J., Deng, J., and Guo, J. (2010). Tio2 nanoparticles co-doped with silver and nitrogen for antibacterial application. *J Nanosci Nanotechnol*, 10(8):4868–74.

Yuk, J. M. and Jo, E. K. (2013). Crosstalk between autophagy and inflammasomes. *Mol Cells*, 36(5):393–9.

Zamboni, W. C., Torchilin, V., Patri, A. K., Hrkach, J., Stern, S., Lee, R., Nel, A., Panaro, N. J., and Grodzinski, P. (2012). Best practices in cancer nanotechnology: Perspective from NCI nanotechnology alliance. *Clin Cancer Res*, 18(12):3229–41.

Zhang, X. F., Liu, Z. G., Shen, W., and Gurunathan, S. (2016). Silver nanoparticles: Synthesis, characterization, properties, applications, and therapeutic approaches. *Int J Mol Sci*, 17(9).

Zhang, Y., Nayak, T. R., Hong, H., and Cai, W. (2013). Biomedical applications of zinc oxide nanomaterials. *Curr Mol Med*, 13(10):1633–45.

Zhang, Z., Berg, A., Levanon, H., Fessenden, R. W., and Meisel, D. (2003). On the interactions of free radicals with gold nanoparticles. *J Am Chem Soc*, 125(26):7959–63.

Zhao, L., Seth, A., Wibowo, N., Zhao, C. X., Mitter, N., Yu, C., and Middelberg, A. P. (2014). Nanoparticle vaccines. *Vaccine*, 32(3):327–37.

Zhao, Y., Sun, X., Zhang, G., Trewyn, B. G., Slowing, I., and Lin, V. S. (2011). Interaction of mesoporous silica nanoparticles with human red blood cell membranes: Size and surface effects. *ACS Nano*, 5(2):1366–75.

Zhong, Z., Umemura, A., Sanchez-Lopez, E., Liang, S., Shalapour, S., Wong, J., He, F., Boassa, D., Perkins, G., Ali, S. R., McGeough, M. D., Ellisman, M. H., Seki, E., Gustafsson, A. B., Hoffman, H. M., Diaz-Meco, M. T., Moscat, J., and Karin, M. (2016). NF-kappaB restricts inflammasome activation via elimination of damaged mitochondria. *Cell*, 164(5):896–910.

Zhong Lin, W. (2004). Zinc oxide nanostructures: Growth, properties and applications. *Journal of Physics: Condensed Matter*, 16(25):R829.

Zhou, F. (2009). Molecular mechanisms of IFN-gamma to up-regulate MHC class I antigen processing and presentation. *Int Rev Immunol*, 28(3-4):239–60.

Zielinski, J. M. and Kettle, L. (2013). Physical characterization: Surface area and porosity. Intertek, London. Retrieved from www.intertek.com/chemical-physical-characterization-surface-area-and-porosity/.

Zolnik, B. S., Gonzalez-Fernandez, A., Sadrieh, N., and Dobrovolskaia, M. A. (2010). Nanoparticles and the immune system. *Endocrinology*, 151(2):458–65.